NAVAL AIR WARFARE CENTER AIRCRAFT DIVISION
PATUXENT RIVER, MARYLAND

TECHNICAL REPORT

REPORT NO: NAWCADPAX--99-112-TR

HEAT DAMAGE ASSESSMENT
FOR NAVAL AIRCRAFT COMPOSITES

by

Henry McShane
El Sayed Arafat
Philip McLaughlin
Roland Cochran
Kevin Miller
Fred Arnold
Randall Cramer

7 September 1999

19991119 031

Aerospace Materials Division
Air Vehicle Department
Naval Air Warfare Center Aircraft Division
Patuxent River, Maryland
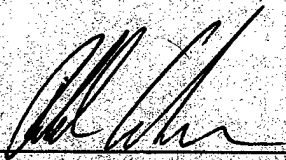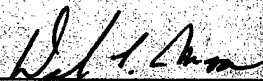
DTIC QUALITY INSPECTED 4

DEPARTMENT OF THE NAVY
NAVAL AIR WARFARE CENTER AIRCRAFT DIVISION
PATUXENT RIVER, MARYLAND

NAWCADPAX--99-112-TR
7 September 1999

RELEASED BY:

8/27/99

ROLAND COCHRAN / DATE
Head, Polymer Composites and Materials Branch

9/2/21

DALE MOORE / DATE
Director, Materials Competency
Naval Air Warfare Center Aircraft Division

REPORT DOCUMENTATION PAGE

1. AGENCY USE ONLY (Leave Blank)	2. REPORT DATE 7 September 1999	3. REPORT TYPE AND DATES COVERED

4. TITLE AND SUBTITLE

Heat Damage Assessment for Naval Aircraft Composites

5. FUNDING NUMBERS

6. AUTHOR(S)

Henry McShane	Roland Cochran	Fred Arnold
El Sayed Arafat	Kevin Miller	Randall Cramer
Philip McLaughlin		

7. PERFORMING ORGANIZATION NAMES(S) AND ADDRESS(ES)

Naval Air Warfare Center Aircraft Division
22347 Cedar Point Road Unit #6
Patuxent River, Maryland 20670-1161

8. PERFORMING ORGANIZATION REPORT NUMBER

NAWCADPAX--99-112-TR

9. SPONSORING / MONITORING AGENCY NAME(S) AND ADDRESS(ES)

Office of Naval Research
800 N. Quincy Street
Arlington, Virginia 22217-5660

10. SPONSORING / MONITORING AGENCY REPORT NUMBER

11. SUPPLEMENTARY NOTES

12a. DISTRIBUTION / AVAILABILITY STATEMENT

Approved for public release; distribution is unlimited.

12b. DISTRIBUTION CODE

13. ABSTRACT (Maximum 200 words)

This report presents results of work funded by the Office of Naval Research to study heat damage in organic matrix composites. The results presented in this report identify the mechanisms of heat damage, and the effects on physical and mechanical properties of composites subjected to high temperatures. A model to describe the heat damage process is presented, and a methodology to determine composite damage is supplied. In addition, specimens and data from this effort were supplied to government and private industry groups developing nondestructive evaluation techniques for heat damage evaluation in naval aircraft.

14. SUBJECT TERMS

Heat Damage
Composite Materials
Thermal Exposure

15. NUMBER OF PAGES
190

16. PRICE CODE

17. SECURITY CLASSIFICATION OF REPORT	18. SECURITY CLASSIFICATION OF THIS PAGE	19. SECURITY CLASSIFICATION OF ABSTRACT	20. LIMITATION OF ABSTRACT
UNCLASSIFIED	UNCLASSIFIED	UNCLASSIFIED	SAR

ABSTRACT

Polymer matrix composites are becoming more widely used for naval aircraft applications. An inherent problem with all organic matrix resins used in advanced composites is their susceptibility to thermal oxidative degradation following exposure to temperatures above their recommended upper service temperature. In current applications, composite heat damage arises from fire, engine exhaust impingement, equipment overheat, or a mishap during composite repair. Composites subjected to these exposure conditions experience a decrease in the glass transition temperature, which serves to effectively lower the upper use temperature, and matrix mass loss, which reduces the mechanical properties of the composite. The composite structure may or may not exhibit visual signs of damage, and this damage is difficult to measure by conventional nondestructive evaluation (NDE) techniques. All naval aircraft that use composites have the potential to succumb to composite heat damage, including the newly developed V-22 Osprey and the F/A-18 E/F.

This report presents results of work funded by the Office of Naval Research to study heat damage in organic matrix composites. The results presented in this report identify the mechanisms of heat damage, and the effects on physical and mechanical properties of composites subjected to high temperatures. A model to describe the heat damage process is presented, and a methodology to determine composite damage is supplied. In addition, specimens and data from this effort were supplied to government and private industry groups developing NDE techniques for heat damage evaluation in naval aircraft.

ACKNOWLEDGMENTS

CONTENTS

SECTION 1
INTRODUCTION

1.1 BACKGROUND

Airframes, propulsion systems, and other structural components are exposed to extreme temperatures from a variety of heat sources that are sufficient to cause damage to composite parts. NAWCAD Patuxent River, Maryland, has defined these high temperature exposure conditions for naval aircraft as fire, engine exhaust impingement, equipment overheat, or mishaps that occur during repairs. The properties of structural composites subjected to high temperature environments needs to be understood in order to intelligently use these materials. This report presents the results of an effort to investigate the process of heat damage. Subtasks in the program included identifying the temperatures and time-at-temperature conditions (within the bounds of Navy heat damage scenarios) that result in structural damage, understanding the effects of moisture on heat damage, and their relation to observed heat-induced property changes. Several techniques were used to evaluate the chemical, physical, and mechanical properties of composites exposed to high temperatures.

The behavior of composites exposed to high temperatures first became of interest for NAWCAD Patuxent River in August of 1991, after a fire in a composite wing of an A-6 aircraft. Questions arose regarding the flightworthiness of the aircraft and of the Navy's thermal damage assessment capabilities for composite materials. Five evaluation methods were initially studied: ultrasonics, Diffuse Reflectance Infrared Fourier Transform (DRIFT) spectroscopy, thermal mechanical analysis, hardness, and thermography (reference 1). After 2 years, the aircraft was certified flightworthy and returned to service. During this investigation, none of the nondestructive evaluation (NDE) methods proved effective in determining the effects of high-temperature exposure to the composite. The need for a method to evaluate composite heat damage led to other programs either conducted or sponsored by NAWCAD Patuxent River. Techniques such as dielectric spectroscopy, Raman spectroscopy, X-ray Photoelectron Spectroscopy (reference 2), Fourier Transform Infrared (FTIR) spectroscopy, and Laser-Pumped Fluorescence (reference 3) were studied. Their results, when correlated to mechanical property losses, showed that none of these techniques could accurately, with repeatable results, define strength losses in a composite. Ultrasonics, the standard depot-level technique, is effective at identifying damage when delaminations are present; however, studies show that there are heat damage scenarios where there is a loss in residual strength without crack formation or delaminations in the laminate (reference 4). This effect, where there are strength reductions not detectable by current nondestructive inspection (NDI) methods, is known as "incipient" heat damage. These evaluations showed the effectiveness as well as the limitations of current heat damage assessment techniques and the need for better, more accurate, nondestructive assessment methods.

Graphite/epoxy composite structures can, in some cases, survive (with some damage) very brief exposures to temperatures in excess of the decomposition temperature of the epoxy (reference 5). Heat transfer limitations can offer some protection during short-time exposures, especially if a porous char layer forms, or if blistering or delamination occurs, or if gas evolved from the outer surface carries away sufficient heat to protect the inner plies (reference 6). To better understand these observations and to investigate the mechanisms of heat damage, information on the chemical mechanisms and kinetics of degradation is needed. Thermal analysis and spectroscopy

1

have been used to investigate decomposition of composites and matrix resins. Global degradation kinetics are typically measured by thermal gravimetric analysis (reference 7). Two Thermal Gravimetric Analyzer (TGA) methods were used by NAWCWD China Lake to measure weight loss kinetics of epoxy resins; an isothermal method and a dynamic, or constant heating rate method. Results were compared to give confidence to predictions based on the kinetic parameters derived from TGA measurements. TGA studies need to be supplemented by spectroscopic methods that can identify chemical changes and measure kinetics of the loss or appearance of identifiable chemical functional groups. Infrared spectroscopy has been used to examine the chemical changes accompanying thermal degradation in epoxies and other resins. In particular, DRIFT has been used to investigate heat damage in epoxy resin composites (references 1, 8, and 9).

1.2 SCOPE OF TESTING

As advanced composites are becoming more widely used in naval aircraft, the incidence of heat damage will continue to increase. Many instances of heat damage have been documented in both fleet and developmental aircraft. A significant amount of time and money are spent evaluating the damaged structures. In addition, the large amount of aircraft downtime that results from investigation and evaluation of heat damage affects fleet readiness. Understanding the mechanisms of heat damage will allow for more efficient and timely assessment techniques than are currently available.

This report presents results of work funded by the Office of Naval Research (ONR) to study heat damage in organic matrix composites. The objective of this work was to evaluate the process of heat damage, document effects on physical and mechanical properties, and develop a method to determine composite heat damage.

There are three main efforts documented in this report. The first effort, MECHANISMS OF LAMINATION PLANE CRACKING, is a study of IM6/977-3 epoxy matrix composites. The results documented in this section describe the effects of temperatures near the onset of thermal decomposition of the matrix in varying moisture conditions. This aids in determining the mechanism that causes cracking and disbonds to occur in a composite exposed to high temperatures. Thermal and mechanical results of the various exposure conditions are given. Two nondestructive techniques for detecting heat damage are evaluated, and areas where mechanical damage occurred but was not identified by nondestructive techniques (incipient heat damage) are documented.

The second effort, OUTGASSING OF EPOXIES, builds upon the results of the first effort. In this section, the outgassed products occurring in IM7/8552 epoxy matrix composites during thermal damage are identified to better understand the thermal degradation process. Identifying the temperature at which these products were generated led to identifying the mechanism of incipient heat damage and a possible heat damage assessment technique.

The third effort, STATIC AND FATIGUE MODEL OF UNIDIRECTIONAL COMPOSITES, presents an analysis of fiber/matrix interface debonding and matrix property degradation due to high-temperature exposure. The model developed assesses the degree of tensile strength and tension-tension fatigue life that are lost due to such damage.

SECTION 2
MECHANISMS OF LAMINATION PLANE CRACKING

2.1   INTRODUCTION

Previous heat damage programs at NAWCAD Patuxent River have shown cracking to occur between the plies of a composite laminate after high-temperature exposure (reference 4). These disbonds run parallel to the plane of the laminate. The candidate mechanisms of lamination-plane cracking have been theorized to be 1) material thermoelastic property (TEP) mismatch, 2) high thermal gradients, 3) thermomechanical interlaminar stresses, and 4) internal pressure buildup due to outgassing of volatiles and/or water. One goal of the heat damage effort is to determine the primary mechanism(s) of lamination-plane cracking. A set of experiments were performed on neat resin and composite samples to evaluate each of these mechanisms.

Thermal effects on polymer composites show that there are heat damage scenarios where there is a loss in residual strength without crack formation or delaminations occurring in the laminate. This type of damage is extremely difficult to detect. In fact, heat damage resulting in a loss of mechanical strength that has not been accurately detected by any nondestructive technique has been documented. This effect, where there are strength reductions in composite materials and where the damage has not to date been nondestructively detectable, is known as "incipient" heat damage. Incipient heat damage requires further identification. A secondary goal is to define the temperature and time-at-temperature scenario where "incipient" heat damage occurs.

2.2   MATERIALS

2.2.1   NEAT RESIN

Neat resin samples were prepared by first degassing Fiberite 977-3 resin in a vacuum oven at 35°C (95°F). The resin was then cast in aluminum cake pans and oven cured at ambient pressure resulting in 2.54 mm (0.1 in.) thick panels. A convection oven was heated to 180°C (356°F) and the degassed resin was then placed in the oven, brought to temperature, and held for 2 hr. The ramp rate to temperature was approximately 5°C/min. To prevent sudden exothermic reactions that were experienced by directly heating to 180°C (356°F), 1 hr temperature holds were incorporated into the cure cycle at 100°C (212°F), 120°C (248°F), and 140°C (284°F). The neat resin panels were subsequently cut into 7.62 x 2.54 x 0.25 cm (3 x 1 x 0.1 in.) coupons.

2.2.2   COMPOSITE LAMINATES

Composite laminates were made from Fiberite IM6/977-3 unidirectional prepreg material containing 64% fiber volume content. Sixteen-ply unidirectional $[0]_{16}$ and quasi-isotropic $[0,\pm45,90,90,\pm45,0]_S$ laminates were hand laid-up using unidirectional prepreg and autoclave cured to Fiberite specifications. After cure, the laminates were cut into 7.62 x 2.54 x 0.25 cm (3 x 1 x 0.1 in.) coupons.

2.3 EXPERIMENTAL PROCEDURE

2.3.1 ENVIRONMENTAL CONDITIONING

The samples were conditioned before thermal exposure to yield dry, ambient stored, and saturated coupons. Drying was performed in a convection oven at 38°C (100°F) until no appreciable weight loss occurred. The ambient samples were stored in open air at prevailing (ambient) conditions. The saturated samples were held in boiling water according to the ASTM D 570-81 testing procedure.

2.3.2 THERMAL EXPOSURE

The conditioned specimens were thermally damaged in a high-temperature furnace. The furnace was heated to a known temperature, and coupons were then placed in the furnace. The coupons were subsequently removed after a period of either 5, 20, or 45 min. Furnace temperatures of 274°C (525°F), 302°C (576°F), and 329°C (623°F) were used. These times and temperatures of exposure were selected based upon a set of preliminary exposures at a wide variety of conditions. The intent of the selected time/temperature exposures was to yield samples that exhibited all forms of lamination-plane cracking, from no damage to extreme damage. Upon removal from the furnace, the samples were air cooled to room temperature. Table A-8 identifies the moisture condition of the specimens before heating and the temperature and time-at-temperature coupon exposure conditions. All samples were stored in open air ambient conditions after heating.

2.3.3 SAMPLE NOMENCLATURE

The convention used to identify each individual sample should be explained. Table A-8 identifies each sample and the exposure conditions. These exposure conditions defined the sample name.

The first character in each sample name identifies the laminate type. There are three different characters in this position, a 9, U, or Q. The "9" stands for a 977-3 neat resin sample. A "U" in this position means it was a unidirectional sample, and a "Q" denotes a quasi-isotropic sample.

The next three characters identify the temperature, in degrees Fahrenheit, of the exposure. There are three different numbers in this position, 525, 576, or 623.

The next two numbers identify the exposure time at the particular temperature. The three times are 5, 20, or 45 min.

The last character in the sample's name identifies the environmental exposure prior to heat damage. The three letters in this position are either "S," "A," or "D." "S" stands for a saturated sample, "A" for ambient, and "D" for dry.

For example, there is the sample identified as 9-525-05-S. The "9" means that it was a 977-3 neat resin sample, exposed at "525" °F, for "5" min, and was fully saturated ("S") before heat damage.

2.3.4 THERMAL GRAVIMETRIC ANALYSIS

TGA testing was conducted on a TA Instrument Model No. 2950. The temperature in the furnace, with the sample mounted, was first raised to a temperature of 30°C and allowed to equilibrate. Then the temperature was ramped to 900°C at 10°C/min. A sample size of 6-8 mg was used for each run; one run was performed on each exposed sample.

2.3.5 DIFFERENTIAL SCANNING CALORIMETRY

Differential Scanning Calorimetry (DSC) testing was conducted on a TA Modulated DSC Instrument Model No. 2920. The temperature in the DSC cell, with the sample mounted, was ramped from room temperature to 300°C at 5°C/min. Typical sample size was 10-11 mg. The modulation temperature was ±1°C at a rate of 60 sec/cycle. One run was made on each exposed sample.

2.3.6 VISUAL INSPECTION

Visual inspection was performed on the samples. Damage in the semitransparent neat resin samples was clearly visible when back-lighting was used. See section 2.4.5 for results.

2.3.7 ULTRASONIC INSPECTION

Ultrasonic testing was performed on a TechTrend International laboratory scanner using Arius II software. Scanning of the samples was performed using a 10 dB gain level and a 5 MHz concave transducer with a 5.08 cm (2 in.) focal length. Index and scan increments were 0.127 cm (0.05 in.) at a rate of 15.24 cm/sec (6 in./sec).

2.3.8 THERMOGRAPHIC INSPECTION

Thermographic testing was performed on an Ambervu infrared imaging system located 46 cm (18 in.) from the coupons. Inspection of the samples was performed using two flash heat lamps, each 2,400 ws, located 61 cm (24 in.) from the sample. Images were taken at 217 frames per second focusing on every seventh frame, resulting in 200 frames of data.

2.3.9 FOUR-POINT FLEXURE TEST

Flexural testing was performed according to ASTM Standard D 790-86, "Flexural Properties of Unreinforced and Reinforced Plastics and Insulating Materials." Four-point loading at one-third point was used. The support span was 4.1 cm (1.6 in.) with a span-to-depth ratio of 16:1. The tests were conducted on an Instron test machine at a cross-head rate of 1.27 mm/min (0.05 in./min).

2.4 RESULTS AND DISCUSSION

2.4.1 EXPERIMENTAL DESIGN

This study was designed for two purposes, to evaluate the mechanisms of lamination plane cracking and to determine the effect of absorbed moisture in heat damage. Temperatures in the range of incipient heat damage were chosen to determine the effectiveness of nondestructive techniques to evaluate this type of damage. As such, temperatures approximately 50°C to 100°C below the onset of the polymer matrix decomposition temperature were chosen, and the samples were exposed for 5 to 45 min. Three sample sets were evaluated, one set of cured neat resin samples and two composite laminate configurations - unidirectional and quasi-isotropic. The neat resin samples were used to isolate the TEP mismatching, which occurs in composite laminates, from the other variables being studied. To provide a range of samples to test the effect of absorbed moisture, the samples were treated under dry, ambient, and saturated environmental conditions. Table A-8 identifies the various coupon configurations. After exposure, the samples were evaluated using thermal gravimetric analysis and DSC. Three nondestructive methods were used to assess the degree of damage resulting from the thermal treatments: visual inspection, ultrasonic inspection, and thermographic inspection.

2.4.2 ENVIRONMENTAL CONDITIONING

Table A-1 lists the neat resin samples and their weight before and after saturation. Table A-2 lists the neat resin samples and their weight before and after drying. Tables A-3 through A-6 similarly list the weights before and after conditioning of the unidirectional and quasi-isotropic samples. Table A-7 shows the average weight loss or weight gain for the different sample groups. The neat resin samples gained an average of 4.2% in weight during the conditioning compared to the composite samples in which the unidirectional samples gained 0.98% in weight and the quasi-isotropic ones gained 0.84% over the 25 days of conditioning. The neat resin samples lost an average of 0.63% in weight during the conditioning compared to the composite samples in which the unidirectional samples lost 0.29% in weight and the quasi-isotropic samples lost 0.32% over the 10 days of drying. The fiber volume content of the composite laminates is the cause for the large difference between the neat resin and the composite samples. Figure B-1 shows the weight gain or loss during conditioning of the 977-3 neat resin samples. Initially, weight gain or loss occurs rapidly and then levels off until equilibrium is reached. For the saturated samples, equilibrium was reached in 25 days. Equilibrium was reached in 10 days during drying.

2.4.3 THERMAL GRAVIMETRIC ANALYSIS

Thermal decomposition versus temperature was determined in order to correlate both the temperature of thermal decomposition initiation (defined as the temperature where 95% of the original weight remains) and the temperature where the maximum rate of decomposition occurs for the different heat damage scenarios. Figure B-2 is a typical TGA plot showing the percent weight loss versus temperature for a neat resin sample. The neat resin sample in this figure was first saturated (section 2.3.1) and then thermally damaged at 274°C (525°F) for a period of 5 min. The onset of thermal decomposition is measured as 357°C. The first derivative of the temperature versus time curve can be calculated resulting in a new curve also shown in figure B-2. The peak of the derivative curve occurs at 420.6°C, indicating that this is the temperature where the maximum rate of decomposition is occurring. These measurements were taken for each of the samples in this study. The TGA plots for every sample are presented in appendix C. Table A-9 summarizes the results of thermal decomposition initiation and the temperature where the maximum rate of decomposition occurs for the different heat damage scenarios for the 977-3 neat resin. Similarly, tables A-10 and A-11 represent similar data for the unidirectional and quasi-isotropic samples, respectively.

Figure B-3 summarizes the results of the onset of decomposition for the neat resin samples. This graph has the onset temperatures grouped according to the heat damage temperature. Comparing the results for the 525°F exposures, it can be seen from this graph that the dry and ambient samples' onset of decomposition temperature stays constant. The saturated samples' onset of decomposition temperature increases with time for the 525°F results. Note that the 5 min exposure value is 357°C and increases to 386°C as the exposure time increases. A similar trend is observed in the 576°F grouped samples; however, the values for the dry and ambient temperatures increase to a smaller extent with the 20 and 45 min exposed samples. The 623°F exposed samples do not show a significant trend. This could be due to the higher temperature exposure of this group. Figure B-4 compares the same data, but groups the samples by similar time of exposure as opposed to temperature of exposure. Again, the shape of the saturated samples' curve is vastly different from the dry and ambient curves. Both of these representations of the data show that the onset of decomposition temperature has increased with both increasing temperature exposure and time exposure.

Figures B-5 and B-6 present the data for the temperature reflecting the maximum rate of weight loss for the neat resin. Figure B-5 groups the data by exposure temperature showing increasing time, and figure B-6 groups the data by exposure time showing the effects of increasing temperature. These two charts reflect no significant trend.

The results for the unidirectional and quasi-isotropic laminates are shown in figures B-7 through B-14. Again, no trend can be observed in the temperature at which the maximum rate of weight loss occurs. But, the onset of decomposition temperature data shows that this value increases as the temperature exposure or the time of exposure increases. The highest temperature exposure, 623°F, shows the largest scatter in the data.

2.4.4 DIFFERENTIAL SCANNING CALORIMETRY

DSC was used to monitor the heat flow through the damaged sample and measure the residual exotherm. From these data, it is possible to derive the glass transition temperature (T_g) and the degree of conversion for the materials.

Figure B-15 shows the results from the degree of conversion measurements. This graph presents data from the dry neat resin samples. To derive the degree of conversion for a sample, the residual heat of reaction for the sample is correlated to the heat of reaction for an uncured sample. A standard value of 300 J/g was used for the uncured resin. For comparative purposes, this value suffices. As is shown on the graph, the specimens heat damaged at the 274°C temperature exhibited further curing as evidenced by the increased degree of conversion from 95% for the 5-min exposure to 98% for the 20-min exposure and to 99% for the 45-min exposure. The higher temperature exposures reveal a fully cured network at greater than 99% degree of conversion.

Results of this increase in degree of conversion can be seen in the T_g measurements. The dry T_g measurements are presented in figure B-16. The data show that the 274°C exposed samples experience an increase in T_g with increasing exposure time rising from 200°C to 219°C, and this is attributed to a postcure resulting from the thermal exposure. This is not experienced in the higher temperature exposed samples. Both the 302°C and the 328°C exposed samples experience a decrease in T_g. The 328°C samples degrade much faster than the 302°C samples. The same trend was observed with the ambient conditioned samples. Figure B-17 presents the results for the saturated samples. These results differ from the dry conditioned samples in that all three temperature exposures for the saturated samples exhibit degradation, with the higher temperature exposed samples showing more degradation than the lower temperature exposed samples. Comparing figure B-16 to figure B-17, note the 274°C exposed T_g values. The 5-min saturated exposure value clearly indicates an increase in T_g from an undamaged resin state. This increase, which occurred over a 5-min span, is a larger increase in T_g than was experienced by the dry sample exposed for 45 min at the same temperature. This is an indication that absorbed moisture accelerates the postcure process when the time/temperature exposure is not great enough to cause matrix degradation.

2.4.5 VISUAL RESULTS

The semitransparent nature of the neat resin lends itself to visual evaluation of the effects of the temperature exposure on the polymer. Figure B-18 shows all of the coupons as they appeared after thermal exposure. The unidirectional and quasi-isotropic coupons are shown in figures B-19 and B-20, respectively. Figure B-21 shows three of the neat resin coupons after thermal exposure. These coupons were saturated at 5-min time exposures with increasing temperature exposure from the top of the figure down. The figure shows that the amount of voids increase as exposure temperature increases. Using back lighting to aid the examination, observations of void formation after heating were noted and are documented in figure B-22. The

degree of damage was then qualitatively rated as either having no damage, some to moderate damage, or being completely damaged, figure B-24. As the temperature and time-at-temperature increased, the degree of damage increased, but no visible damage was observed at the low temperature and short time-at-temperature exposures. Also noteworthy is the comparison of the ambient and dry conditions showing similar behavior, which is not surprising since their moisture content are approximately equal. Typical damage modes observed are shown in figures B-21, B-22, and B-23. Note the striation marks in figure B-22 indicating stress buildup initiating in the middle of the resin and continuing to the surface. This spalling damage mode was observed in all neat resin samples. As has occurred in this example, a piece of the neat resin coupon was ejected during thermal exposure. The manifestation of this phenomena in composite laminates is shown in figure B-23. The fibers contained within the matrix prevent the laminate from spalling like the neat resin, and instead the damage mode is delamination.

2.4.6 ULTRASOUND AND THERMOGRAPHY INSPECTION

Ultrasonic and thermographic scans were made on each of the specimens. Signal attenuation in the sonograms indicated damage from the thermal exposure. Figure B-25 shows a typical ultrasonic c-scan for the saturated neat resin samples. All of the saturated samples are shown and labeled in this figure. Similarly, all of the dry neat resin and ambient conditioned neat resin c-scans are shown in figures B-26 and B-27, respectively. Figures B-28 through B-33 show the results for the unidirectional and quasi-isotropic laminates. The c-scans were then rated by estimating the percent of the total area that exhibited defects, as noted by decibel loss. This grading system uses 25% increments in an effort to develop a tool for qualitatively comparing the c-scan results with the visual, mechanical, and other evaluation techniques used in the project. It also provides a way to determine overall trends in the c-scan data. Samples with less than 25% inhomogenieties were classified as undamaged and greater than 25% were rated as damaged to some degree. Samples with deterioration so extensive that they could not be evaluated by these techniques were noted as totally damaged. This was done to distinguish intact 100% damaged samples from those that had entirely lost their structural integrity. The results of this scheme are shown in figure B-43.

Note according to this evaluation protocol, ultrasound inspection indicated no detectable damage at the lower temperatures and the lower time-at-temperature exposures for the dry and ambient stored samples. Again, the dry and ambient conditioned samples were comparable for the most part due to the fact that there is not an appreciable difference in their moisture content. The saturated samples did tend to show damage under any time/temperature condition except at the lowest temperature/time exposure of 5 min at 274°C. These ultrasonic results correlate well with the visual results as shown in section 2.4.5 for all sample types. It is also apparent that the higher degrees of damage were detected as temperature, time at temperature, and moisture content increased.

The results of the thermography inspections are rated in the same fashion. The thermography results are given in figures B-34 through B-42. Figure B-44 is the rated figure of the thermography scans similar to figure B-43 for the ultrasonic c-scans. The general trends are the same as those found by ultrasound inspection, damage detection increases with temperature, time at temperature, and moisture content. However, the results of the saturated samples for the unidirectional and quasi-isotropic materials yielded unusual results. The c-scan results show those sample groups to be extremely damaged although the thermography results show little damage for any of the coupons. Perhaps the extent of damage in these samples hindered penetration of heat and thus effected detection by thermography in the most severely damaged samples or perhaps they were uniformly damaged.

2.4.7 FOUR-POINT FLEXURE TEST

Limited mechanical testing was conducted on the specimens after all other testing was completed. Flexure testing was conducted on the specimens to see if any trends could be established. It must be noted that the flexure testing results are based on one sample at each heat damage condition and, therefore, the results are not statistically based, but define trends in the data. The flexure test was chosen because resin properties are assumed to degrade faster than fiber properties under the influence of heat, and a flexure test is a matrix dependent property. Table A-12 gives the results of the four-point flexure test for the neat resin samples. Similarly, tables A-13 and A-14 give the results for the unidirectional and quasi-isotropic coupons. Included in these tables are the physical dimensions of each coupon, the peak load that was reached during testing, and the corresponding flexural strength. Note that in table A-13 many of the unidirectional tests were aborted. This was due to the fact that the peak load needed to break the specimen was greater than the limit of the load cell on the test machine. Figure B-45 is a graphical representation of the flexure strength for the saturated neat resin samples. A large decrease in T_g is observed from the 5-min 274°C saturated neat resin exposed sample to both the 20- and 45-min exposed samples. The same trend was observed in the 302°C sample set. The highest temperature exposure, 329°C, exhibits total flexural strength loss immediately from the 5- to the 45-min exposure. These data demonstrate that greater temperature exposure leads to greater structural damage in the resin. Figures B-46 and B-47 give the results for the dry exposed and ambient exposed neat resin samples, respectively. These two graphs are almost identical with little difference between the dry and ambient exposed samples, as is demonstrated with all the other evaluation methods. It must be noted that the 329°C 20- and 45-min exposed samples from each of these two groups have zero values for their flexural strength. As noted in table A-12, these samples completely crumbled upon removal from the high-temperature furnace after heating and, therefore, no sample was available to test. This also happened for the 329°C 45-min saturated sample. The 274°C exposed sample shows an increase in flexure strength from the 5-min exposed sample. This could be explained by the increase in T_g that was experienced by these samples. Figures B-48, B-49, and B-50 are the results for the quasi-isotropic coupons. The same trends are observed as were shown in the neat resin samples.

Flexural strength decreased very significantly in most cases with increases in temperature, time at temperature, and moisture content, which is very consistent with the damage detected by the above inspection techniques. Some of the exposures evidenced loss in flexural strength when the damage detected by NDI was either minimal or borderline. This was observed in the case of the dry and ambient conditioned samples. The saturated samples almost immediately experienced significant loss in flexural strength when compared to the decrease in the dry and ambient results.

The test matrix chosen for this study does not allow comprehensive analysis and correlation with the degree of damage detected by the above techniques; however, the results do illustrate some very definite trends when the decrease in flexural strength is compared to the inspection results.

2.5   CONCLUSIONS

The visual results revealed that at the 274°C temperature, no damage occurs at any of the time periods for either the dry or ambient samples. The 5-min exposure time yielded no visible damage at any of the temperatures for the dry or ambient samples. The saturated samples did show spalling in the neat resin at both the 20- and 45-min 274°C exposures and at the 5-min exposure for the 302°C and 328°C temperatures. From this and the results from other inspection techniques, it was concluded that internal pressure from volatiles and/or trapped moisture was the primary degradation mechanism in the samples over the temperatures and times studied. All of the samples showed the trend of increasing damage with both increasing temperature and time-at-temperature exposures. The T_g of the dry samples at the 274°C exposure increased. This increase is attributed to a post cure. All other samples showed a decrease in T_g when compared to the undamaged samples. All tests showed that the dry and ambient conditioned samples exhibited almost identical behavior, most likely due to the small difference in moisture content between them. All tests revealed that the saturated samples exhibited degraded properties much earlier and much more severely than the dry/ambient samples. Ultrasonic inspection was capable of detecting heat damage that induced blistering, ply delaminations, and void formations. However, NDE techniques were not capable of detecting changes in samples that showed degradation of other properties.

SECTION 3
OUTGASSING OF EPOXIES

3.1 INTRODUCTION

This study focuses on developing a technique to detect and estimate heat damage in a graphite/epoxy composite composed of Hexcel 8552 resin by STA-FTIR technique. Simultaneous Thermal Analyses (STA) performs DSC and TGA procedures simultaneously. DSC provides heat flow characteristics while TGA measures weight loss, both as a function of temperature and time. FTIR identifies the presence of specific molecular groups or bonds by their absorption of energy in the infrared range. Combining the three techniques allows simultaneous quantification and identification of evolved decomposition products as a function of weight loss, time, and temperature.

3.2 EXPERIMENTAL

3.2.1 MATERIALS

Sixteen-ply quasi-isotropic composite laminates were made from Hexcel IM7/8552 unidirectional prepreg material. The laminates were hand laid-up and autoclave cured according to Hexcel specifications. The laminate ply layup is $[0,\pm45,90,90,\pm45,0]_s$.

3.2.2 THERMAL EXPOSURE

The laminates were thermally damaged using a high-temperature platen press. The lower surface of the press was first heated to 315°C (600°F), and the laminates were then placed on the heated surface. The laminates were thermally damaged for either 5, 20, or 45 min. Upon removal from the press, the samples were air cooled to room temperature. All samples were stored in open air ambient conditions after heating.

3.2.3 SIMULTANEOUS THERMAL ANALYZER

Thermal gravimetric experiments are performed with a Rheometric Scientific Instrument "Simultaneous Thermal Analyzer 625" (STA). STA consists of a DSC and a TGA. The system is calibrated for the base line, sample temperature, balance and furnace temperature. The TGA furnace is equipped with a heated transfer line to the gas cell in the FTIR instrument. The analysis is performed under dynamic and isothermal conditions to measure the kinetic parameters of thermal decomposition. The heating rates for the dynamic runs are 3, 5, 10, 15, and 20°C/min from room temperature to 550°C. The isothermal condition is reached by a rapid heating rate of 60°C/min to the isothermal temperatures at 290, 300, 310, 320, 330, 340, 350, 360, and 370°C. The temperature of the transfer line and the gas cell is controlled by the gas cell controller. The temperature of the gas cell is kept at 200°C and the transfer line at 155°C. The composite sample was cut in thin slices by a water-cooled, diamond-bladed saw and then into

smaller pieces using scissors. The weight loss is measured by using 13 to 17 mg of crushed composite material in an aluminum pan. The sample was purged with high-purity nitrogen gas (99.998%) for 30 min before and during the analysis at a flow rate of 50 ml/min. Five samples were analyzed at each condition.

3.2.4 FOURIER TRANSFORM INFRARED SPECTROSCOPY

The Nicolet 560 Magna FTIR Instrument in line with the STA system was used to obtain the FTIR spectra of the evolved gases from the heated composite sample. The instrument is equipped with an MCT-B liquid nitrogen cooled detector. The transfer line and the gas cell are purged with nitrogen gas at a flow rate of 50 ml/min. The gas cell compartment is purged with nitrogen gas at a flow rate of 100 SCFH for 10 min before the run and then reduced to 30 SCFH during the run. A background spectra is collected before each experiment at 128 scans and 4 cm^{-1} resolution. The correction for carbon dioxide (CO_2) gas and water moisture, as determined by the background spectra, is programmed and automatically subtracted from the final results. The sample spectra are collected every 30 sec at 32 scans per spectra at 4 cm^{-1} resolution. The Gram-Schmidt chromatogram is recorded for all experiments. The Gram-Schmidt measures the total gases evolved as a function of time.

3.3 RESULTS AND DISCUSSION

The samples were studied under both isothermal and dynamic conditions in the TGA cell. During these runs, the outgassed products were transferred to the FTIR cell and analyzed. Figure B-51 shows the weight loss measurement of undamaged 8552 resin from the TGA instrument as a function of temperature. The TGA data show a one-step weight loss of 20% during the dynamic run from room temperature to 550°C at 10°C/min. Figure B-52 shows the Gram-Schmidt chromatogram for this dynamic run. At approximately 25 min into thermal decomposition, corresponding to an STA cell temperature of 280°C, evolution of gasses were indicated. This corresponds with the TGA weight loss analysis in which weight loss begins at approximately 280°C.

The evolved gases of 8552 resin during heating were identified by FTIR as CO_2, carbon monoxide (CO), water (H_2O), carbonyl sulfide (COS), acid anhydride (R-CO-O-CO-R), and phenol (C6H5-OH). The decomposition products appear in two stages, first at 280°C and then at 340°C. Figure B-53 shows the FTIR spectra for the evolved gasses of 8552 resin at 290°C. This is during the first stage of thermal decomposition and consists of CO_2, CO, H_2O, and R-CO-O-CO-R. This grouping of evolved gasses continues from 280°C to 340°C. Table A-15 provides a listing of the associated vibrational frequencies used to identify these products. The FTIR data show three carbonyl groups at 1725, 1759, and 1790 cm^{-1} frequencies during the first stage of decomposition. The possible identification of the carbonyl groups are acid anhydride and ester. At 340°C, a second grouping of evolved gasses begins. Figure B-54 is a spectrum collected at 350°C identifying this stage, and consists of COS and C6H5-OH. Figure B-55 is a comparison

of the FTIR spectra for 290°C, 350°C, and 500°C showing how the peaks change between the two stages. Note that the 500°C spectra is similar to the one at 350°C, indicating that the second phase is the final phase of decomposition.

The first stage of decomposition causes up to 8% weight loss, as observed during an isothermal TGA run at 330°C (table A-16). Figure B-56 is a TGA plot showing the total weight loss percent associated with 8552 resin at isothermal temperatures ranging from 300°C to 370°C. This amount of weight loss causes the mechanical properties of the composite to greatly decrease (section 2.4.7). In section 2, MECHANISMS OF LAMINATION PLANE CRACKING, it was shown that incipient heat damage occurs at temperatures near the onset of thermal decomposition, which occurred in the 274°C and 302°C exposed samples in that study. Therefore, this first stage of thermal decomposition characterizes heat damage situations that induce incipient heat damage. This is the most difficult heat damage to detect nondestructively because there is no visible damage, and delaminations in the composite do not occur due to the relatively low-exposure temperatures.

To estimate heat damage, the peak height of the carbonyl groups and the CO_2 peak was tracked over the temperature range of 290°C to 370°C, see table A-16. Figure B-57 is a graph of the average peak height versus the TGA isothermal temperature. A good correlation is seen in both the CO_2 and the carbonyl group peak heights with temperature. There is a definite slope change for both groups in the range of 330°C to 340°C, which corresponds to the thermal decomposition mechanism change identified from the FTIR spectra. This correlation can be used to develop a calibration curve to estimate the heat damage of a composite. To test this approach, data were collected on thermally damaged composites at 315°C for 5, 20, and 45 min, and analyzed by the STA-FTIR technique at 330°C isothermal (section 3.2.2). The damaged composite data are given in table A-17. The peak height/mg of the carbonyl group of the undamaged composite is measured at 4.25, which compares to the damaged group with peaks of 3.92, 3.53, 2.91 as damage time increases from 5 to 45 min and is plotted in figure B-59. There is not a good correlation with the CO_2 peaks. A linear regression was plotted through the carbonyl data with an R^2 value of 0.978. By developing calibration curves, STA-FTIR has the capability to track heat damage and to estimate the amount of heat damage in a composite.

3.4 CONCLUSIONS

Analysis of Hexcel IM7/8552 composite material by STA/FTIR shows two distinct stages of degradation, beginning at 280°C and then at 340°C. The outgassed products of the first stage of thermal decomposition consist of CO_2, CO, H_2O, and a carbonyl group identified as either acid anhydride or ester. This first stage occurs from 280°C to 340°C. At 340°C, a second stage of thermal decomposition begins and continues for the duration of the decomposition process. The second stage is characterized by the outgassing of COS and C6H5-OH.

Heat damage can be evaluated by STA/FTIR by correlating the peak heights of the carbonyl group to exposure temperature. There is the potential to develop a heat damage assessment technique using STA/FTIR by developing more extensive calibration curves of this type. In section 2, incipient heat damage was shown to occur near the onset of thermal decomposition. Stage one of the heat damage process begins at the onset of thermal decomposition of the polymer; this initial stage results in incipient damage. During stage 2, more severe damage occurs resulting in delamination and blistering, which are detectable by ultrasonic techniques.

SECTION 4
STATIC AND FATIGUE MODEL OF UNIDIRECTIONAL COMPOSITES

4.1 INTRODUCTION

This section presents an analysis of fiber/matrix interface debonding and matrix property degradation due to a single step-function of temperature, investigates the mechanisms of damage, and assesses the degree of tensile strength and tension-tension fatigue life that might be lost due to such damage.

In the analysis, the fundamental mode of unidirectional fiber composite tensile failure is assumed to be that of the "chain of bundles" cumulative weakening failure mechanism proposed by Rosen (reference 17) and extended by Zweben (reference 22), McLaughlin and Rosen (reference 14), Phoenix, et al. (reference 15), McLaughlin (reference 13), and others wherein the "ineffective length" (unstressed fiber length encompassing a fiber break) and appropriate fiber strength Weibull probability distribution parameters control structural failure. It is clear from the work of Zweben (reference 20), Zweben and Rosen (reference 23), and Zhou and Curtin (reference 19), for example, that other mechanisms than cumulative weakening can be operative during composite tensile failure, most notably a transverse fiber break propagation mode caused by adjacent fiber overstress near single or multiple fiber breaks. However, it has been shown (Zweben, reference 21) that the cumulative weakening mode is an upper bound to failure and may be a good representation for glass/polymer and graphite/polymer composites with weak interfaces (Hahn, reference 12).

The cumulative weakening model has been modified (McLaughlin, reference 13) to include a linear elastic fracture mechanics micromechanics model of the growth of fiber disbonds and hence ineffective length with both increasing quasi-static load and number of cycles of constant-amplitude tension-tension fatigue load. The ineffective length damage growth model was combined with Weibull fiber failure statistics to obtain a predictive tool for determining either the life or the residual strength of a unidirectional fiber composite under any combination of static or variable amplitude tension-tension fatigue loading. This work adds the effects of thermal stress, residual and otherwise, to the analysis and, using temperature-dependent material properties, predicts the reduction in static strength and fatigue life that might occur as functions of the applied temperature and time at temperature.

4.2 CUMULATIVE WEAKENING WITH THERMAL STRESSES

4.2.1 CUMULATIVE WEAKENING AND CHAIN-OF-BUNDLES MODEL

In the cumulative weakening mode of tensile failure, a unidirectional composite is considered to be a series chain of links composed of short lengths of dry fiber bundles. In the latter mode, bundle strength is dictated by fiber strength (s) versus length (δ) statistics that can be expressed, for example, by the Weibull cumulative distribution function (α, β are constants):

$$F(s) = 1 - e^{\alpha \delta s^{\beta}} \tag{1}$$

which results in bundle strength S_f of

$$S_f = (\alpha \beta e \delta)^{1/\beta} \tag{2}$$

In a composite, the effective bundle length, δ, is the ineffective length, which is the distance from a fiber break over which the fiber is ineffective in carrying tensile load (figure B-60). Remaining fibers in the bundle "link" of length δ are assumed to share equally the broken fiber's load as if they were in a dry bundle of that length. Until fiber stress is high enough to initiate and propagate a crack in the fiber/matrix interface, the ineffective length is assumed to equal the length δ_E of an equivalent step function of zero stress extending in either direction from the fiber break (figure B-61). This elastic ineffective length δ_E has been computed with a shear-lag analysis in McLaughlin (reference 13) for a broken fiber in a hexagonal array of intact fibers that have been "smeared" into an equivalent ring of surrounding fiber material (figure B-62):

$$\delta_E / d = (1/2)\sqrt{2E_f \ \ln(d'/d)/G_m} \tag{3}$$

where E_f is fiber axial Young's modulus, G_m is matrix shear modulus, d is fiber diameter, and d' = 2r' is inner diameter of intact ring. Once an average shear-lag shear stress of T is exceeded at the crack tip (shown in McLaughlin, reference 13, to be equivalent to exceeding a critical mode II energy release rate of G_{IIc}), the crack propagates and the ineffective length becomes equal to $\delta_E + 2a$. In the cracked region, due to friction and/or mechanical interference, the shear stress may maintain a constant value of ηT where η , the post-failure shear stress fraction, is between 0 and 1.0. The ineffective length δ as a function of applied far-field of fiber stress σ_{f0} following fiber/matrix crack initiation at a fiber stress s_T is shown in McLaughlin and Rosen (reference 14) to be:

$$\delta = \delta_E + 2a = \delta_E + \frac{(\sigma_f 0 - s_T)d}{2\eta T} \ ; \quad s_T = 2T\delta_E/d \tag{4}$$

As composite stress σ_c increases and, with it, fiber far-field stress σ_{f0}, the ineffective length increases until the bundle strength S_f, given by equation (2), reduces to σ_{f0}. Equating equation (2) solved for δ to equation (4) with S_f in place of σ_{f0} will give the fiber stress S_f at composite failure, which in turn gives composite failure stress S_c from

$$S_c = S_f E_c / E_f \tag{5}$$

McLaughlin (reference 13) developed a procedure for using the cumulative weakening model to predict fatigue life and residual strength under any history of tension-tension composite axial stress. If a Paris-type crack growth equation is applicable for the fiber/matrix interface, it can be shown that the resulting rate of crack extension with cycles N as a function of amplitude fiber stress $\Delta\sigma_{f0}$ is

$$\frac{da}{dN} = C_\sigma (\Delta\sigma_f 0)^m \tag{6}$$

and the growth of ineffective length with number of cycles for constant amplitude stress becomes

$$\delta \, \delta_i = C_\sigma (\Delta\sigma_f 0)^m (N \, N_i) \tag{7}$$

where C_σ and m are constants from the Paris equation, and δ_i and N_i are the preexisting ineffective length and total number of cycles, respectively, before a block of cycles at fiber stress amplitude $\Delta\sigma_{f0}$.

The growth of ineffective length with static loading, equation (4), and constant-amplitude fatigue loading, equation (7), are sufficient to determine the ineffective length that will occur under any history of static and cyclic tension-tension stresses. The first instance where the ineffective length reaches a value

$$\delta_f = \frac{1}{\alpha\beta e} \sigma_{f0\,max}^{\,\beta} \tag{8}$$

at the same time the maximum fiber stress level is at σ_{f0max} causes the composite to fail. Several examples of this that include fatigue strength versus cycles (S/N) curve determination under constant-amplitude loading and residual strength after a history of cyclic stressing are presented in McLaughlin (reference 13).

4.2.2 CUMULATIVE WEAKENING WITH THERMAL STRESSES

The difference in thermal expansion properties of the fiber and matrix usually causes residual thermal stresses in each phase. These stresses have not been included in the preceding analysis, and it is important to determine their effect upon strength and fatigue life. Also, when subjected to elevated temperatures, the properties of the matrix, fiber/matrix interface, and fiber change.

18

Therefore, high temperatures may cause damage in the composite because of stresses created due to thermal expansion *and* the modified properties that affect the damage development. This section includes thermal expansion in the cumulative weakening analysis .

Let T_0 be the stress-free temperature (approximately the cure temperature) of a composite. The composite is at instantaneous temperature T with the resulting temperature difference from the stress-free-state being $\Delta T = T - T_0$. The composite (*c*), fiber (*f*), and matrix (*m*) are each assumed to be represented by one-dimensional constitutive laws between stress **F**, strain ε, and temperature difference (α is linear thermal expansion coefficient):

$$\varepsilon_i = \sigma_i / E_i + \alpha_i \Delta T , \quad i = c, f, \text{ or } m \tag{9}$$

Let the axial coordinate along a fiber be x with origin at a fiber break (figure B-61), axial displacement be $u(x)$, cross-sectional area be A, and subscripts $c, f,$ and m refer to composite, fiber, and matrix, respectively. The matrix has a shear modulus of G_m, and $\tau(x) = G_m \gamma(x)$ is the shear stress at the fiber/matrix interface due to the shear-lag engineering shear strain γ. Force equilibrium in the x-direction in the cracked and uncracked regions becomes, using $\varepsilon_f = du_f / dx$,

$$E_f A_f \frac{d^2 u_f}{dx^2} - \eta T \pi d = 0, \qquad\qquad 0 \_ x \_ a$$

$$E_f A_f \frac{d^2 u_f}{dx^2} - \tau(x)\pi d = 0, \quad \tau(x) = 2 G_m \frac{u_f - u_c}{d_f \ln(d'/d)} , \quad a \_ x \_ \infty \tag{10}$$

To obtain u_f, these equations are integrated using $u_c = \varepsilon_c x$ and the boundary/continuity conditions

$$\frac{du_f}{dx}_{-x=0} = 0$$

$$\frac{du_f}{dx}_{-x \to \infty} = \sigma_{0T} \tag{11}$$

$$u_f \text{ and } \frac{du_f}{dx} \text{ continuous at } x = a$$

where

$$\sigma_{0T} = \sigma_{f0} + E_f \alpha_f \Delta T \tag{12}$$

and the shear stress at the crack tip is found to be

$$\tau(a) = \left[\frac{G_m}{2 E_f \ln(d'/d)} \right]^{1/2} [\sigma_{0T} - 4\frac{a}{d}\eta T] \tag{13}$$

A comparison with McLaughlin (reference 13) shows that the difference between formulations with and without thermal expansion is in the constitutive equation (9), the appearance of the term σ_{0T} in place of σ_{f0} in equation (13) and subsequent developments, and the variation of material properties with temperature.

4.2.3 ISOTHERMAL STATIC STRENGTH AND FATIGUE LIFE

The growth of ineffective length with monotonic increasing fiber thermomechanical tensile stress σ_{0T} becomes

$$\delta = \delta_E + \frac{(\sigma_{0T} \quad s_T)d}{2\eta T} \; ; \quad s_T = 2T\delta_E/d \tag{14}$$

where δ_E remains unaffected by temperature and is still given by equation (3). Composite static tensile strength is determined by first finding fiber stress S_f at failure using equations (2), (12), and (14), and then computing composite failure stress from

$$\sigma_c = \frac{E_c}{E_f}\sigma_{0f} - E_c(\alpha_c - \alpha_f)\Delta T \tag{15}$$

with $\sigma_c = S_c$ and $S_f = \sigma_{0f}$. Following McLaughlin (reference 13), the equation for isothermal fatigue life under constant-amplitude tension-tension cyclic stress is obtained as follows. From equation (13), it can be shown that the cyclic (maximum minus minimum) component of shear-lag shear stress $\Delta \tau(a)$ under isothermal conditions is proportional to the cyclic component of fiber stress $\Delta\sigma_{f0}$. Therefore, the Paris equation (6) for fiber/matrix crack extension and the resulting equation (7) for growth of ineffective length remain unaltered. Fatigue failure occurs when ineffective length (equation (7)) grows and bundle strength given by equation (2) falls to the maximum applied fiber stress σ_{f0max}, resulting in

$$\frac{(\sigma_{f0max})^\beta}{\alpha\beta e} \delta_i = C_\sigma(\Delta\sigma_f 0)^m (N \quad N_i) \tag{16}$$

where δ_i is the ineffective length immediately prior to the inception of cyclic loading and N_i is the cycle number at the beginning of the particular block of cyclic loading defined by σ_{f0max} and $\Delta\sigma_{f0}$.

Two forms of equation (16) are of interest. The first is when the composite is in its virgin state with no prior fiber/matrix interface damage, and the initial ineffective length is due solely to the initial half-cycle of fatigue loading given by equations (12) and (14) with $\sigma_{f0} = \sigma_{f0max}$:

$$\delta_i = \frac{d_f}{2\eta T}(\sigma_{f0max} + E_f\alpha_f\Delta T - s_T) \tag{17}$$

The resulting fatigue life equation in terms of composite stress is, using equation (15) and nondimensionalizing,

$$\frac{(\sigma_{cn} + \sigma_{cnT})^{\beta} - C_s \sigma_{cn} - C_{\delta T}}{\Delta \sigma_{cn}{}^m} = C_N(N \ 1/2) \tag{18}$$

where

$$\sigma_{cn} = \sigma_c / S_c$$

$$\sigma_{cnT} = \frac{E_C}{S_C}\left(\alpha_c - \alpha_f\right)\Delta T$$

$$C_s = \alpha\beta e \frac{d}{2\eta T}\left(\frac{E_f}{E_c}S_c\right)^{\beta+1} \tag{19}$$

$$C_N = \alpha\beta e C_\sigma \left(\frac{E_f}{E_c}S_c\right)^{\beta+m}$$

$$C_\delta T = \alpha\beta e \left[\frac{d}{2\eta T}\left(E_f\alpha_c\Delta T - s_T\right) + \delta_E\right]\left(\frac{E_f}{E_c}S_c\right)^{\beta}$$

The other form of equation (16) occurs when the composite is not in its virgin state due to prior cyclic loading or static stressing to a level above the current cyclic stress. Then δ_i and N_i have predetermined values, and δ_i is not a function of σ_{f0max}. In this case, equation (16) becomes

$$\frac{(\sigma_{cn} + \sigma_{cnT})^{\beta} - C_{\delta i}}{\Delta \sigma_{cn}{}^m} = C_N(N \ N_i) \tag{20}$$

with

$$C_{\delta i} = \delta_i \alpha\beta e \left(\frac{E_f}{E_c}S_c\right)^{\beta} \tag{21}$$

4.3   HEAT DAMAGE IN UNIDIRECTIONAL GRAPHITE/EPOXY COMPOSITES

4.3.1   MATERIAL-RELATED HEAT DAMAGE PROCESSES

In the temperature range from 20°C to 600°C, fiber properties do not change significantly. On the other hand, matrix and fiber/matrix interface properties and those composite properties that they affect will change significantly with temperature. Tests have been carried out by the

authors and others (references 1 through 11) on neat epoxy resin and graphite/epoxy composites showing that:

a. Increasing temperature causes reductions in stiffness and strength properties in epoxies. If the material is heated to a high enough temperature, there will be permanent, residual changes. Tests were performed on Hercules 3501-6 and Fiberite 977-3 neat epoxy resin samples using a Rheometrics RDA II dynamic analyzer. Storage and loss moduli were dynamically measured on a single specimen as temperature increased from 20°C to above 300°C. Figure B-63 shows the temperature variation of shear modulus (normalized to 40°C values) for both resins. Note that the curves are nearly identical. At 300°C, the shear moduli of both resins were negligible and remained so as the samples cooled back down to room temperature. Upon test completion, the samples were observed to be severely cracked and oxidized with significant mass loss.

b. Heat causes damage in the form of micro- and/or macro-cracks to form in the resin, most probably caused by out gassing of water vapor and organic volatiles (Arafat, reference 10). Figure B-64 shows c-scans of 25 x 50 x 4 mm 977-3 neat resin samples subjected to temperatures from 270°C to 330°C for times varying from 5 to 45 min. Greater darkness indicates greater damage. Figure B-65a shows the spallation cracks (about 5-mm across) that typically appear in these samples. Figure B-65b is a photograph of the surface of a laminated woven composite heated to 370°C. The dark "craters" are holes through which gasses escaped from inside the composite after causing the specimen to delaminate.

c. All of these phenomena are magnified with increasing time at temperature and moisture content (see, for example, figure B-64 and Mehrkam, et al., reference 4; Arafat, reference 10; and Tuttle, et al., reference 18).

In order to predict the static strength and fatigue life of a unidirectional composite with a given moisture content, there are three material property issues to address. The first is the variation of properties with temperature as it increases to a given level. These properties will control thermal damage occurring during the heating process. The second is the degradation of properties as the temperature is maintained at a given level. Many studies, including those at NAWCAD Patuxent River on neat resin samples, have shown that greater time at temperature generally produces more damage. Other work shows that mass loss occurs at elevated temperatures and the loss is also time dependent. The third issue is whether the heat has permanently altered material properties at room temperature once the heat has been removed. The altered properties will affect the manner in which damage grows under mechanical loads following the heat exposure. The consideration of temperature dependence, time dependence, and residual effects are all necessary to determine the effects of heat exposure on residual strength and life of the composite.

From a practical standpoint, it will be important to determine the relative importance of the following two main damage mechanisms:

1. Residual fiber/matrix interface damage may be caused during the heating process that could manifest itself as an increased initial ineffective length and, therefore, reduce fatigue life even if there were no residual matrix property alterations. Such damage is practically impossible to detect in the field using current NDE techniques. If it is important, such techniques will need to be developed.

2. Matrix property alterations that are nonreversible upon cool down will clearly affect strength and life. It is necessary to know at which temperatures and for what application times critical reductions in important material stiffness and strength properties occur. Most of the important property variations are due to mass loss and chemical changes, and techniques are under development that may allow surface chemistry changes to be readily detected in the field and thus assist in determining heat damage criticality.

4.3.2 THERMAL DAMAGE EFFECTS FOR A PARTICULAR GRAPHITE/EPOXY SYSTEM

4.3.2.1 General

Test results for T300B, 6000-50B/AralditeLY553 graphite/epoxy from Radhakrishnan (reference 16) are used in conjunction with data from the literature to estimate a consistent set of properties for use in the current analysis to study the relative importance of the mechanisms described above and to quantitatively estimate the effects of thermal history on strength and fatigue life. A presentation is given here of available data and the methods used to estimate unavailable properties. The temperature- and time-dependent properties are then used to determine how much fiber/matrix damage occurs during the heating process. Finally, S/N curves are constructed that result from thermomechanical damage and altered material properties for two heat-application scenarios: a short time of less than 5 min and a long time of greater than 1 hr.

4.3.2.2 Time/Temperature Property Variations

Room-temperature properties of T300B, 6000-50B/Araldite LY553 graphite/epoxy from Radhakrishnan (reference 16) are shown in table A-18. Since the fatigue parameters C_N and m were unavailable, they were calculated from constant-amplitude fatigue data that were presented in his paper by using a least-squares curve fit and procedures outlined in McLaughlin (reference 13), but with the current thermal development and a stress-free temperature of 180°C.

For short heating times of 5 min or less, the variation with temperature of Araldite LY553 epoxy nondimensional shear modulus was assumed to follow that of Fiberite 977-3 since results for the two resins shown in figure B-63 were so close. Matrix Poisson's ratio was assumed not to vary with temperature, and Young's modulus was found from $E_m = 2G_m(1+\nu)$. While it is likely that the epoxy coefficient of thermal expansion will be temperature-dependent, it is likely to be much less so than the elastic constants as long as the material is not significantly chemically altered, and was assumed constant here until above 300°C. Tests on both neat resin systems and graphite/977-3 composites show that at 350°C and higher, the material rapidly ablates or oxidizes, leaving effectively a bundle of dry fibers in the region to which heat is applied.

For long heating times of 60 min or greater, it was also assumed that matrix thermal expansion coefficient and Poisson's ratio are unaffected by temperature until the matrix is destroyed. For shear modulus, it was noted that the resins tested became fluid at a temperature near 300°C and ablated within the hour, leaving a region of dry fibers. Tuttle (reference 18) has shown that significant mass loss (greater than 2%) and a drop of 80% in matrix-dominated composite properties occur when composites are exposed to several hours at 260°C. Arafat (reference 10) found significant mass loss at temperatures of 200°C. Following the data trends in these references and tests performed under the current program, it was assumed for long-time heating above 200°C that epoxy shear modulus suffers additional loss (10% at 210°C, 75% at 250°C, 100% at 300°C), and that any property loss is permanent upon cooling to room temperature. The resulting variation in matrix shear modulus with temperature is shown in table A-19. Note the differences between long- and short-time at-temperature and residual values.

To estimate the temperature variation of fiber/matrix interface properties, it is noted that (see McLaughlin (reference 13)) the energy release rate for fiber pullout is primarily mode II and is proportional to the square of the average shear stress at the crack tip calculated from a shear-lag analysis of fiber pullout. Therefore, the fiber/matrix interface shear stress T at which a crack extends is proportional to the square root of the critical mode II energy release rate G_{IIc} of the fiber/matrix interface. Tuttle (reference 18) found that, following exposure to 260°C, G_{Ic} of graphite/epoxy panels reduced 7% after 15 min, 40% after 45 min, 33% after 1 hr, and 80% after a 10-hr exposure. This is consistent with neat resin tests at NAWCAD Patuxent River that also show a strong time effect and greater matrix cracking and apparent out-gassing effects at higher temperatures. In addition, test data were examined from 11 unidirectional composite material systems and from unpublished data from NAVAIRSYSCOM Structures Division and other sources on the temperature variation of transverse tensile strength, transverse compressive strength, axial shear strength, and interlaminar shear strength. These are all matrix- or fiber/matrix-interface-dominated properties that should have similar variations with temperature as does the shear-lag fracture stress T. The numerical values thus obtained and the results of Tuttle (reference 18) are fairly consistent with the degradation in epoxy shear modulus given above. As a result, T is assumed to decrease proportionately with shear modulus.

An epoxy-matrix composite is cured at a temperature of approximately 180°C. When it is cooled to room temperature, the usually greater thermal expansion coefficient of the matrix will impart radial normal compressive stress to the fiber/matrix interface. Heating the composite will lessen this clamping force until at cure temperature, the radial stress at the interface becomes tensile. This may do several things: the shear stress T at which a crack propagates along the fiber/matrix interface may decrease because of the added mode I loading; and the cracked interface stress ratio η in the cracked region will decrease. As a result, the additional effects of thermal microstresses must be dealt with.

A constant-axial-strain thermal stress analysis was performed on a three-phase composite cylinder model consisting of a fiber surrounded by a ring of matrix, which is in turn surrounded by an infinite cylinder of composite. Temperature-dependent material properties were used. It was found that interface normal stress was significantly reduced with temperature and even became slightly tensile as temperatures increased, but even the highest tensile and compressive stresses were judged too small compared to epoxy fracture properties to affect the interface fracture stress T. The cracked shear stress interface ratio, η, on the other hand, should depend heavily upon radial normal stress. In the absence of other data, it was assumed that η is proportional to the ratio of radial normal compressive stresses at temperature to that at room temperature. Table A-20 shows the results of the analysis.

4.3.2.3   At-Temperature Fiber/Matrix Interface Damage

As previously discussed, it is useful for NDE purposes to know if significant fiber/matrix cracking occurs during the heat application period. It is also a necessary preliminary to determination of residual fatigue life once the heat has been removed. The procedure is to determine, as described in section 2.3, the static fiber failure stress at temperature using temperature-dependent properties and equations (2, 3, 12, and 14). The residual thermal fiber stress at temperature is then found using equation (15) with $\sigma_c = 0$. Initially, fiber stress is compressive due to residual stresses caused during cure. Results for both the short- and long-heat application times showed that the fiber stress at which fiber/matrix interface begins to crack is significantly reduced with increasing temperature. However, by the time temperature rises above the stress-free state and begins to cause fiber axial tensile stress, matrix elastic modulus has decreased to the point where fiber stress is considerably below that required to initiate interface cracking. It is concluded that, for the graphite/epoxy composite material analyzed here, no significant thermal stress-created fiber/matrix interface damage occurs throughout a thermal cycle.

4.3.2.4   Residual (Upon Cool Down) Fatigue Strength Versus Cycles Curves

Since there is no thermomechanically induced fiber/matrix interface damage for either long- or short-heat application times until the matrix is driven off by temperatures above 250°C to 300°C, the appropriate equations for fatigue life are equations (18) and (19). For cyclic stress ratio $R = 0$, S/N curves were calculated that give residual fatigue properties upon cool down from

maximum temperatures ranging from room (no applied heat) to the temperature at which the matrix has been driven off (350°C for short-heat application times and 300°C for long-heat application times). Results are shown in figure B-66. It is important to note that for short-application times, the matrix was assumed to recover to its virgin state with no loss in properties. The resulting short-application time S/N curves will be unchanged from the virgin one until the matrix is gone at 350°C. The long-application time S/N curves will show changes from 100°C reflecting matrix chemical and mechanical changes due to the long time at temperature. Interestingly, at 150°C and below, strength reductions are limited to about 15%. Temperatures above glass transition T_g (about 185°C here) produce a marked and sudden strength decrease: nearly 50% at 200°C, 95% at 250°C. This is not unexpected due to the equivalent drop observed in matrix and fiber/matrix interface properties. In addition, the S/N curves indicate that life of the composite is not strongly affected for cyclic stress levels that are below the level of the heat-degraded static strength.

Finally, it is important to realize that the results presented above pertain to the region of heating only. This is important because in the damaged region, the fibers are *at worst* still continuous, and the strength can be no less than the static strength of a dry fiber bundle of length equal to the size of the damage zone. In fact, above 300°C for short-application times and 250°C for long-application times, there is no matrix inside the damage zone. Outside the zone, however, the matrix is still intact. This creates a scenario in which the initial (static) composite strength is determined by an ineffective length that is equal to the size of the damage zone. Continued cyclic stressing will cause cracks to form at the fiber/matrix interface and grow into the unheated region where matrix properties are intact. This will further increase the ineffective length and decrease residual strength. The effect of the size of the damaged region can be determined by using equations (19, 20, and 21). For illustrative purposes, damage zone (and δ_i) was varied from 15 to 150 mm. Figure B-67 shows that the 150-mm long damage zone causes a drop of nearly 70% in initial static strength, but the fatigue strength remains constant until about 10^{15} cycles where it rejoins the unheated material S/N curve.

4.4 CONCLUSIONS

A model has been developed for strength and fatigue life of unidirectional composite materials in tension that includes thermal as well as mechanical loading. The model is capable of treating any combination of thermal and mechanical stress histories as long as temperature-dependent properties are known. The model has been applied to investigating the damage processes caused in a particular unidirectional graphite/epoxy composite due to the application of heat and maintaining a constant temperature in the composite for short-time (less than 5 min) and long-time (greater than 60 min) scenarios. The following results show that:

1. According to the model developed, while the composite is at temperature, damage in the form of fiber/matrix interface cracking due to thermal stresses probably does not occur for either short- or long-time heat application, and the primary loss in strength and fatigue life is due to matrix shear and fiber/matrix interface degradation with temperature.

2. According to the model, heat application for less than 5 min at 300°C or lower will not have a significant effect on residual matrix properties after cool down to room temperature because matrix mass loss, chemical changes, and cracking do not occur to a significant degree. Maintaining composite temperatures of greater than 150°C for longer than 60 min will cause large reductions in strength due to matrix degradation at temperature. Interestingly, life does not appear to be significantly affected for cyclic stresses below the heat-degraded static strength level.

3. The model predicts that short-time application of heat resulting in temperatures higher than 300°C and long-time heating resulting in temperatures above 250°C will remove the matrix, leaving at best a dry bundle of fibers in the heated zone. Strength and life of the composite in the immediate vicinity of this zone are strongly affected by the size of the zone.

These conclusions are based upon one graphite/epoxy material system for which incomplete at-temperature property data were available and for which many assumptions had to be made. While care must be taken if applying them to other composites with larger fiber volume fractions and stronger interface properties, it appears reasonable that less matrix and a stronger interface will have little effect upon results 1 and 3. However, it is possible that such changes will push the failure mode from cumulative weakening to fiber-break propagation, in which case, the cumulative weakening results would be an upper bound (Zweben, reference 21).

SECTION 5
CONCLUSIONS

Heat damage occurs over a wide variety of temperature ranges in the naval environment. The damage begins when composite structures are exposed to temperatures beginning near the T_g of the material and continues with increasing temperature such as in the case of fire exposure. The time of exposure is critical in determining the amount of damage. At temperatures near the onset of thermal decomposition, the damage becomes so subtle that it becomes very hard to detect using current evaluation techniques. The most critical of these cases is known as incipient heat damage. This is damage that is undetectable using current nondestructive assessment techniques. Higher temperature exposures leave visual clues and delaminations in the structure, but with incipient damage, a composite structure may have reduced strength and life without any indication.

Section 2, MECHANISMS OF LAMINATION PLANE CRACKING, addresses the phenomenon of incipient heat damage. It is observed that at temperatures near the onset of thermal decomposition, longer time exposures cause incipient heat damage. Matrix mass loss is observed as the primary degradation mechanism in the case of incipient damage. When damage is nondestructively detectable, outgassing from volatiles and/or moisture was the degradation mechanism that caused voids and delaminations in a composite. The presence of absorbed moisture in a structure was shown to lower the temperature/time exposure necessary to cause delaminations and void formation.

In Section 3, OUTGASSING OF EPOXIES, the products that are given off during heat damage causing matrix mass loss were shown to occur in two distinct ranges of temperature. The first occurred over the temperature range of 280°C to 340°C. The evolved gases of 8552 resin were identified by FTIR as CO_2, CO, H_2O, and a carbonyl group identified as either acid anhydride or ester. The first stage of decomposition caused up to 8% weight loss in the composite and it is, therefore, during this phase of damage that mechanical properties are reduced. Incipient heat damage was shown to occur near the thermal decomposition temperature (section 2). This first stage begins at the onset of thermal decomposition, therefore, it is in this stage that incipient heat damage occurs. At 340°C, a second stage of thermal decomposition begins and continues for the duration of the decomposition process. The second stage is characterized by the outgassing of COS and $C6H5-OH$. Heat damage can be evaluated by STA/FTIR by correlating the peak heights of the carbonyl group given off during heat damage to exposure temperature. The STA/FTIR technique shows great promise as a means to detect and determine the degree of heat damage in composites. Further studies to develop more extensive calibration curves correlated to mechanical properties are necessary.

An analytical model was developed to aid in predicting heat damage. The model can predict strength and fatigue life of unidirectional composite materials in tension, to include thermal as well as mechanical loading. The model is capable of treating any combination of thermal and mechanical stress histories as long as temperature-dependent properties are known. According

to the model developed, heat application for less than 5 min at 300°C or lower will not have a significant effect on residual matrix properties after cool down to room temperature because matrix mass loss, chemical changes, and cracking do not occur to a significant degree. Maintaining composite temperatures of greater than 150°C for longer than 60 min will cause large reductions in strength due to matrix degradation at temperature. The life of a composite does not appear to be significantly affected for cyclic stresses below the heat-degraded static strength level.

THIS PAGE INTENTIONALLY LEFT BLANK

REFERENCES

1. P. A. Mehrkam, E. Armstrong-Carroll, and R. Cochran, "Fire Damage Assessment of A-6 Composite Wing BuNo 152951", Report No. NAWCADWAR-93058-60, of Sep 1993.

2. F. D. Hardcastle, R. I. Johnson, and R. W. Brotzman, "Evaluation of Heat Damage In Carbon/Epoxy Composites", TPL-2061-Fr, Jun 1994.

3. R. Collins, et al., "NDI for Heat Damaged Advanced Composites", Volumes 1 and 2, Great Lakes Composites Consortium, Feb 1995.

4. Armstrong-Carroll, E., Mehrkam, P. A., and Cochran, R., "Heat Damage Evaluation of Painted Graphite/Epoxy Composites", Conference on Characterization and NDE of Heat Damage in Graphite Epoxy Composites, Organized by the Nondestructive Information Analysis Center (NTIAC) located in Austin, Texas, Apr 1993.

5. L. B. Greszczuk, "Mechanical Properties and Thermal Degradation of Advanced Composites Under Rapid Heating," Defense Nuclear Agency Report No. DNA-TR-85-71-V2, of Jun 1985.

6. M. R. Tant, H. L. N. McManus, and M. E. Rogers, in M. R. Tant, J. W. Connell, and H. L. N. McManus, eds., High-Temperature Properties and Applications of Polymeric Materials, American Chemical Society, Washington, DC, 1995, pp. 10-12.

7. W. W. Wendlandt, Thermal Analysis, 3rd ed., Wiley, New York 1986, pp. 9-86.

8. C. J. Janke, J. D. Muhs et al., "Composite Heat Damage Spectroscopic Analysis," Oak Ridge National Laboratory Report ORNL/ATD-42, Sep 1990.

9. P. A. Mehrkam and E. Armstrong-Carroll, SAMPE International Symposium, 38, 217 (1993).

10. Arafat, E. S., 1995, Rust College, Holly Springs, MS. Personal Communication.

11. Armstrong-Carroll, E., Mehrkam, P. A., and Cochran, R., 1994, A Characterization of Heat Damage in Composites, 12th ASTM Symposium on Composite Materials: Testing and Design.

12. Hahn, H. T., 1979, "Fatigue Behavior and Life Prediction of Composite Laminates," in Composite Materials: Testing and Design (Fifth Conference), ASTM STP 674, S. W. Tsai, Ed., pp. 383-417.

13. McLaughlin, P.V.D., Jr., 1994, Life and Residual Strength of Unidirectional Fiber Composites, in Wetherhold, R. C, ed., *Durability of Composite Materials*, MD Vol. 51, ASME, pp. 59-73.

14. McLaughlin, P. V., and Rosen, B. W., 1974, "Combined Stress Effects Upon Failure of Fiber Composites," TFR/7404/1112, Materials Sciences Corporation, Final Report, Contract N62269-73-0800, Naval Air Development Center, Warminster, PA.

15. Radhakrishnan, K., 1984, "Fatigue and Reliability Evaluation of Unnotched Carbon Epoxy Laminates," *Journal of Composite Materials*, Vol. 18, pp. 21-31.

16. Rosen, B. W., 1965, "Mechanics of Composite Strengthening," in *Fiber Composite Materials*, ASM, Metals Park, OH.

17. Tuttle, M., *et al.*, 1995, Thermo-Mechanics of Structural Composites Under Conditions of Fire Impact, Navy Council on Materials and Structures.

18. Zhou, S. J., and Curtin, W.A, (1995), A Failure of Fiber Composites: A Lattice Green=s Function, *Acta Met.*, Vol. 43, pp. 3093-3104.

19. Zweben, C., 1968, "Tensile Failure Analysis of Fibrous Composites," *AIAA Journal*, Vol. 6, pp. 2325-2331.

20. Zweben, C., 1972, "A Bounding Approach to the Strength of Composite Materials," *Engineering Fracture Mechanics*, Vol. 4, pp. 1-8.

21. Zweben, C., 1974, "Failure Analysis of Unidirectional Fiber Composites under Combined Axial Tension and Shear," *J. of the Mechanics and Physics of Solids*, Vol. 22, pp. 193-215.

22. Zweben, C., and Rosen, B. W., 1970, "A Statistical Theory of Material Strength with Applications to Composite Materials," *J. of the Mechanics and Physics of Solids*, Vol. 18, pp. 189-206.

APPENDIX A
TABLES

Table A-1
SATURATING STATISTICS OF 977-3 NEAT RESIN SAMPLES

Sample	Ambient Weight (g)	Saturated Weight (g)	Weight Gain (g)	% Gain (Ambient)
9-525-05-S	4.3211	4.5005	0.1794	4.15
9-525-20-S	4.3949	4.5790	0.1841	4.19
9-525-45-S	4.4514	4.6374	0.1860	4.18
9-576-05-S	4.3924	4.5896	0.1972	4.49
9-576-05-S	4.3494	4.5280	0.1786	4.11
9-576-05-S	3.4827	3.6265	0.1438	4.13
9-623-05-S	3.8963	4.0566	0.1603	4.11
9-623-20-S	4.2336	4.4078	0.1742	4.11
9-623-45-S	3.8566	4.0157	0.1591	4.13
Avg ==>	4.1532	4.3268	0.1736	4.18

Table A-2
DRYING STATISTICS OF 977-3 NEAT RESIN SAMPLES

Sample	Ambient Weight (g)	Dry Weight (g)	Weight Loss (g)	% Loss (Ambient)
9-525-05-D	3.9869	3.9600	0.0269	0.67
9-525-20-D	3.9321	3.9094	0.0227	0.58
9-525-45-D	4.0273	4.0037	0.0236	0.59
9-576-05-D	3.9002	3.8759	0.0243	0.62
9-576-20-D	3.9001	3.8748	0.0253	0.65
9-576-45-D	4.2966	4.2704	0.0262	0.61
9-623-05-D	4.5908	4.5616	0.0292	0.64
9-623-20-D	4.6132	4.5850	0.0282	0.61
9-623-45-D	3.9541	3.9277	0.0264	0.67
Avg ==>	4.1335	4.1076	0.0259	0.63

APPENDIX A

Table A-3
SATURATING STATISTICS OF UNIDIRECTIONAL COMPOSITE SAMPLES

Sample	Ambient Weight (g)	Saturated Weight (g)	Weight Gain (g)	% Gain (Ambient)
U-525-05-S	3.9877	4.0255	0.0378	0.95
U-525-20-S	4.4007	4.4442	0.0435	0.99
U-525-45-S	4.4032	4.4469	0.0437	0.99
U-576-05-S	4.4036	4.4465	0.0429	0.97
U-576-05-S	4.4537	4.4975	0.0438	0.98
U-576-05-S	4.5609	4.6062	0.0453	0.99
U-623-05-S	4.4258	4.4701	0.0443	1.00
U-623-20-S	4.3643	4.4070	0.0427	0.98
U-623-45-S	4.3976	4.4405	0.0429	0.98
Avg ==>	4.3775	4.4205	0.0430	0.98

Table A-4
DRYING STATISTICS OF UNIDIRECTIONAL COMPOSITE SAMPLES

Sample	Ambient Weight (g)	Dry Weight (g)	Weight Loss (g)	% Loss (Ambient)
U-525-05-D	4.5226	4.5076	0.0150	0.33
U-525-20-D	4.3862	4.3721	0.0141	0.32
U-525-45-D	4.3276	4.3163	0.0113	0.26
U-576-05-D	4.2424	4.2308	0.0116	0.27
U-576-05-D	4.3911	4.3779	0.0132	0.30
U-576-05-D	4.4185	4.4059	0.0126	0.29
U-623-05-D	4.5125	4.4983	0.0142	0.31
U-623-20-D	4.5156	4.5029	0.0127	0.28
U-623-45-D	4.4004	4.3886	0.0118	0.27
Avg ==>	4.4130	4.4000	0.0129	0.29

APPENDIX A

Table A-5
SATURATING STATISTICS OF QUASI-ISOTROPIC COMPOSITE SAMPLES

Sample	Ambient Weight (g)	Saturated Weight (g)	Weight Gain (g)	% Gain (Ambient)
Q-525-05-S	4.6294	4.6688	0.0394	0.85
Q-525-20-S	4.3628	4.3994	0.0366	0.84
Q-525-45-S	4.1261	4.1590	0.0329	0.80
Q-576-05-S	4.6150	4.6547	0.0397	0.86
Q-576-05-S	4.3294	4.3665	0.0371	0.86
Q-576-05-S	4.3034	4.3397	0.0363	0.84
Q-623-05-S	4.2344	4.2693	0.0349	0.82
Q-623-20-S	4.3893	4.4266	0.0373	0.85
Q-623-45-S	4.4021	4.4405	0.0384	0.87
Avg ==>	4.3769	4.4138	0.0370	0.84

Table A-6
DRYING STATISTICS OF QUASI-ISOTROPIC COMPOSITE SAMPLES

Sample	Ambient Weight (g)	Dry Weight (g)	Weight Loss (g)	% Loss (Ambient)
Q-525-05-D	4.4575	4.4415	0.0160	0.36
Q-525-20-D	4.4003	4.3838	0.0165	0.37
Q-525-45-D	4.3629	4.3480	0.0149	0.34
Q-576-05-D	4.5276	4.5126	0.0150	0.33
Q-576-05-D	4.2894	4.2757	0.0137	0.32
Q-576-05-D	4.6505	4.6341	0.0164	0.35
Q-623-05-D	4.3769	4.3633	0.0136	0.31
Q-623-20-D	4.2767	4.2650	0.0117	0.27
Q-623-45-D	4.1944	4.1838	0.0106	0.25
Avg ==>	4.3929	4.3786	0.0143	0.32

APPENDIX A

Table A-7
AVERAGE PERCENT WEIGHT GAIN OR LOSS RESULTING FROM
ENVIRONMENTAL CONDITIONING

Samples	Average Dry Weight Loss (%)	Average Wet Weight Gain (%)
977-3 Neat Resin	0.63	4.18
Unidirectional	0.29	0.98
Quasi-Isotropic	0.32	0.84

Table A-8
COUPON LEVEL IDENTIFICATION OF EXPOSURE CONDITIONS

Sample Set Coupon Label			Exposure Conditions		
977-3 Neat Resin	Unidirectional Laminates	Quasi-Isotropic Laminates	Temperature (°C)	Time (min)	Moisture Condition
9-525-05-S	U-525-05-S	Q-525-05-S	274	5	Saturated
9-525-20-S	U-525-20-S	Q-525-20-S	274	20	Saturated
9-525-45-S	U-525-45-S	Q-525-45-S	274	45	Saturated
9-576-05-S	U-576-05-S	Q-576-05-S	302	5	Saturated
9-576-20-S	U-576-20-S	Q-576-20-S	302	20	Saturated
9-576-45-S	U-576-45-S	Q-576-45-S	302	45	Saturated
9-623-05-S	U-623-05-S	Q-623-05-S	328	5	Saturated
9-623-20-S	U-623-20-S	Q-623-20-S	328	20	Saturated
9-623-45-S	U-623-45-S	Q-623-45-S	328	45	Saturated
9-525-05-D	U-525-05-D	Q-525-05-D	274	5	Dry
9-525-20-D	U-525-20-D	Q-525-20-D	274	20	Dry
9-525-45-D	U-525-45-D	Q-525-45-D	274	45	Dry
9-576-05-D	U-576-05-D	Q-576-05-D	302	5	Dry
9-576-20-D	U-576-20-D	Q-576-20-D	302	20	Dry
9-576-45-D	U-576-45-D	Q-576-45-D	302	45	Dry
9-623-05-D	U-623-05-D	Q-623-05-D	328	5	Dry
9-623-20-D	U-623-20-D	Q-623-20-D	328	20	Dry
9-623-45-D	U-623-45-D	Q-623-45-D	328	45	Dry
9-525-05-A	U-525-05-A	Q-525-05-A	274	5	Ambient
9-525-20-A	U-525-20-A	Q-525-20-A	274	20	Ambient
9-525-45-A	U-525-45-A	Q-525-45-A	274	45	Ambient
9-576-05-A	U-576-05-A	Q-576-05-A	302	5	Ambient
9-576-20-A	U-576-20-A	Q-576-20-A	302	20	Ambient
9-576-45-A	U-576-45-A	Q-576-45-A	302	45	Ambient
9-623-05-A	U-623-05-A	Q-623-05-A	328	5	Ambient
9-623-20-A	U-623-20-A	Q-623-20-A	328	20	Ambient
9-623-45-A	U-623-45-A	Q-623-45-A	328	45	Ambient

APPENDIX A

Table A-9
ONSET OF DECOMPOSITION TEMPERATURE AND THE TEMPERATURE WHERE
THE MAXIMUM RATE OF DECOMPOSITION OCCURS FOR
THE 977-3 NEAT RESIN SAMPLES

Sample	Exposure Time (min)	Exposure Temperature (°C)	Temperature at 5% Weight Loss (°C)	Temperature at Maximum Decomposition Rate (°C)
Undamaged	0	0	379.5	433.8
9-525-05-S	5	274	357.1	420.6
9-525-20-S	20	274	368.3	426.5
9-525-45-S	45	274	386.2	428.6
9-576-05-S	5	302	357.1	424.8
9-576-20-S	20	302	377.2	421.3
9-576-45-S	45	302	393.9	430.1
9-623-05-S	5	329	373.9	428.8
9-623-20-S	20	329	385.0	428.8
9-623-45-S	45	329	390.6	425.7
9-525-05-D	5	274	386.2	436.1
9-525-20-D	20	274	385.0	433.3
9-525-45-D	45	274	388.4	430.5
9-576-05-D	5	302	381.7	429.8
9-576-20-D	20	302	388.4	427.5
9-576-45-D	45	302	395.1	425.3
9-623-05-D	5	329	381.7	413.2
9-623-20-D	20	329	371.6	423.9
9-623-45-D	45	329	358.3	425.2
9-525-05-A	5	274	379.5	417.6
9-525-20-A	20	274	379.5	421.9
9-525-45-A	45	274	381.7	425.5
9-576-05-A	5	302	377.2	410.7
9-576-20-A	20	302	383.9	420.5
9-576-45-A	45	302	397.3	428.1
9-623-05-A	5	329	377.2	424.7
9-623-20-A	20	329	390.6	415.9
9-623-45-A	45	329	363.8	415.9

Table A-10
ONSET OF DECOMPOSITION TEMPERATURE AND THE TEMPERATURE
WHERE THE MAXIMUM RATE OF DECOMPOSITION OCCURS FOR
THE 977-3 UNIDIRECTIONAL SAMPLES

Sample	Exposure Time (min)	Exposure Temperature (°C)	Temperature at 5% Weight Loss (°C)	Temperature at Maximum Decomposition Rate (°C)
Undamaged	0	0	410.7	421.4
U-525-05-S	5	274	413.0	428.2
U-525-20-S	20	274	413.0	428.0
U-525-45-S	45	274	417.4	428.2
U-576-05-S	5	302	410.7	425.9
U-576-20-S	20	302	413.0	422.1
U-576-45-S	45	302	412.9	425.1
U-623-05-S	5	329	410.7	426.1
U-623-20-S	20	329	417.4	422.7
U-623-45-S	45	329	415.2	425.0
U-525-05-D	5	274	408.5	423.7
U-525-20-D	20	274	413.0	424.0
U-525-45-D	45	274	413.0	422.5
U-576-05-D	5	302	410.7	423.0
U-576-20-D	20	302	414.0	421.9
U-576-45-D	45	302	417.4	430.5
U-623-05-D	5	329	415.2	424.7
U-623-20-D	20	329	417.4	422.0
U-623-45-D	45	329	416.3	418.2
U-525-05-A	5	274	410.7	420.5
U-525-20-A	20	274	415.2	425.5
U-525-45-A	45	274	411.8	421.3
U-576-05-A	5	302	409.6	417.7
U-576-20-A	20	302	414.0	423.8
U-576-45-A	45	302	416.3	422.6
U-623-05-A	5	329	413.0	423.9
U-623-20-A	20	329	412.5	422.5
U-623-45-A	45	329	417.4	427.4

Table A-11
ONSET OF DECOMPOSITION TEMPERATURE AND THE TEMPERATURE
WHERE THE MAXIMUM RATE OF DECOMPOSITION OCCURS FOR
THE 977-3 QUASI-ISOTROPIC SAMPLES

Sample	Exposure Time (min)	Exposure Temperature (°C)	Temperature at 5% Weight Loss (°C)	Temperature at Maximum Decomposition Rate (°C)
Undamaged	0	0	414.0	425.6
Q-525-05-S	5	274	415.2	431.0
Q-525-20-S	20	274	413.0	427.4
Q-525-45-S	45	274	418.5	427.8
Q-576-05-S	5	302	411.8	426.2
Q-576-20-S	20	302	413.0	427.0
Q-576-45-S	45	302	417.4	429.4
Q-623-05-S	5	329	413.0	428.5
Q-623-20-S	20	329	417.4	427.3
Q-623-45-S	45	329	419.6	428.9
Q-525-05-D	5	274	416.3	424.8
Q-525-20-D	20	274	415.2	427.9
Q-525-45-D	45	274	415.2	429.2
Q-576-05-D	5	302	416.3	429.6
Q-576-20-D	20	302	416.3	432.5
Q-576-45-D	45	302	413.0	425.1
Q-623-05-D	5	329	413.0	422.6
Q-623-20-D	20	329	417.4	426.6
Q-623-45-D	45	329	419.6	422.0
Q-525-05-A	5	274	410.7	425.9
Q-525-20-A	20	274	415.2	426.8
Q-525-45-A	45	274	420.7	428.2
Q-576-05-A	5	302	413.0	426.2
Q-576-20-A	20	302	415.2	428.3
Q-576-45-A	45	302	417.4	420.3
Q-623-05-A	5	329	413.0	426.2
Q-623-20-A	20	329	415.2	424.4
Q-623-45-A	45	329	409.6	422.5

APPENDIX A

Table A-12
FLEXURAL TEST RESULTS FOR THE 977-3 NEAT RESIN SAMPLES

977-3 Neat Resin (Four-Point Flex, ASTM D-790)							
Temp (°F)	Time (min)	Moisture Condition	Width (b) (in.)	Depth (d) (in.)	Length (l) (in.)	Peak Load (lb)	Flex Strength (KSI)
0	0	Ambient	0.421	0.109	1.600	25.49	12.338
525	5	Saturated	1.024	0.102	1.600	135.25	30.468
525	20	Saturated	1.019	0.101	1.600	26.08	6.021
525	45	Saturated	1.013	0.104	1.600	37.65	8.247
575	5	Saturated	1.025	0.107	1.600	100.76	20.607
575	20	Saturated	0.973	0.108	1.600	24.82	5.249
575	45	Saturated	0.960	0.092	1.600	7.36	2.174
625	5	Saturated	0.964	0.099	1.600	10.52	2.672
625	20	Saturated	0.980	0.111	1.600	13.88	2.759
625	45	Saturated	Samples Crumbled Upon Cooling				
525	5	Dry	0.983	0.098	1.600	84.56	21.497
525	20	Dry	0.956	0.100	1.600	130.42	32.741
525	45	Dry	0.964	0.100	1.600	82.88	20.634
575	5	Dry	0.959	0.102	1.600	120.95	29.094
575	20	Dry	0.961	0.096	1.600	21.67	5.872
575	45	Dry	0.952	0.108	1.600	15.99	3.456
625	5	Dry	0.978	0.112	1.600	176.48	34.525
625	20	Dry	Samples Crumbled Upon Cooling				
625	45	Dry	Therefore Nontestable				
525	5	Ambient	1.001	0.099	1.600	144.72	35.403
525	20	Ambient	0.990	0.116	1.600	177.11	31.908
525	45	Ambient	0.986	0.117	1.600	140.93	25.059
575	5	Ambient	1.009	0.100	1.600	157.76	37.525
575	20	Ambient	1.009	0.105	1.600	29.24	6.308
575	45	Ambient	1.009	0.105	1.600	12.62	2.723
625	5	Ambient	0.994	0.109	1.600	186.16	37.832
625	20	Ambient	Samples Crumbled Upon Cooling				
625	45	Ambient	Therefore Nontestable				

APPENDIX A

Table A-13
FLEXURAL TEST RESULTS FOR THE IM6/977-3 UNIDIRECTIONAL SAMPLES

Unidirectional (Four-Point Flex, ASTM D-790)							
Temp (°F)	Time (Min)	Moisture Condition	Width (b) (in.)	Depth (d) (in.)	Length (l) (in.)	Peak Load (lb)	Flex Strength (KSI)
0	0	Ambient	1.003	0.089	1.600	1,003.89	303.261
525	5	Saturated	1.004	0.084	1.600	918.09	311.031
525	20	Saturated	1.002	0.089	1.600	795.69	240.607
525	45	Saturated	0.997	0.089	1.600	549.21	166.907
575	5	Saturated	1.005	0.090	1.600	875.6	258.146
575	20	Saturated	0.994	0.091	1.600	553.21	161.299
575	45	Saturated	0.996	0.092	1.600	528.39	150.429
625	5	Saturated	1.000	0.090	1.600	428.08	126.839
625	20	Saturated	0.989	0.090	1.600	497.06	148.915
625	45	Saturated	0.993	0.109	1.600	63.83	12.985
525	5	Dry	0.999	0.091	1.600	1,002.84	**Test Abort**
525	20	Dry	0.981	0.090	1.600	986.65	298.003
525	45	Dry	0.996	0.087	1.600	961.83	306.205
575	5	Dry	1.000	0.085	1.600	1,001.58	**Test Abort**
575	20	Dry	0.997	0.089	1.600	623.66	189.533
575	45	Dry	0.987	0.091	1.600	646.16	189.737
625	5	Dry	0.993	0.092	1.600	1,004.52	**Test Abort**
625	20	Dry	0.999	0.091	1.600	497.48	144.324
625	45	Dry	0.988	0.089	1.600	328.18	100.644
525	5	Ambient	0.998	0.089	1.600	1,002.84	**Test Abort**
525	20	Ambient	0.972	0.089	1.600	1,000.11	**Test Abort**
525	45	Ambient	0.985	0.087	1.600	951.31	306.238
575	5	Ambient	0.999	0.089	1.600	1,004.73	**Test Abort**
575	20	Ambient	0.988	0.092	1.600	584.96	167.882
575	45	Ambient	0.988	0.090	1.600	570.66	171.138
625	5	Ambient	0.988	0.090	1.600	1,002.21	**Test Abort**
625	20	Ambient	0.990	0.091	1.600	483.81	141.634
625	45	Ambient	0.990	0.101	1.600	105.68	25.115

Table A-14
FLEXURAL TEST RESULTS FOR THE IM6/977-3 QUASI-ISOTROPIC SAMPLES

Quasi-Isotropic (Four-Point Flex, ASTM D-790)							
Temp (°F)	Time (min)	Moisture Condition	Width (b) (in.)	Depth (d) (in.)	Length (l) (in.)	Peak Load (lb)	Flex Strength (KSI)
0	0	Ambient	0.976	0.089	1.600	626.63	194.533
525	5	Saturated	0.999	0.089	1.600	666.35	202.101
525	20	Saturated	0.983	0.087	1.600	294.11	94.870
525	45	Saturated	0.983	0.083	1.600	267.61	94.843
575	5	Saturated	1.001	0.088	1.600	343.32	106.295
575	20	Saturated	0.989	0.087	1.600	214.62	68.809
575	45	Saturated	0.981	0.086	1.600	229.97	76.071
625	5	Saturated	0.991	0.086	1.600	217.35	71.171
625	20	Saturated	0.985	0.088	1.600	248.05	78.046
625	45	Saturated	0.971	0.092	1.600	60.04	17.533
525	5	Dry	0.981	0.089	1.600	628.94	194.255
525	20	Dry	0.982	0.088	1.600	540.81	170.679
525	45	Dry	0.987	0.088	1.600	383.47	120.409
575	5	Dry	0.994	0.088	1.600	740.85	230.988
575	20	Dry	0.992	0.086	1.600	287.76	94.131
575	45	Dry	1.000	0.088	1.600	305.22	94.593
625	5	Dry	0.997	0.084	1.600	517.67	176.608
625	20	Dry	0.989	0.085	1.600	248.84	83.579
625	45	Dry	0.991	0.084	1.600	110.43	37.902
525	5	Ambient	0.999	0.086	1.600	674.17	218.987
525	20	Ambient	0.994	0.087	1.600	523.98	167.148
525	45	Ambient	0.988	0.088	1.600	363.06	113.885
575	5	Ambient	0.999	0.089	1.600	684.27	207.536
575	20	Ambient	0.998	0.088	1.600	316.58	98.310
575	45	Ambient	0.981	0.088	1.600	249.89	78.945
625	5	Ambient	0.987	0.088	1.600	616.74	193.656
625	20	Ambient	0.985	0.090	1.600	227.6	68.464
625	45	Ambient	1.000	0.084	1.600	89.61	30.480

Table A-15
IR VIBRATIONAL FREQUENCIES OF 8552 OUTGASSED PRODUCTS

Compound	Symbol	Vibrational Frequency (cm^{-1})
Carbon Dioxide	CO_2	672, 2,307, 2,372, 3,729
Carbon Monoxide	CO	2,189, 2,254
Water	H_2O	1,337, 1,379, 1,505, 1,596
Acid Anhydride	R-CO-O-CO-R	752, 1,170, 1,721, 1,759, 1,794, 2,942
Carbonyl Sulfide	COS	866, 2,045, 2,068
Phenol	C6H5OH	1,250, 1,486, 1,623, 3,011, 3,383

Table A-16
RAW STA DATA FOR UNDAMAGED 8552 COMPOSITES

Samples Were Undamaged Prior to Testing				
Isothermal Temperature (°C)	Sample Weight (mg)	Weight Loss at 1 Hr	Peak Height/mg (Carbonyl)	Peak Height/mg (CO_2)
290	17.40	2.00	1.09	0.70
290	15.70	2.25	1.58	0.83
Average ==>	**16.55**	**2.13**	**1.34**	**0.76**
300	16.20	3.48	1.97	1.44
300	16.30	3.32	1.73	1.57
300	12.20	4.01	1.71	1.62
Average ==>	**14.90**	**3.60**	**1.80**	**1.54**
310	13.50	4.35	2.64	2.08
310	12.50	4.83	2.50	2.27
310	14.70	4.18	2.40	1.51
Average ==>	**13.57**	**4.45**	**2.52**	**1.95**
320	14.10	5.62	3.21	3.06
320	16.10	5.89	3.39	2.53
320	12.80	5.92	3.32	3.01
Average ==>	**14.33**	**5.81**	**3.31**	**2.87**
330	17.10	7.58	3.76	3.87
330	15.80	8.09	4.26	3.28
330	14.30	7.96	4.74	3.54
Average ==>	**15.73**	**7.88**	**4.25**	**3.56**
340	17.00	9.99	5.07	4.38
340	12.80	10.15	6.24	5.73
Average ==>	**14.90**	**10.07**	**5.66**	**5.06**
350	15.20	12.31	7.11	7.17
350	12.90	12.18	6.59	7.32
Average ==>	**14.05**	**12.25**	**6.85**	**7.24**
360	15.30	13.82	7.97	9.74
360	15.10	13.71	7.78	8.83
Average ==>	**15.20**	**13.77**	**7.88**	**9.28**
370	15.90	16.37	9.13	11.33
Average ==>	**15.90**	**16.37**	**9.13**	**11.33**

APPENDIX A

Table A-17
RAW STA DATA FOR PREDAMAGED 8552 COMPOSITES

Samples Were Predamaged at 315°C Prior to Testing				
Damage Time (min)	Sample Weight (mg)	Weight Loss at 1 Hr	Peak Height/mg (Carbonyl)	Peak Height/mg (CO_2)
5	15.20	7.90	3.98	2.98
5	13.10	8.47	3.86	3.17
Average ==>	**14.15**	**8.19**	**3.92**	**3.07**
20	13.70	7.47	3.41	3.61
20	13.10	7.22	3.66	3.62
Average ==>	**13.40**	**7.35**	**3.53**	**3.61**
45	13.10	6.97	3.07	3.50
45	14.60	7.03	2.76	3.34
Average ==>	**13.85**	**7.00**	**2.91**	**3.42**

Table A-18
PROPERTIES OF GRAPHITE FIBERS IN EPOXY

Fiber Axial Modulus, E_f	177 GPa[1]
Fiber Transverse Modulus, E_{2f}	25 GPa[2]
Fiber Axial Thermal Expansion Coefficient, α_f	-0.5×10^{-6} °C^{-1}[3]
Fiber Transverse Thermal Expansion Coefficient, α_{2f}	30×10^{-6} °C^{-1}[2]
Fiber Volume Fraction, v_f	0.35[1]
Fiber Diameter, d	0.0035 mm[3]
Weibull Fiber Parameter, α	6.89×10^{-9} MPa$^{-1.961}$ mm^{-1}[4]
Weibull Fiber Parameter, β	1.961[4]
Matrix Shear Modulus, G_m	0.7 GPa[1]
Matrix Poisson's Ratio, v_m	0.35[2]
Matrix Thermal Expansion Coefficient, αm	65×10^{-6} °C^{-1}[1]
Fiber-Matrix Interface Shear Strength, T	10 MPa[1]
Postfailure Shear Stress Fraction, η	0.035[1]
Fatigue Crack Propagation Exponent, m	22.5[1]
Fatigue Crack Propagation Constant, C_N	3.9×10^{-4} cycles^{-1}[1]

NOTES: (1) Reference 16 (and micromechanics).
(2) Estimate.
(3) THORNEL Brochure.
(4) Reference 13.

APPENDIX A

Table A-19
DEGRADED EPOXY SHEAR MODULUS FOR
TWO-HEAT EXPOSURE HISTORIES

Temperature (°C)	Matrix Shear Modulus, G_m, MPa			
	Short-Time Exposure		Long-Time Exposure	
	At Temperature	Resid (Cool)	At Temperature	Resid (Cool)
20	700	700	700	700
100	607	700	607	607
150	568	700	568	568
200	301	700	301	301
250	23	700	6	6
300	23	700	0	0
350	0	0	0	0

Table A-20
CRACKED INTERFACE SHEAR STRESS RATIO FOR
TWO-HEAT EXPOSURE HISTORIES

Temperature (°C)	Cracked Interface Dhear Stress Ratio, η			
	Short-Time Exposure		Long-Time Exposure	
	At Temperature	Resid (Cool)	At Temperature	Resid (Cool)
20	0.0346	0.0346	0.0346	0.0346
100	0.0150	0.0346	0.0150	0.0299
150	0.0056	0.0346	0.0056	0.0281
200	0	0.0346	0	0.0150
250	0	0.0346	0	0.0003
300	0	0.0346	0	0
350	0	0	0	0

APPENDIX B
FIGURES

977-3 Neat Resin
Moisture Conditioning Averages
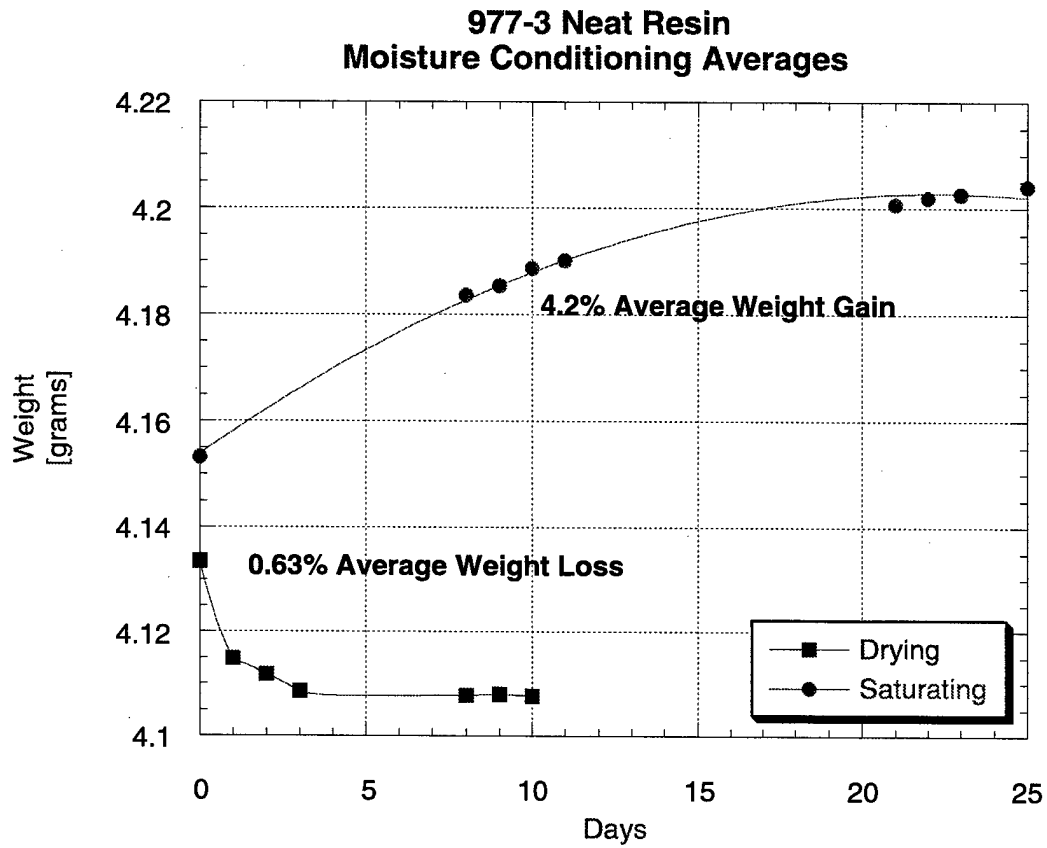
Figure B-1
ENVIRONMENTAL CONDITIONING RESULTS FOR THE 977-3 NEAT RESIN
SAMPLES SHOWING THE AVERAGE WEIGHT GAIN AND LOSS DURING
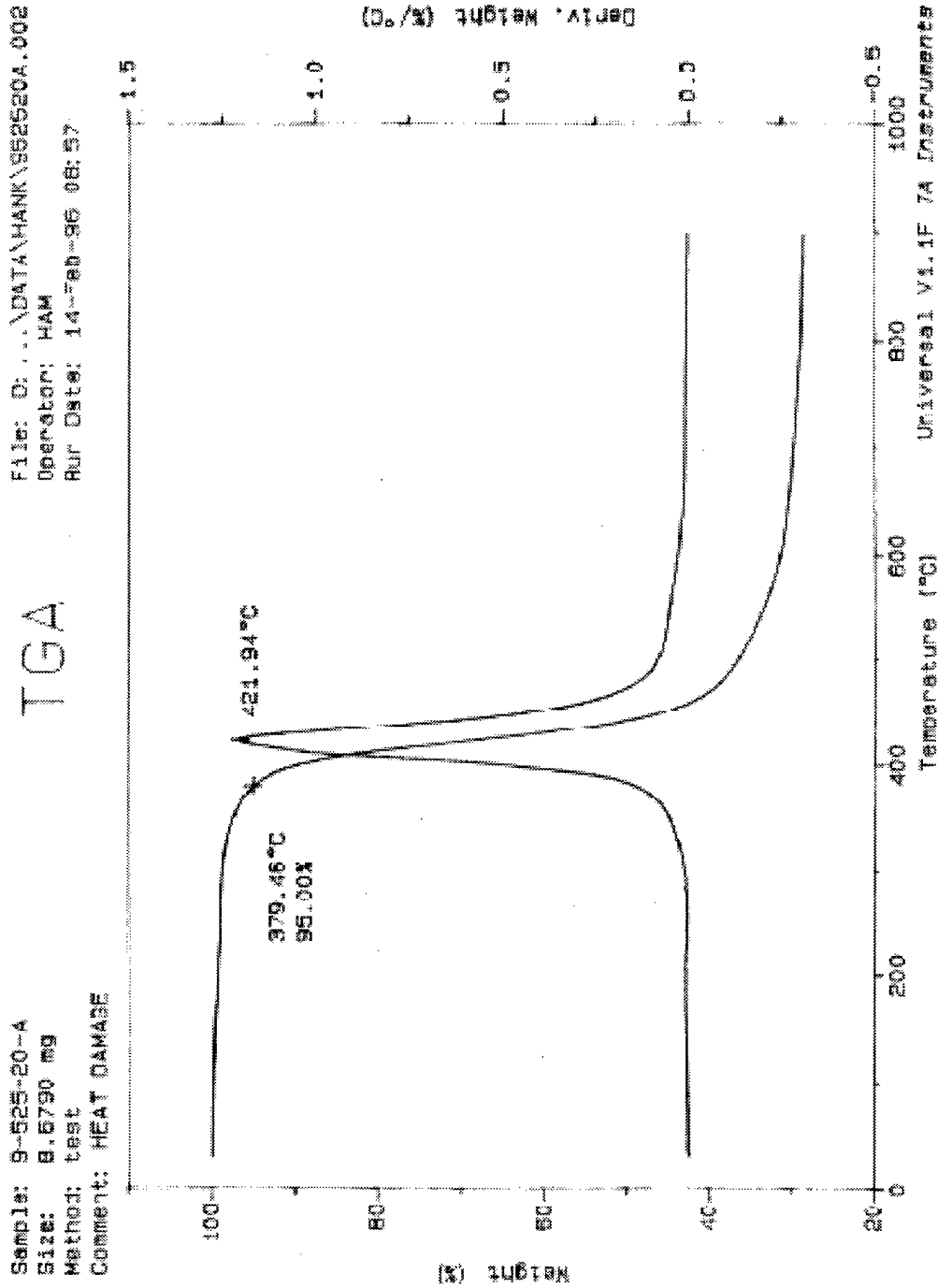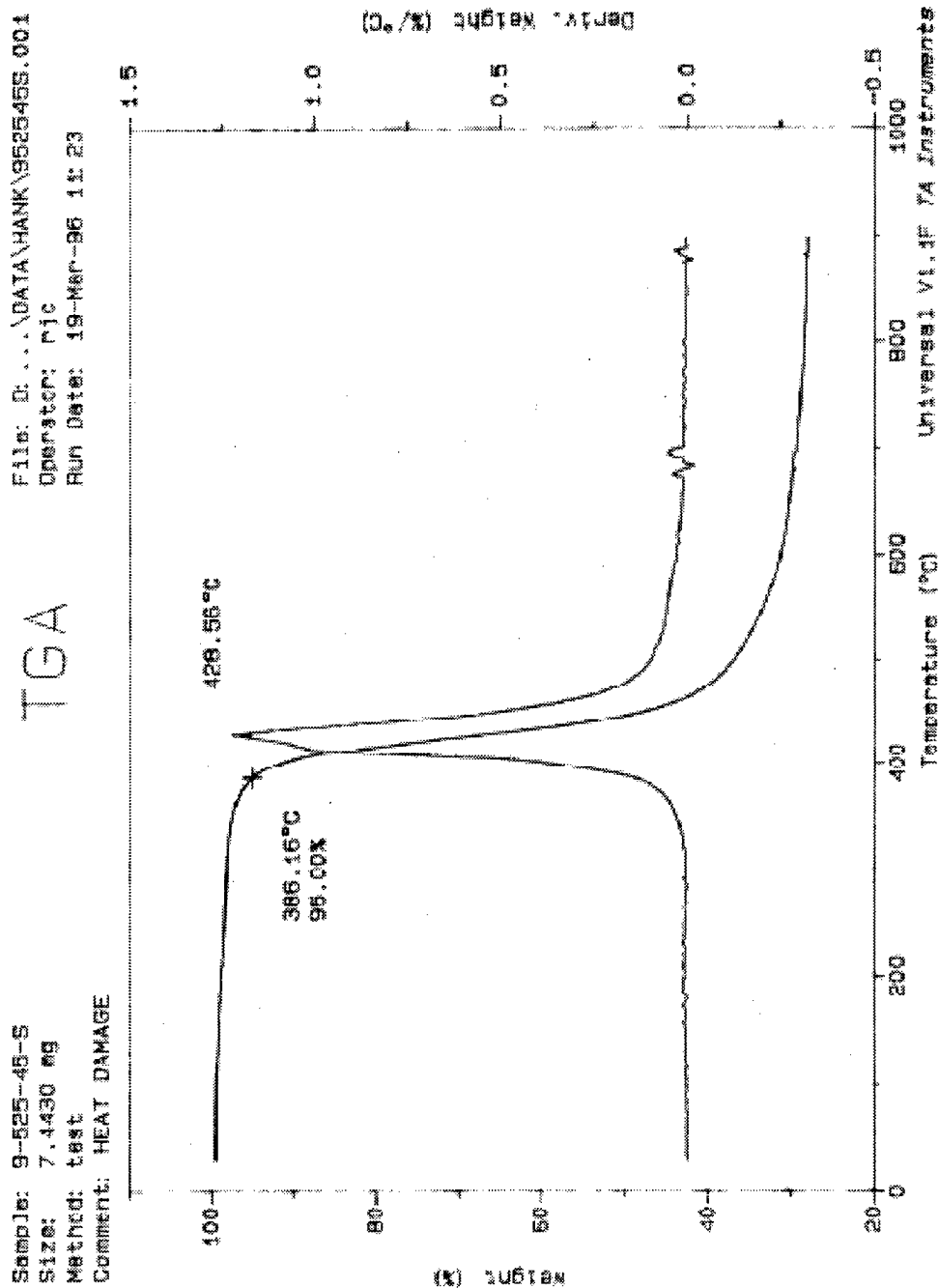THE DAYS OF THE CONDITIONING

APPENDIX B
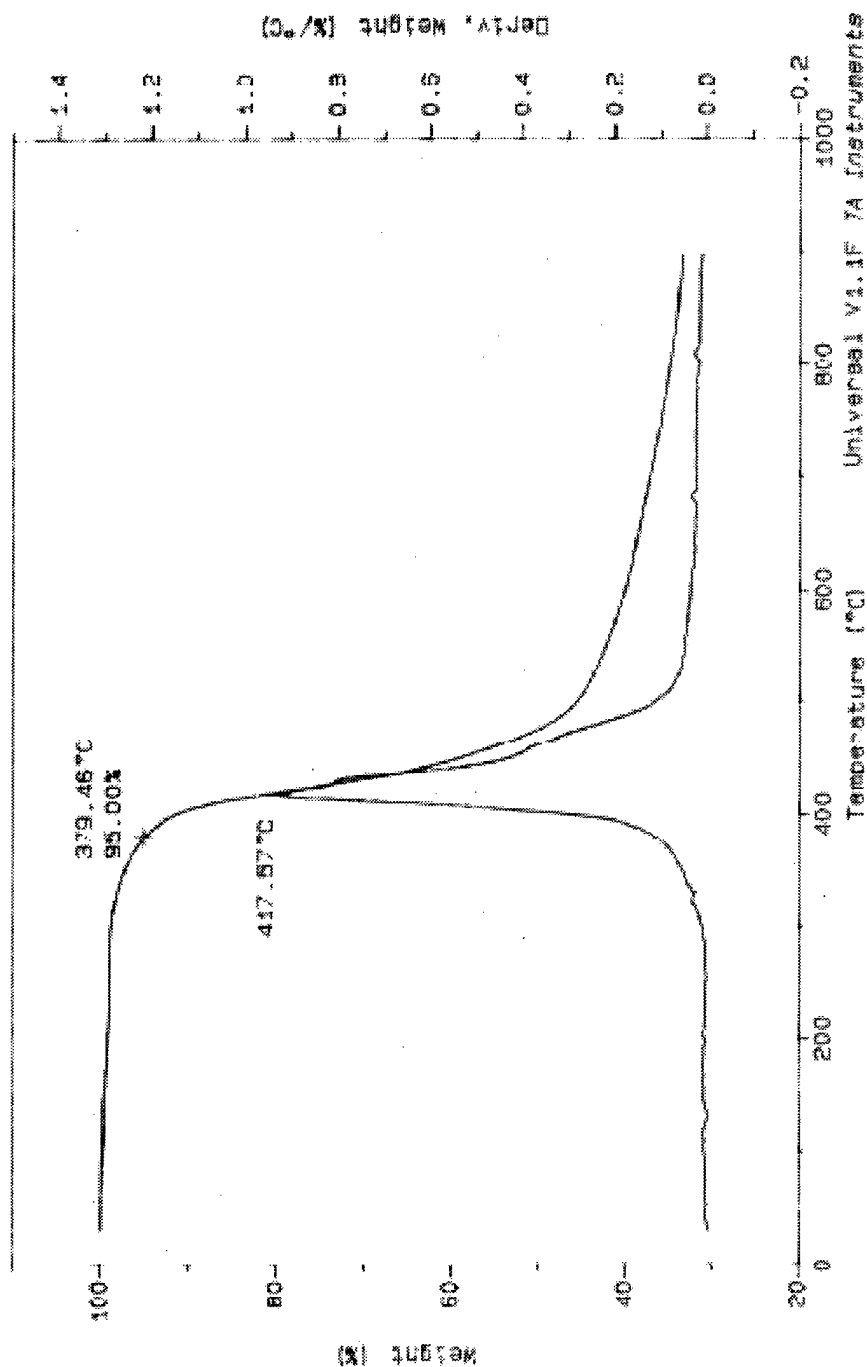
Figure B-2
TGA RESULTS SHOWING WEIGHT LOSS VERSUS TEMPERATURE OF THE 977-3
NEAT RESIN SATURATED SAMPLE THAT WAS HEAT DAMAGED AT 274°C FOR 5 MIN

APPENDIX B
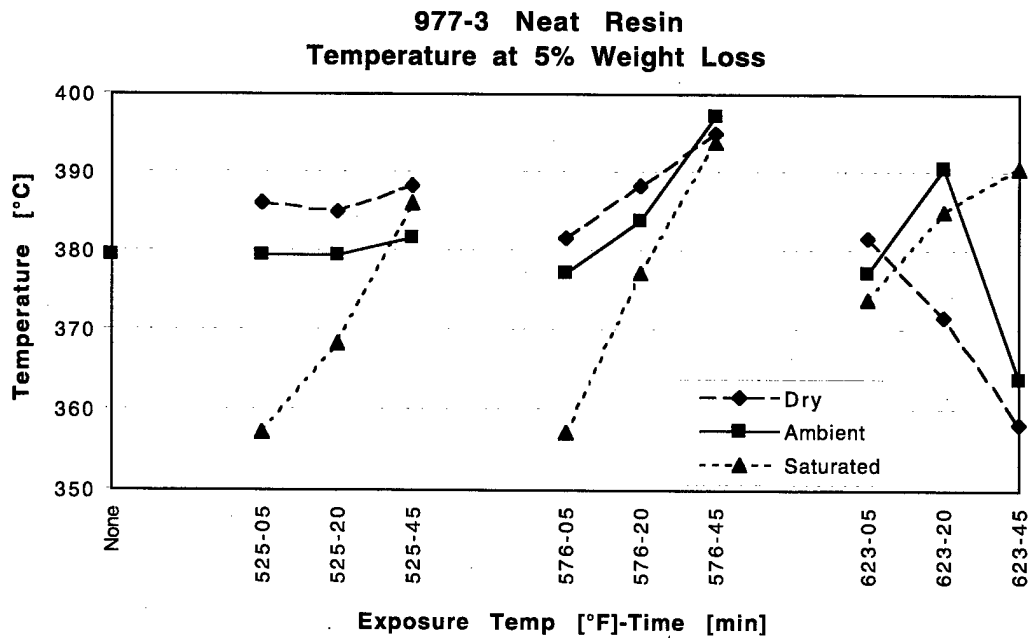
Figure B-3
COMPARISON OF THE ONSET TEMPERATURE OF DECOMPOSITION FOR
THE 977-3 NEAT RESIN SAMPLES GROUPED BY TEMPERATURE EXPOSURE
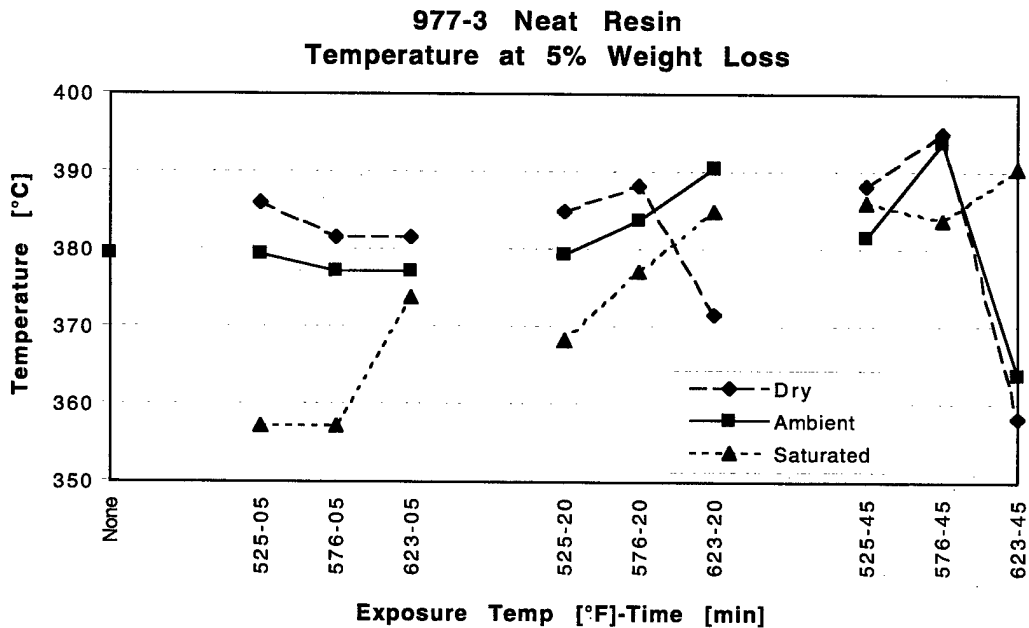
Figure B-4
COMPARISON OF THE ONSET TEMPERATURE OF DECOMPOSITION FOR
THE 977-3 NEAT RESIN SAMPLES GROUPED BY TIME EXPOSURE

52   APPENDIX B
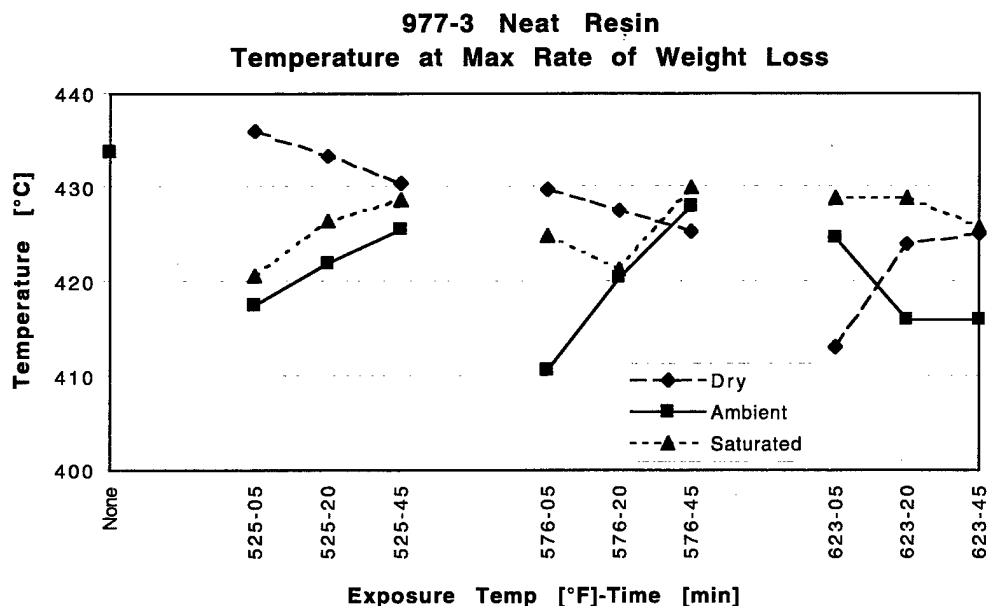
Figure B-5
COMPARISON OF THE TEMPERATURE AT WHICH THE MAXIMUM RATE
OF WEIGHT LOSS OCCURS FOR THE 977-3 NEAT RESIN SAMPLES GROUPED
BY TEMPERATURE EXPOSURE
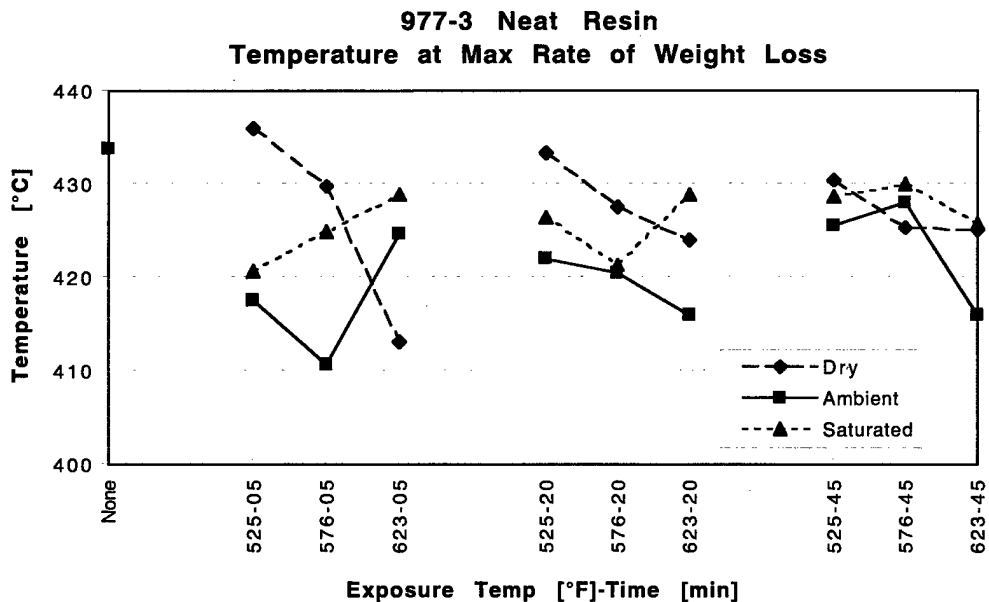
Figure B-6
COMPARISON OF THE TEMPERATURE AT WHICH THE MAXIMUM RATE
OF WEIGHT LOSS OCCURS FOR THE 977-3 NEAT RESIN SAMPLES GROUPED
BY TIME EXPOSURE

53   APPENDIX B
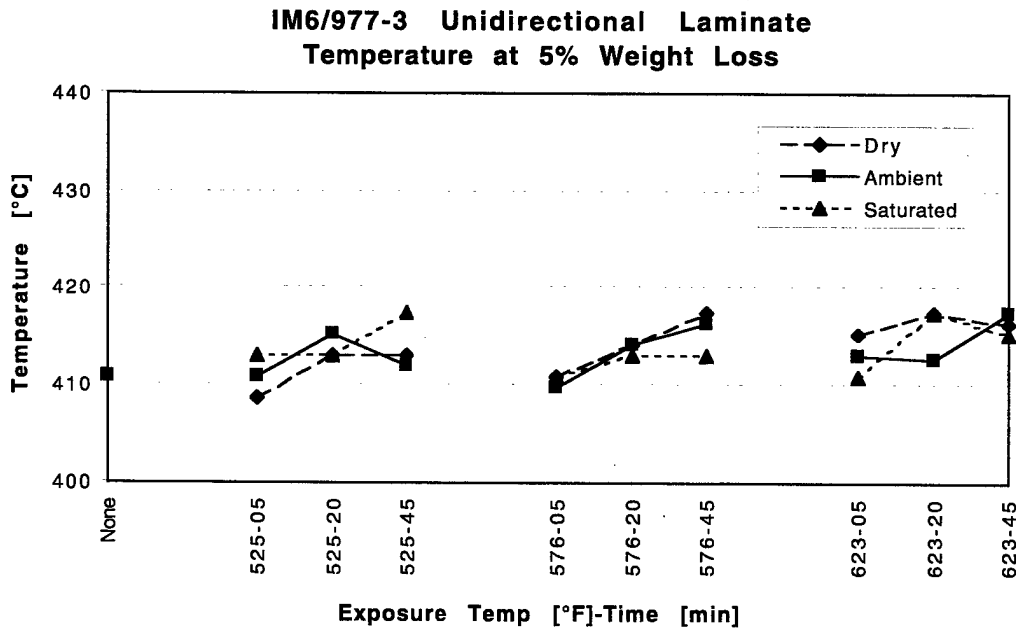
Figure B-7
COMPARISON OF THE ONSET TEMPERATURE OF DECOMPOSITION FOR THE
UNIDIRECTIONAL LAMINATE SAMPLES GROUPED BY TEMPERATURE EXPOSURE
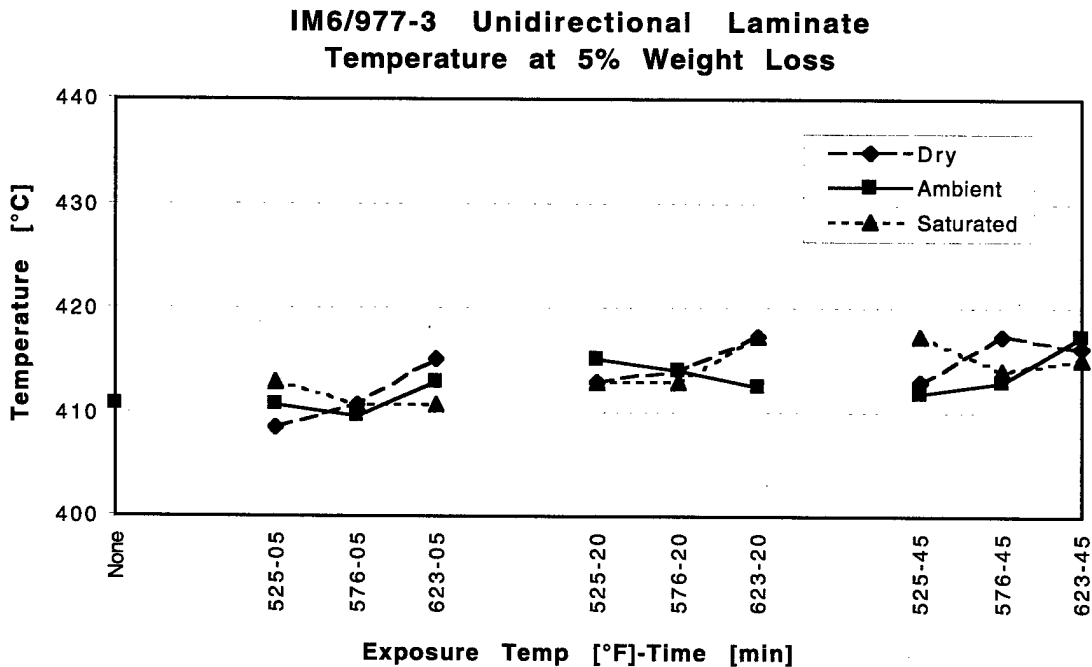
Figure B-8
COMPARISON OF THE ONSET TEMPERATURE OF DECOMPOSITION FOR THE
UNIDIRECTIONAL LAMINATE SAMPLES GROUPED BY TIME EXPOSURE

54   APPENDIX B
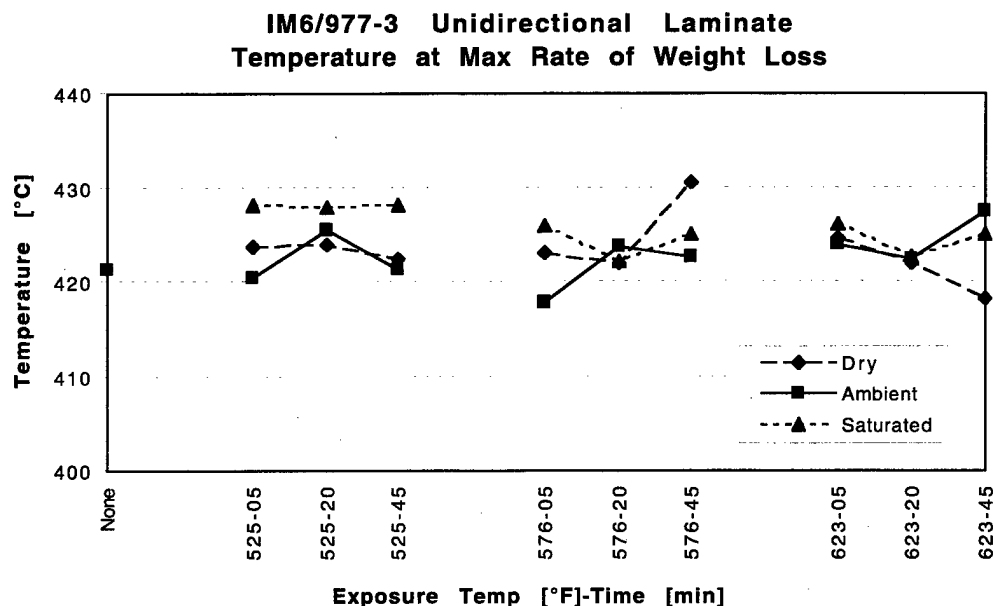
Figure B-9
COMPARISON OF THE TEMPERATURE AT WHICH THE MAXIMUM RATE OF
WEIGHT LOSS OCCURS FOR THE UNIDIRECTIONAL LAMINATE SAMPLES
GROUPED BY TEMPERATURE EXPOSURE
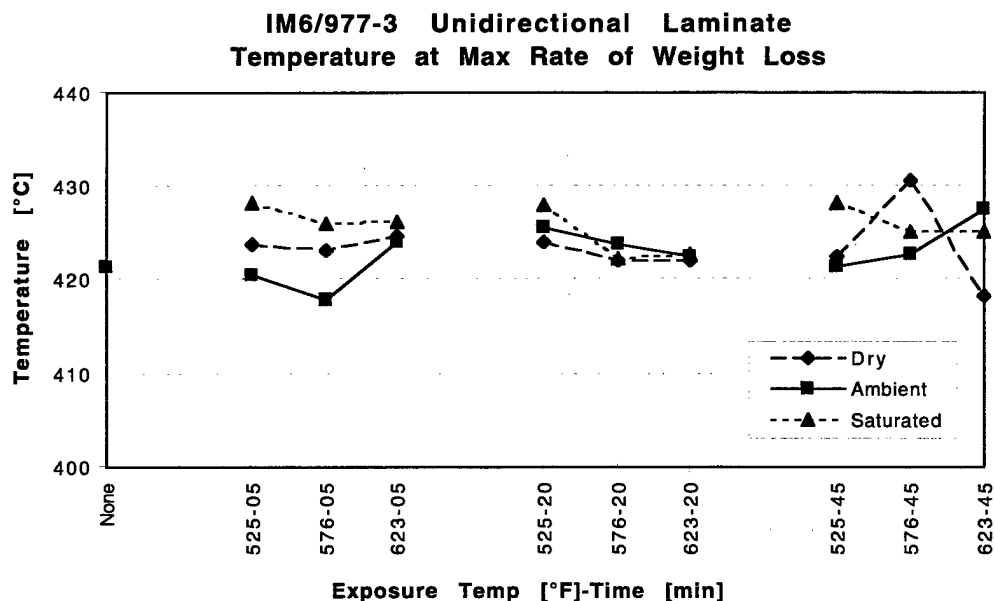
Figure B-10
COMPARISON OF THE TEMPERATURE AT WHICH THE MAXIMUM RATE OF
WEIGHT LOSS OCCURS FOR THE UNIDIRECTIONAL LAMINATE SAMPLES
GROUPED BY TIME EXPOSURE
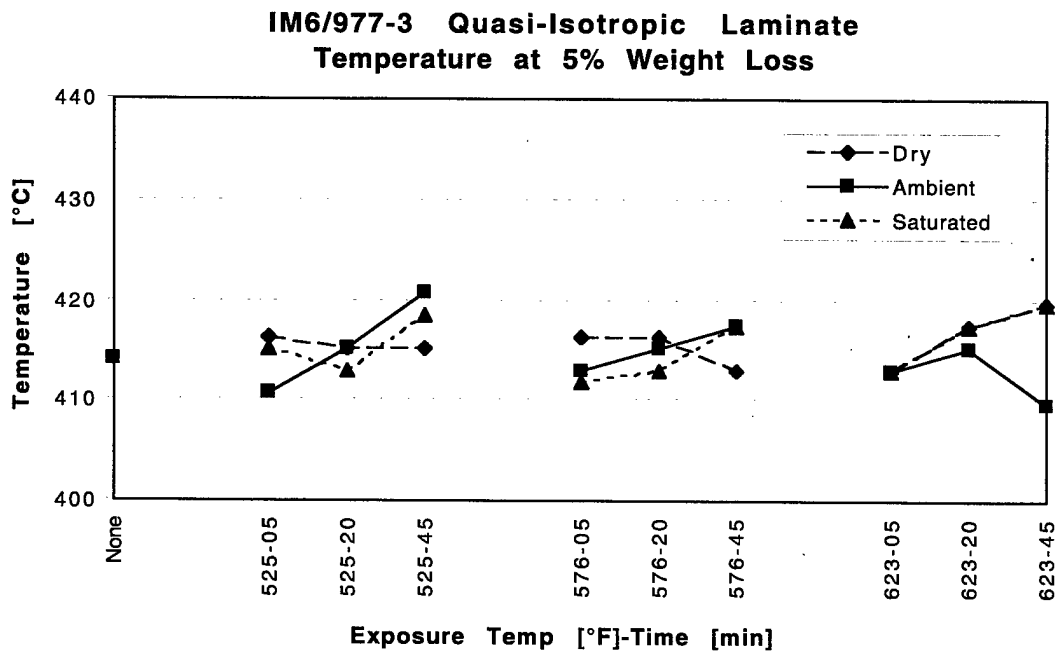
Figure B-11
COMPARISON OF THE ONSET TEMPERATURE OF DECOMPOSITION FOR THE
QUASI-ISOTROPIC LAMINATE SAMPLES GROUPED BY TEMPERATURE EXPOSURE
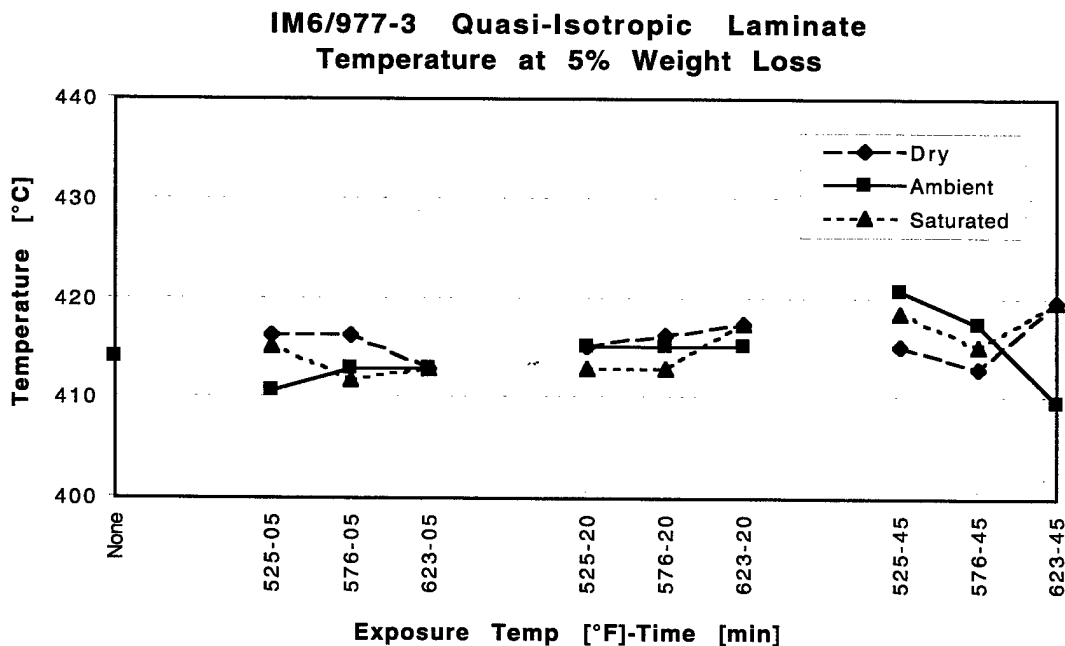
Figure B-12
COMPARISON OF THE ONSET TEMPERATURE OF DECOMPOSITION FOR THE
QUASI-ISOTROPIC LAMINATE SAMPLES GROUPED BY TIME EXPOSURE
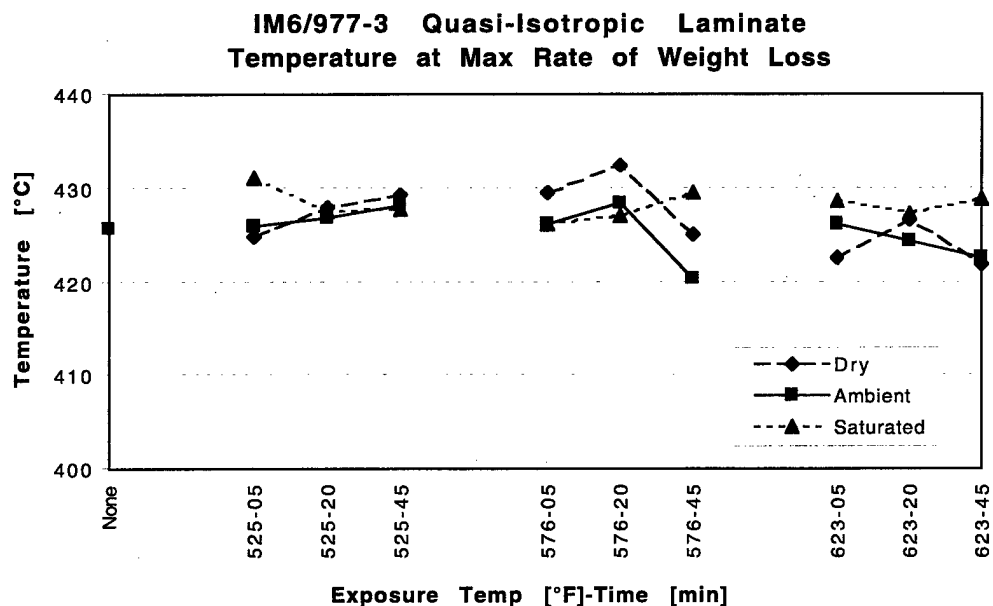
Figure B-13
COMPARISON OF THE TEMPERATURE AT WHICH THE MAXIMUM RATE OF
WEIGHT LOSS OCCURS FOR THE QUASI-ISOTROPIC LAMINATE SAMPLES
GROUPED BY TEMPERATURE EXPOSURE
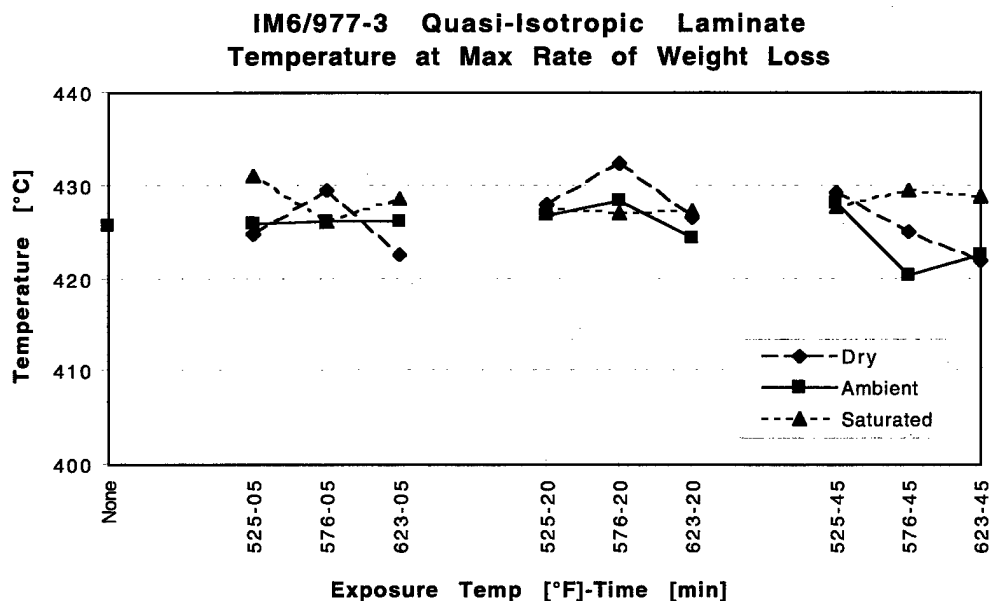
Figure B-14
COMPARISON OF THE TEMPERATURE AT WHICH THE MAXIMUM RATE OF
WEIGHT LOSS OCCURS FOR THE QUASI-ISOTROPIC LAMINATE SAMPLES
GROUPED BY TIME EXPOSURE
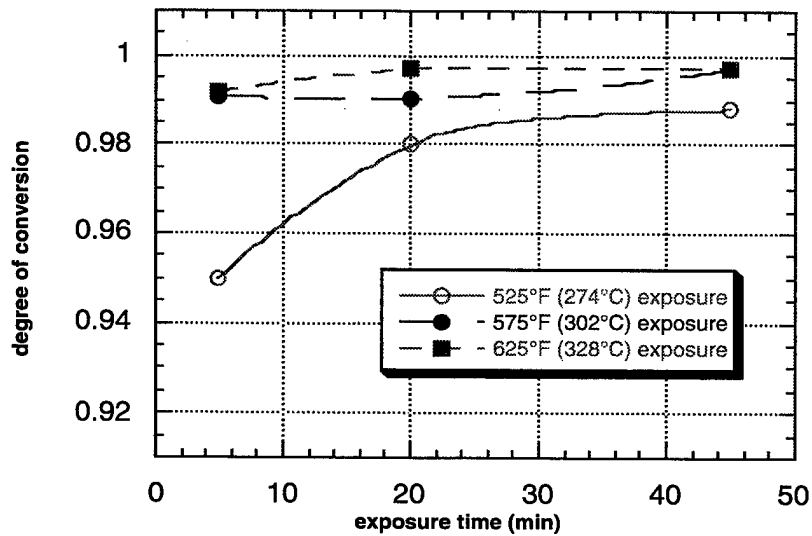
Figure B-15
DEGREE OF CONVERSION VALUES FOR THE 977-3 NEAT RESIN SAMPLES
DRIED PRIOR TO HEAT DAMAGE
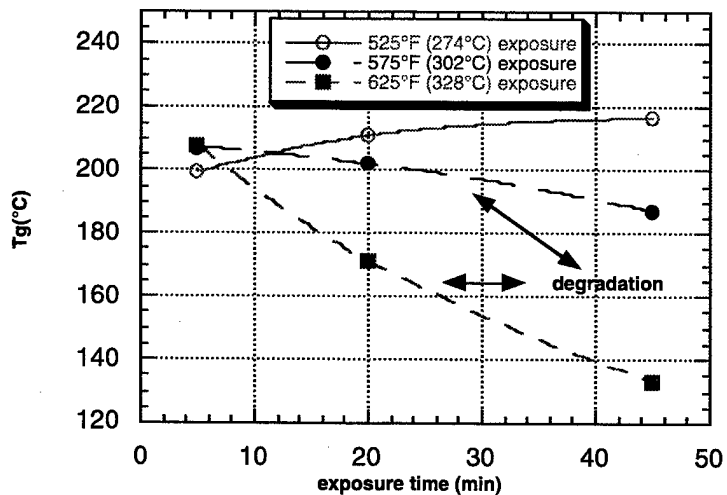
Figure B-16
GLASS TRANSITION MEASUREMENTS FOR THE 977-3 NEAT RESIN SAMPLES
DRIED PRIOR TO HEAT DAMAGE

58   APPENDIX B
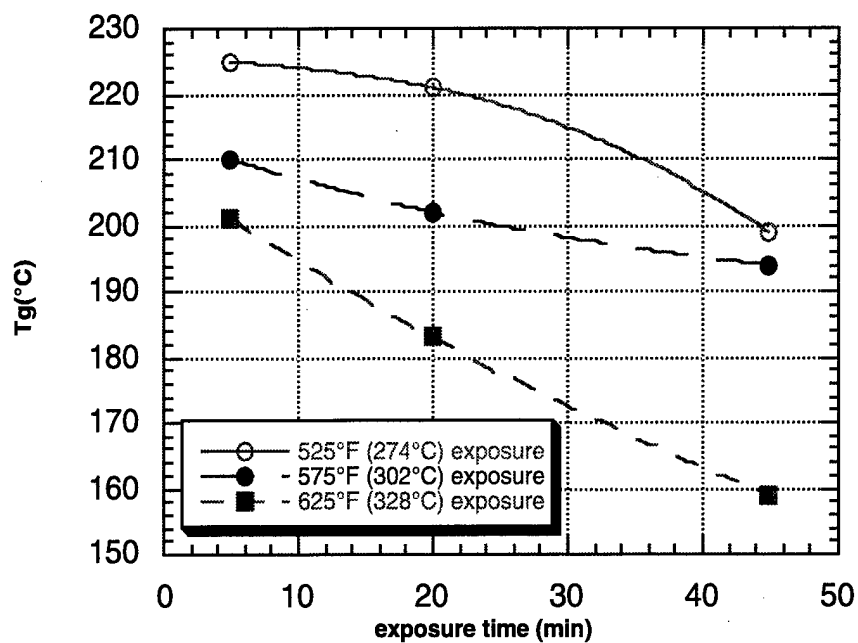
Figure B-17
GLASS TRANSITION MEASUREMENTS FOR THE 977-3 NEAT RESIN SAMPLES
SATURATED PRIOR TO HEAT DAMAGE
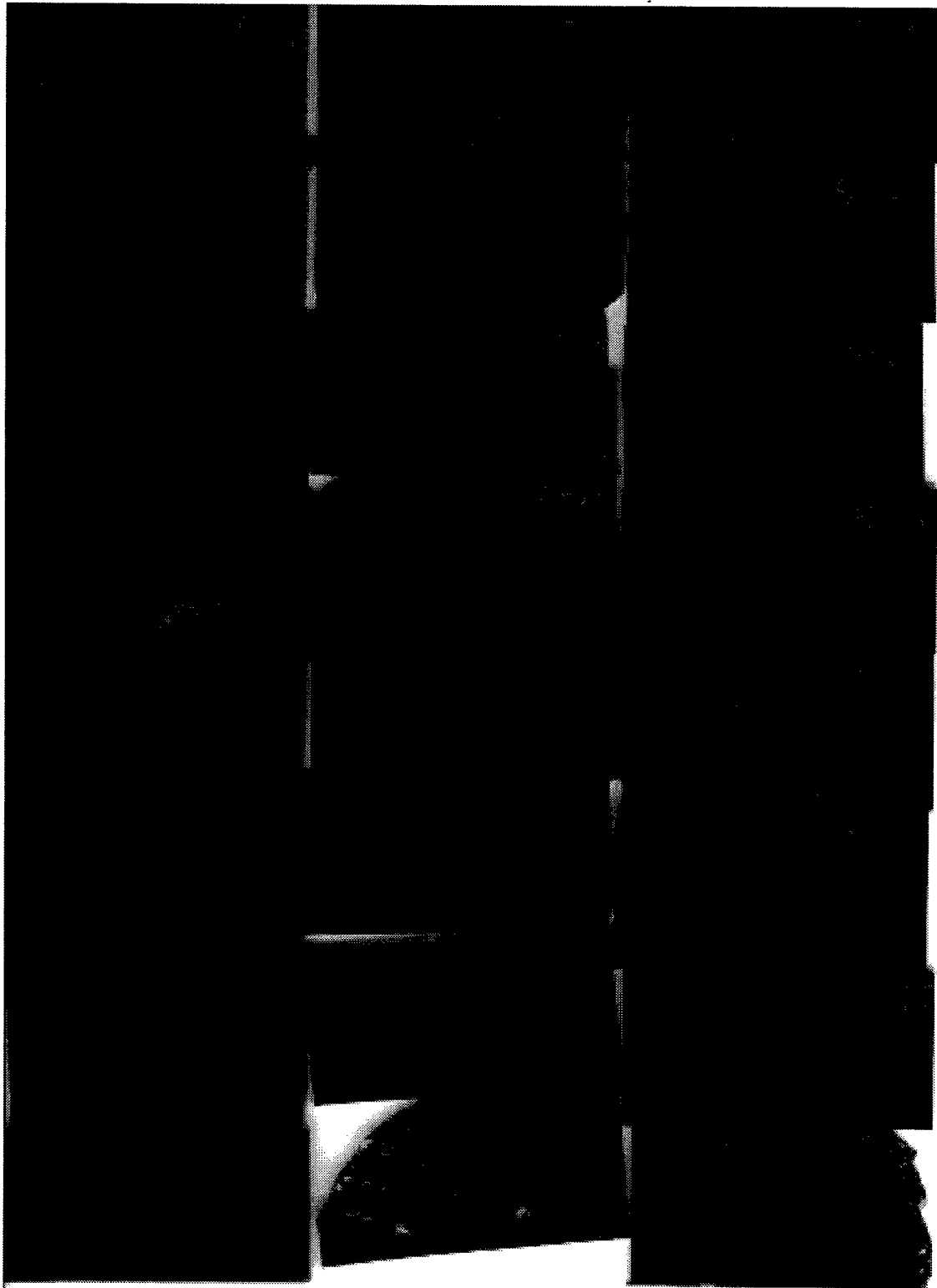
Figure B-18
977-3 NEAT RESIN SAMPLES AFTER ENVIRONMENTAL
AND THERMAL EXPOSURE
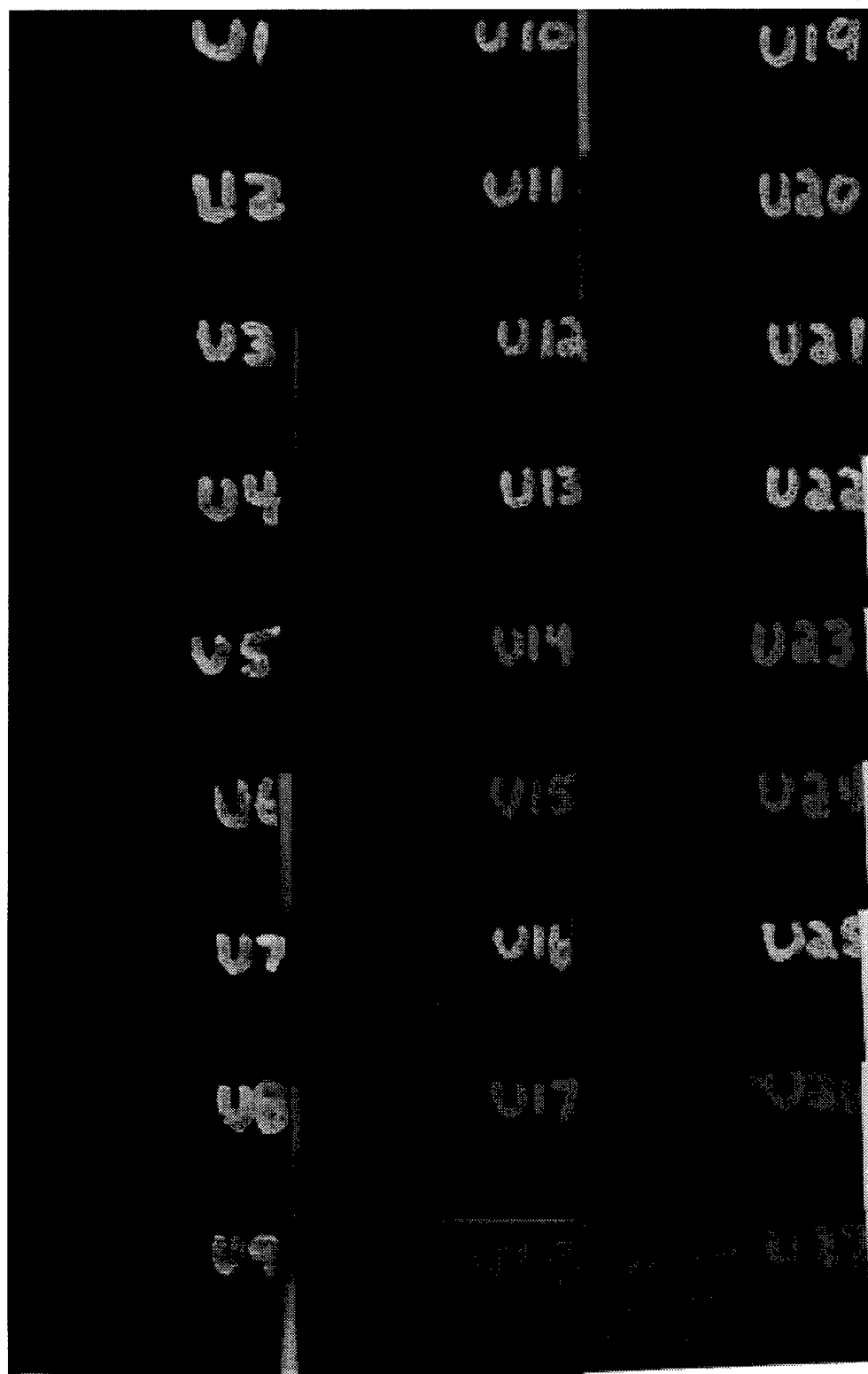
Figure B-19
UNIDIRECTIONAL SAMPLES AFTER ENVIRONMENTAL
AND THERMAL EXPOSURE
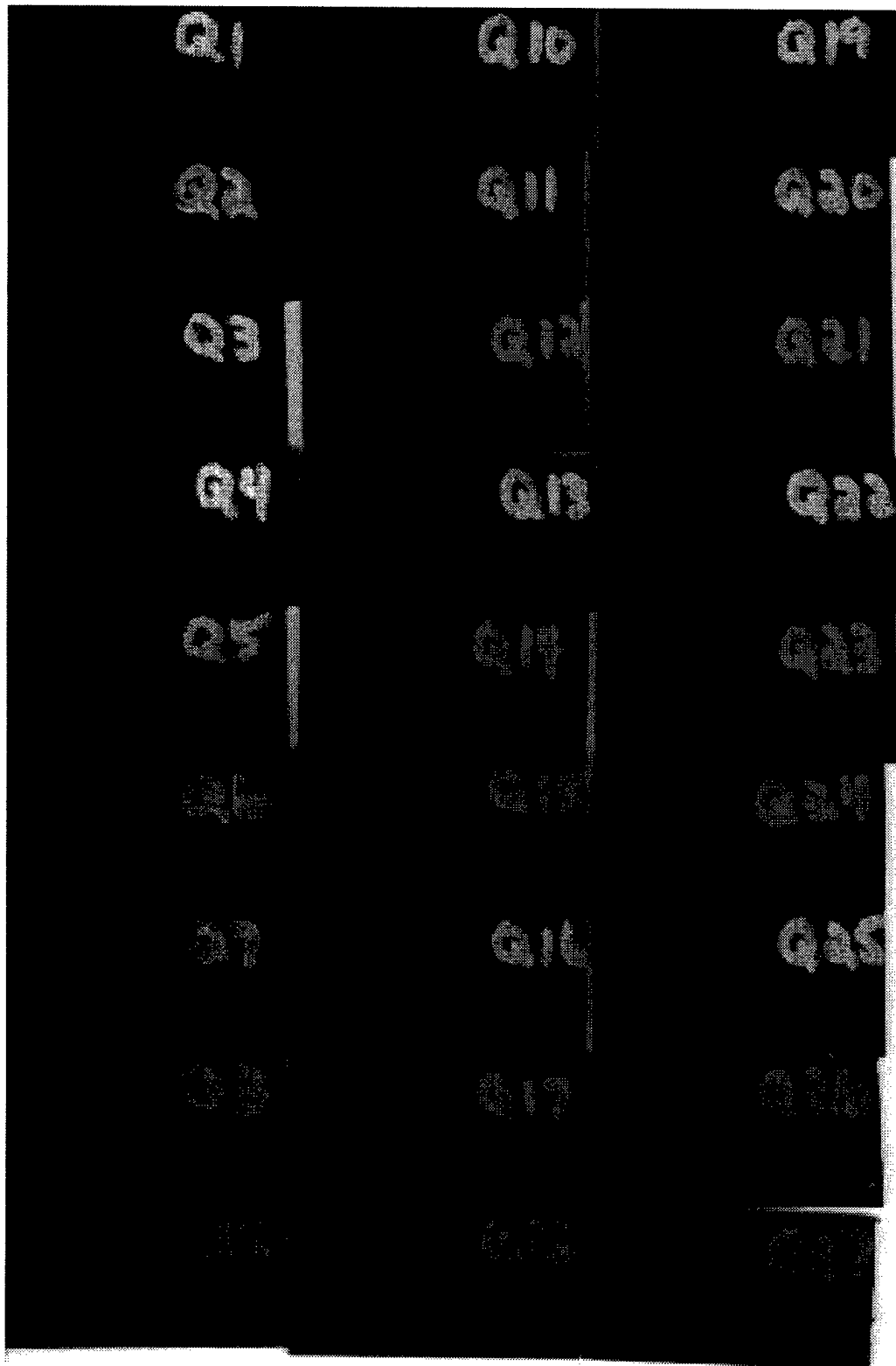
Figure B-20
QUASI-ISOTROPIC SAMPLES AFTER ENVIRONMENTAL
AND THERMAL EXPOSURE

APPENDIX B
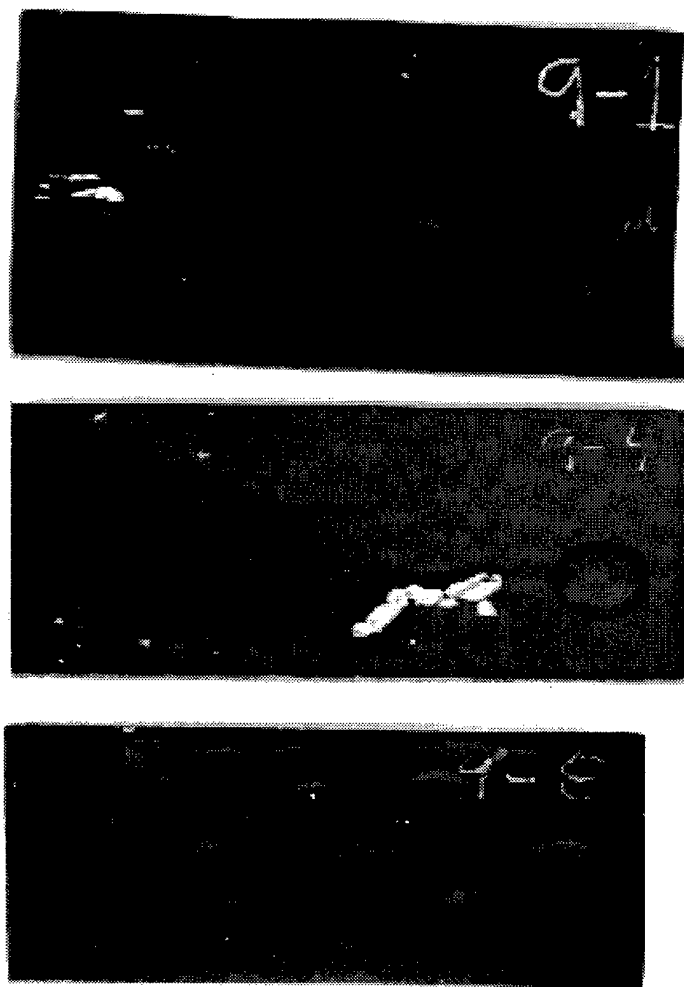
Figure B-21
SATURATED 977-3 NEAT RESIN COUPONS 9-525-5-S, 9-576-5-S, AND 9-623-5-S
(FROM TOP TO BOTTOM) SHOWING INCREASING DAMAGE DUE
TO INCREASING THERMAL EXPOSURE
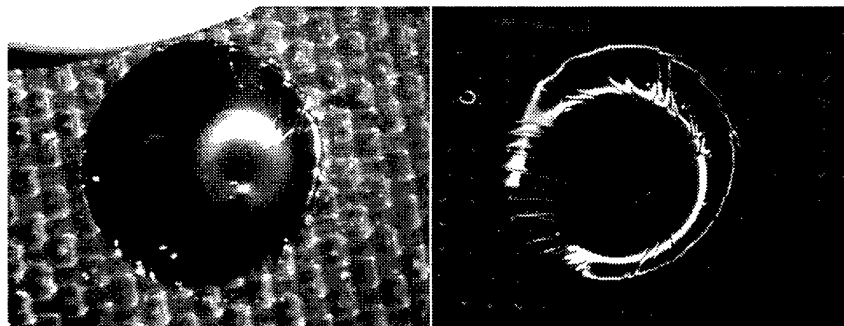
Figure B-22
SPALLING DUE TO OUT-GASSING IN 977-3 HEAT-DAMAGED NEAT RESIN
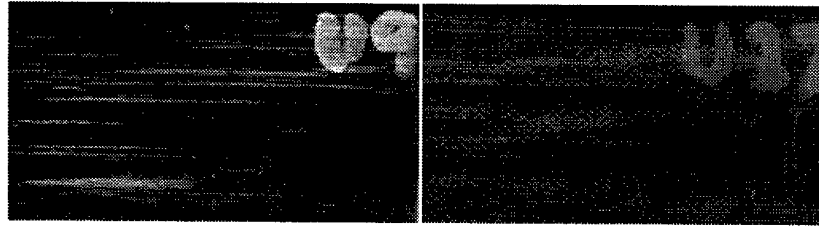
Figure B-23
AMBIENT (LEFT) AND SATURATED (RIGHT) CONDITIONED IM6/977-3
UNIDIRECTIONAL COMPOSITES EXPOSED FOR 45 MIN AT 625°F
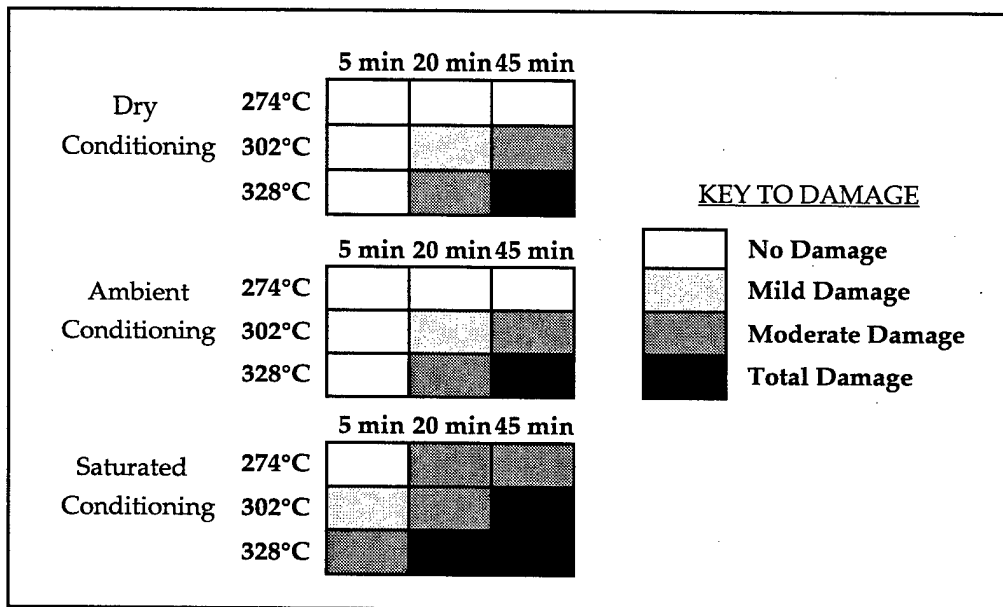
Figure B-24
DEGREE OF DAMAGE RATING FOR 977-3 NEAT RESIN
VISUAL INSPECTION RESULTS

APPENDIX B

977-3 Neat Resin
Moisture Condition: Saturated

525 °F - 45 min
576 °F - 45 min
Total Damage
(Sample Crumbled Upon Cooling)
623 °F - 45 min

525 °F - 20 min
576 °F - 20 min
623 °F - 20 min

525 °F - 05 min
576 °F - 05 min
623 °F - 05 min

NDI Technique: Ultrasonic C-Scan
Darker Areas Are More Damaged
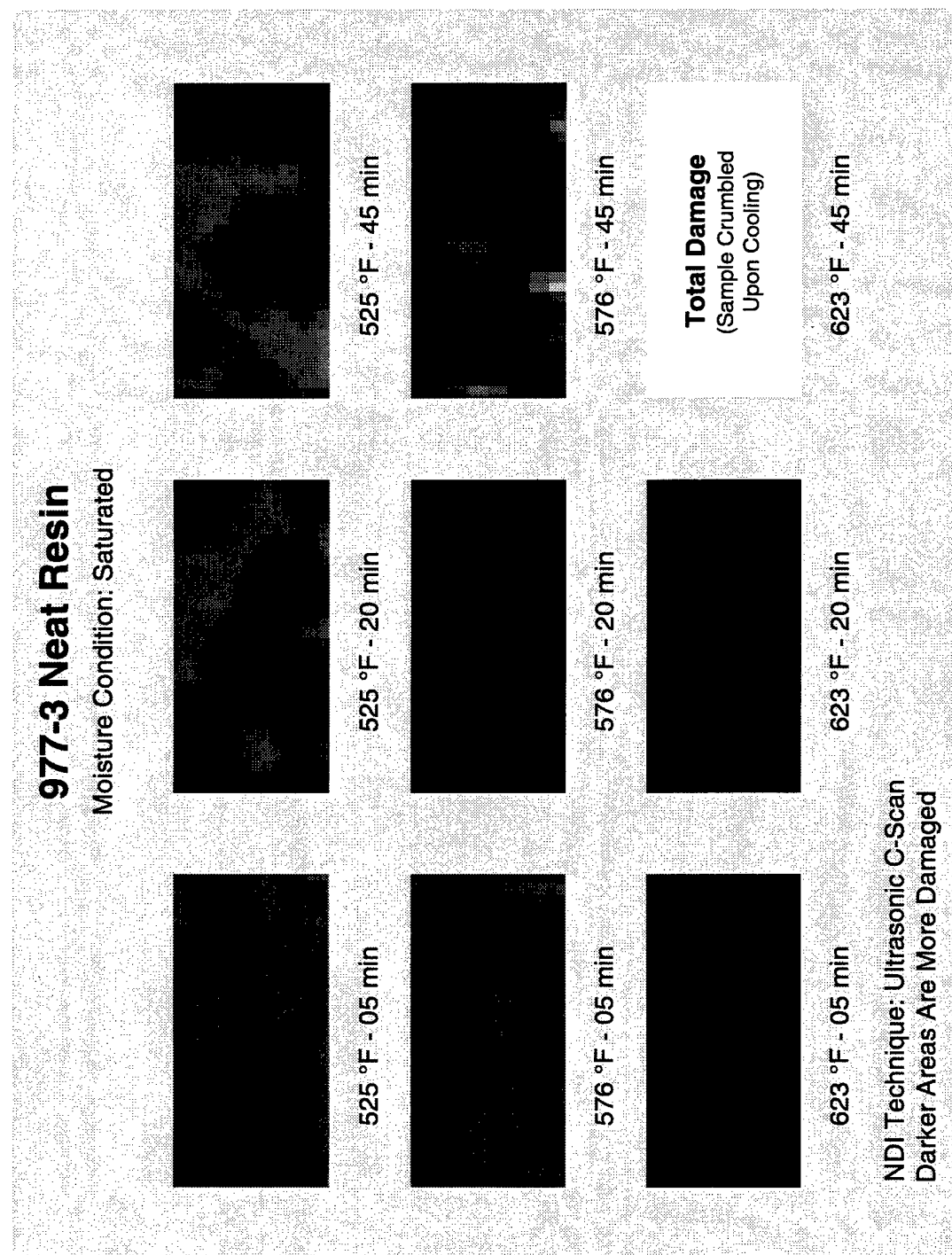
Figure B-25
ULTRASONIC C-SCAN RESULTS FOR THE SATURATED 977-3 NEAT RESIN SAMPLES
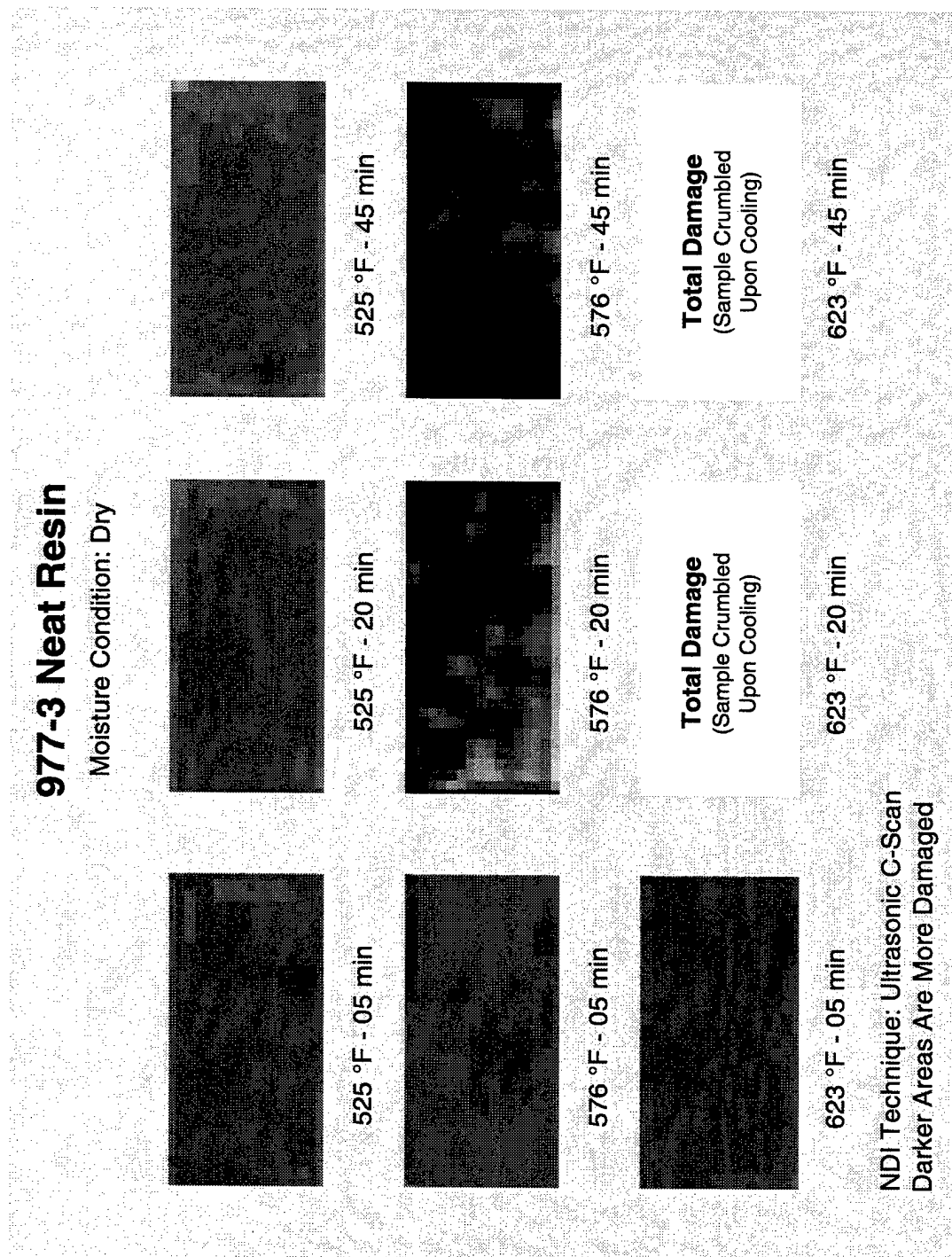
Figure B-26
ULTRASONIC C-SCAN RESULTS FOR THE DRY 977-3 NEAT RESIN SAMPLES

APPENDIX B

977-3 Neat Resin
Moisture Condition: Ambient

525 °F - 45 min

576 °F - 45 min

Total Damage
(Sample Crumbled Upon Cooling)

623 °F - 45 min

525 °F - 20 min

576 °F - 20 min

623 °F - 20 min

525 °F - 05 min

576 °F - 05 min

623 °F - 05 min

NDI Technique: Ultrasonic C-Scan
Darker Areas Are More Damaged
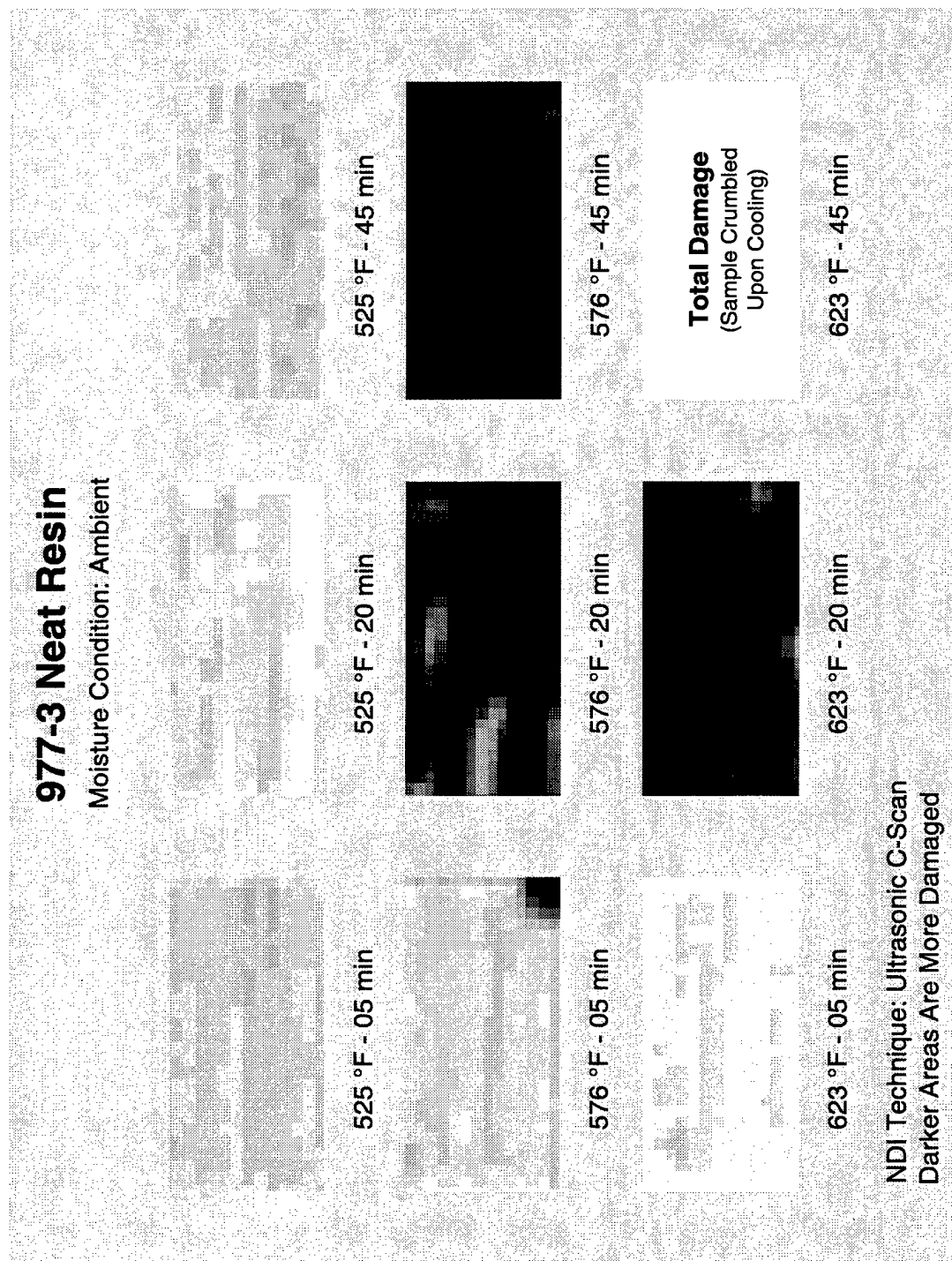
Figure B-27
ULTRASONIC C-SCAN RESULTS FOR THE AMBIENT 977-3 NEAT RESIN SAMPLES

IM6/977-3 Unidirectional Laminate

Moisture Condition: Saturated

525 °F - 45 min

576 °F - 45 min

623 °F - 45 min

525 °F - 20 min

576 °F - 20 min

623 °F - 20 min

525 °F - 05 min

576 °F - 05 min

623 °F - 05 min

NDI Technique: Ultrasonic C-Scan
Darker Areas Are More Damaged
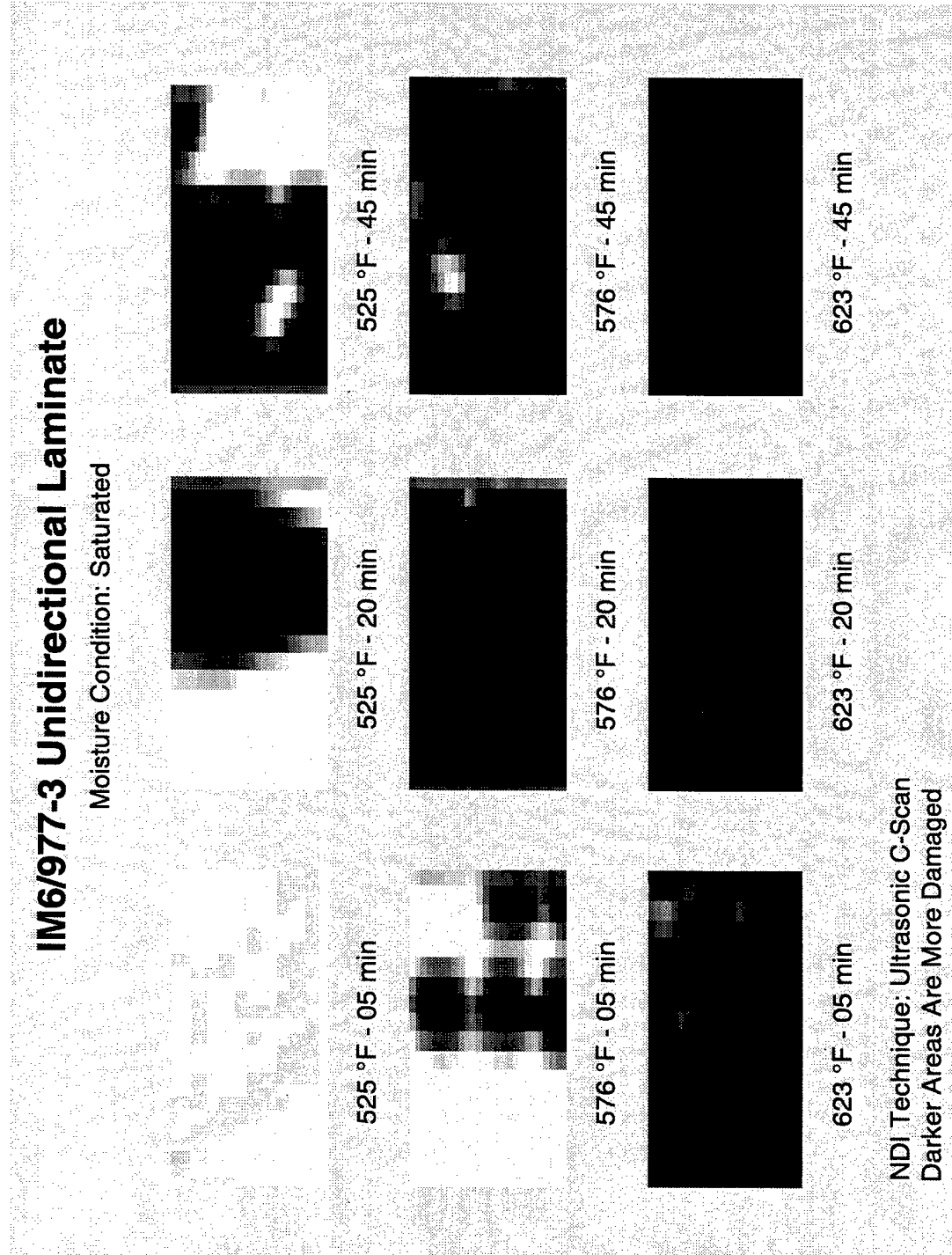
Figure B-28
ULTRASONIC C-SCAN RESULTS FOR THE SATURATED UNIDIRECTIONAL SAMPLES

IM6/977-3 Unidirectional Laminate

Moisture Condition: Dry

525 °F - 45 min

576 °F - 45 min

623 °F - 45 min

525 °F - 20 min

576 °F - 20 min

623 °F - 20 min

525 °F - 05 min

576 °F - 05 min

623 °F - 05 min

NDI Technique: Ultrasonic C-Scan
Darker Areas Are More Damaged
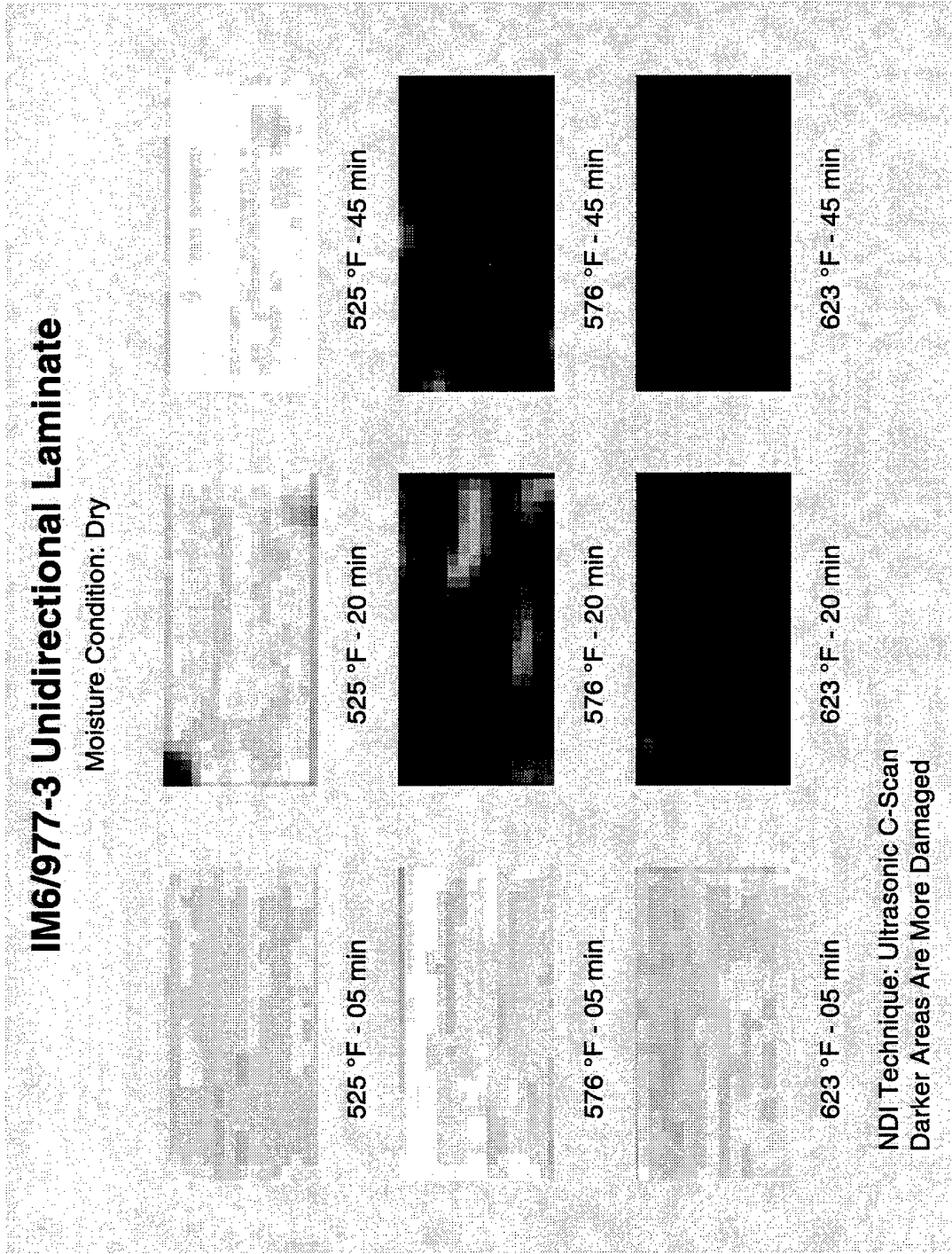
Figure B-29
ULTRASONIC C-SCAN RESULTS FOR THE DRY UNIDIRECTIONAL SAMPLES
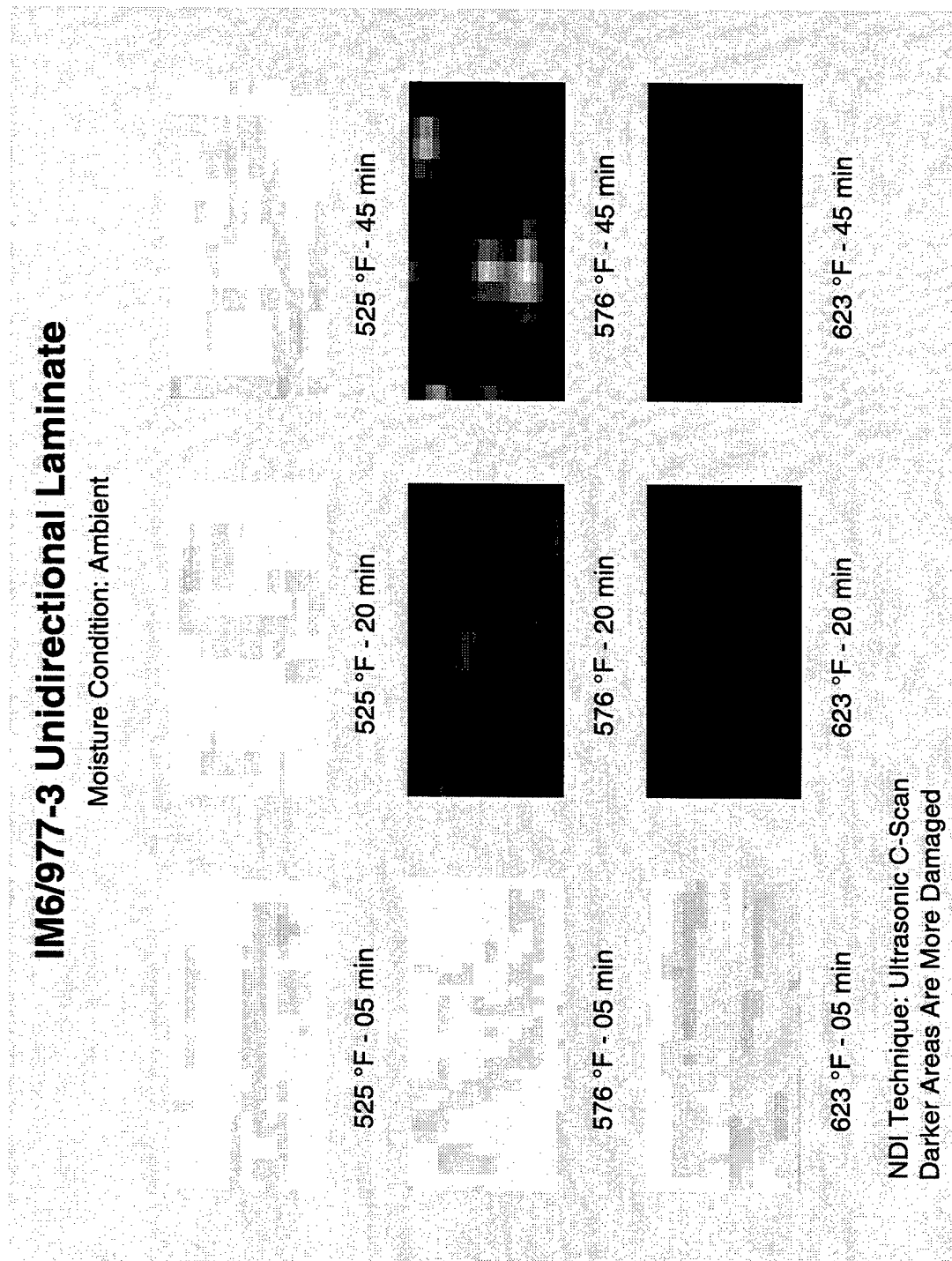
Figure B-30

ULTRASONIC C-SCAN RESULTS FOR THE AMBIENT UNIDIRECTIONAL SAMPLES
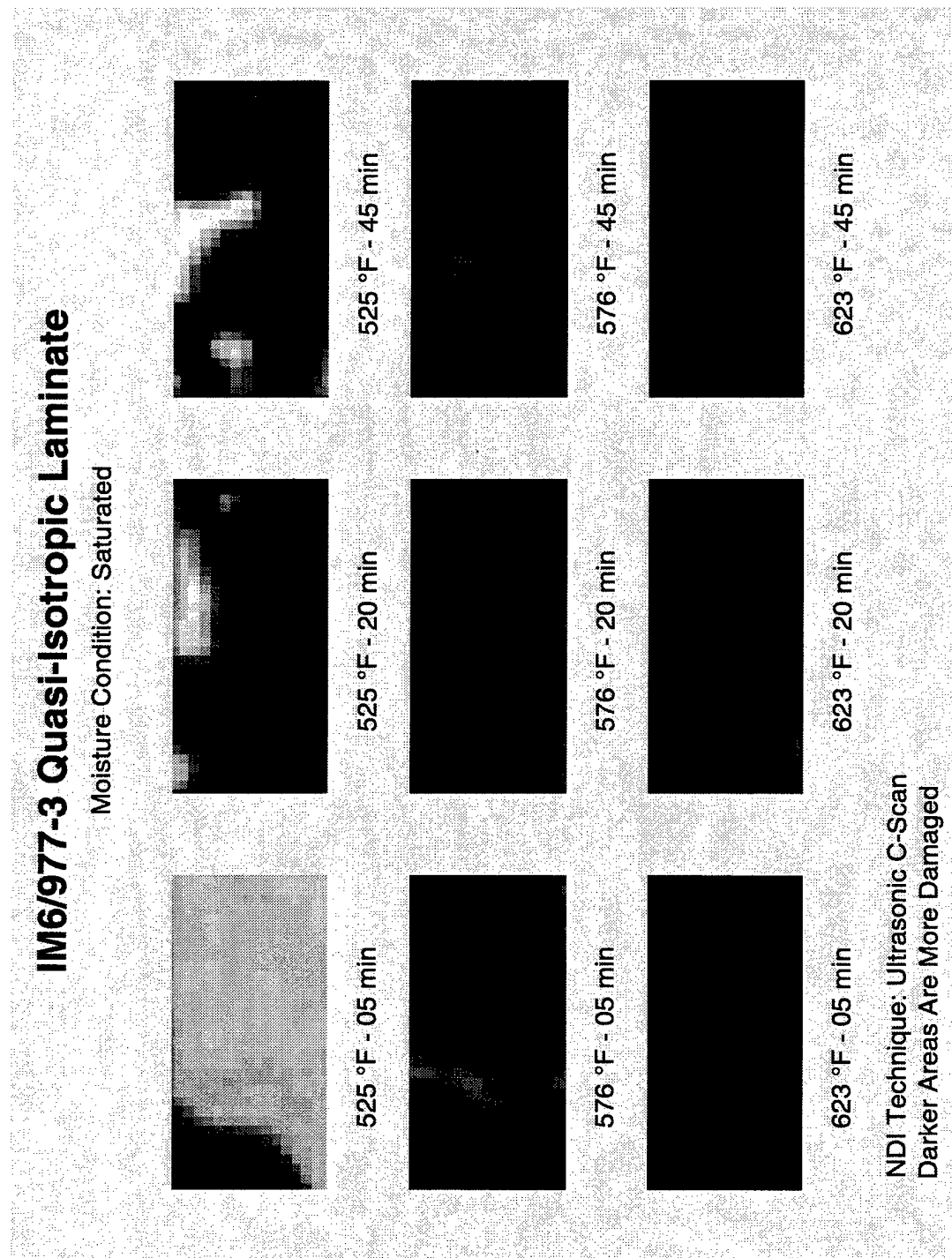
Figure B-31
ULTRASONIC C-SCAN RESULTS FOR THE SATURATED QUASI-ISOTROPIC SAMPLES

APPENDIX B
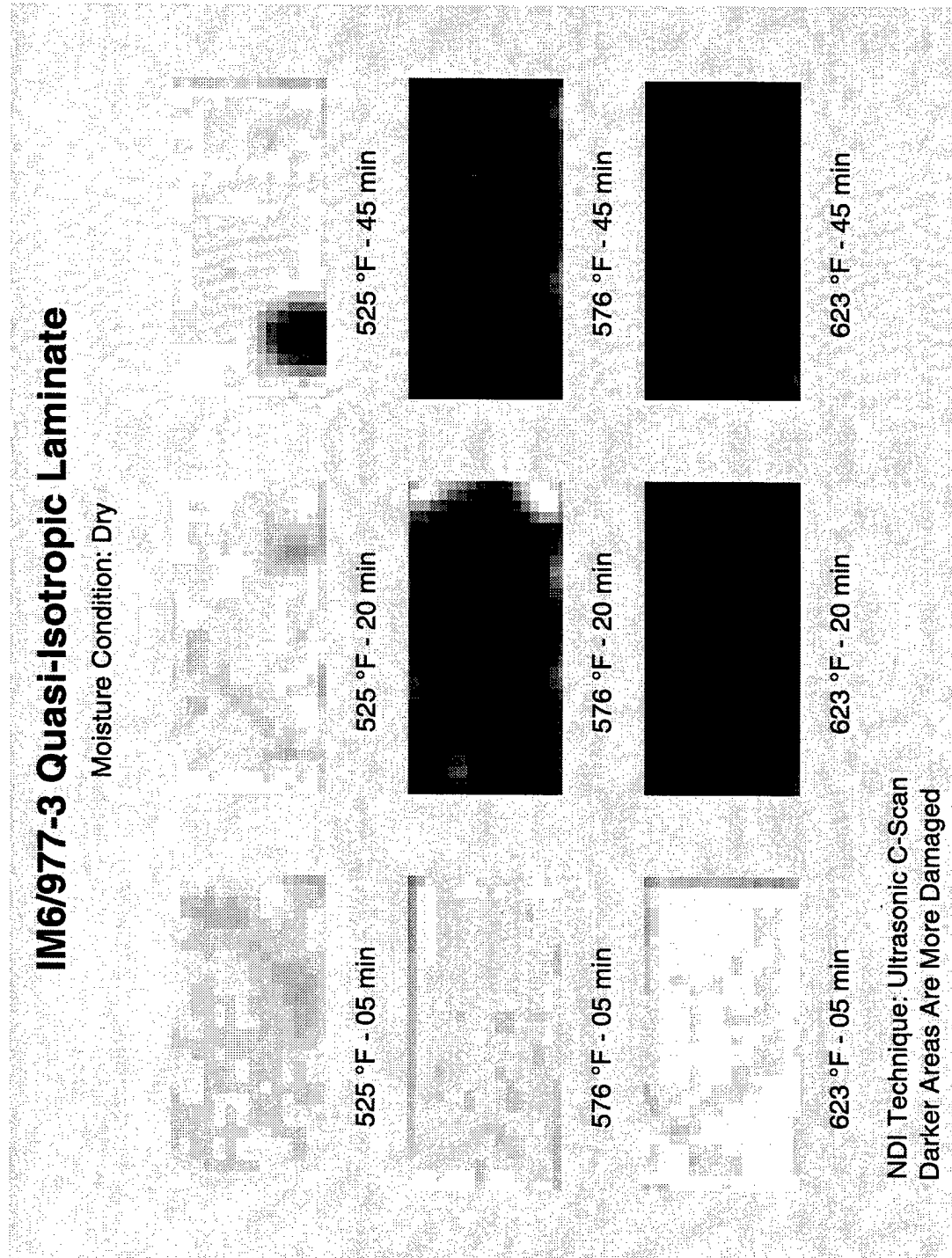
Figure B-32
ULTRASONIC C-SCAN RESULTS FOR THE DRY QUASI-ISOTROPIC SAMPLES
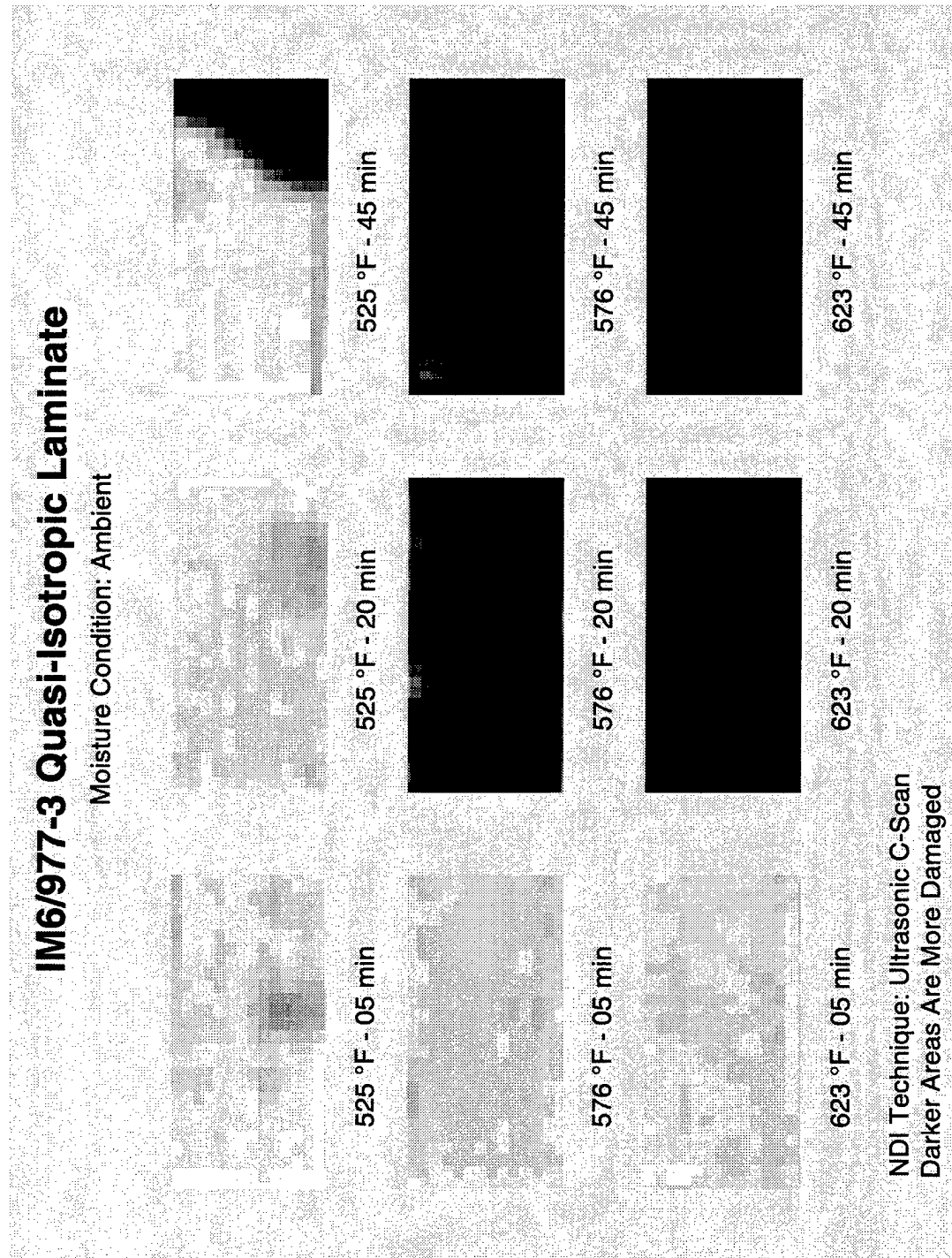
Figure B-33
ULTRASONIC C-SCAN RESULTS FOR THE AMBIENT QUASI-ISOTROPIC SAMPLES

APPENDIX B

977-3 Neat Resin
Moisture Condition: Saturated

525 °F - 45 min

525 °F - 20 min

525 °F - 05 min

576 °F - 45 min

576 °F - 20 min

576 °F - 05 min

Total Damage
(Sample Crumbled Upon Cooling)

623 °F - 45 min

623 °F - 20 min

623 °F - 05 min

NDI Technique: Thermography
Darker Areas Are More Damaged
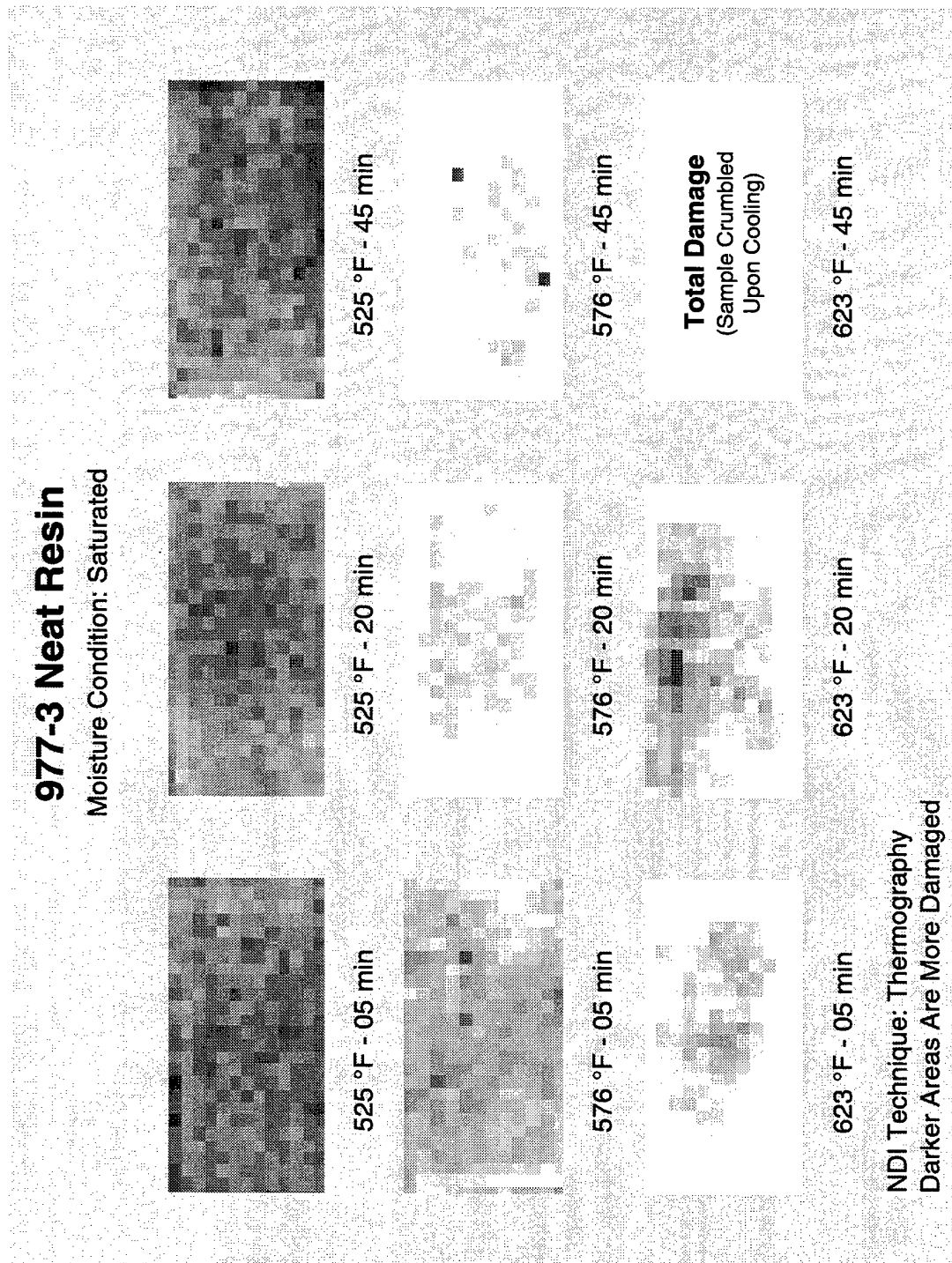
Figure B-34
THERMOGRAPHY RESULTS FOR THE SATURATED 977-3 NEAT RESIN SAMPLES

APPENDIX B
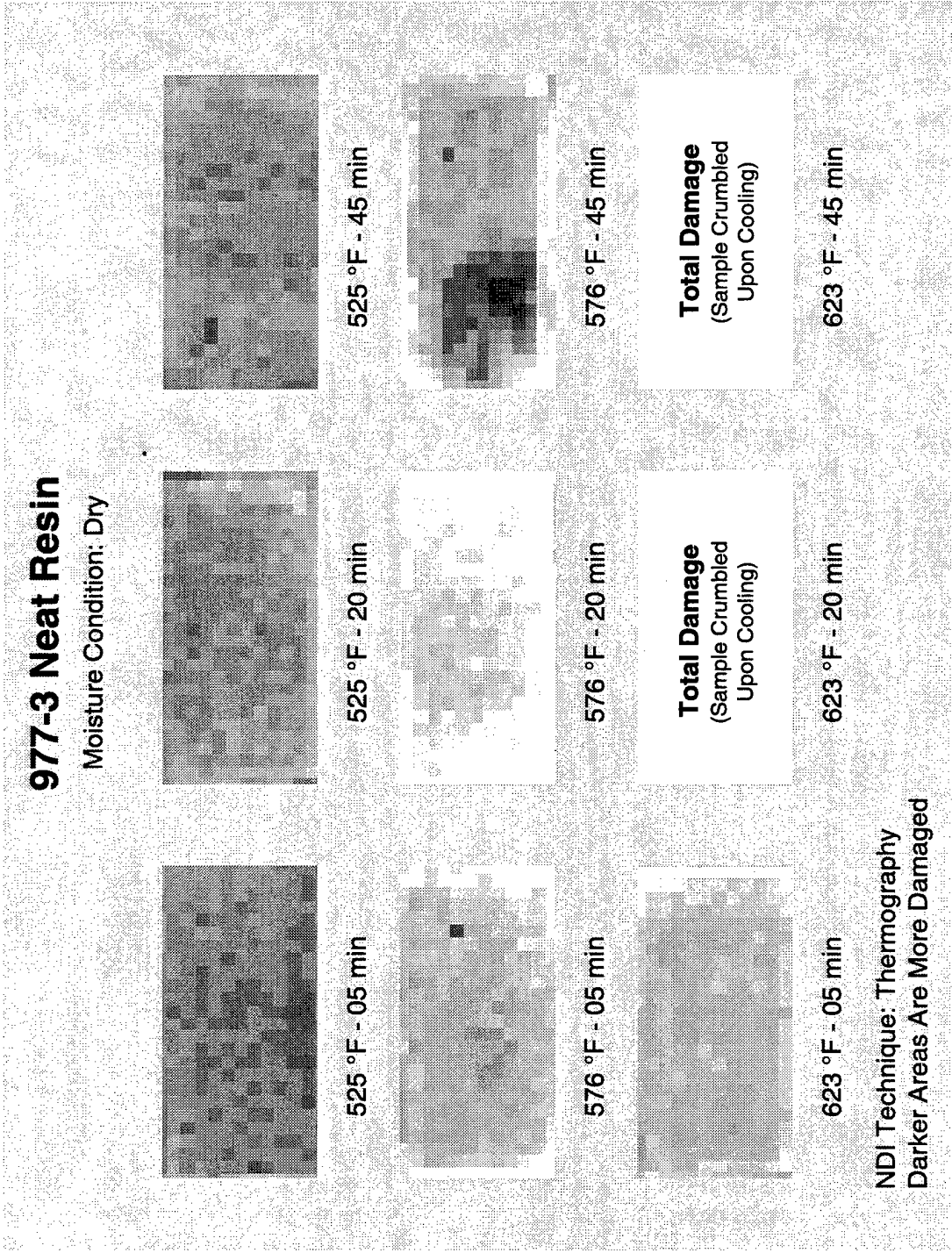
Figure B-35

THERMOGRAPHY RESULTS FOR THE DRY 977-3 NEAT RESIN SAMPLES
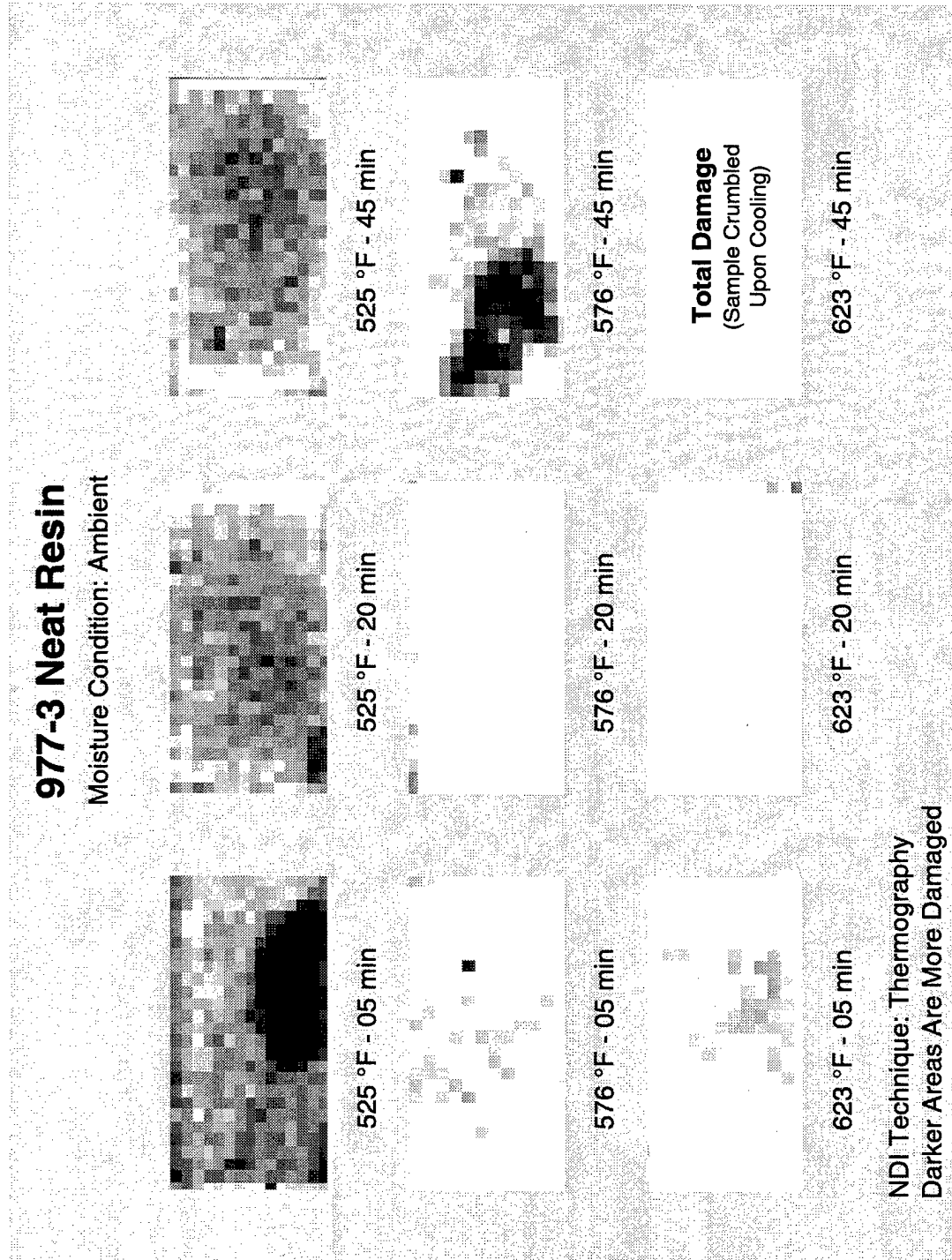
Figure B-36

THERMOGRAPHY RESULTS FOR THE AMBIENT 977-3 NEAT RESIN SAMPLES
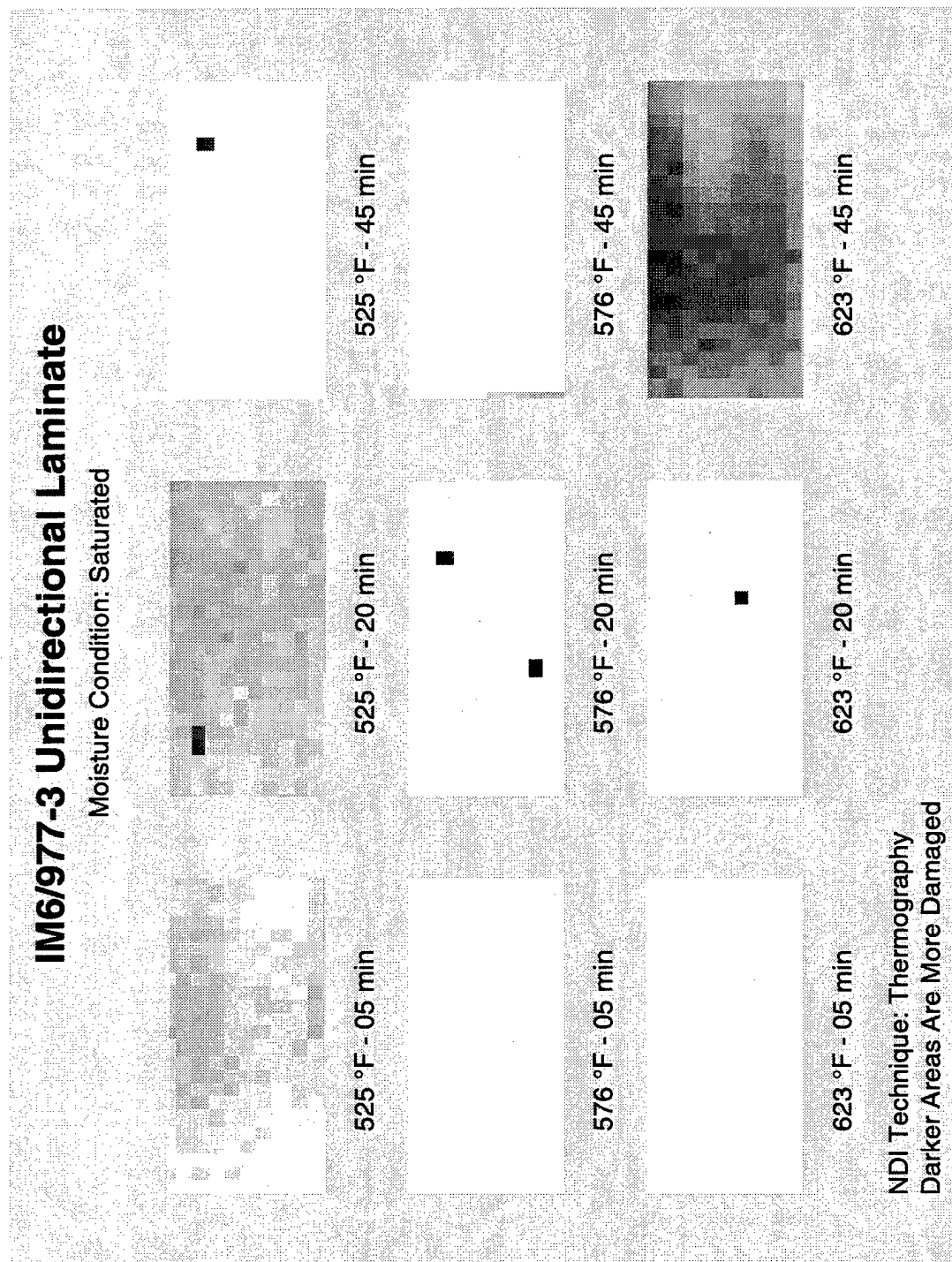
Figure B-37

THERMOGRAPHY RESULTS FOR THE SATURATED UNIDIRECTIONAL SAMPLES

APPENDIX B

IM6/977-3 Unidirectional Laminate

Moisture Condition: Dry

525 °F - 45 min

576 °F - 45 min

623 °F - 45 min

525 °F - 20 min

576 °F - 20 min

623 °F - 20 min

525 °F - 05 min

576 °F - 05 min

623 °F - 05 min

NDI Technique: Thermography
Darker Areas Are More Damaged
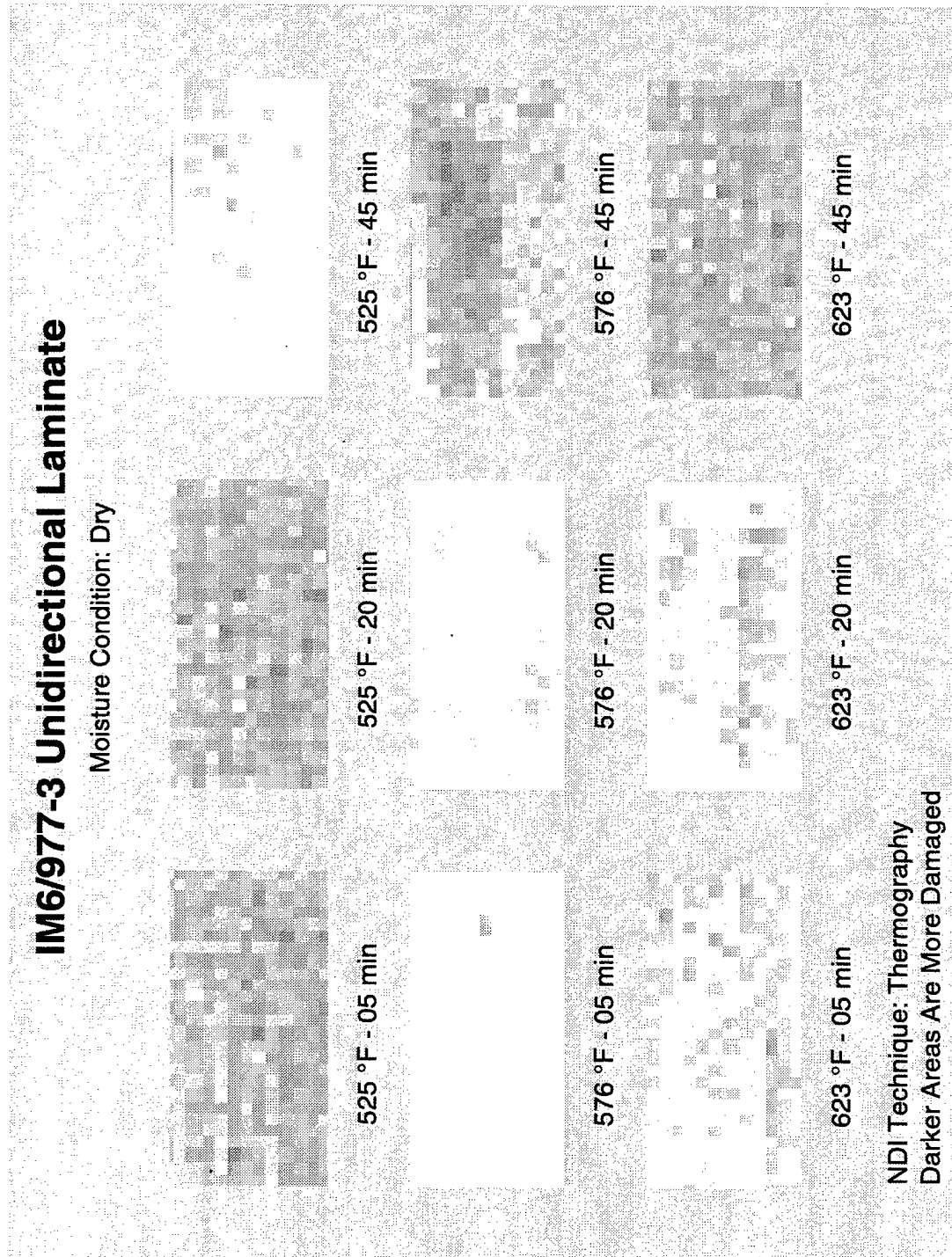
Figure B-38

THERMOGRAPHY RESULTS FOR THE DRY UNIDIRECTIONAL SAMPLES

IM6/977-3 Unidirectional Laminate
Moisture Condition: Ambient

525 °F - 45 min

576 °F - 45 min

623 °F - 45 min

525 °F - 20 min

576 °F - 20 min

623 °F - 20 min

525 °F - 05 min

576 °F - 05 min

623 °F - 05 min

NDI Technique: Thermography
Darker Areas Are More Damaged
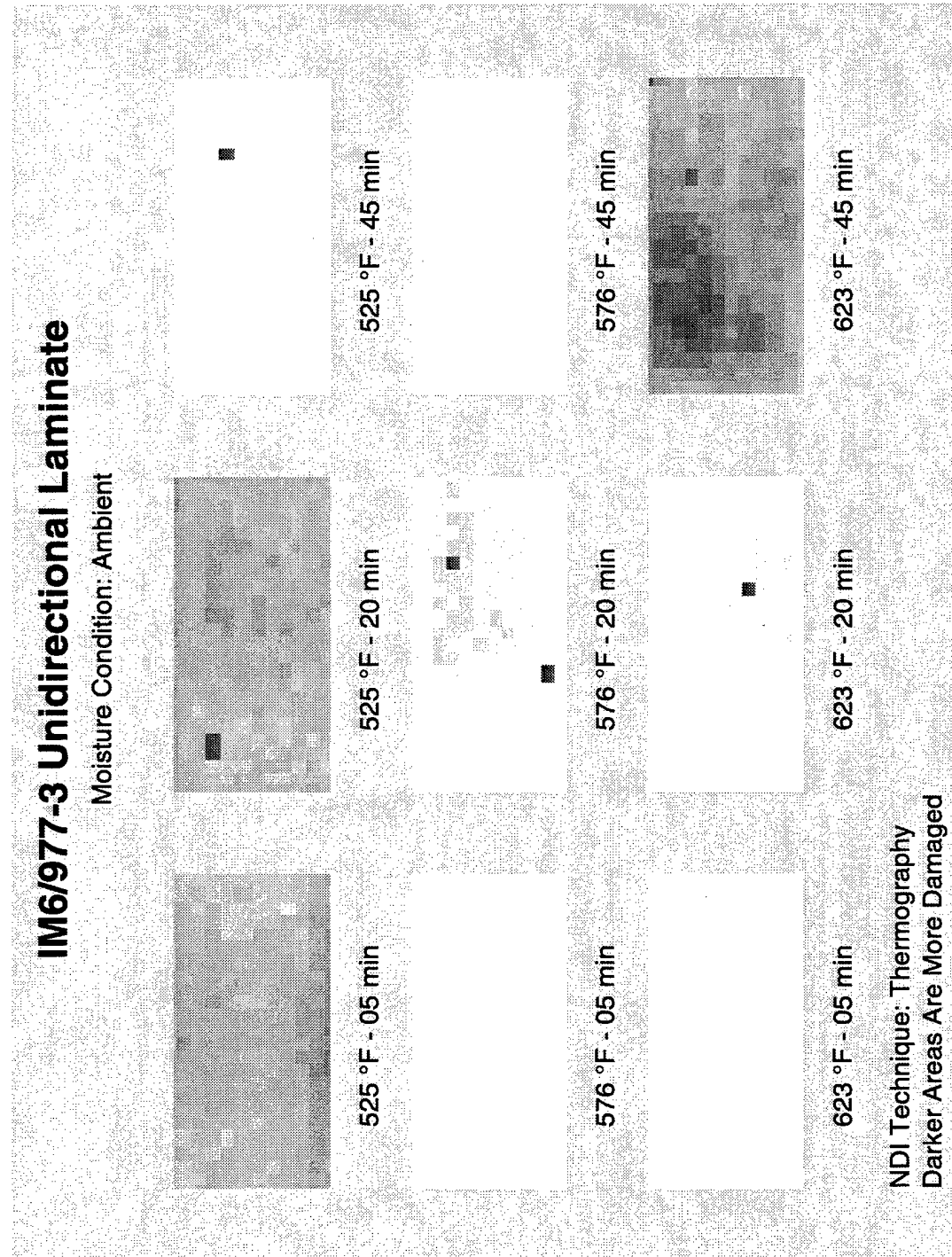
Figure B-39
THERMOGRAPHY RESULTS FOR THE AMBIENT UNIDIRECTIONAL SAMPLES
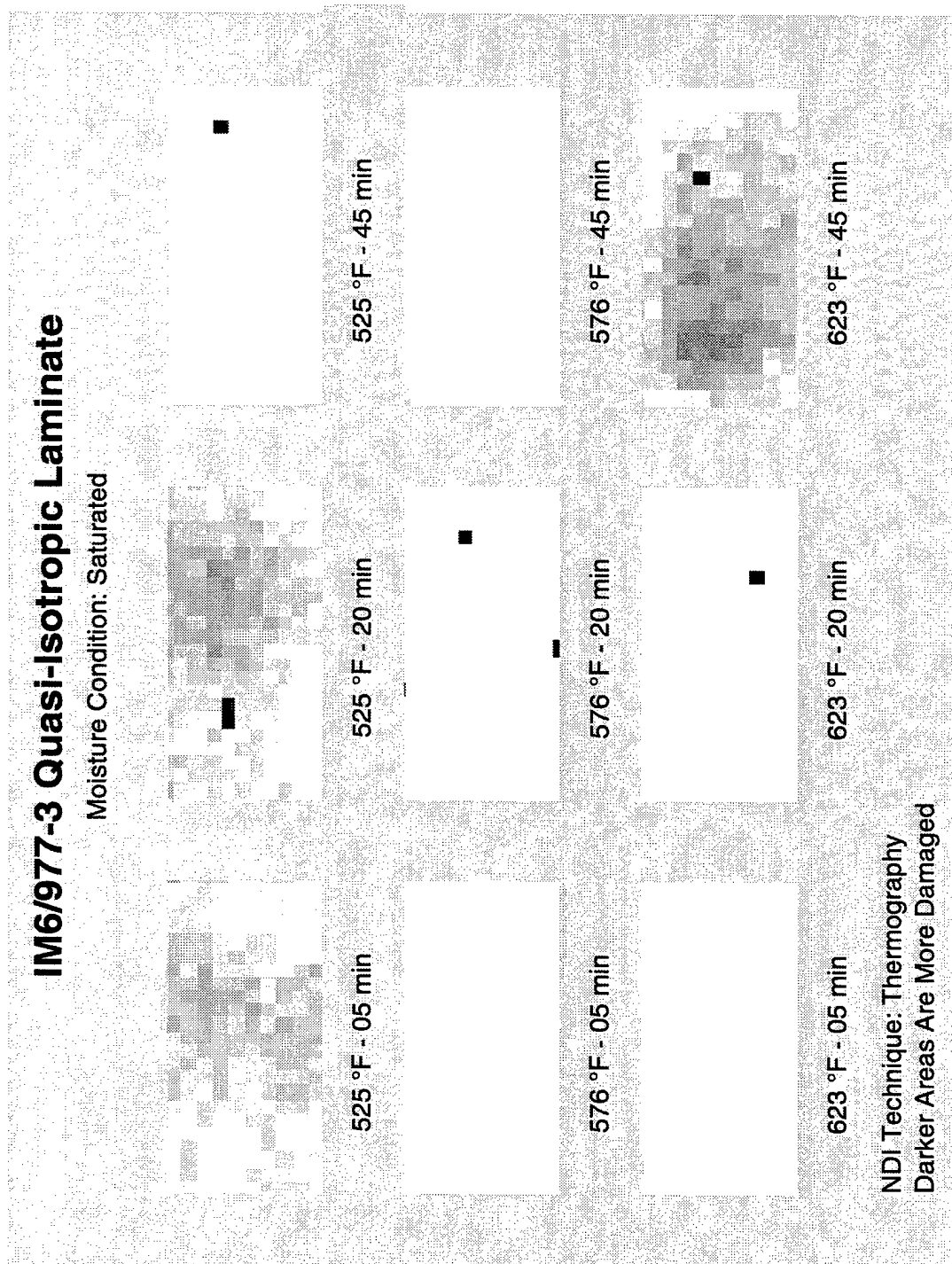
Figure B-40

THERMOGRAPHY RESULTS FOR THE SATURATED QUASI-ISOTROPIC SAMPLES
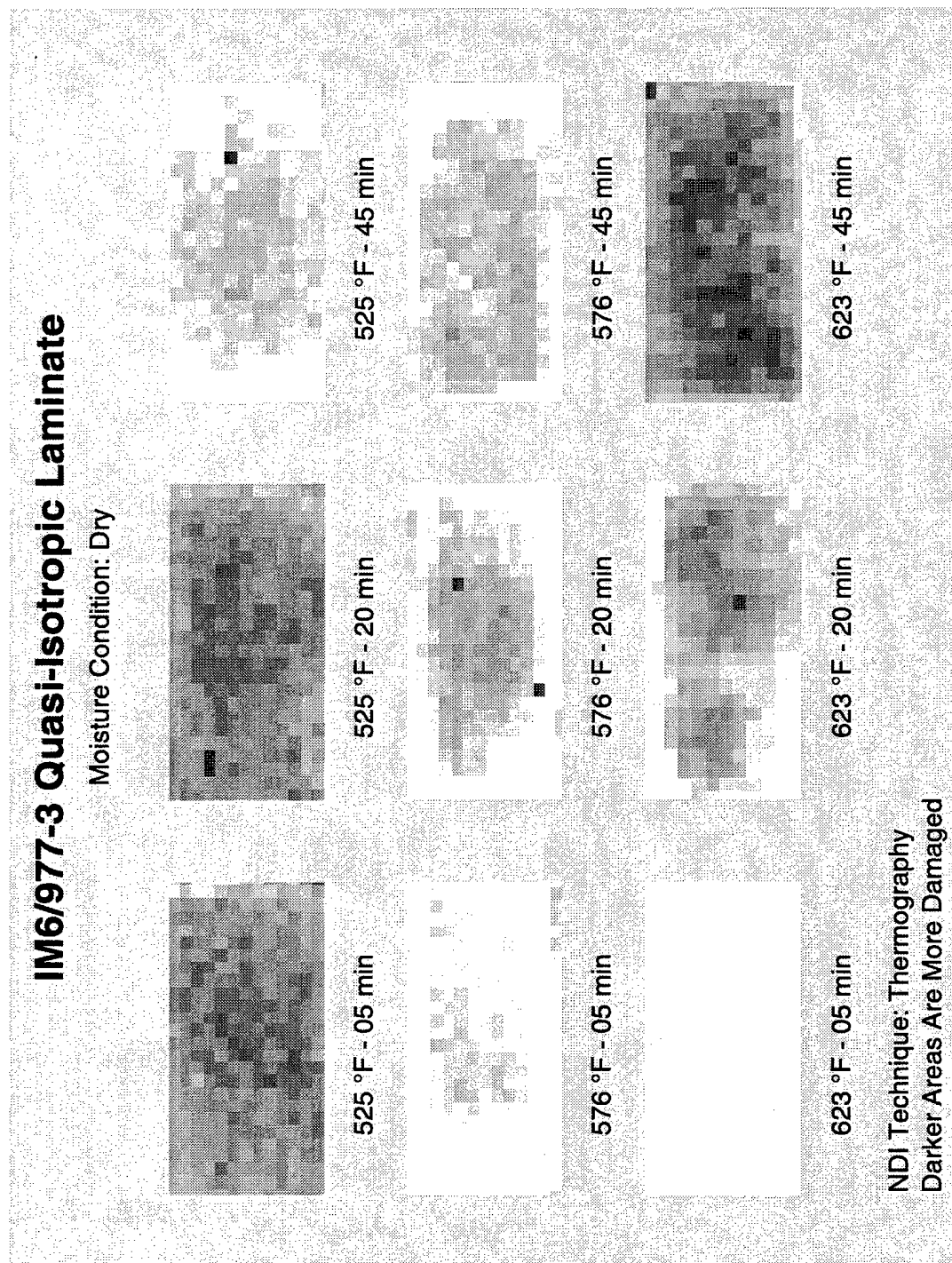
Figure B-41
THERMOGRAPHY RESULTS FOR THE DRY QUASI-ISOTROPIC SAMPLES
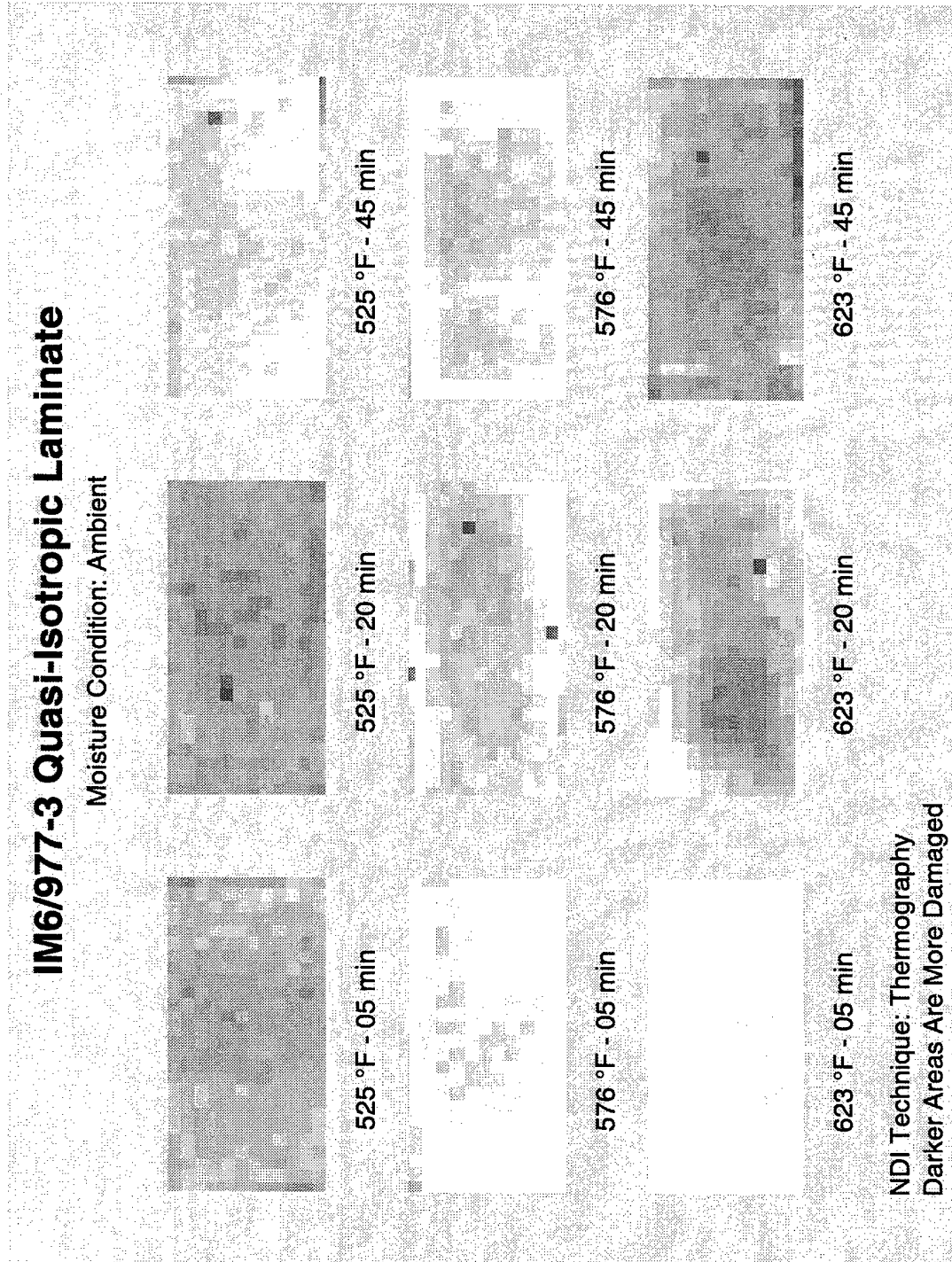
Figure B-42
THERMOGRAPHY RESULTS FOR THE AMBIENT QUASI-ISOTROPIC SAMPLES
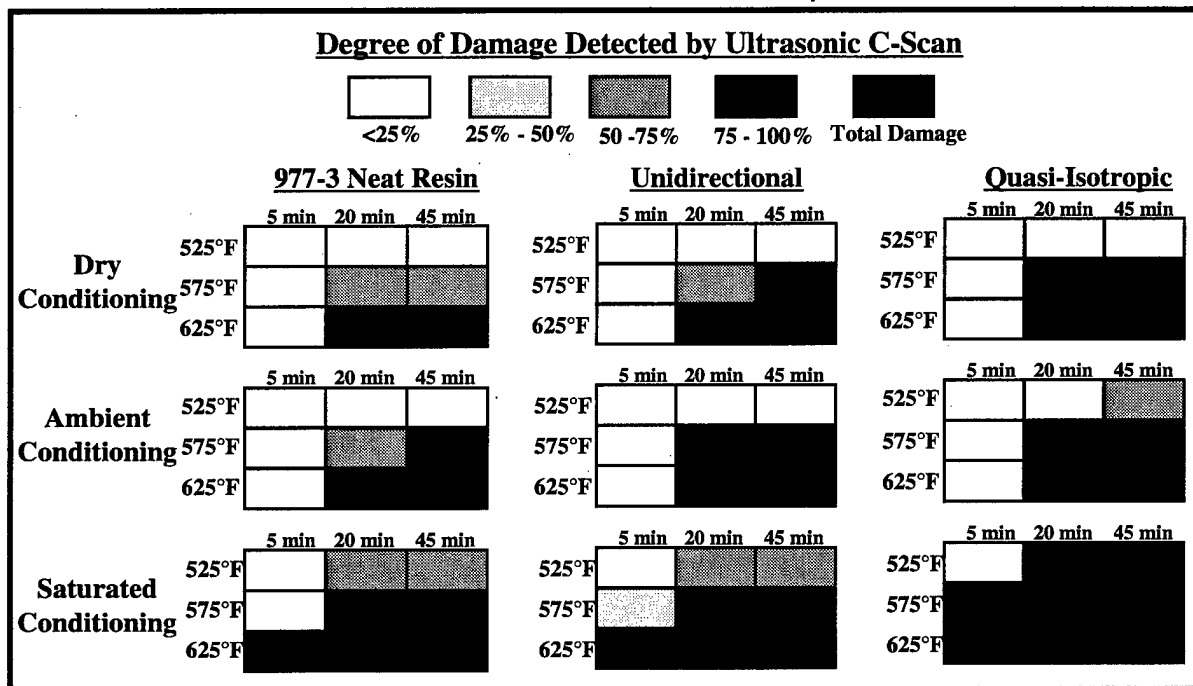
Figure B-43
DEGREE OF DAMAGE DETECTED BY ULTRASONIC C-SCAN
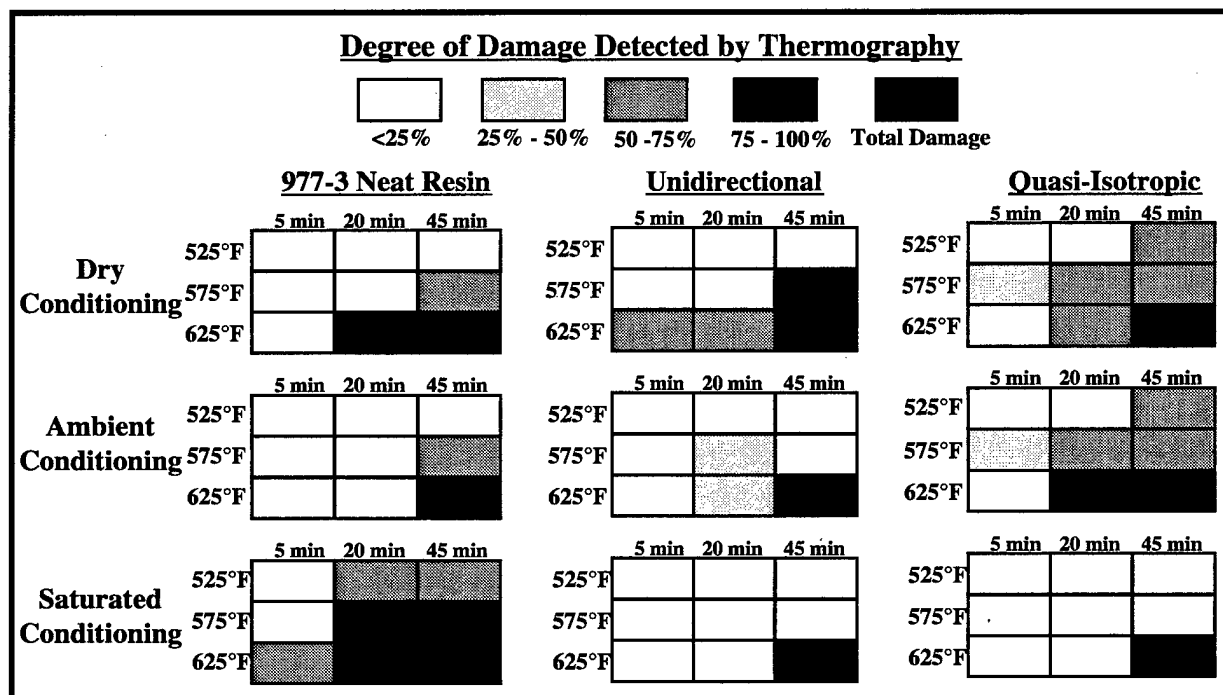
Figure B-44
DEGREE OF DAMAGE DETECTED BY THERMOGRAPHY

977-3 Neat Resin
Saturated Exposures
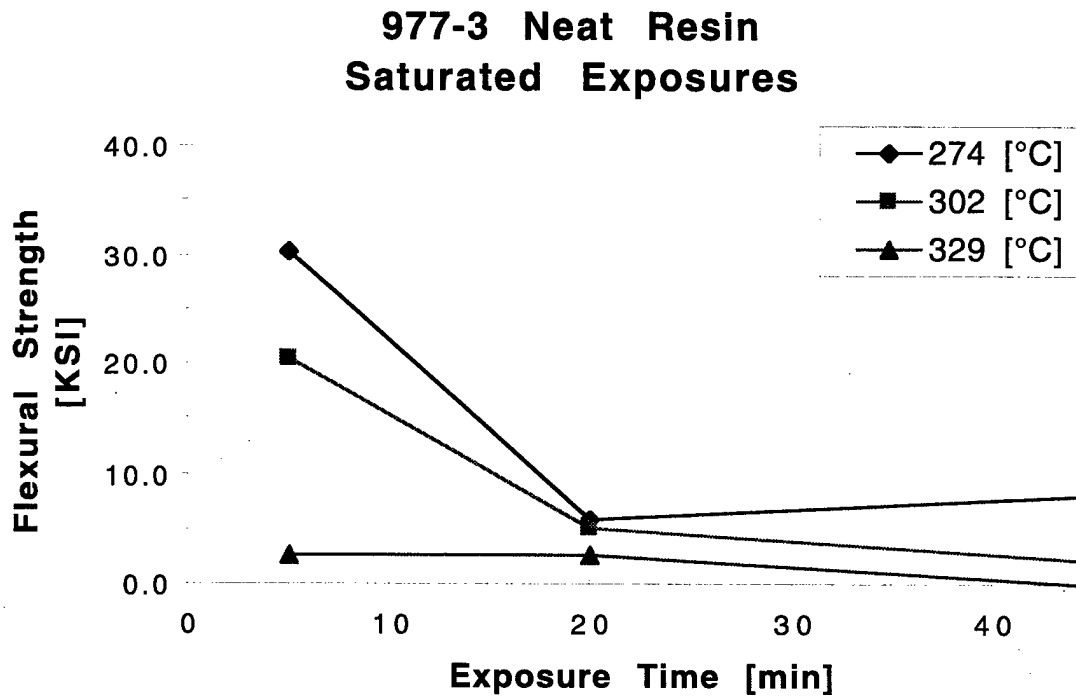
Figure B-45
FLEXURE RESULTS FOR SATURATED 977-3 NEAT RESIN COUPONS

977-3 Neat Resin
Dry Exposures
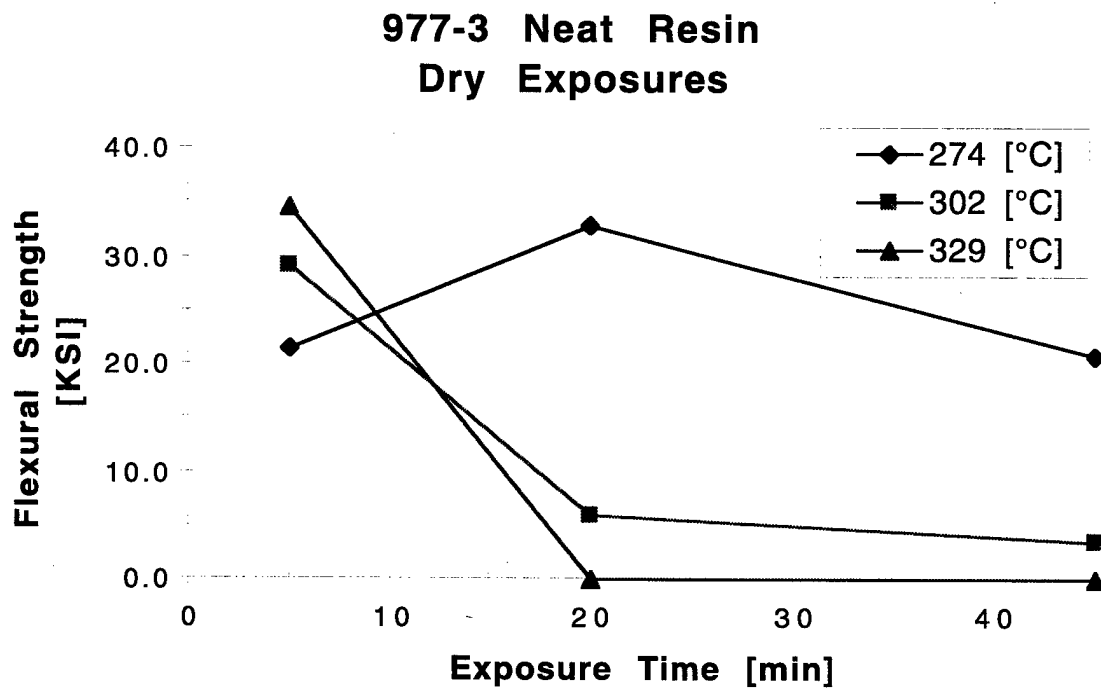
Figure B-46
FLEXURE RESULTS FOR DRY 977-3 NEAT RESIN COUPONS

977-3 Neat Resin
Ambient Exposures
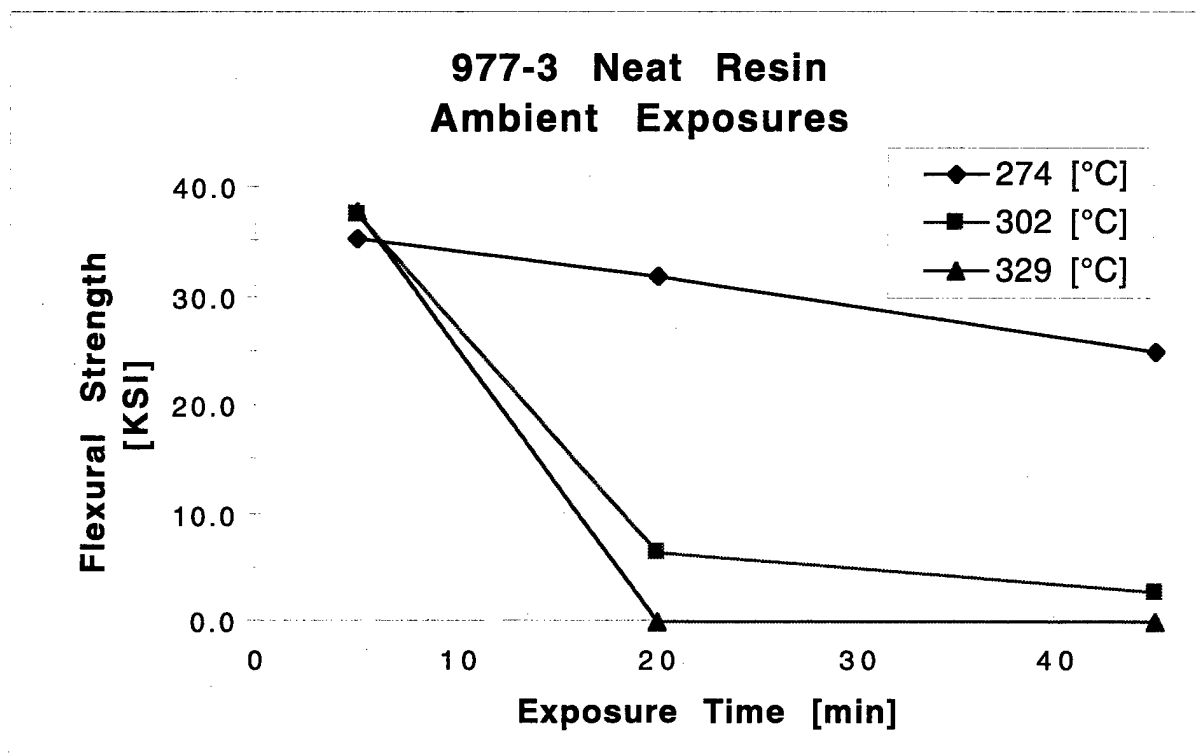
Figure B-47
FLEXURE RESULTS FOR AMBIENT 977-3 NEAT RESIN COUPONS

IM6/977-3 Quasi-Isotropic
Saturated Exposures
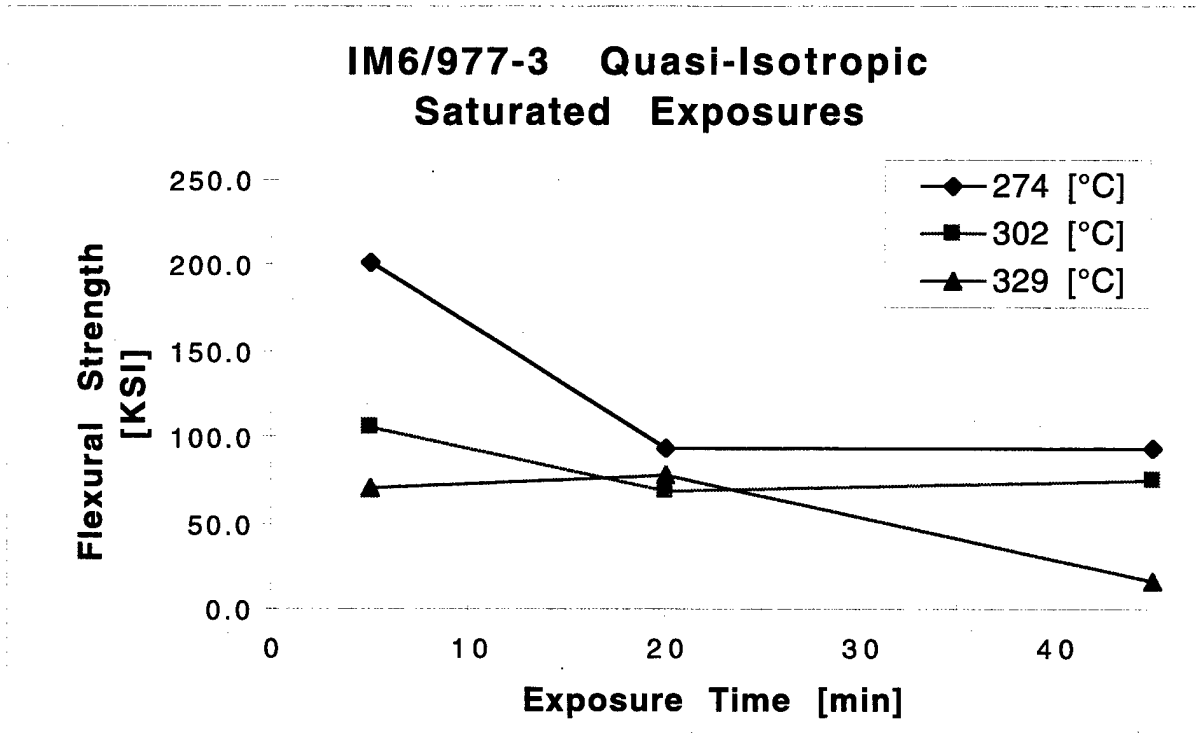
Figure B-48
FLEXURE RESULTS FOR SATURATED IM6/977-3 QUASI-ISOTROPIC COUPONS
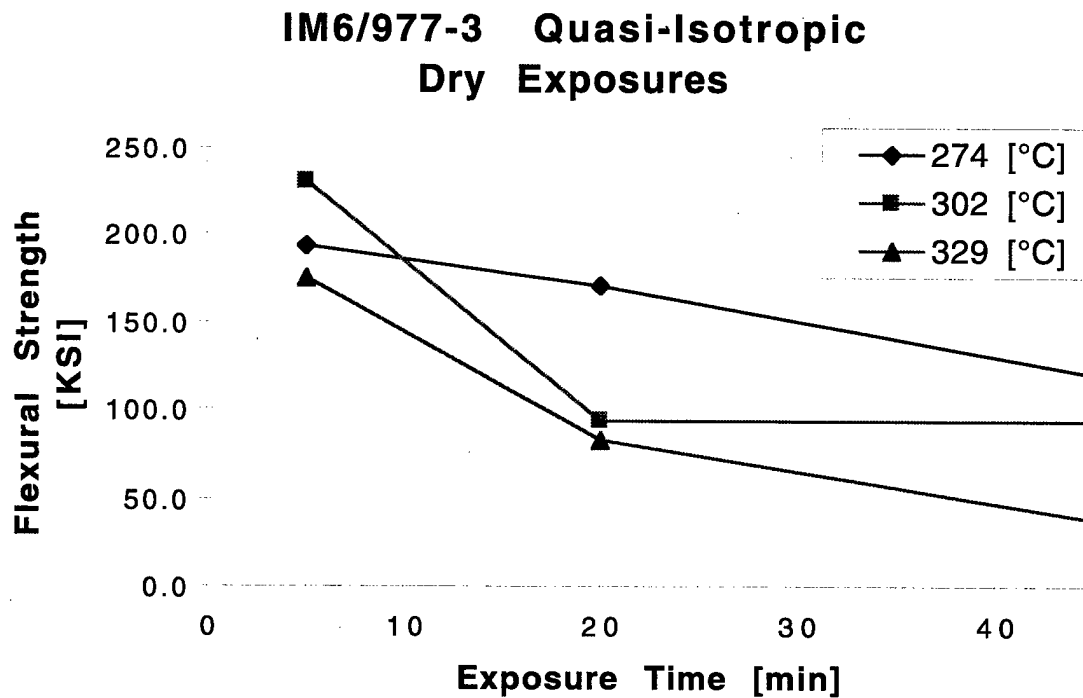
Figure B-49
FLEXURE RESULTS FOR DRY IM6/977-3 QUASI-ISOTROPIC COUPONS
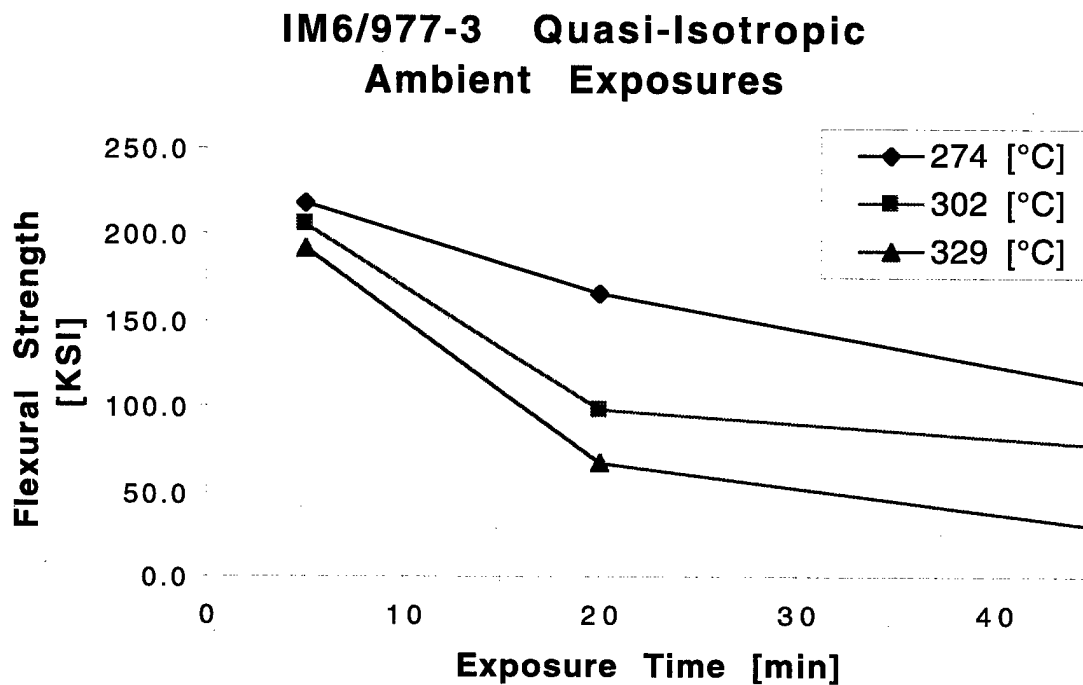
Figure B-50
FLEXURE RESULTS FOR AMBIENT IM6/977-3 QUASI-ISOTROPIC COUPONS
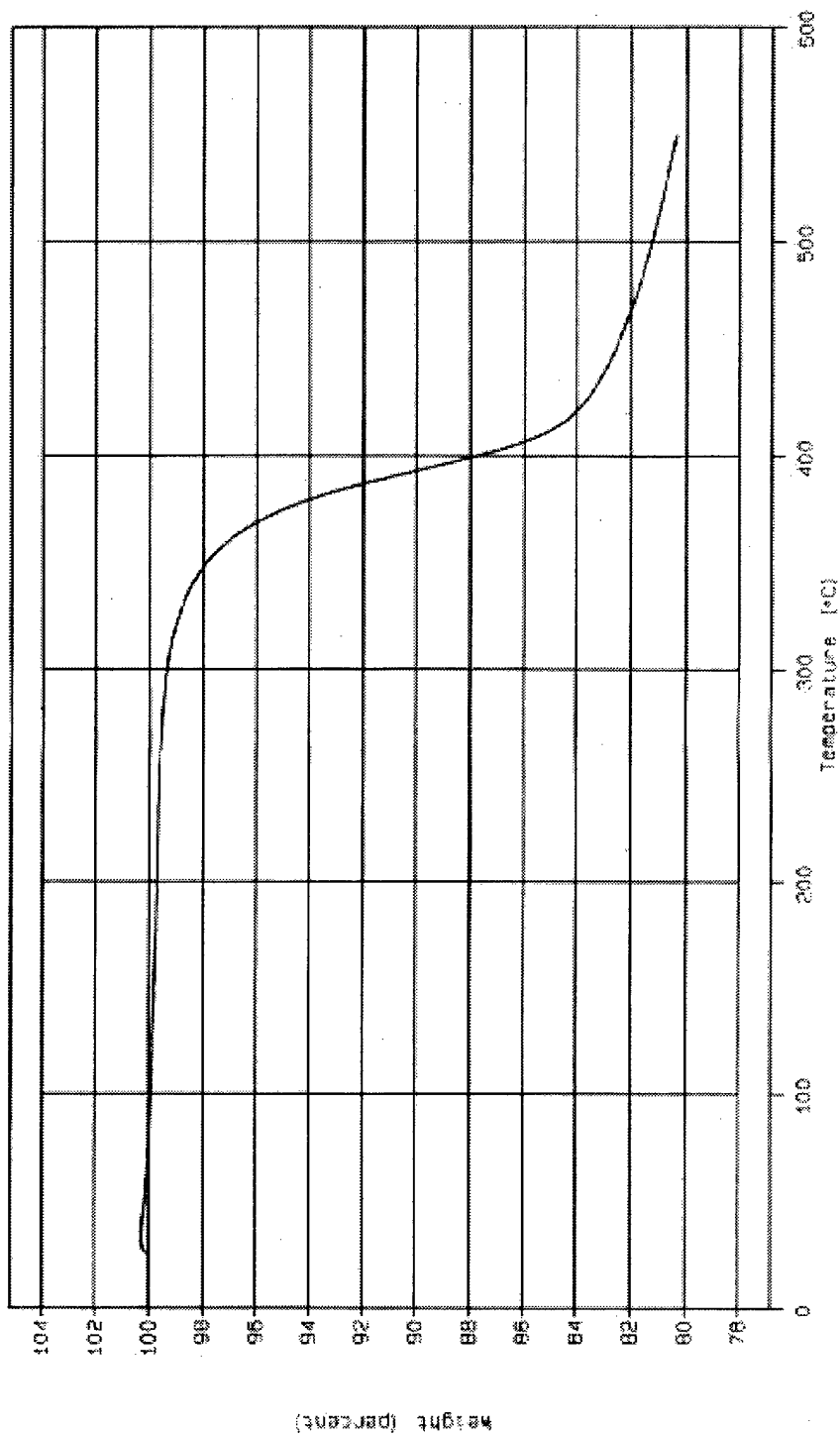
Figure B-51

WEIGHT LOSS MEASUREMENT FROM TGA AS A FUNCTION OF TIME FOR UNDAMAGED 8552 RESIN
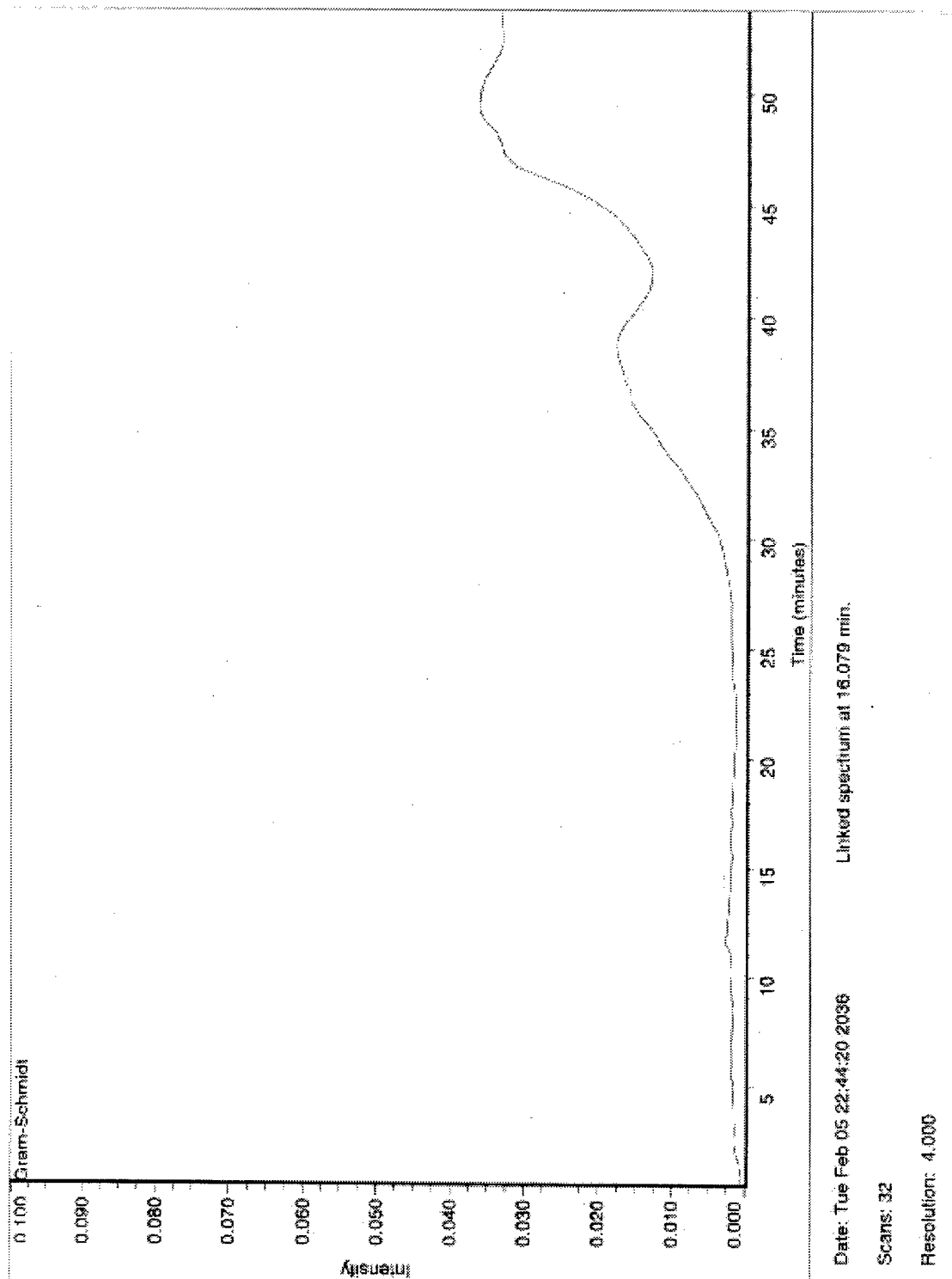
Figure B-52
GRAM-SCHMIDT CHROMATOGRAM FOR UNDAMAGED 8552 RESIN

APPENDIX B
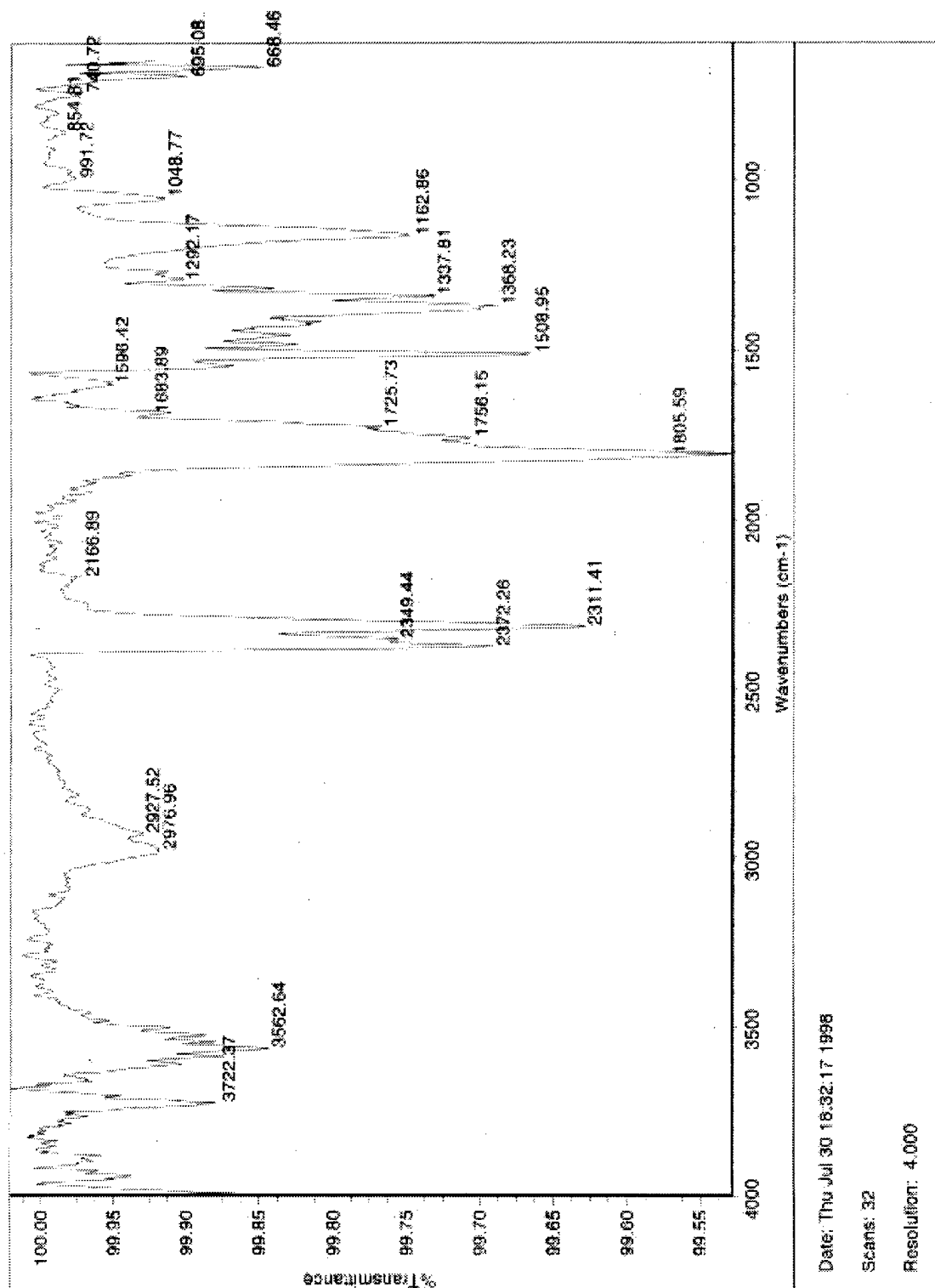
Figure B-53
FTIR SPECTRA COLLECTED AT 290°C

APPENDIX B
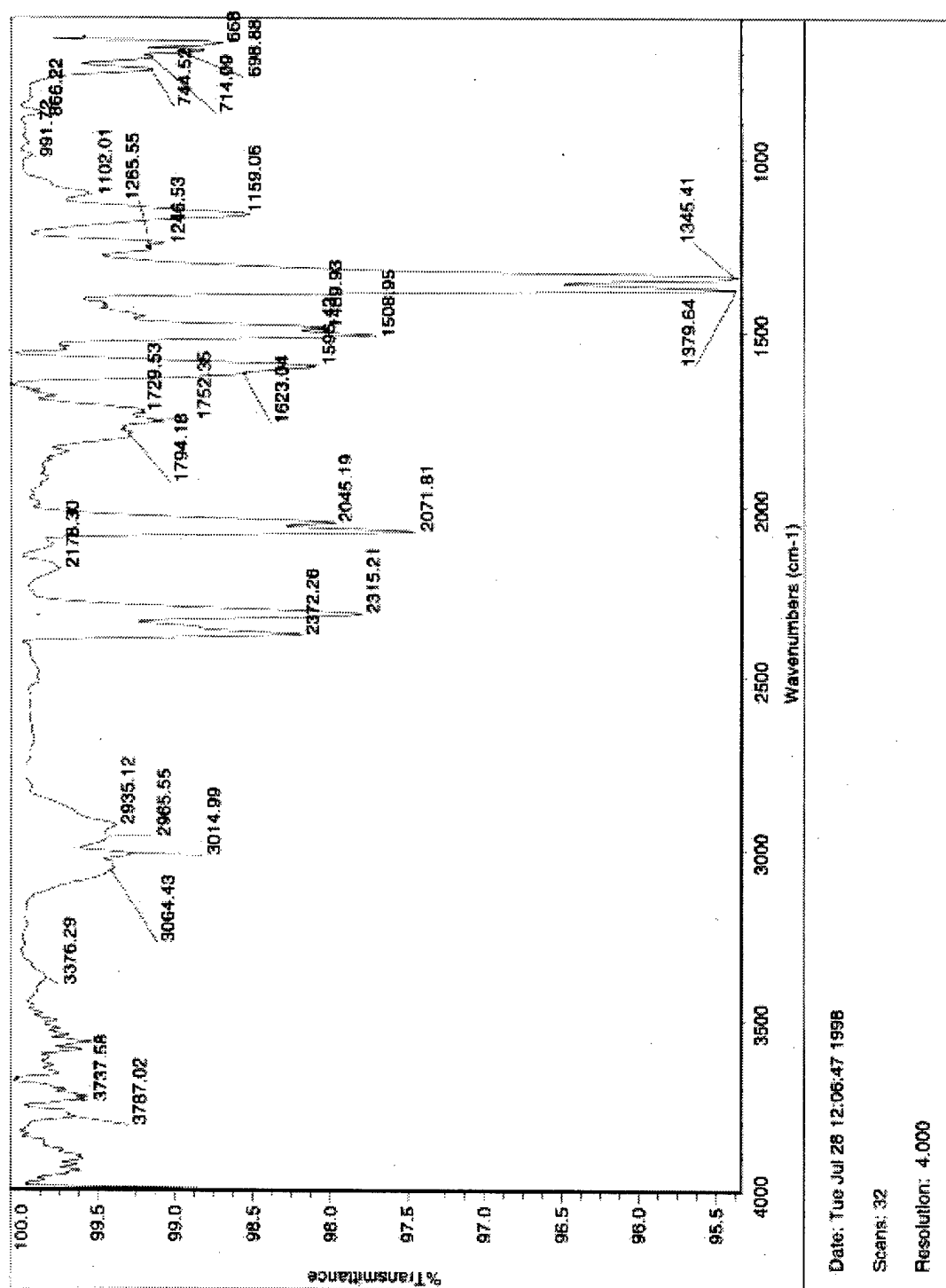
Figure B-54
FTIR SPECTRA COLLECTED AT 350°C
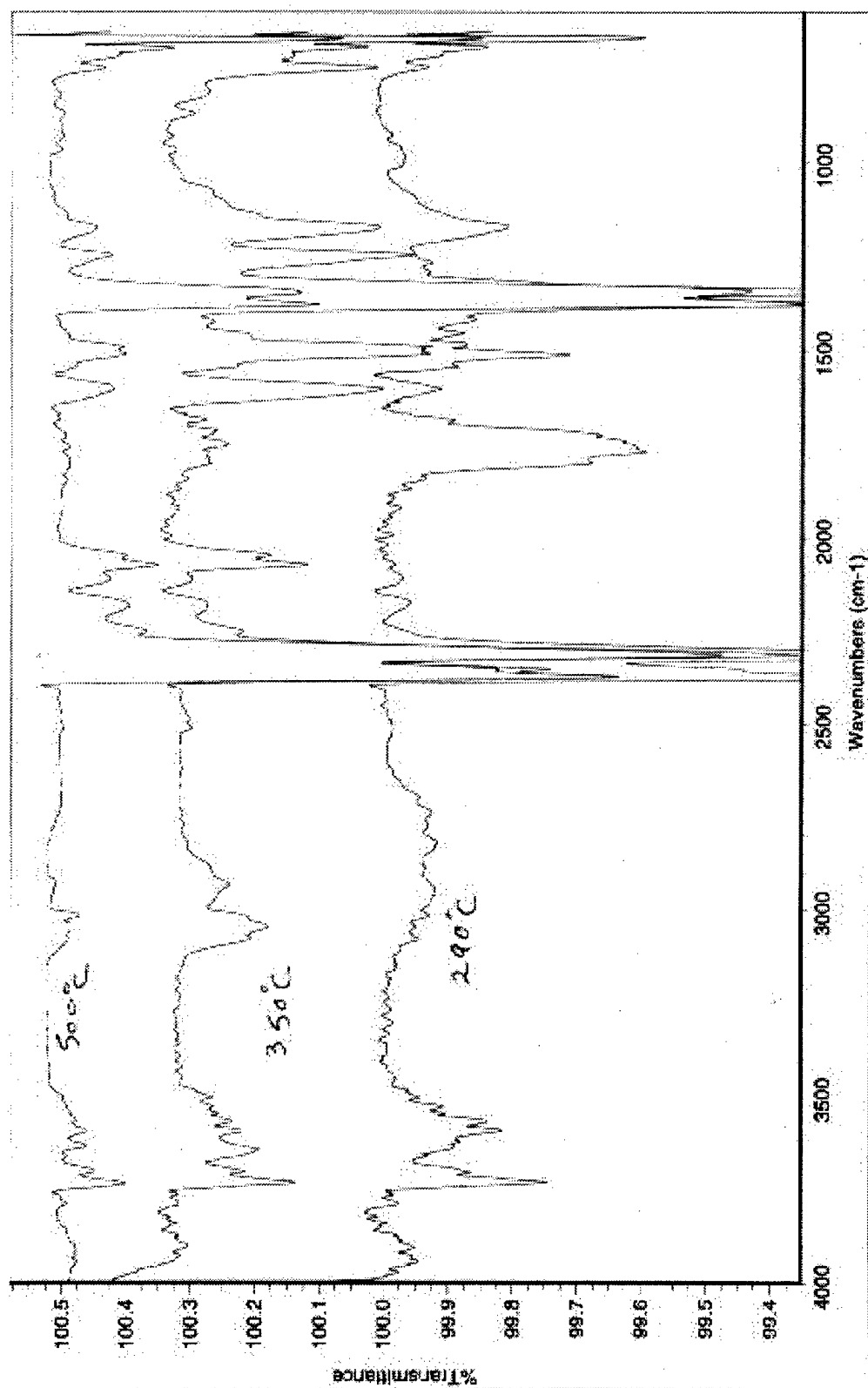
Figure B-55
FTIR SPECTRA COMPARISON OF 8552 EVOLVED GASSES AT DIFFERENT TEMPERATURES
DURING THERMAL DECOMPOSITION

APPENDIX B
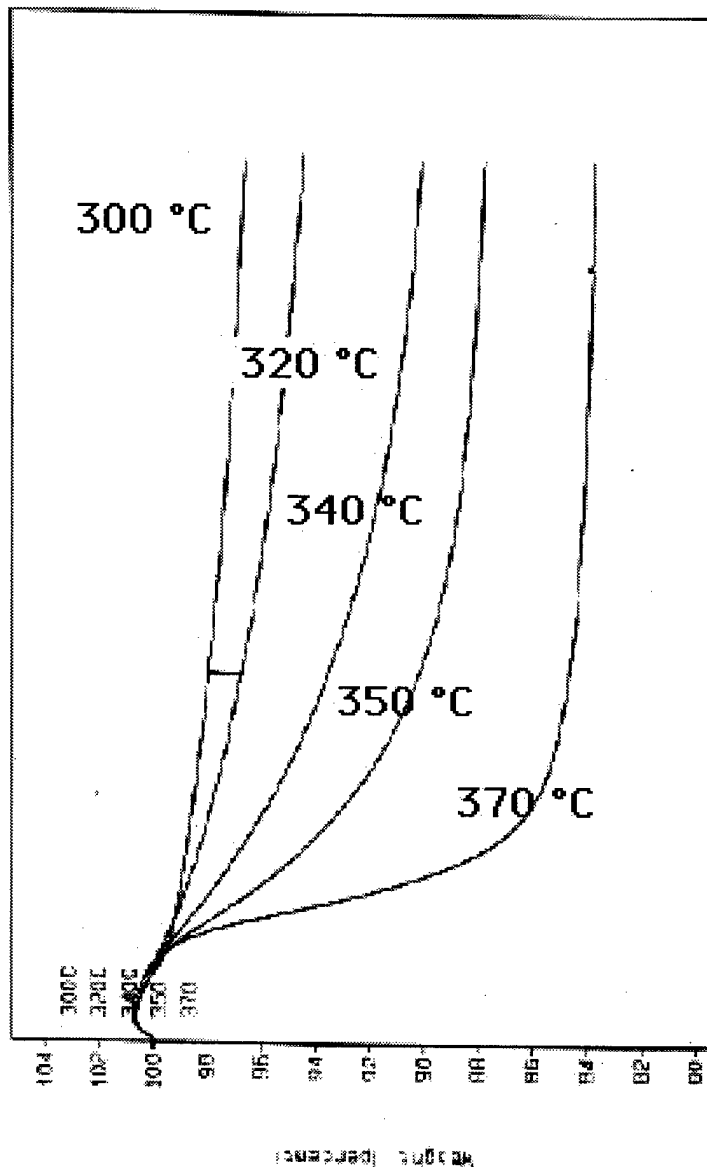
Figure B-56
ISOTHERMAL TGA WEIGHT LOSS RESULTS FOR VARIOUS TEMPERATURES

APPENDIX B
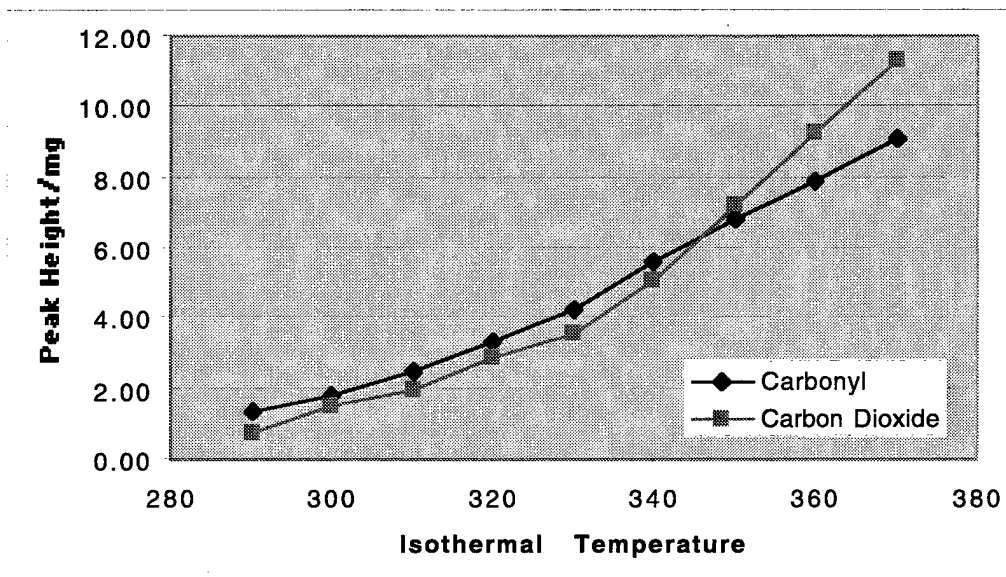
Figure B-57
PEAK HEIGHT OF CARBONYL AND CARBON DIOXIDE VERSUS TEMPERATURE
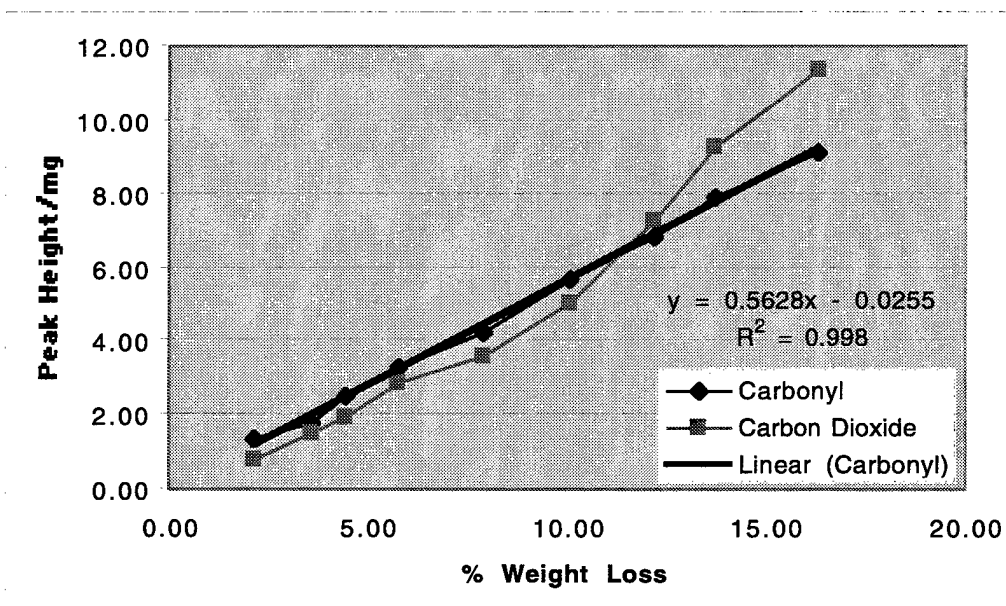
Figure B-58
PEAK HEIGHT OF CARBONYL AND CARBON DIOXIDE VERSUS WEIGHT LOSS
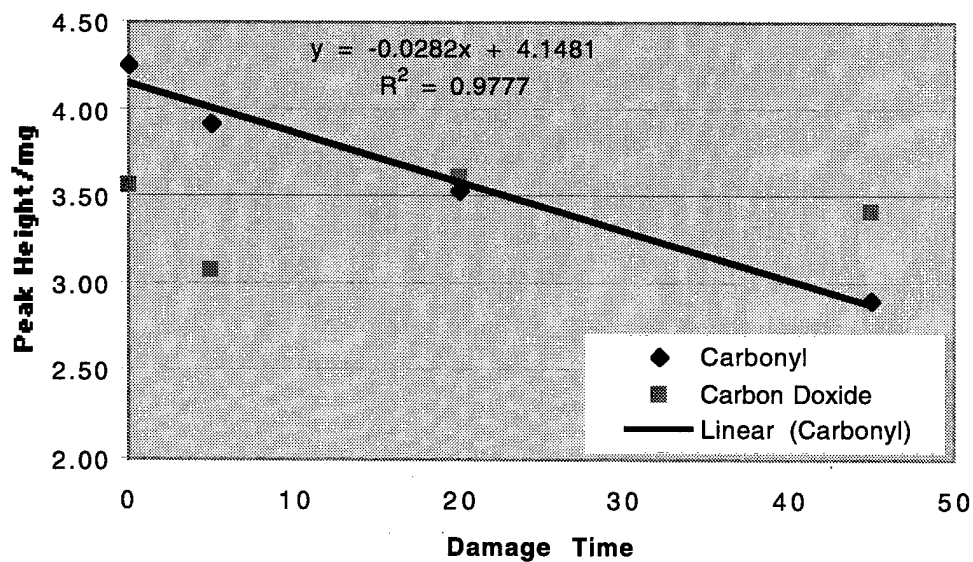
Figure B-59
UNDAMAGED VERSUS 315°C DAMAGED PEAK HEIGHT VERSUS DAMAGE TIME
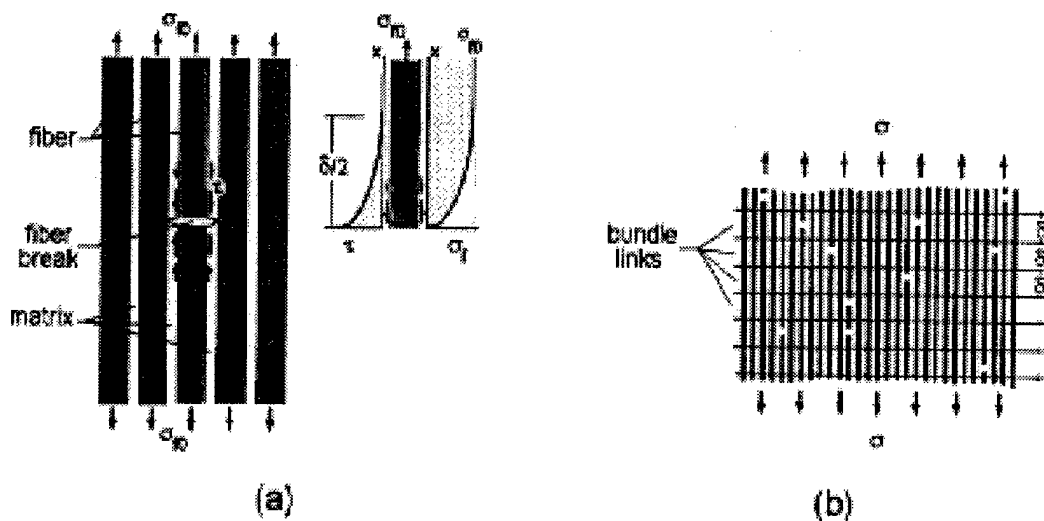
Figure B-60
(a) STRESS DISTRIBUTION NEAR FIBER BREAK (b) CHAIN-OF-BUNDLES MODEL
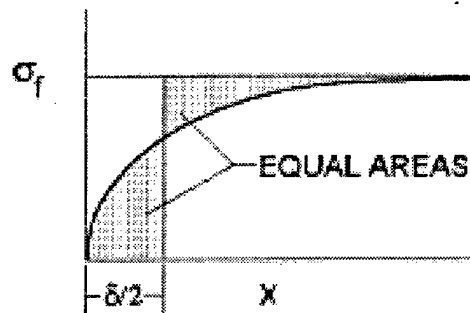
Figure B-61
EQUIVALENT STEP FUNCTION LENGTH FOR δ_E

Figure B-62
BROKEN FIBER IN INTACT FIBER RING SHOWING CRACKED
FIBER/MATRIX INTERFACE OF LENGTH 2a
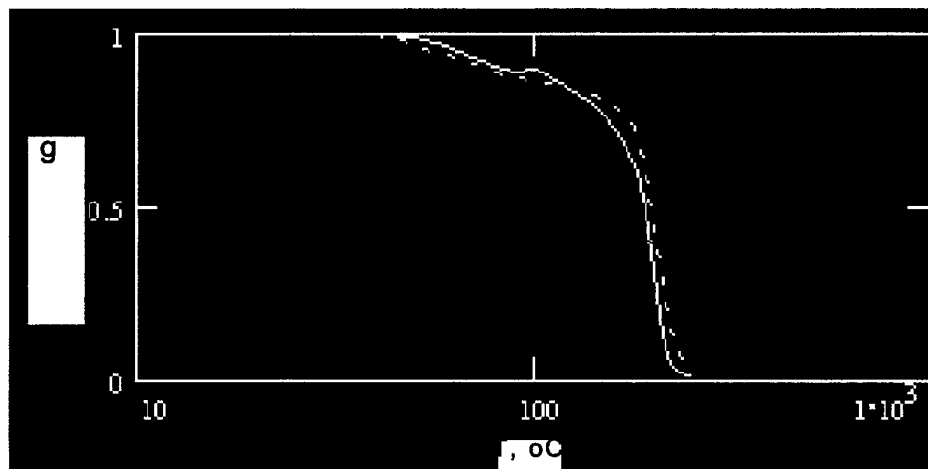
Figure B-63
NONDIMENSIONAL STORAGE MODULUS g AS A FUNCTION OF TEMPERATURE
FOR HERCULES 3501-6 (gh) AND FIBERITE 977-3 (gf)

977-3 Neat Resin
Moisture Condition: Ambient

525 °F - 05 min   525 °F - 20 min   525 °F - 45 min

576 °F - 05 min   576 °F - 20 min   576 °F - 45 min

623 °F - 05 min   623 °F - 20 min   623 °F - 45 min

Total Damage
(Sample Crumbled
Upon Cooling)

* DARKER AREAS ARE MORE DAMAGED
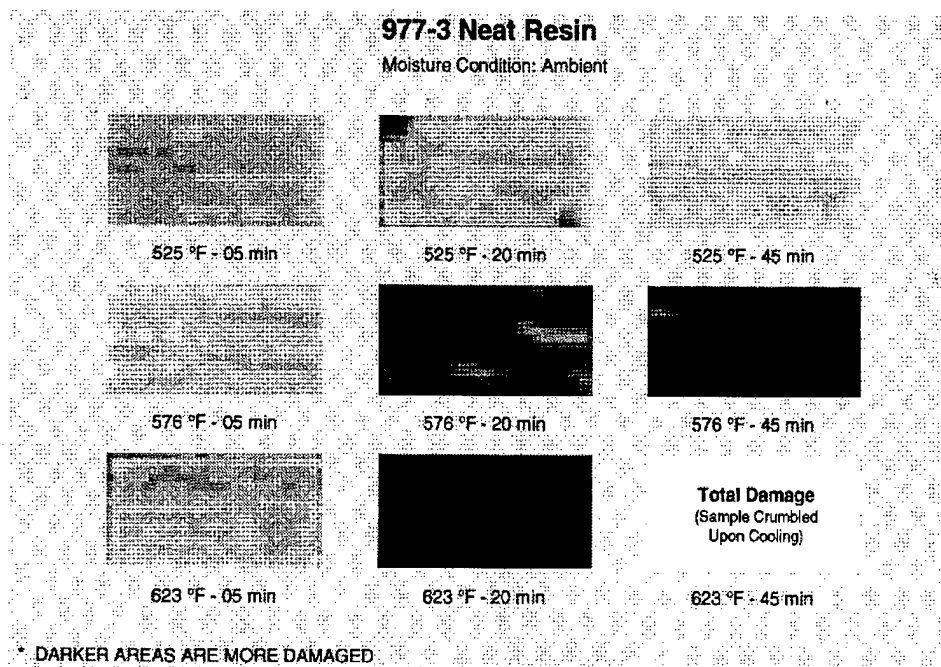
Figure B-64
C-SCANS OF FIBERITE 977-3 NEAT RESIN EPOXY SAMPLES SHOWING EFFECT
OF TEMPERATURE AND TIME AT TEMPERATURE

(a)   (b)
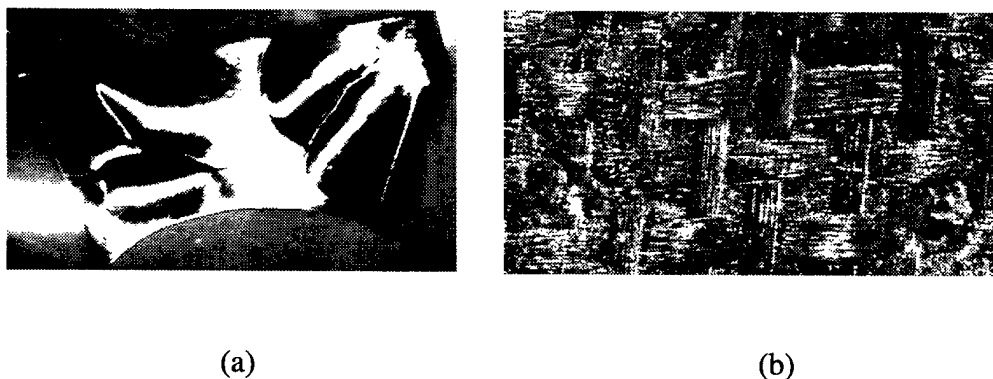
Figure B-65
(a) HEAT-INDUCED CRACKS IN 3501-6 RESIN EXPOSED FOR 15 MIN AT 260°C
(b) OUT-GASSING VENTS IN WOVEN Gr/Ep LAMINATE EXPOSED
FOR 3.3 MIN AT 370°C
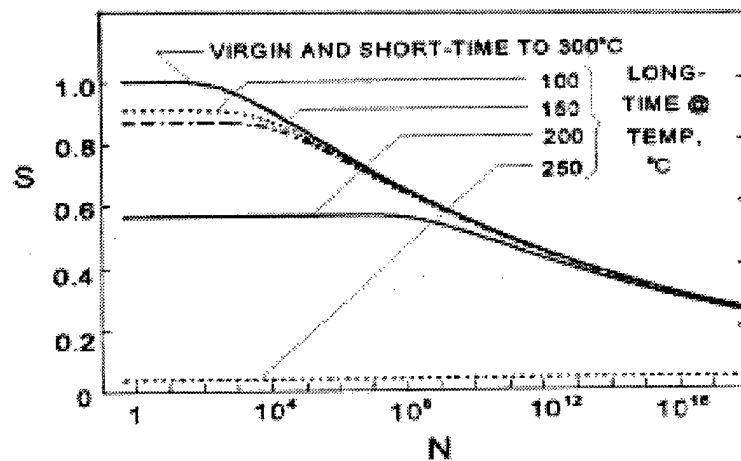
Figure B-66
RESIDUAL NONDIMENSIONAL FATIGUE STRENGTH, S, VERSUS CYCLES, N
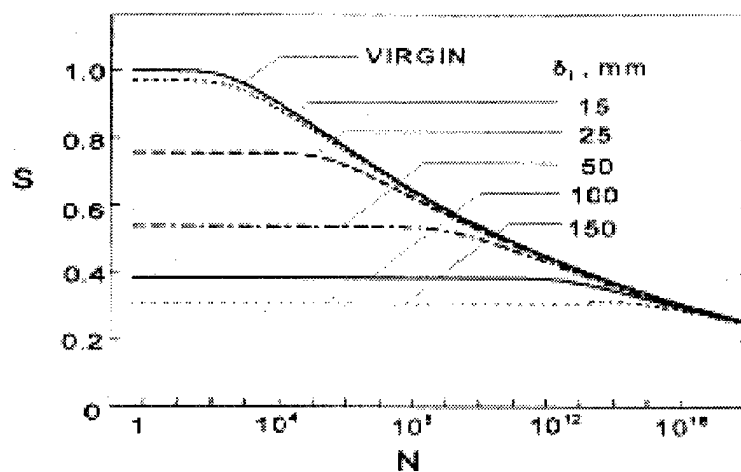
Figure B-67
NONDIMENSIONAL FATIGUE STRENGTH, S, VERSUS CYCLES, N; MATRIX
GONE IN ZONE LENGTH δ_i

THIS PAGE INTENTIONALLY LEFT BLANK
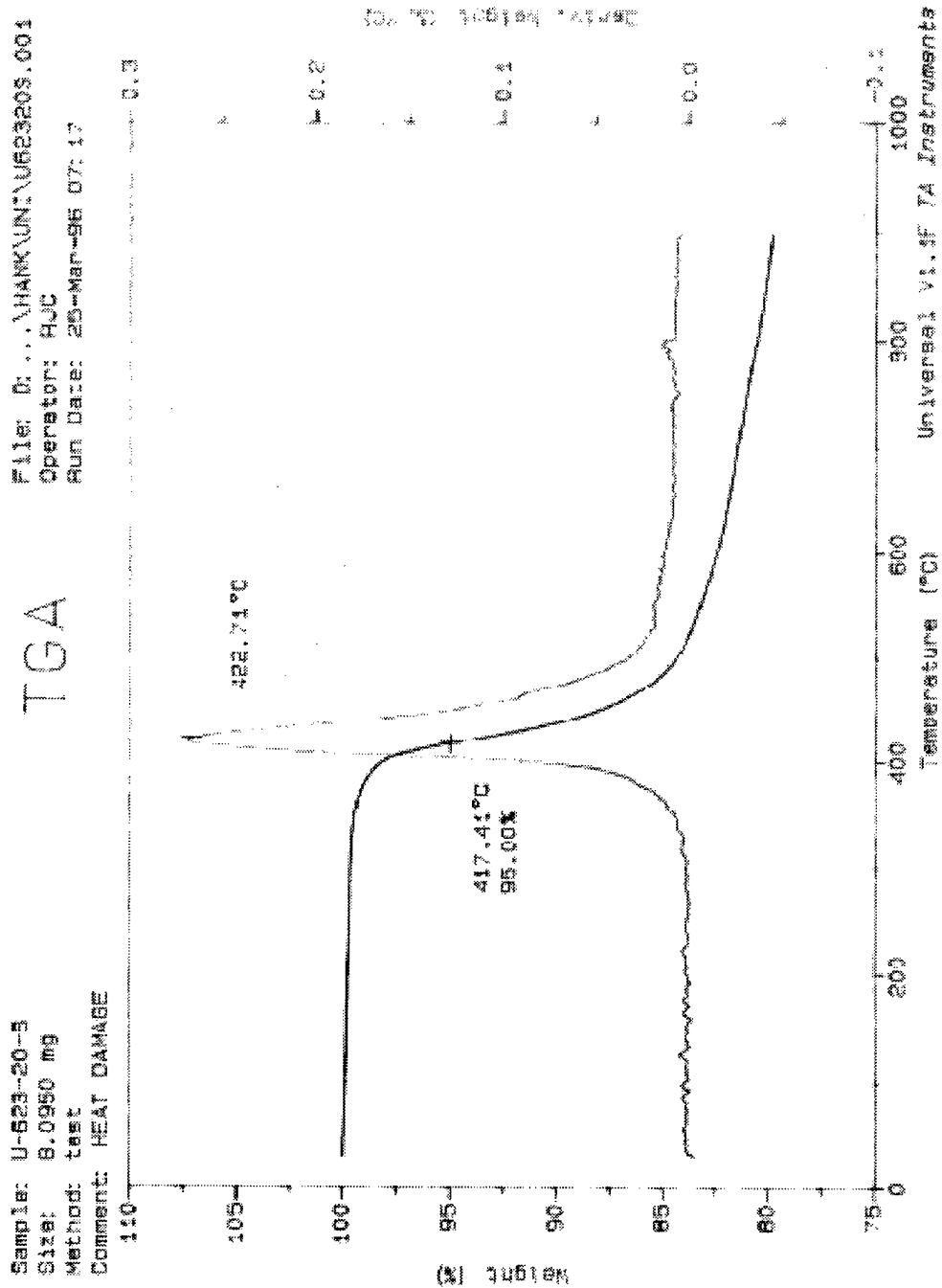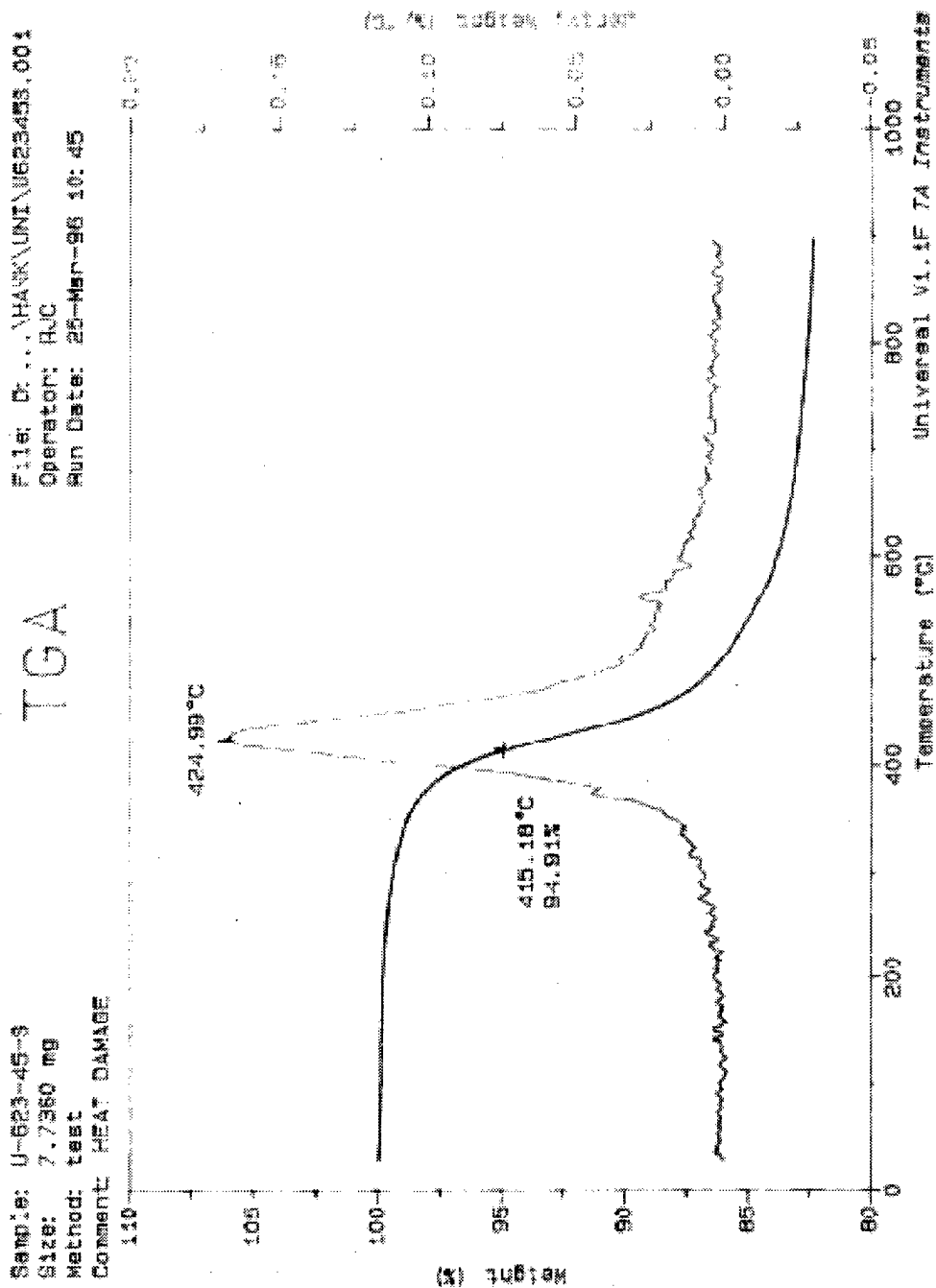
APPENDIX C
THERMAL GRAVIMETRIC ANALYZER PLOTS

APPENDIX C

Figure C-1

TGA RESULTS SHOWING WEIGHT LOSS VERSUS TEMPERATURE OF THE 977-3 NEAT
RESIN SATURATED SAMPLE THAT WAS HEAT DAMAGED AT 274°C FOR 20 MIN

APPENDIX C

Figure C-2

TGA RESULTS SHOWING WEIGHT LOSS VERSUS TEMPERATURE OF THE 977-3 NEAT
RESIN SATURATED SAMPLE THAT WAS HEAT DAMAGED AT 274°C FOR 45 MIN
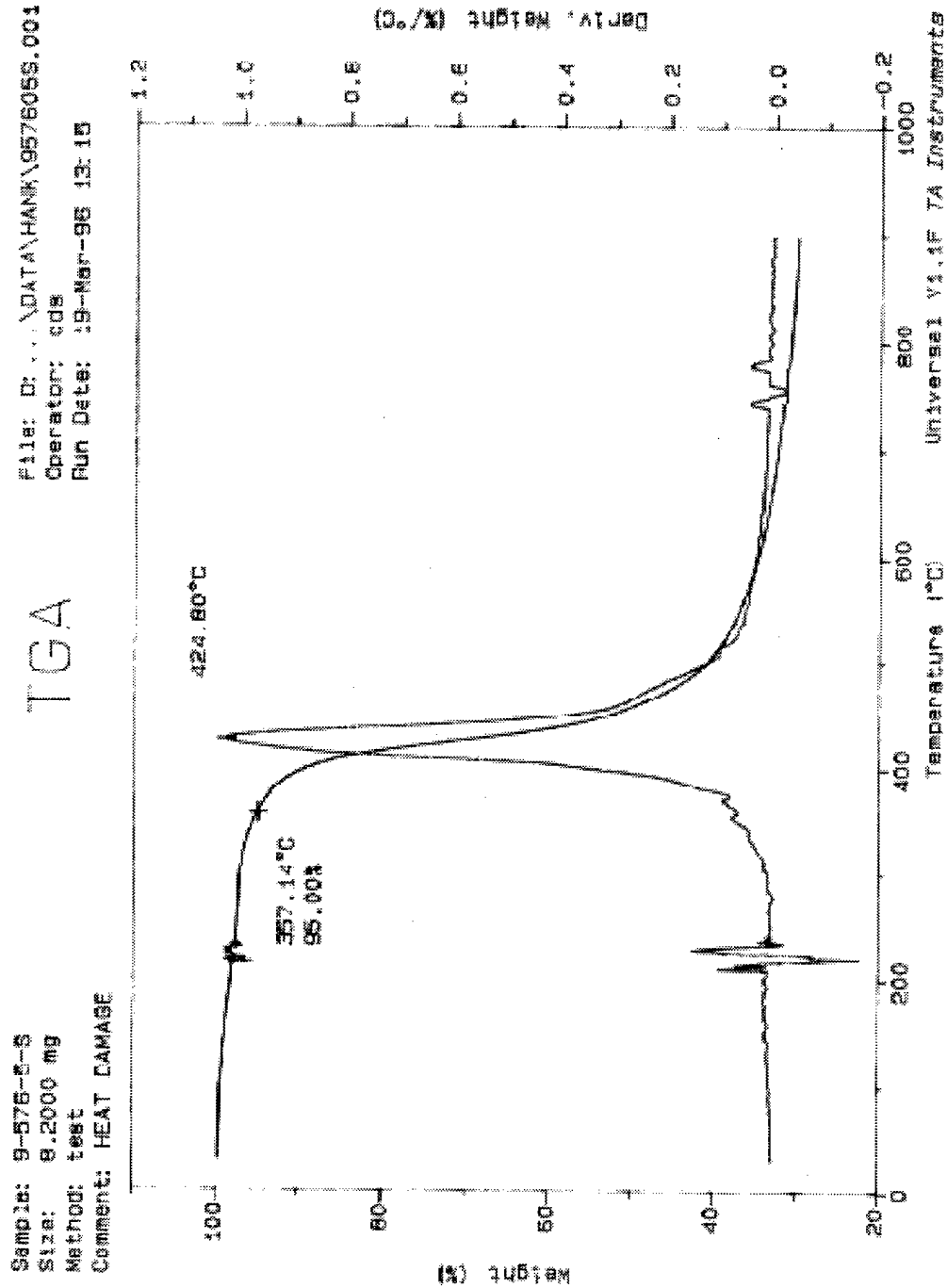
Figure C-3

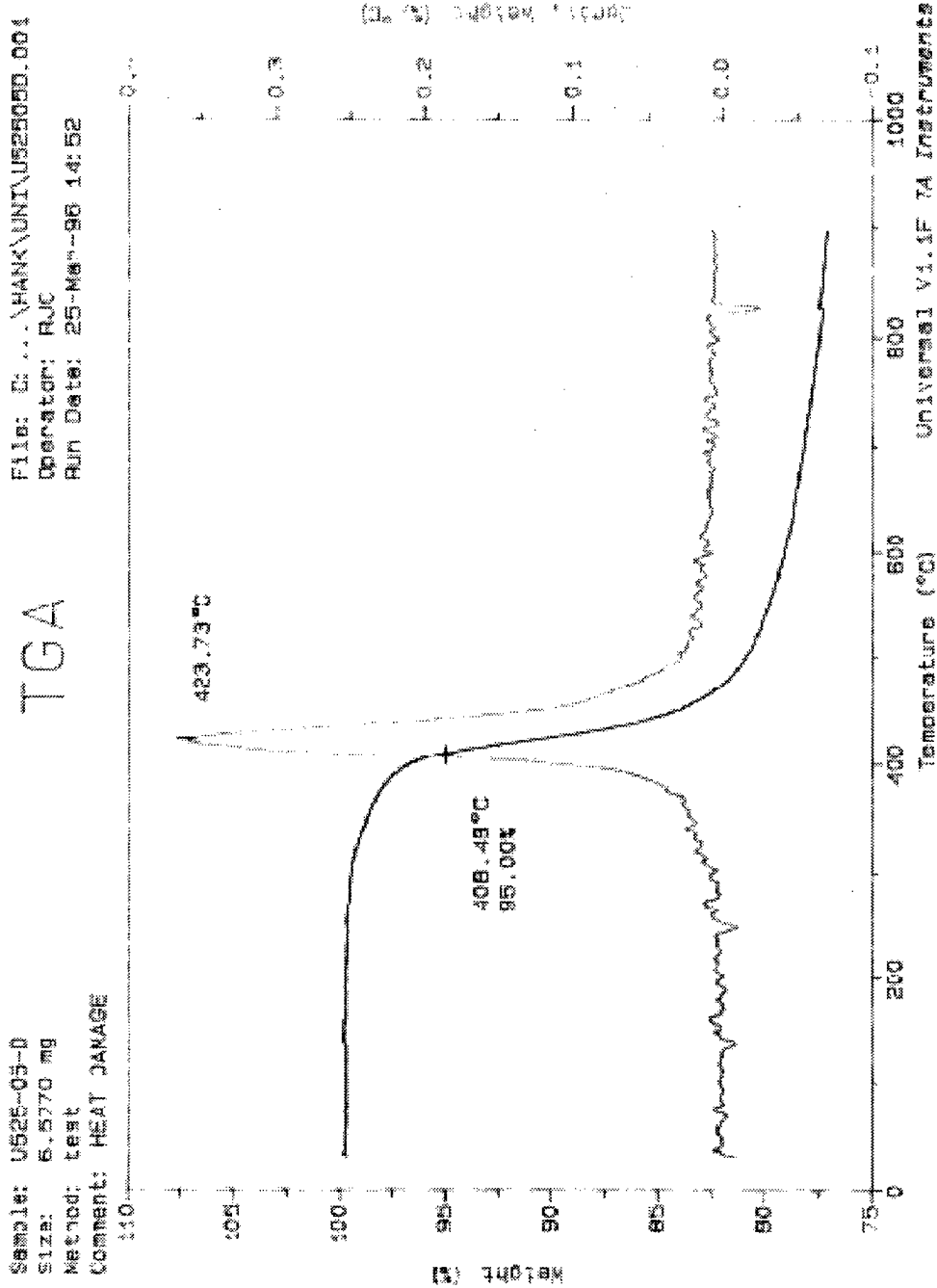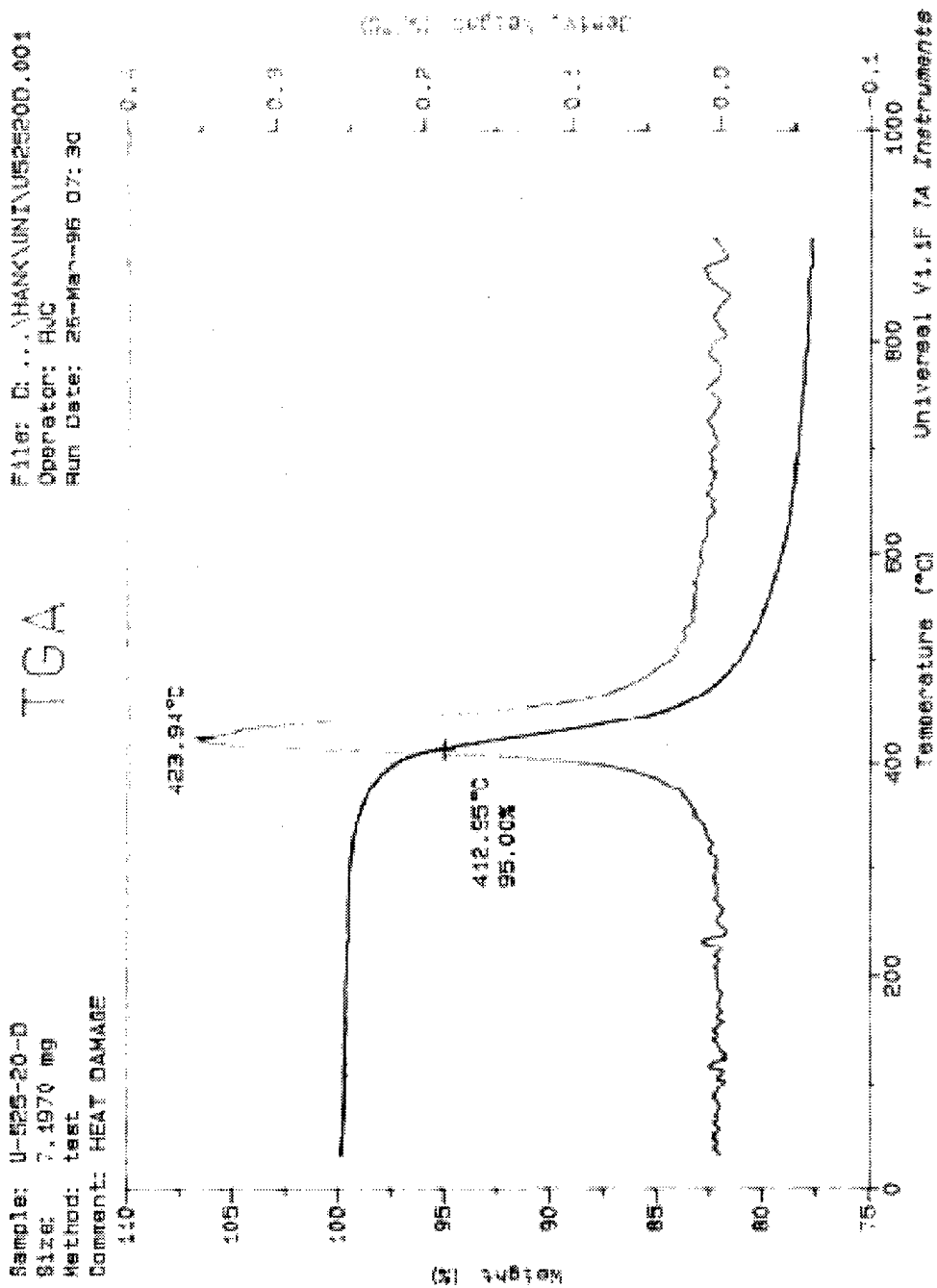TGA RESULTS SHOWING WEIGHT LOSS VERSUS TEMPERATURE OF THE 977-3 NEAT
RESIN SATURATED SAMPLE THAT WAS HEAT DAMAGED AT 302°C FOR 5 MIN

APPENDIX C
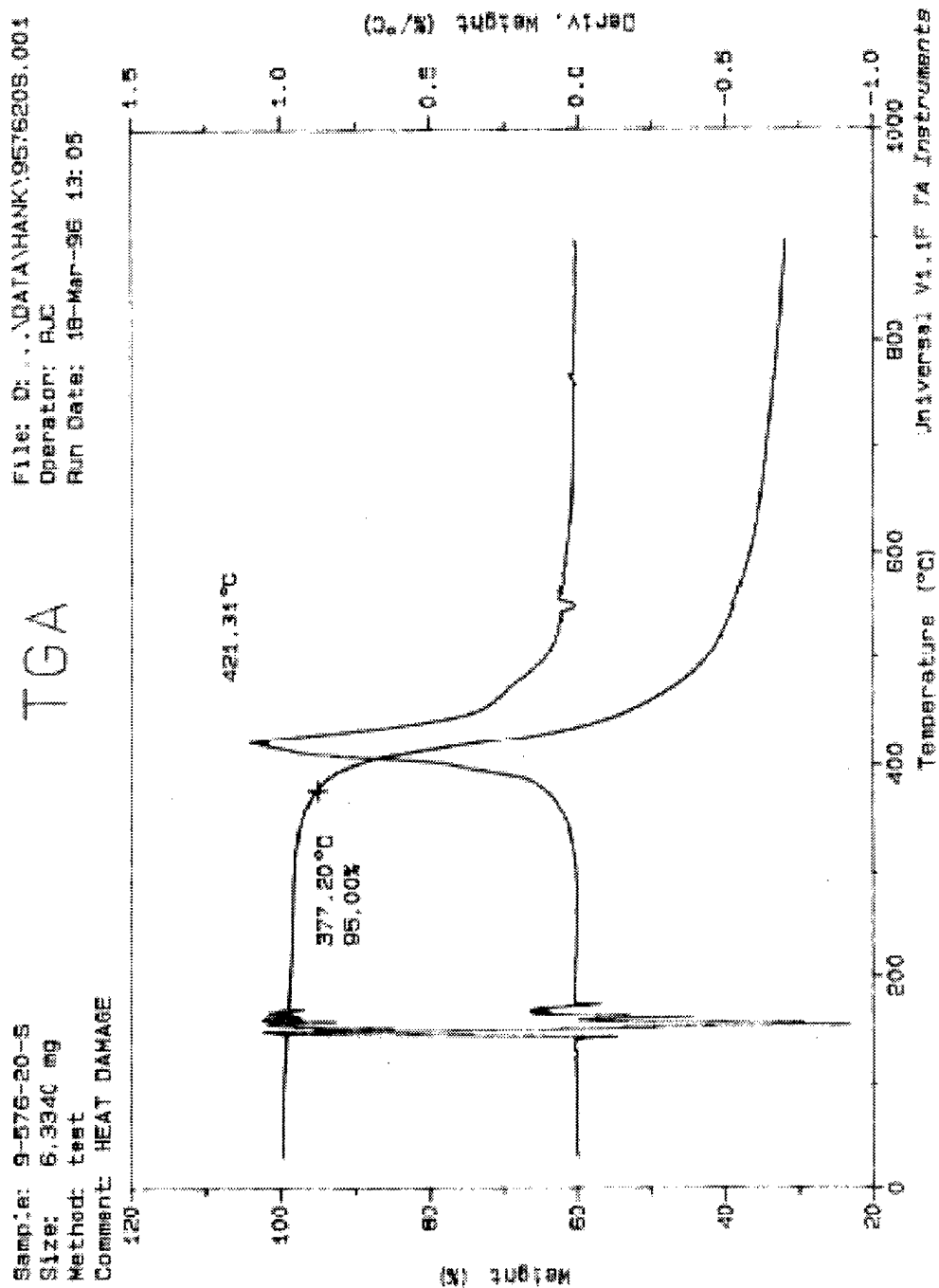
Figure C-4

TGA RESULTS SHOWING WEIGHT LOSS VERSUS TEMPERATURE OF THE 977-3 NEAT RESIN SATURATED SAMPLE THAT WAS HEAT DAMAGED AT 302°C FOR 20 MIN

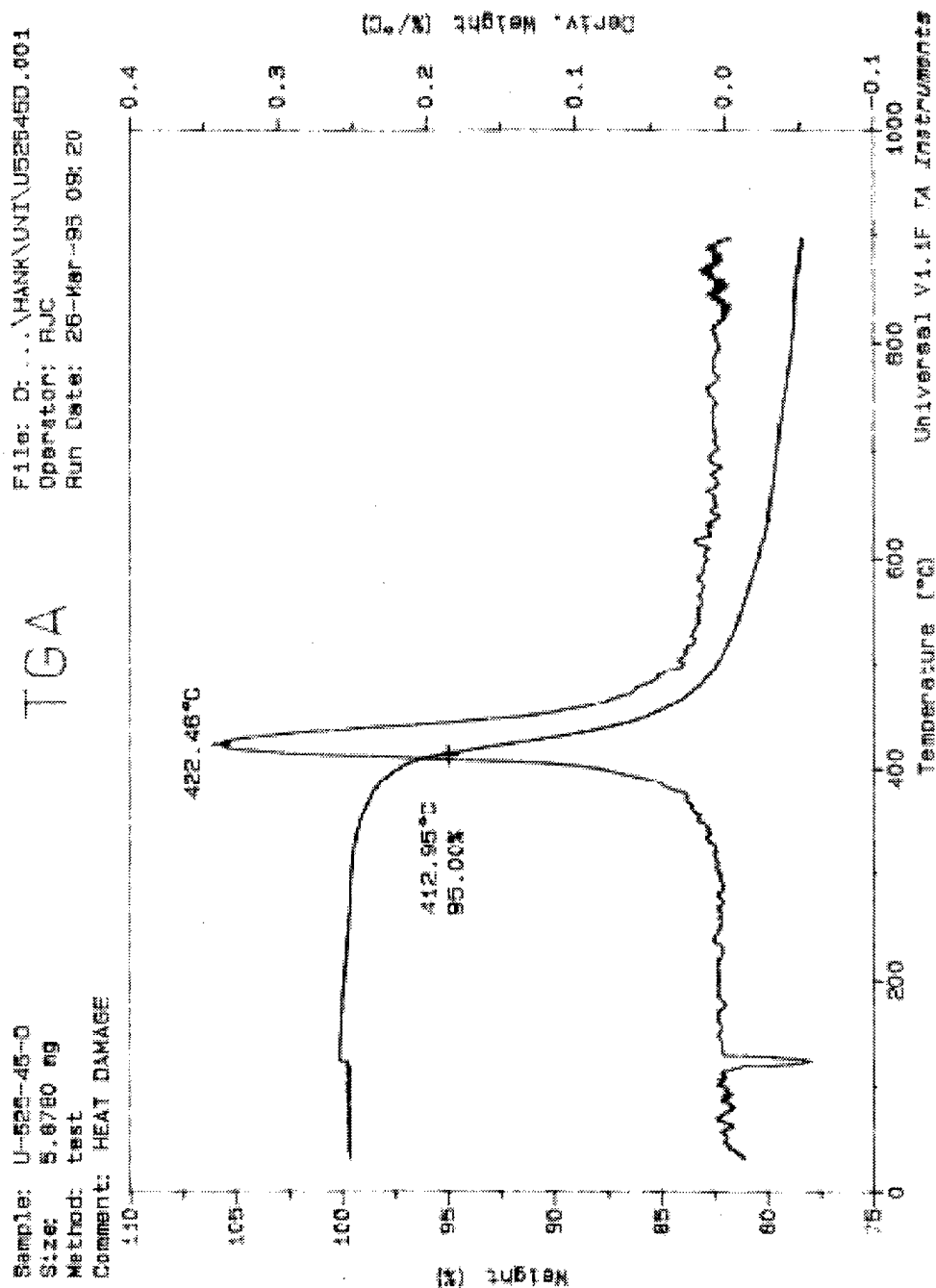103   **APPENDIX C**
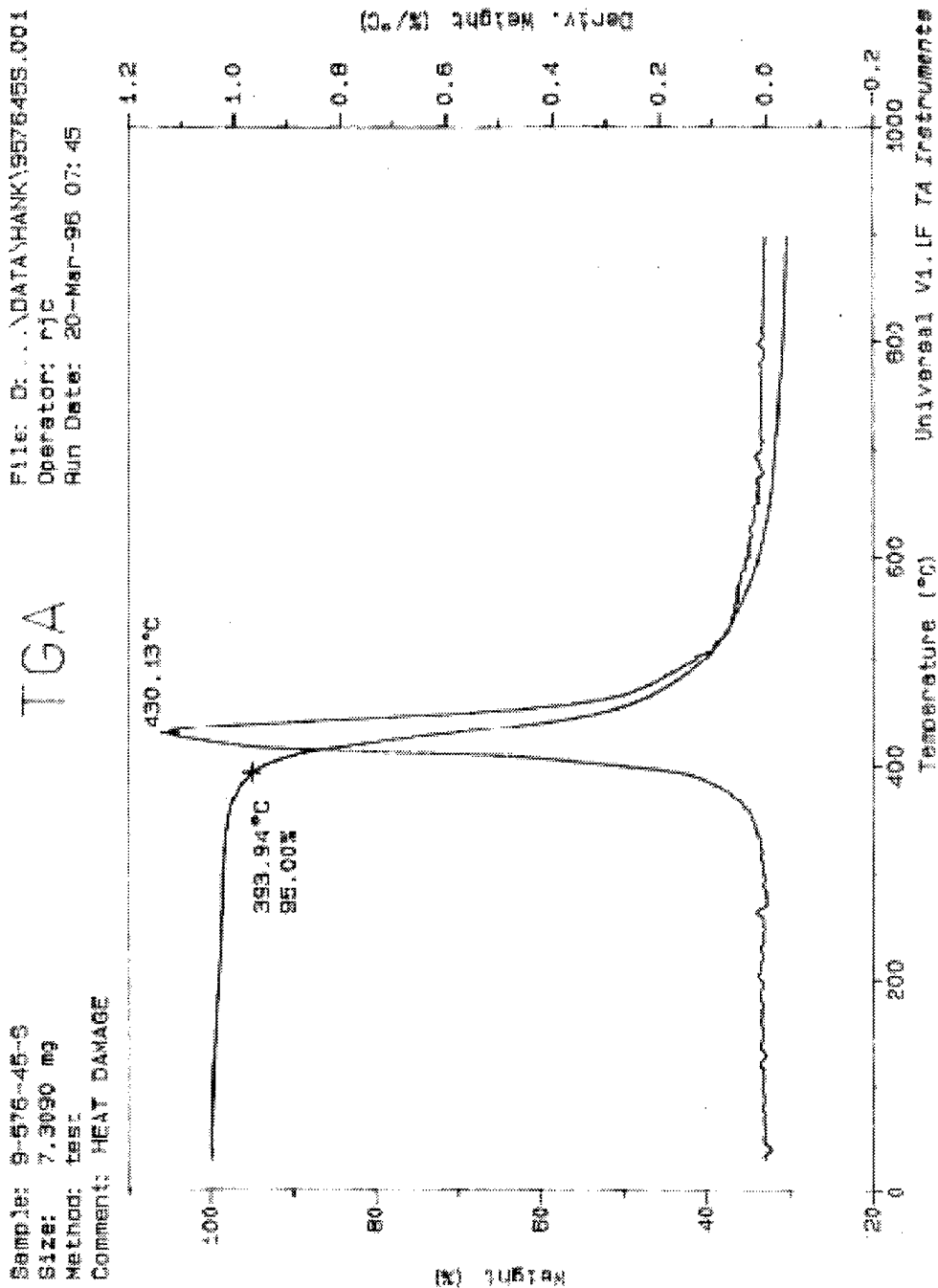
Figure C-5

TGA RESULTS SHOWING WEIGHT LOSS VERSUS TEMPERATURE OF THE 977-3 NEAT
RESIN SATURATED SAMPLE THAT WAS HEAT DAMAGED AT 302°C FOR 45 MIN

APPENDIX C
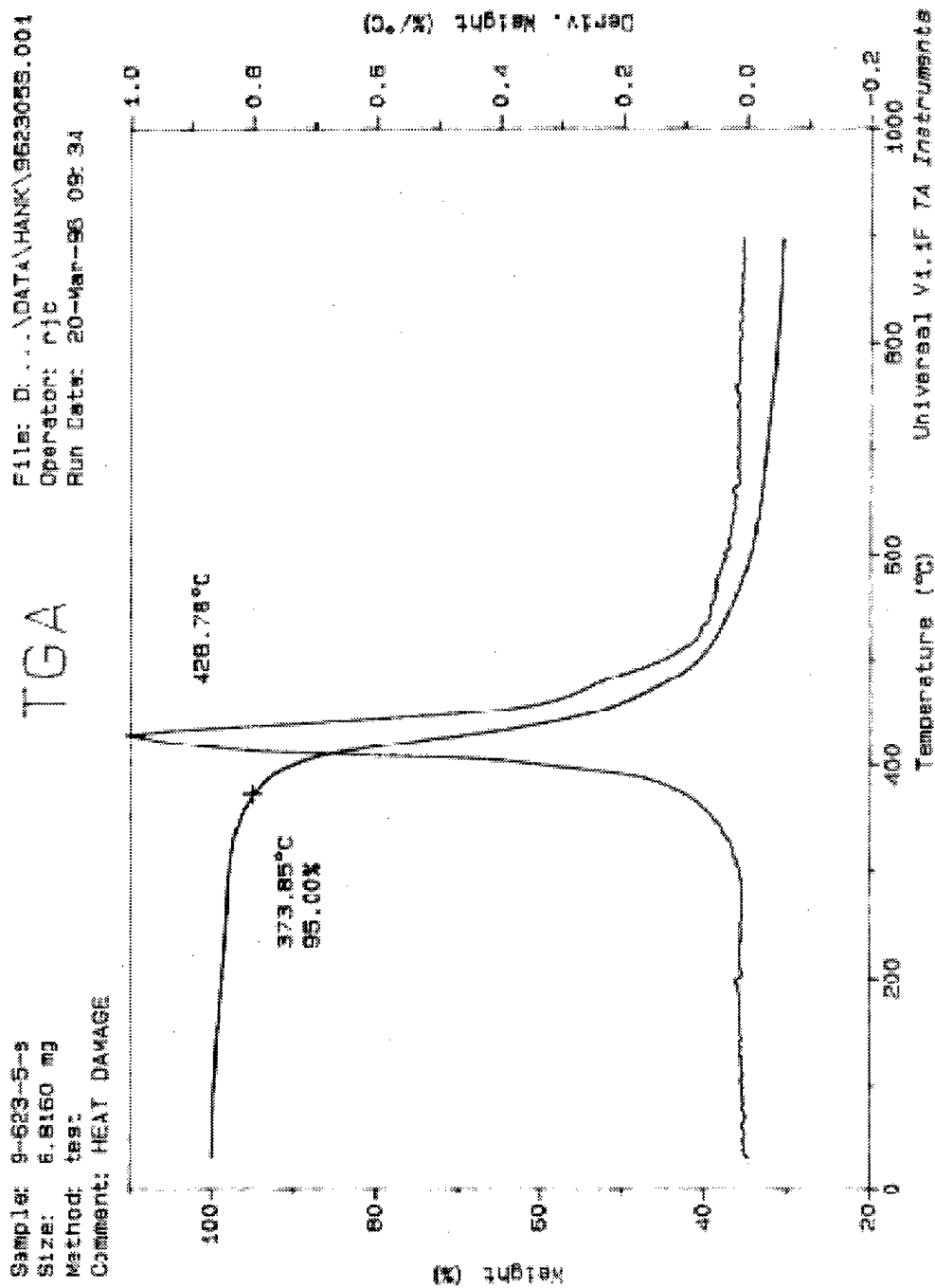
Figure C-6

TGA RESULTS SHOWING WEIGHT LOSS VERSUS TEMPERATURE OF THE 977-3 NEAT RESIN SATURATED SAMPLE THAT WAS HEAT DAMAGED AT 329°C FOR 5 MIN
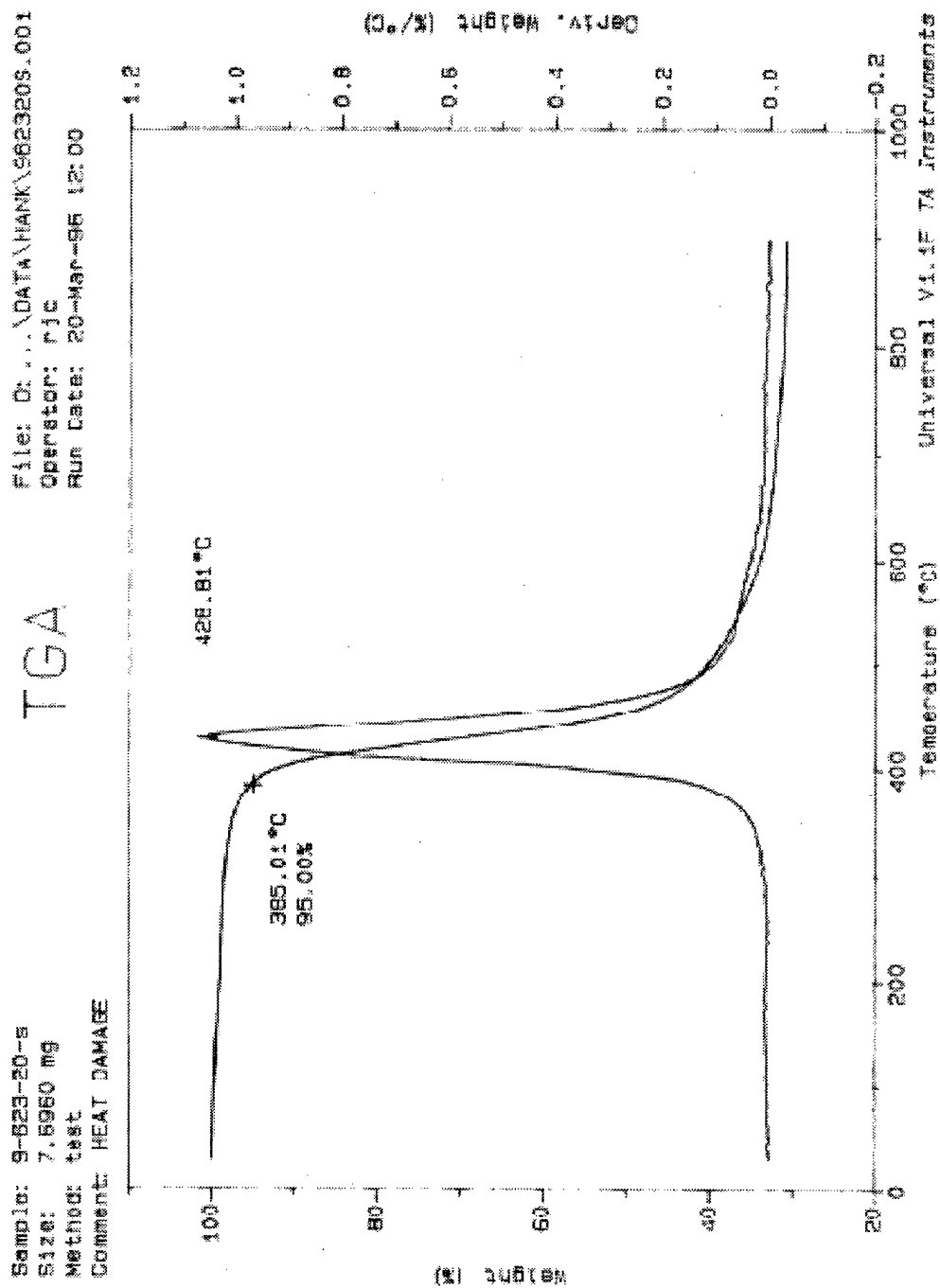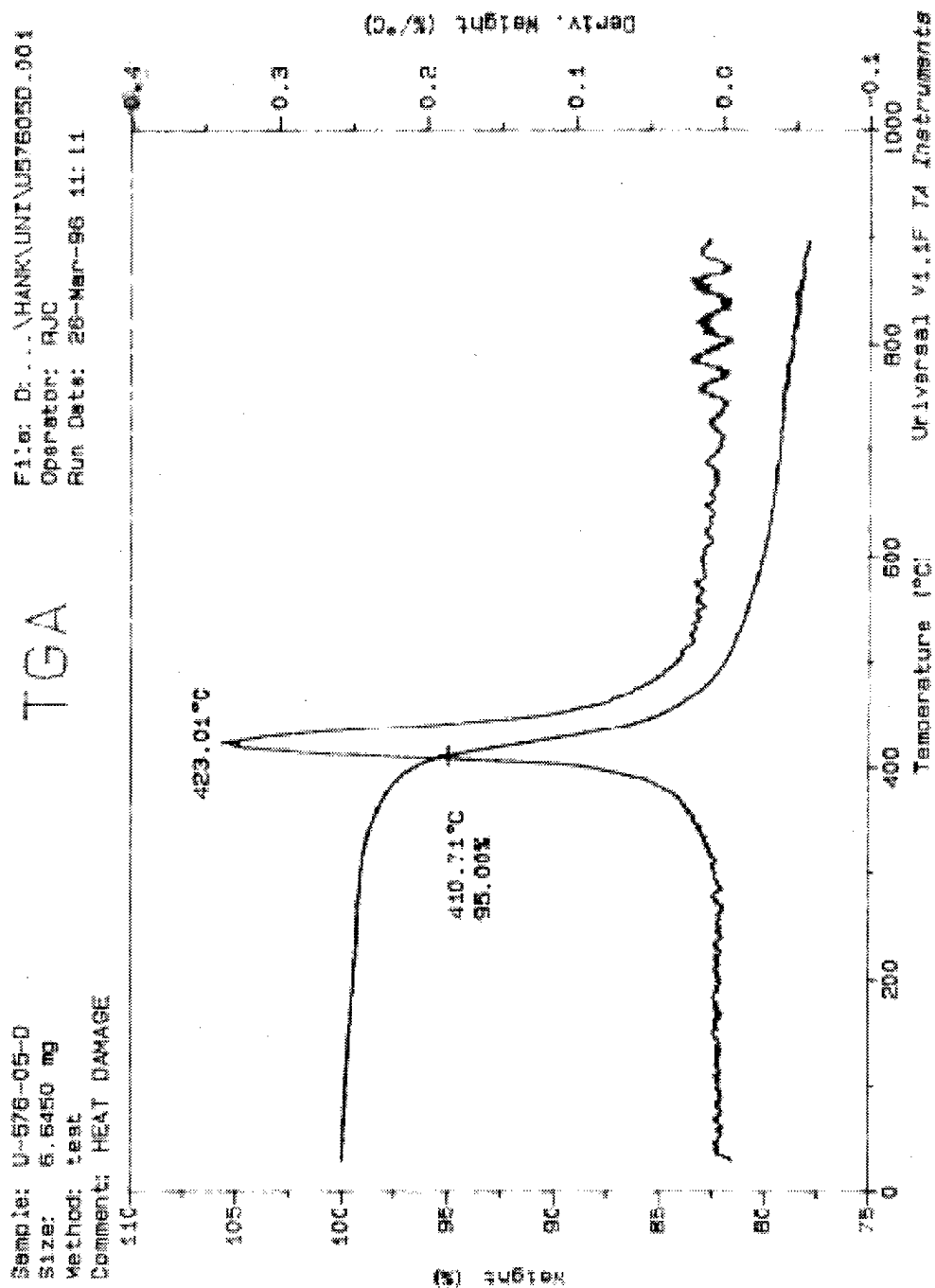
Figure C-7

TGA RESULTS SHOWING WEIGHT LOSS VERSUS TEMPERATURE OF THE 977-3 NEAT
RESIN SATURATED SAMPLE THAT WAS HEAT DAMAGED AT 329°C FOR 20 MIN

APPENDIX C
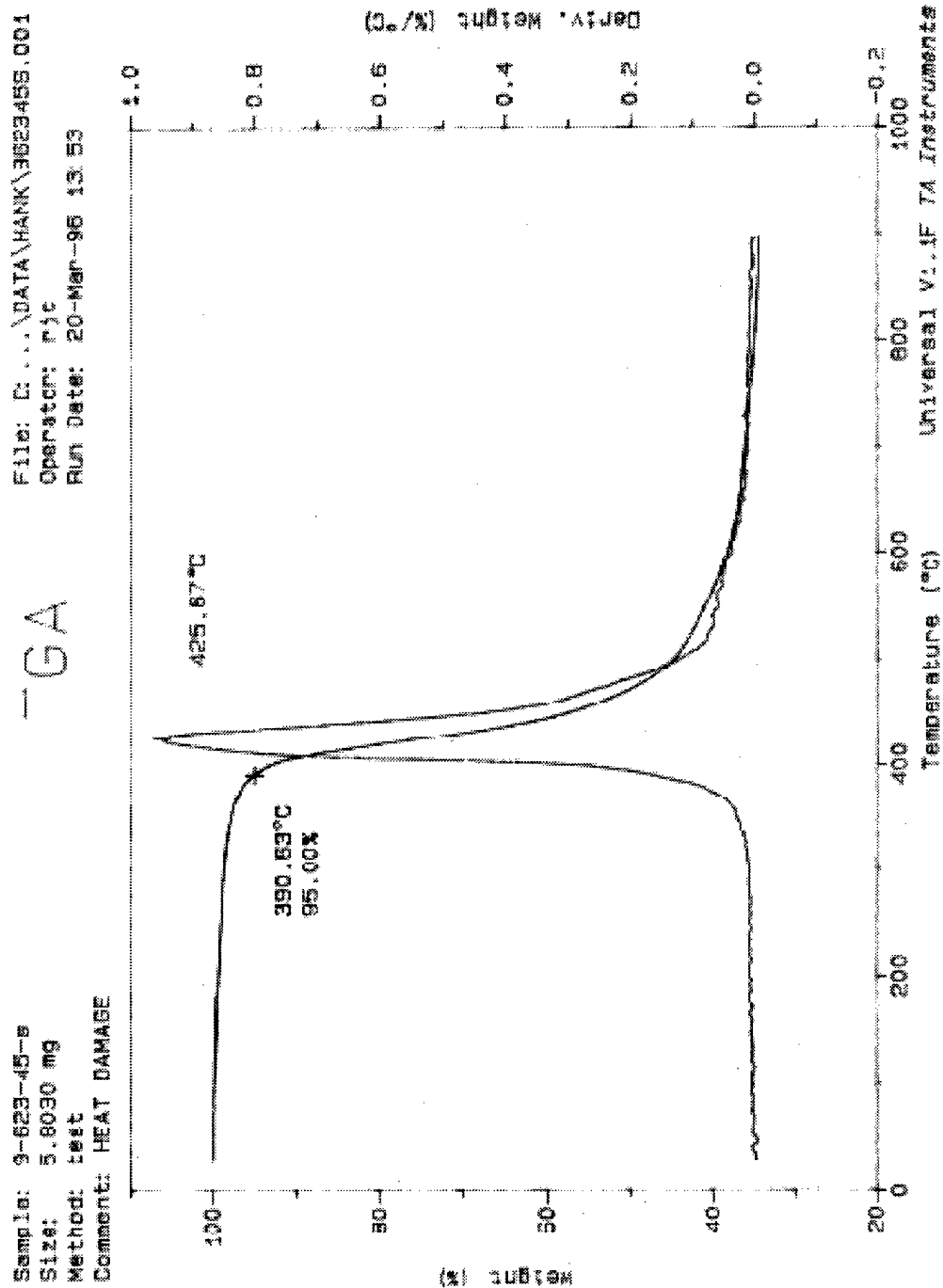
Figure C-8

TGA RESULTS SHOWING WEIGHT LOSS VERSUS TEMPERATURE OF THE 977-3 NEAT
RESIN SATURATED SAMPLE THAT WAS HEAT DAMAGED AT 329°C FOR 45 MIN
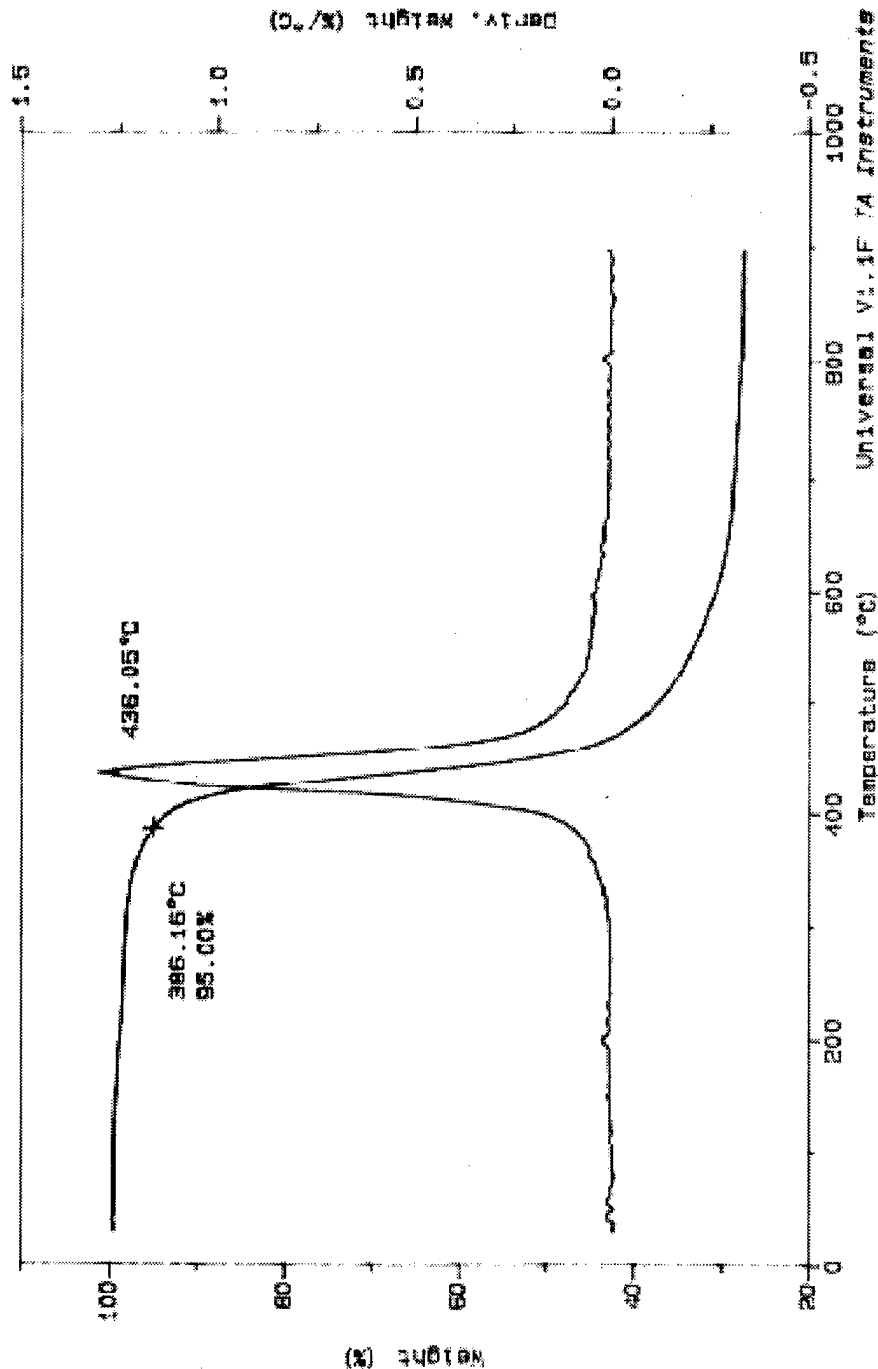
Figure C-9

TGA RESULTS SHOWING WEIGHT LOSS VERSUS TEMPERATURE OF THE 977-3 NEAT
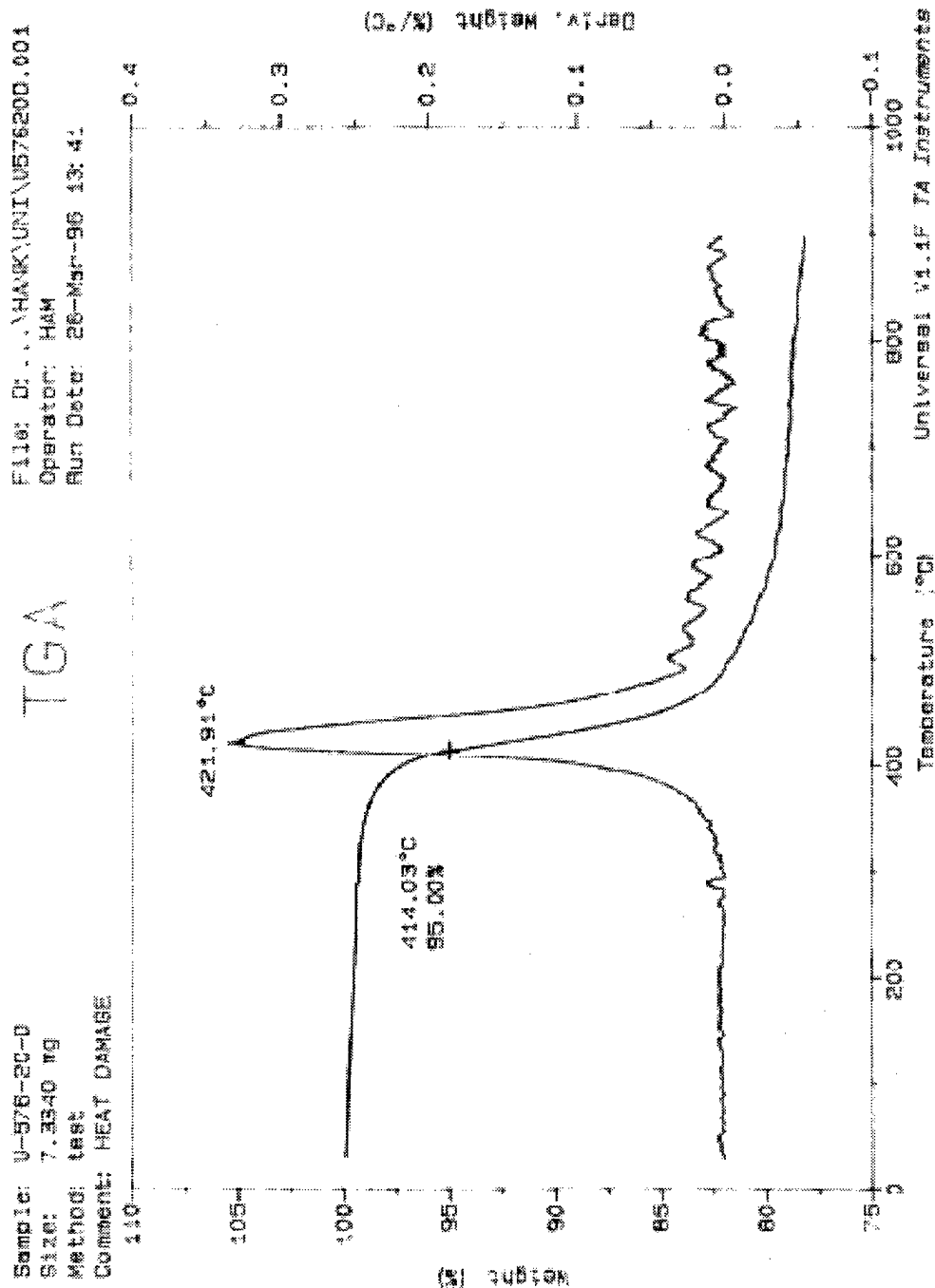RESIN DRY SAMPLE THAT WAS HEAT DAMAGED AT 274°C FOR 5 MIN
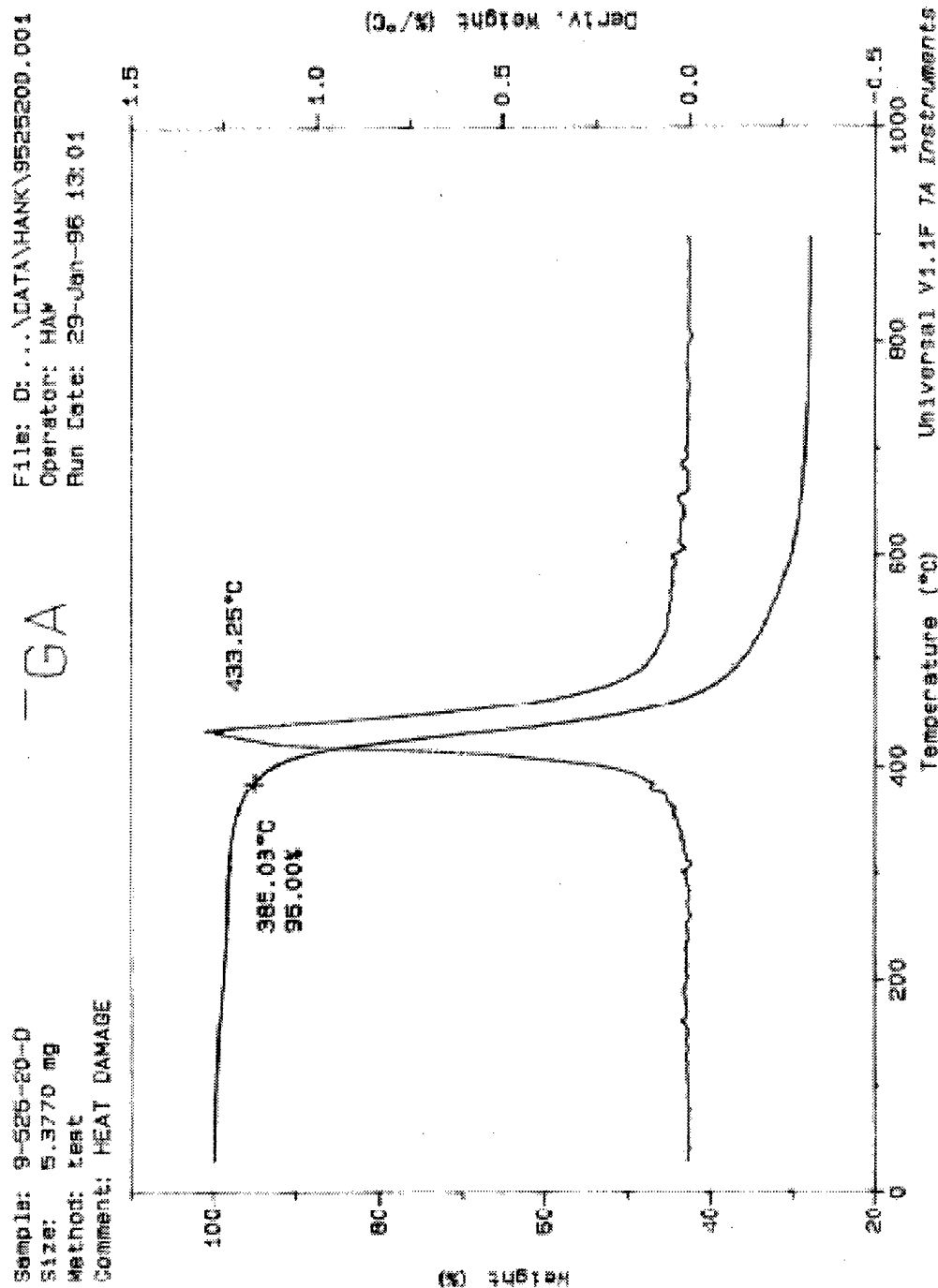
Figure C-10

TGA RESULTS SHOWING WEIGHT LOSS VERSUS TEMPERATURE OF THE 977-3 NEAT
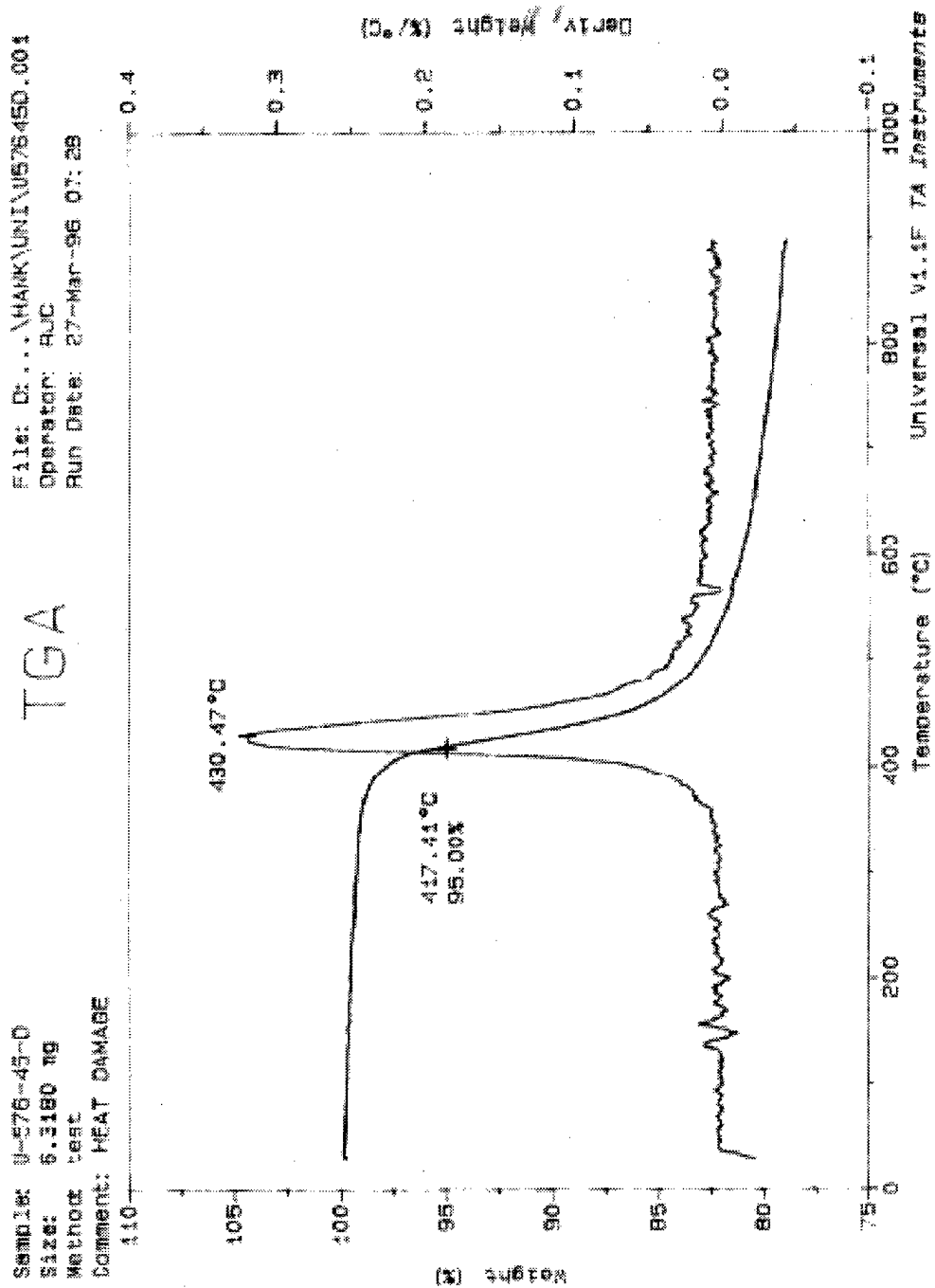RESIN DRY SAMPLE THAT WAS HEAT DAMAGED AT 274°C FOR 20 MIN
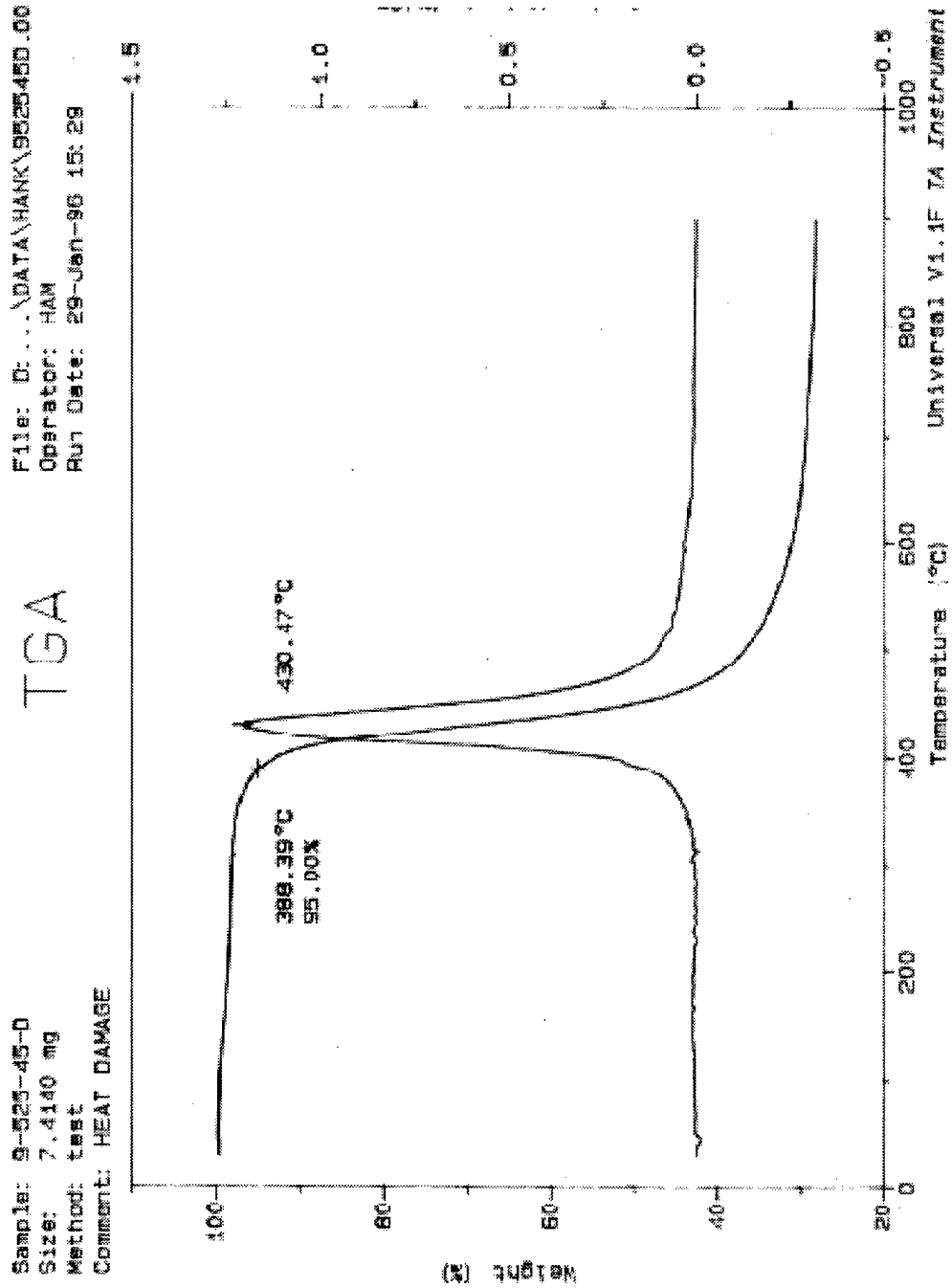
Figure C-11

TGA RESULTS SHOWING WEIGHT LOSS VERSUS TEMPERATURE OF THE 977-3 NEAT
RESIN DRY SAMPLE THAT WAS HEAT DAMAGED AT 274°C FOR 45 MIN
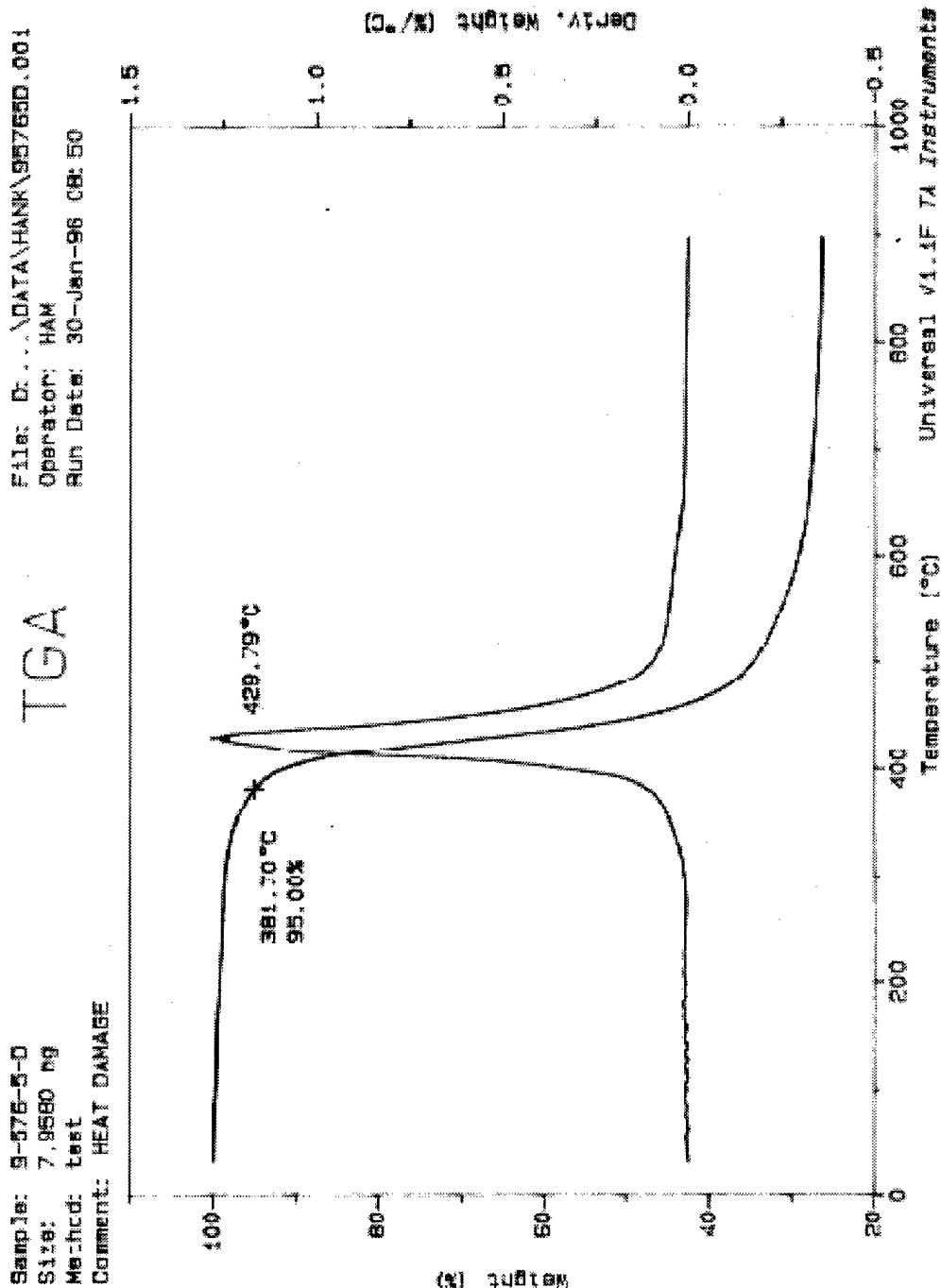
Figure C-12

TGA RESULTS SHOWING WEIGHT LOSS VERSUS TEMPERATURE OF THE 977-3 NEAT
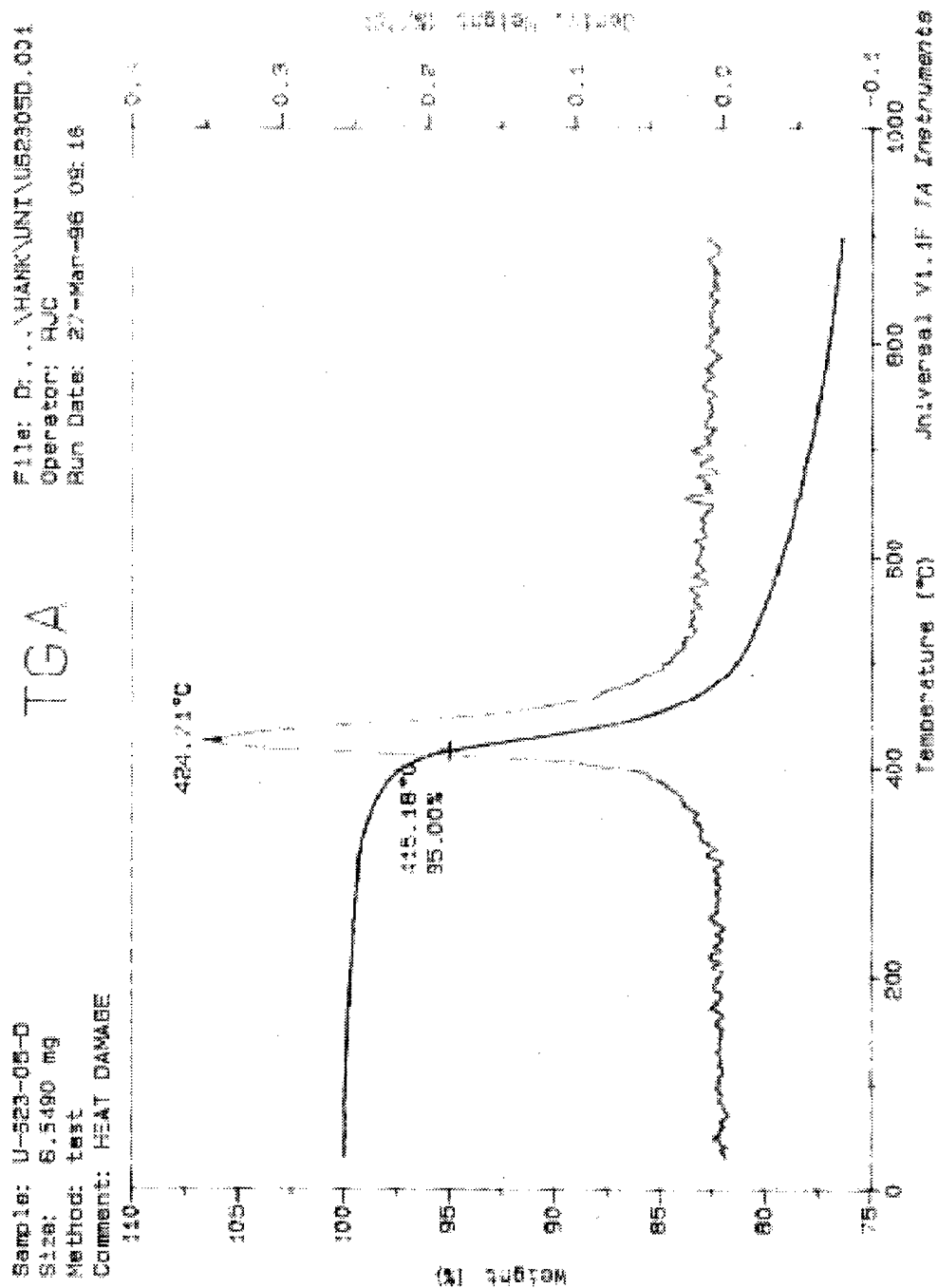RESIN DRY SAMPLE THAT WAS HEAT DAMAGED AT 302°C FOR 5 MIN
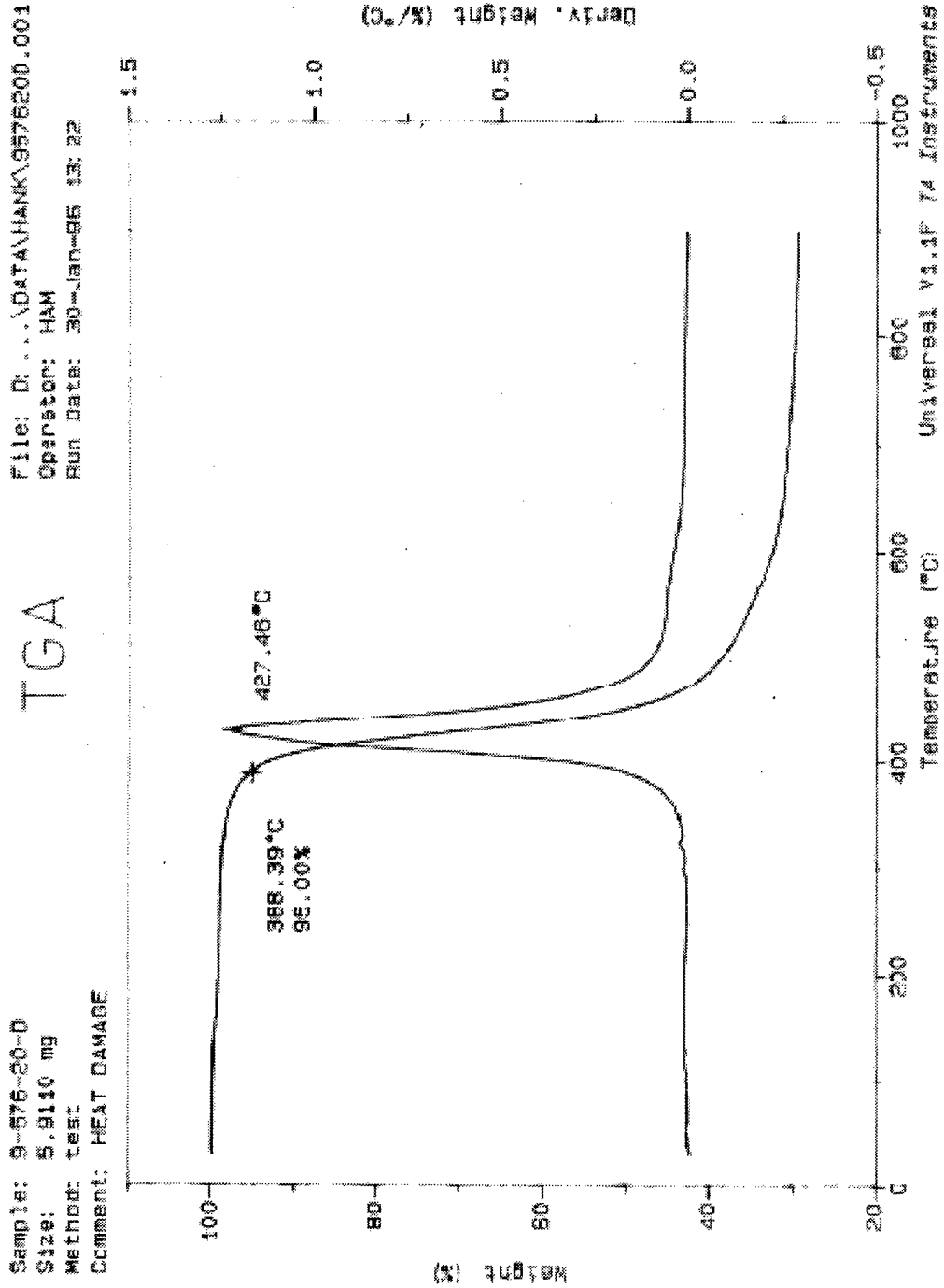
Figure C-13

TGA RESULTS SHOWING WEIGHT LOSS VERSUS TEMPERATURE OF THE 977-3 NEAT
RESIN DRY SAMPLE THAT WAS HEAT DAMAGED AT 302°C FOR 20 MIN

APPENDIX C
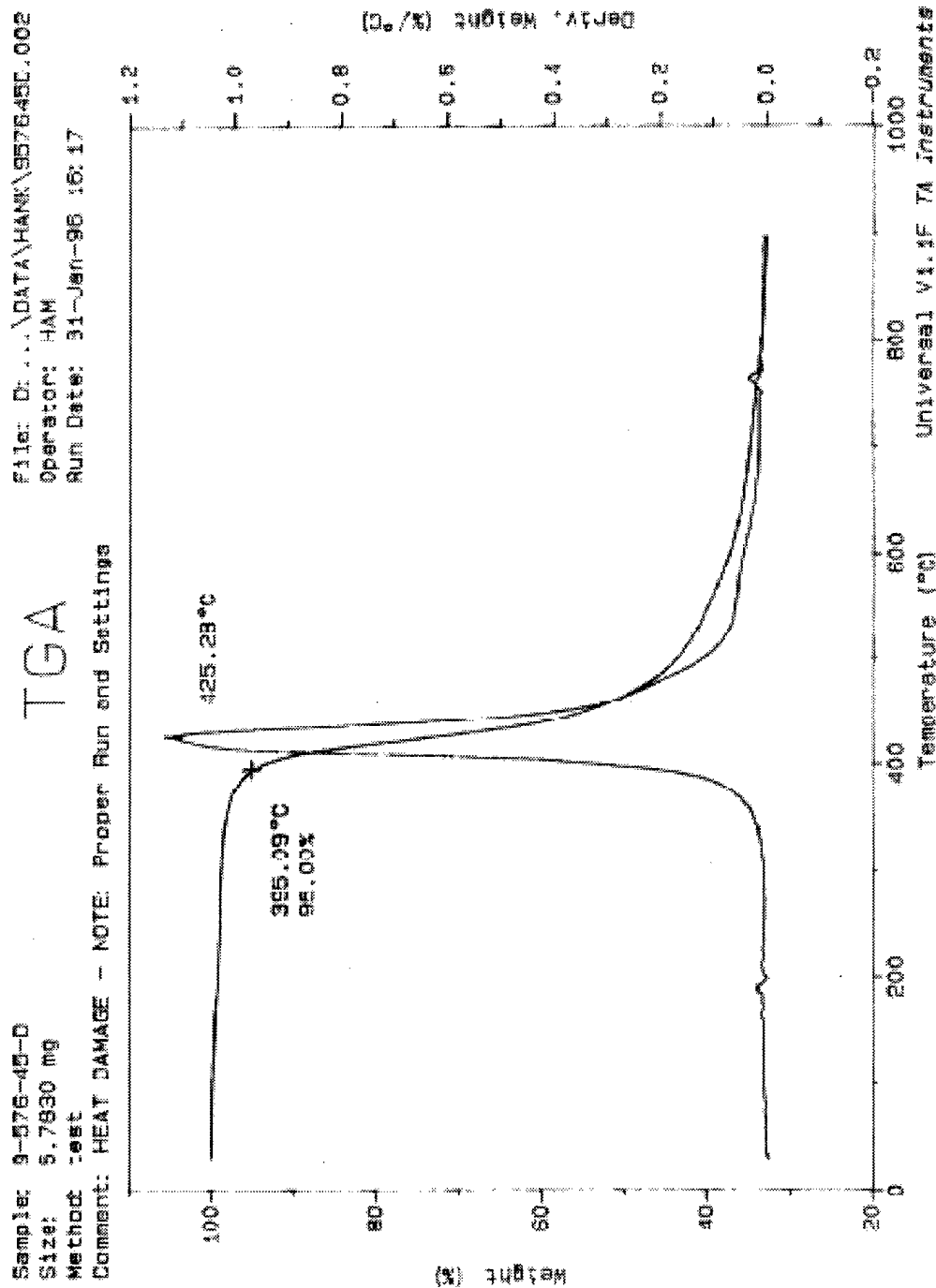
Figure C-14

TGA RESULTS SHOWING WEIGHT LOSS VERSUS TEMPERATURE OF THE 977-3 NEAT
RESIN DRY SAMPLE THAT WAS HEAT DAMAGED AT 302°C FOR 45 MIN
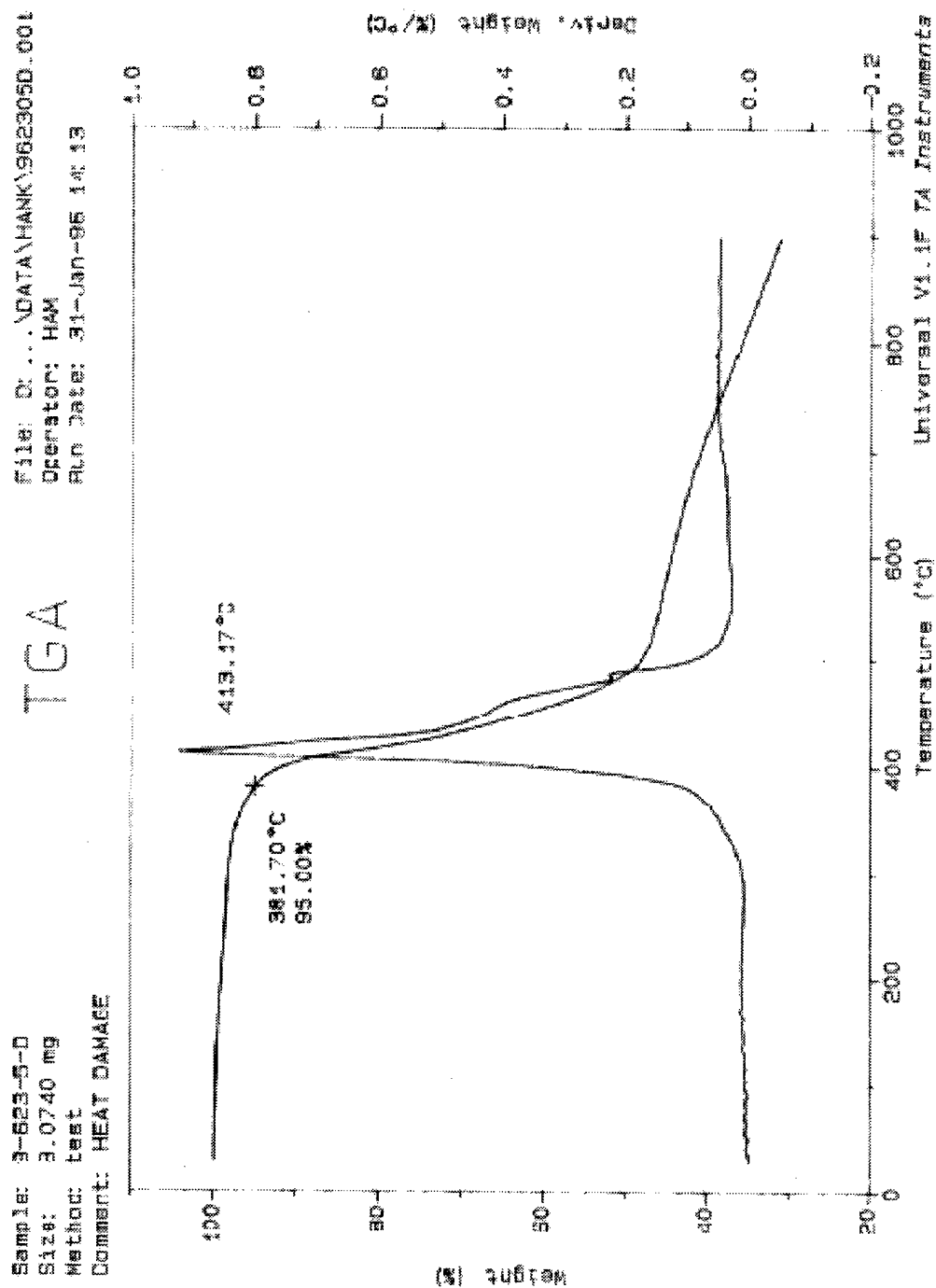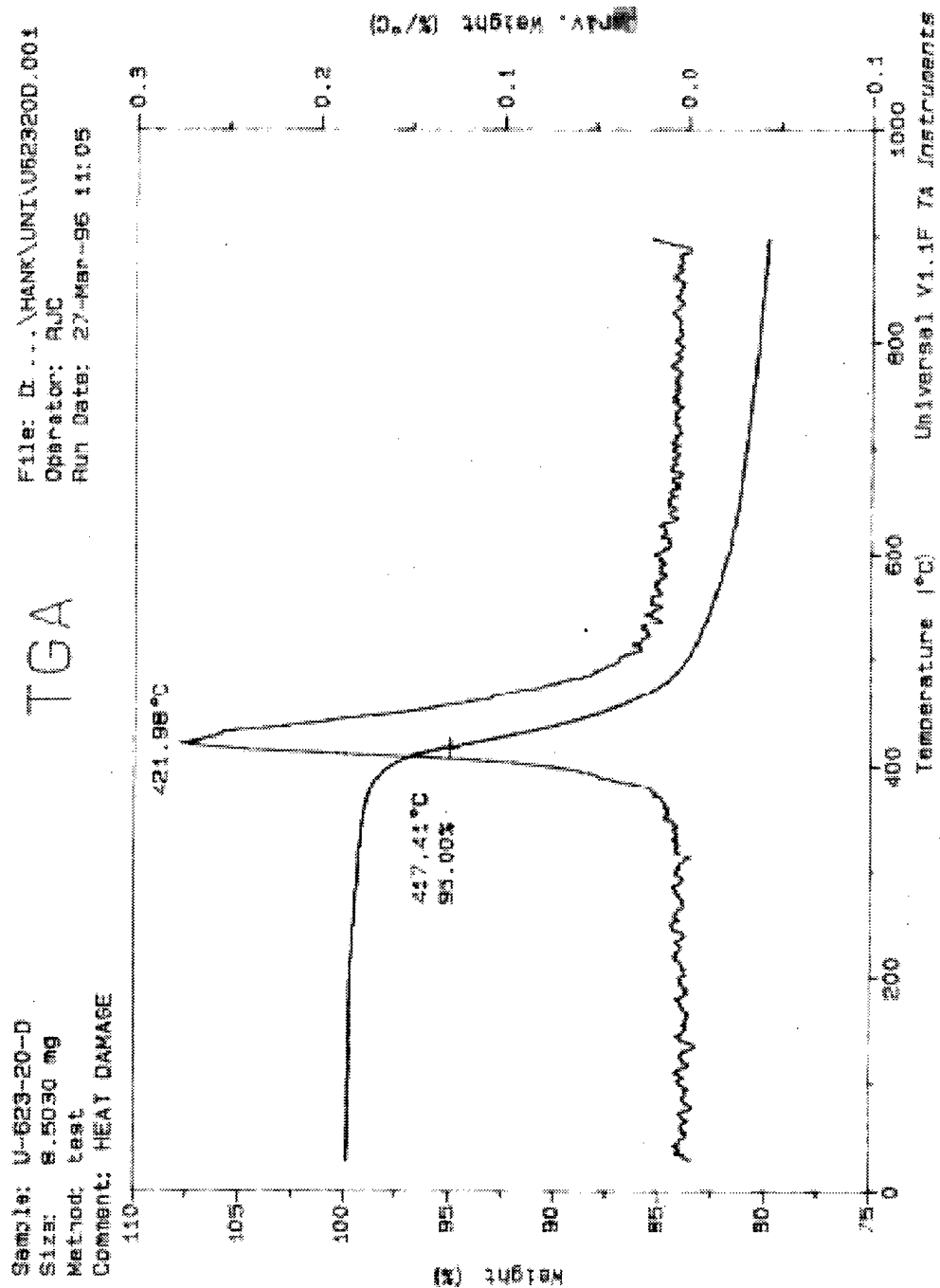
Figure C-15
TGA RESULTS SHOWING WEIGHT LOSS VERSUS TEMPERATURE OF THE 977-3 NEAT
RESIN DRY SAMPLE THAT WAS HEAT DAMAGED AT 329°C FOR 5 MIN
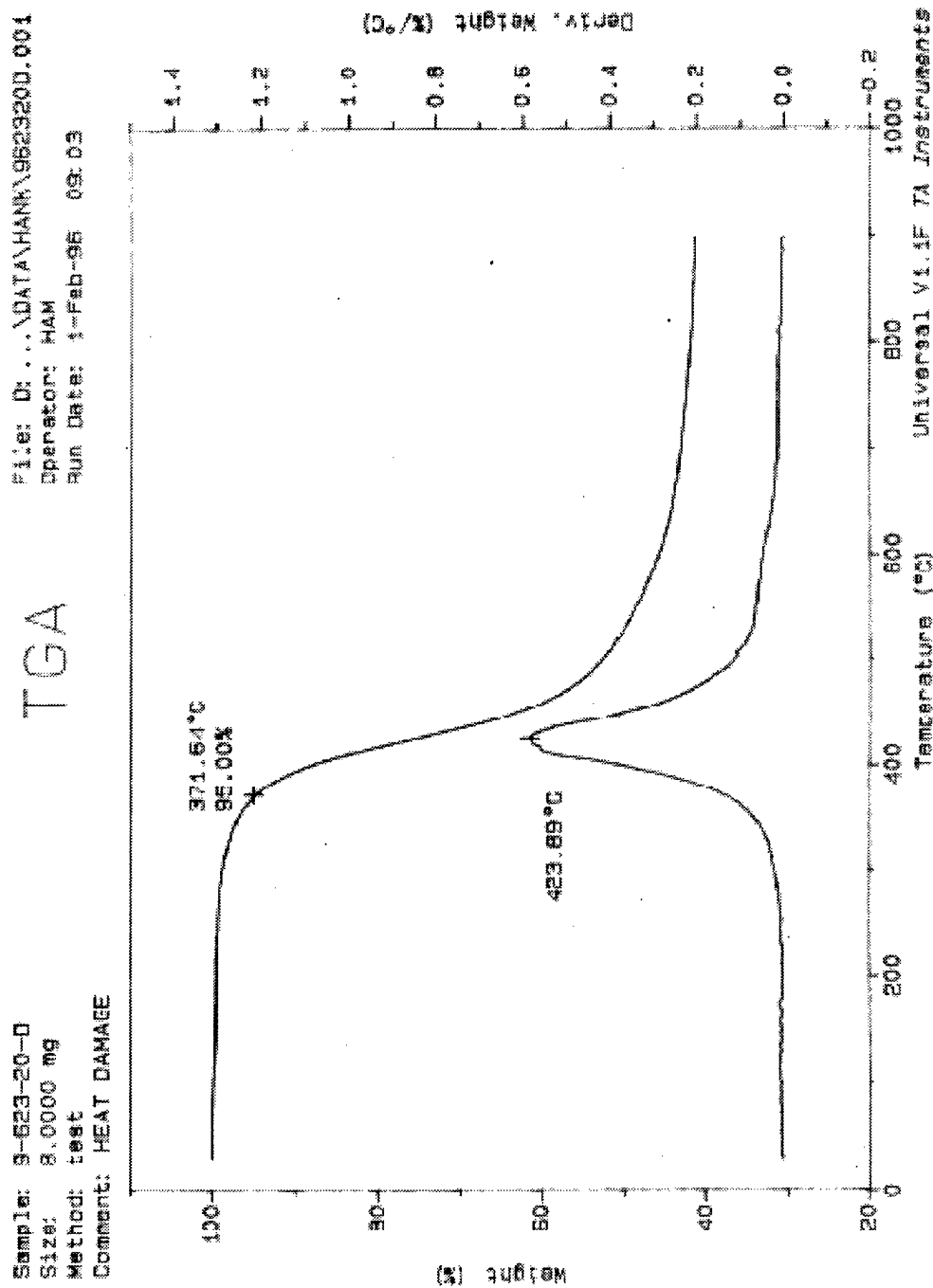
Figure C-16

TGA RESULTS SHOWING WEIGHT LOSS VERSUS TEMPERATURE OF THE 977-3 NEAT
RESIN DRY SAMPLE THAT WAS HEAT DAMAGED AT 329°C FOR 20 MIN
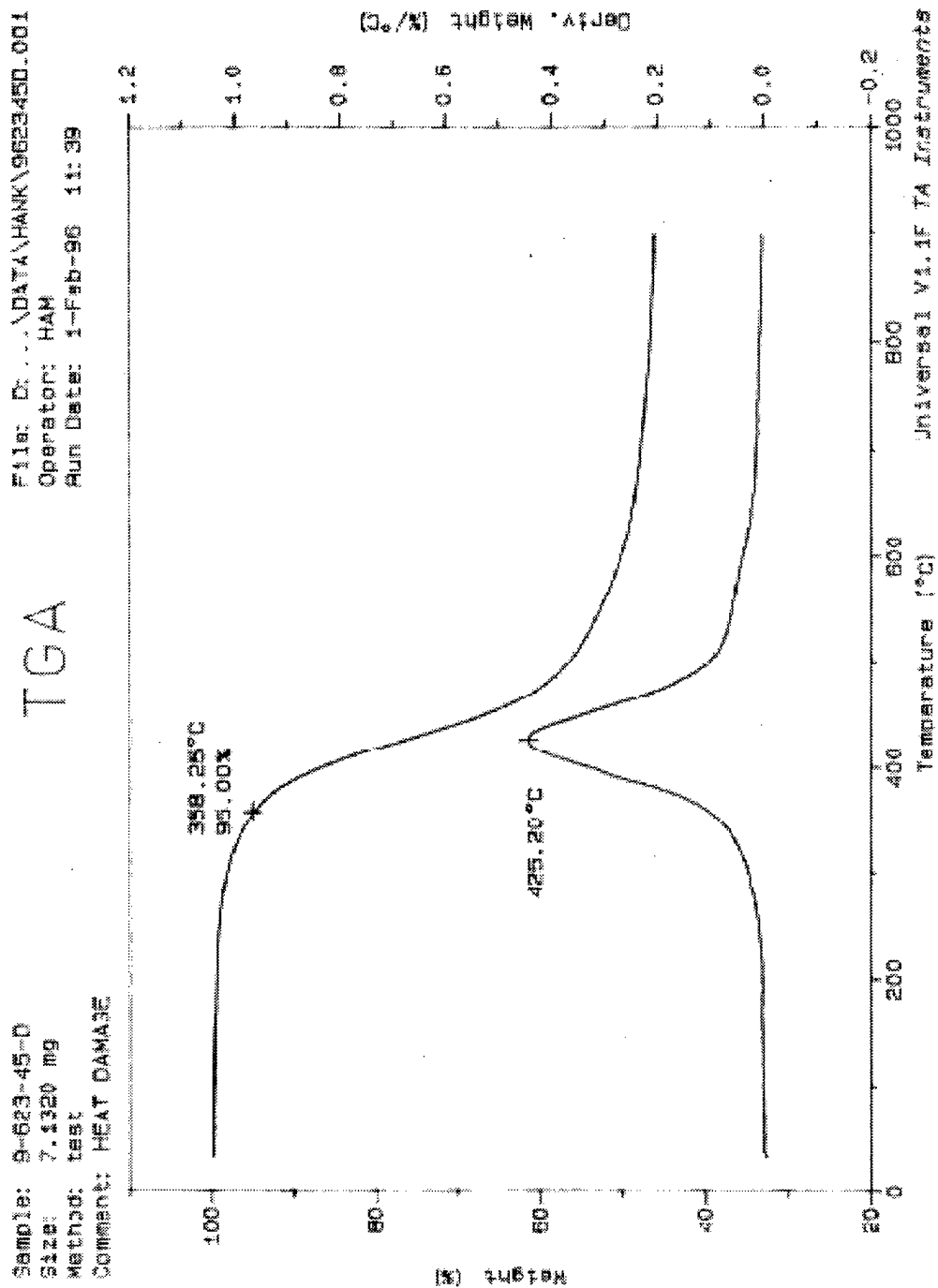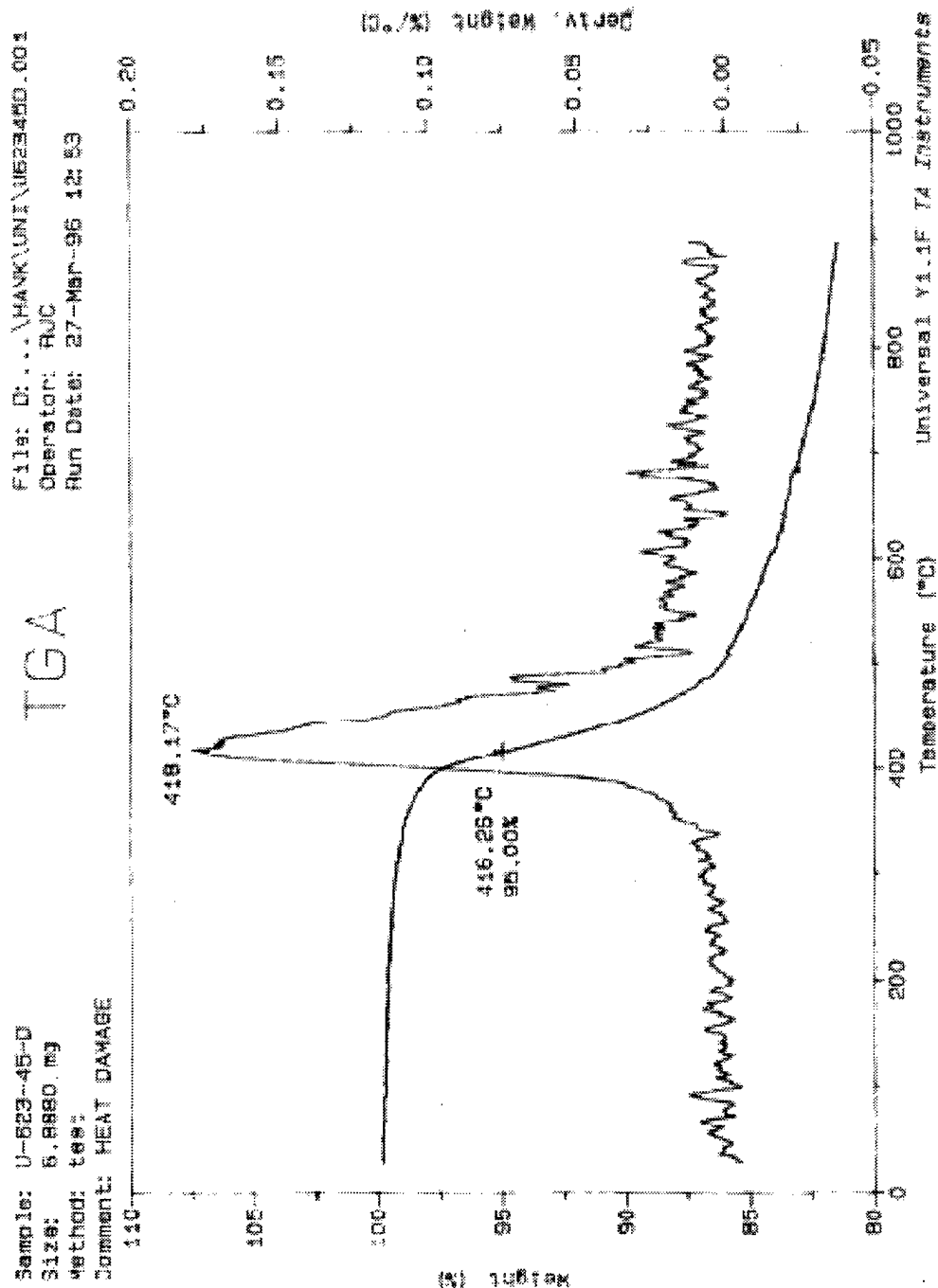
Figure C-17
TGA RESULTS SHOWING WEIGHT LOSS VERSUS TEMPERATURE OF THE 977-3 NEAT
RESIN DRY SAMPLE THAT WAS HEAT DAMAGED AT 329°C FOR 45 MIN
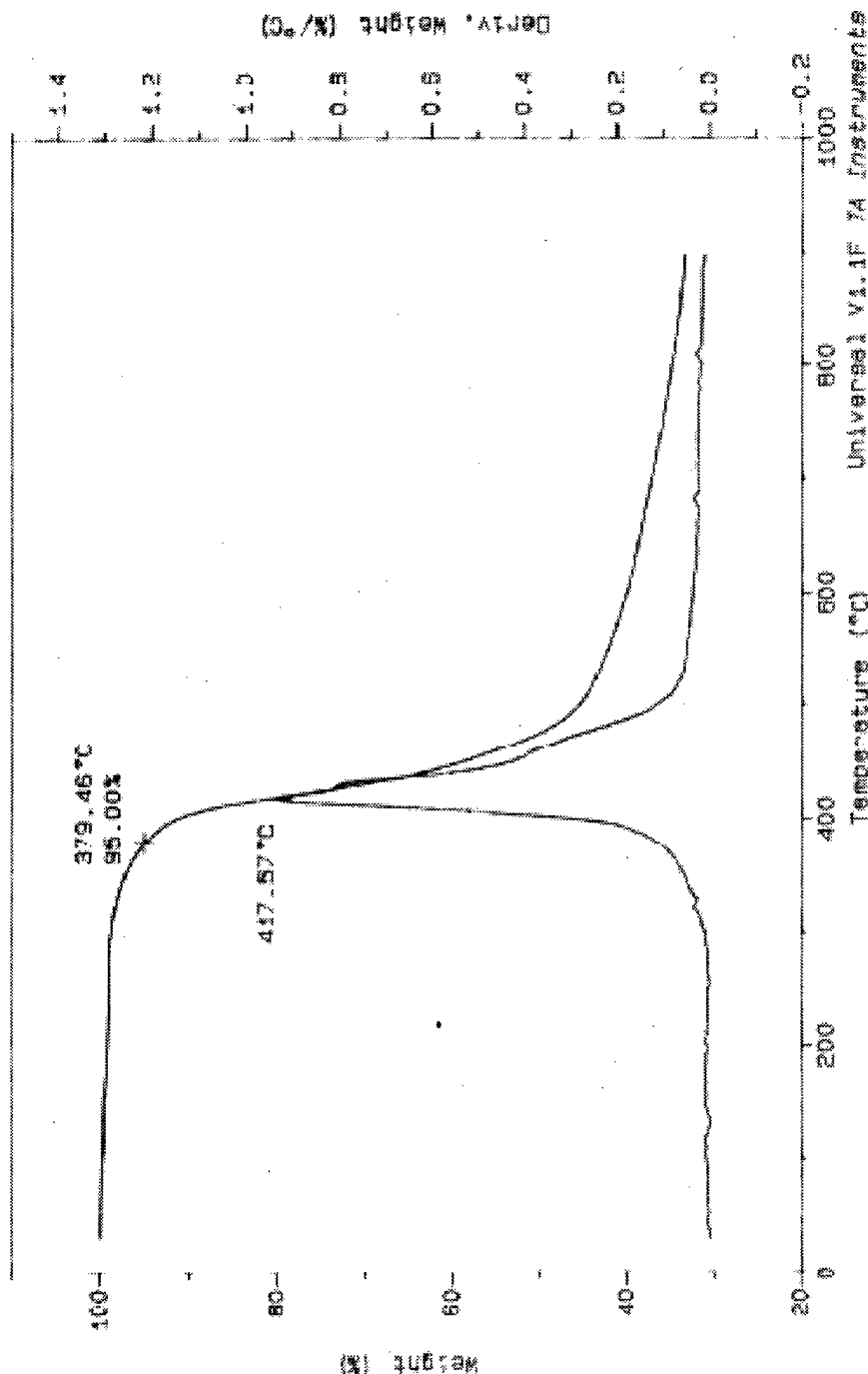
Figure C-18

TGA RESULTS SHOWING WEIGHT LOSS VERSUS TEMPERATURE OF THE 977-3 NEAT
RESIN AMBIENT SAMPLE THAT WAS HEAT DAMAGED AT 274°C FOR 5 MIN
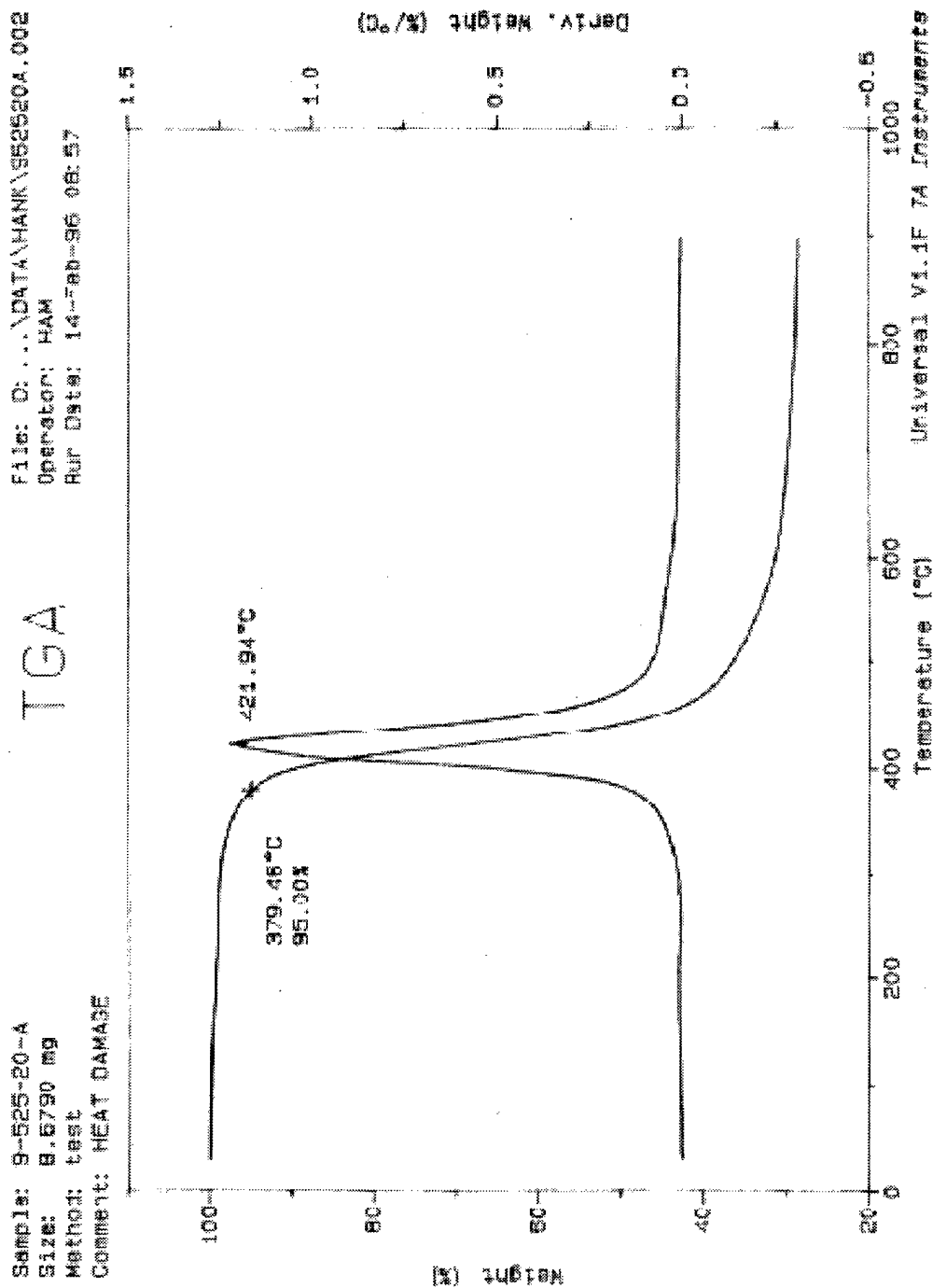
Figure C-19

TGA RESULTS SHOWING WEIGHT LOSS VERSUS TEMPERATURE OF THE 977-3 NEAT
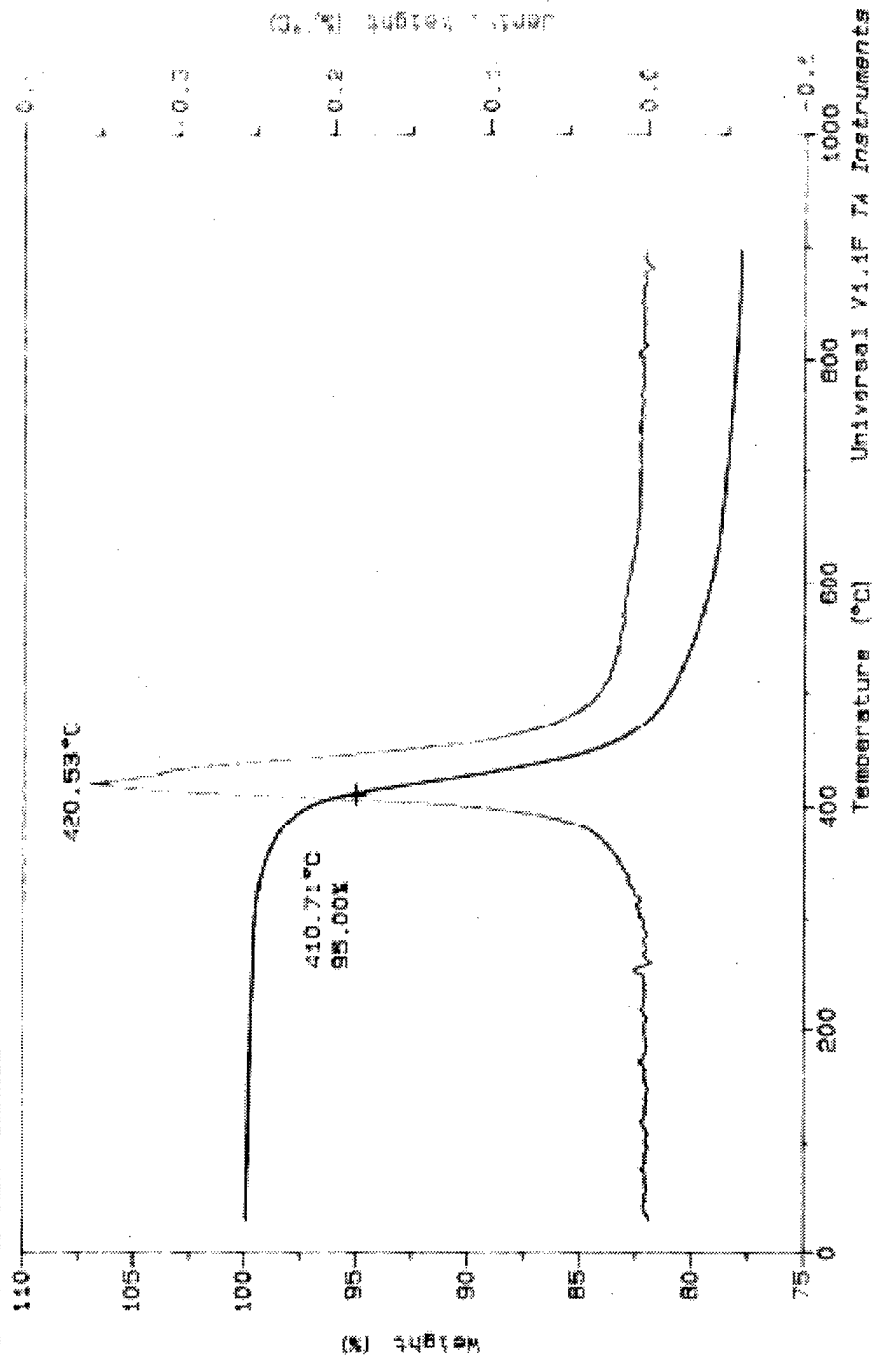RESIN AMBIENT SAMPLE THAT WAS HEAT DAMAGED AT 274°C FOR 20 MIN

APPENDIX C
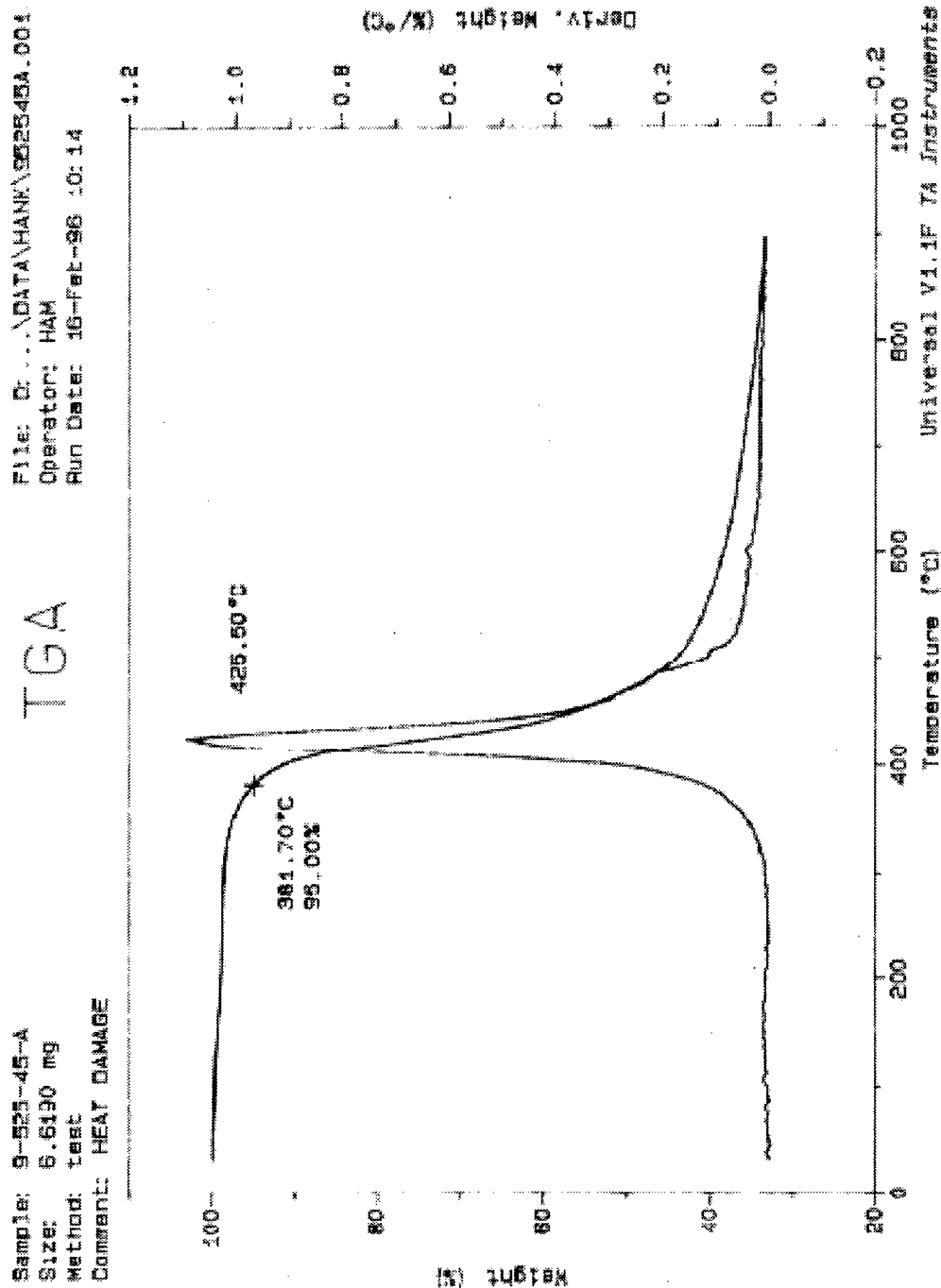
Figure C-20

TGA RESULTS SHOWING WEIGHT LOSS VERSUS TEMPERATURE OF THE 977-3 NEAT
RESIN AMBIENT SAMPLE THAT WAS HEAT DAMAGED AT 274°C FOR 45 MIN

APPENDIX C
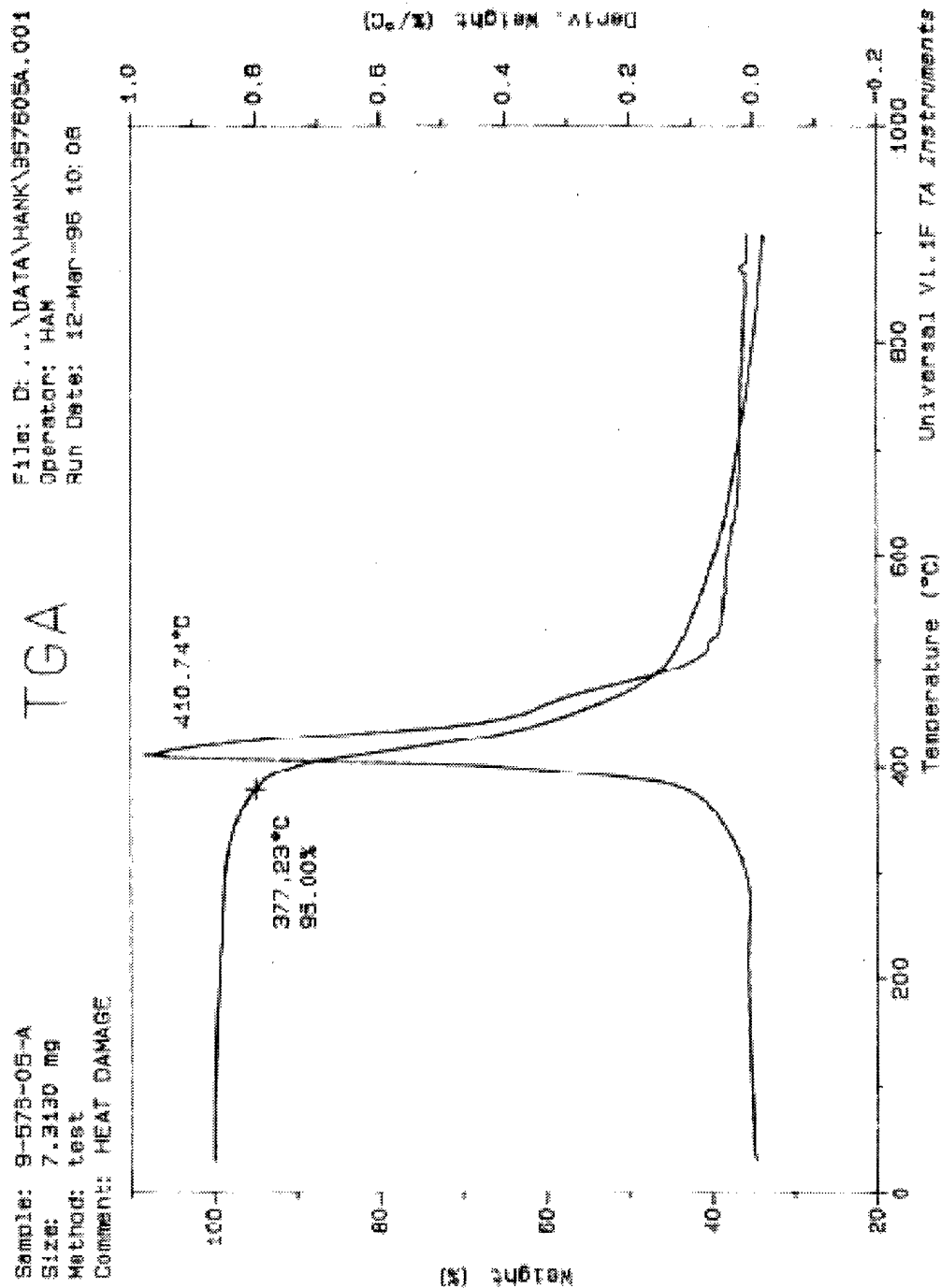
Figure C-21

TGA RESULTS SHOWING WEIGHT LOSS VERSUS TEMPERATURE OF THE 977-3 NEAT
RESIN AMBIENT SAMPLE THAT WAS HEAT DAMAGED AT 302°C FOR 5 MIN

APPENDIX C
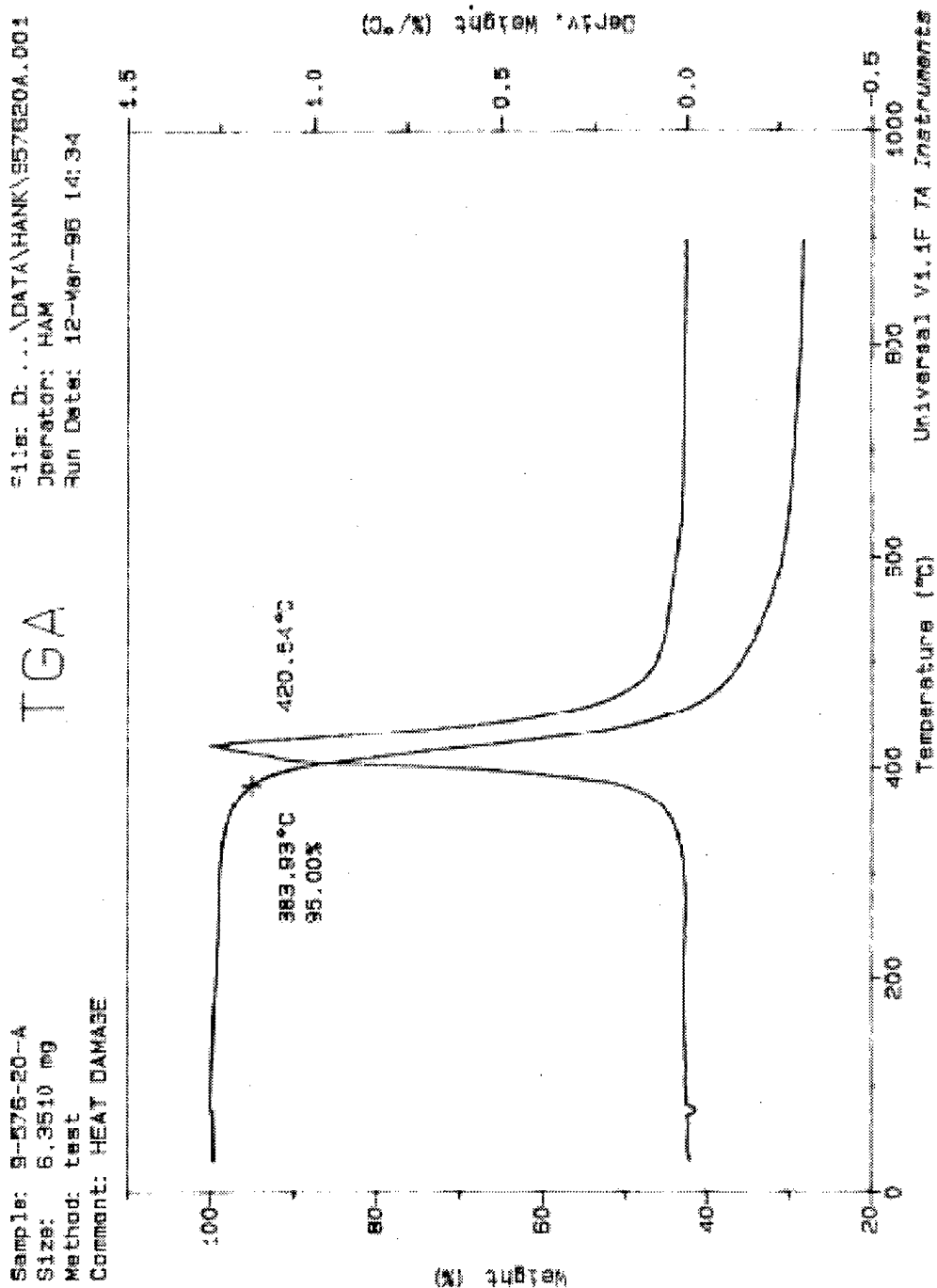
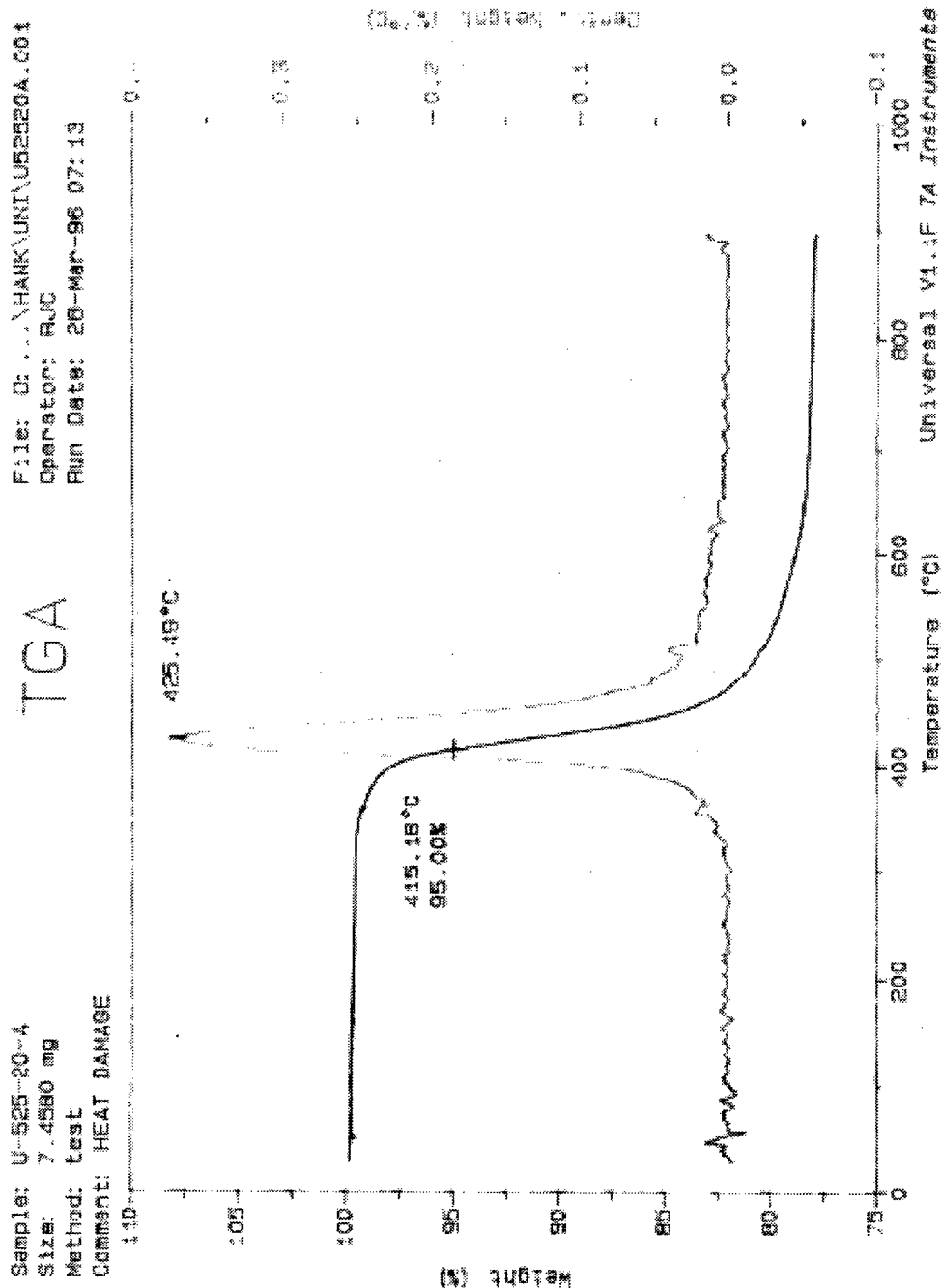Figure C-22

TGA RESULTS SHOWING WEIGHT LOSS VERSUS TEMPERATURE OF THE 977-3 NEAT
RESIN AMBIENT SAMPLE THAT WAS HEAT DAMAGED AT 302°C FOR 20 MIN
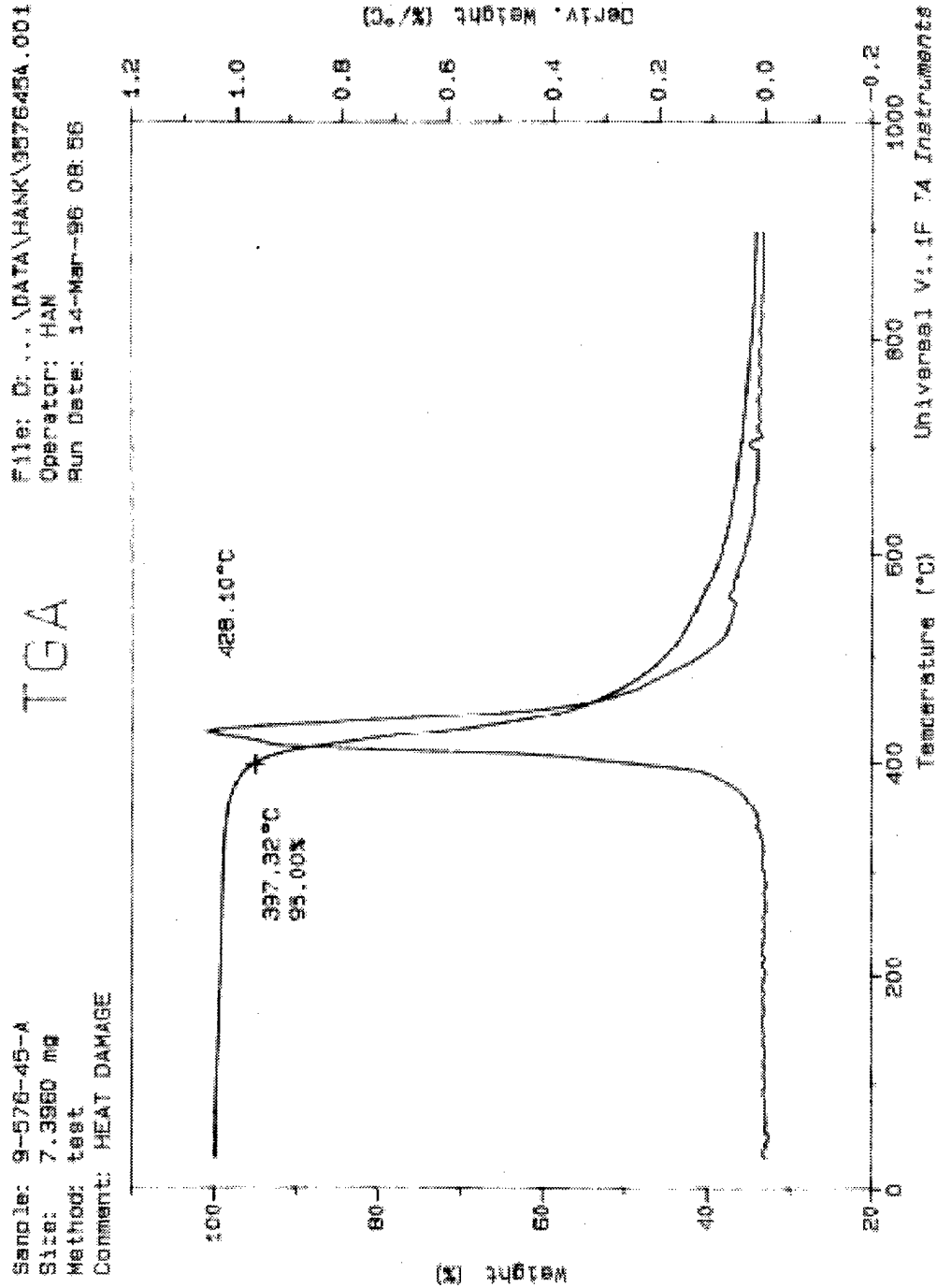
Figure C-23
TGA RESULTS SHOWING WEIGHT LOSS VERSUS TEMPERATURE OF THE 977-3 NEAT
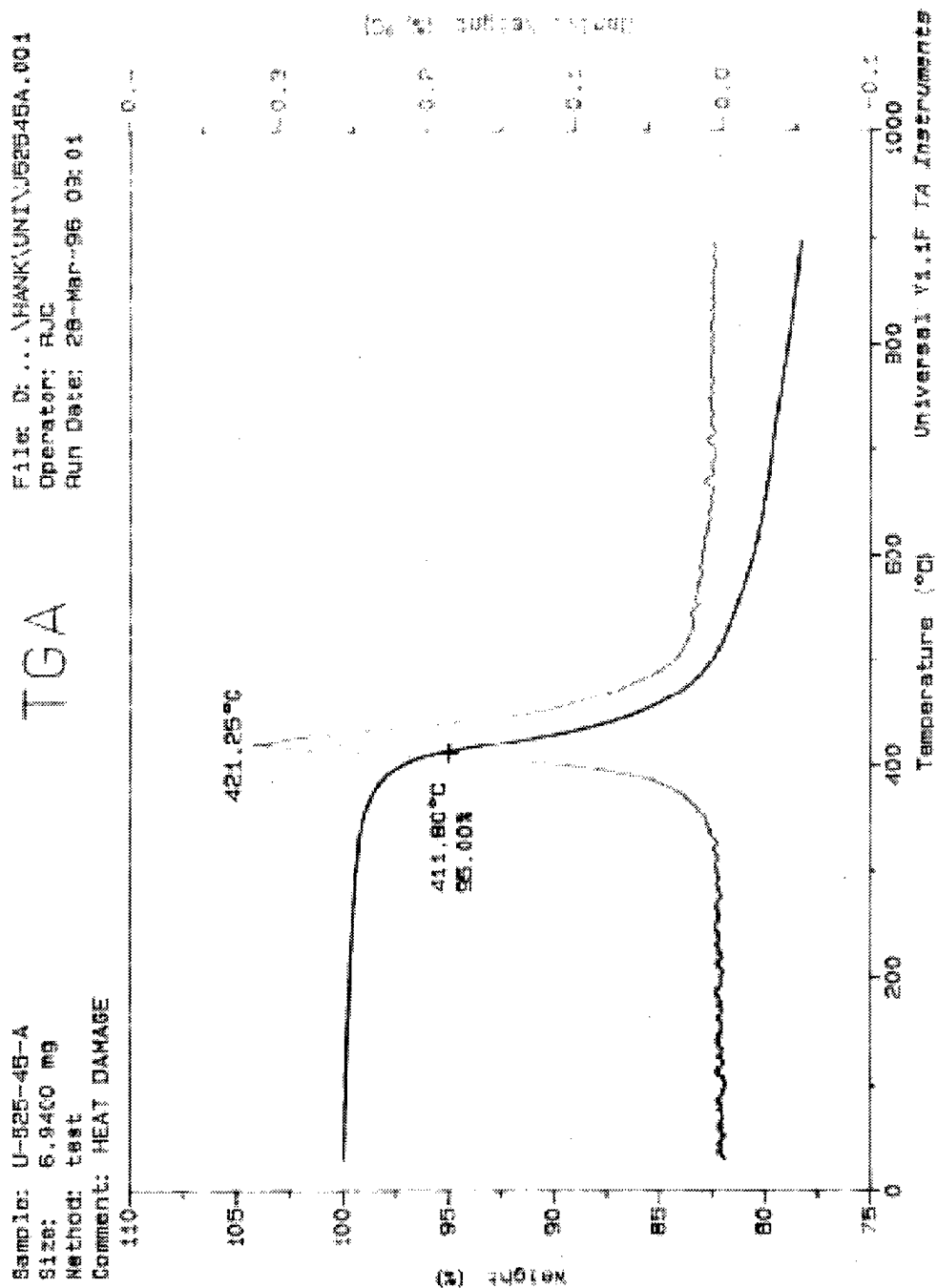RESIN AMBIENT SAMPLE THAT WAS HEAT DAMAGED AT 302°C FOR 45 MIN

APPENDIX C
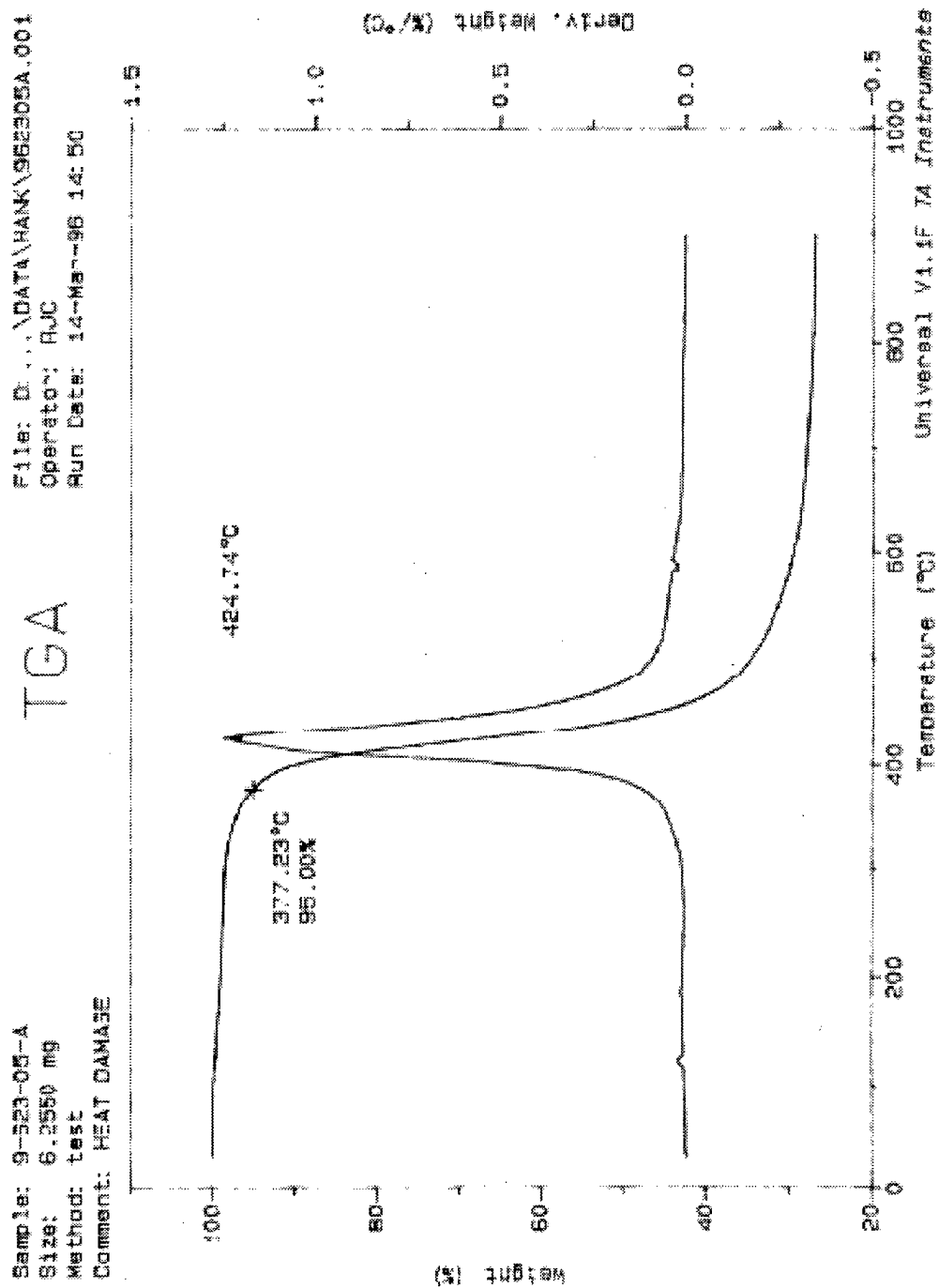
Figure C-24

TGA RESULTS SHOWING WEIGHT LOSS VERSUS TEMPERATURE OF THE 977-3 NEAT
RESIN AMBIENT SAMPLE THAT WAS HEAT DAMAGED AT 329°C FOR 5 MIN

APPENDIX C
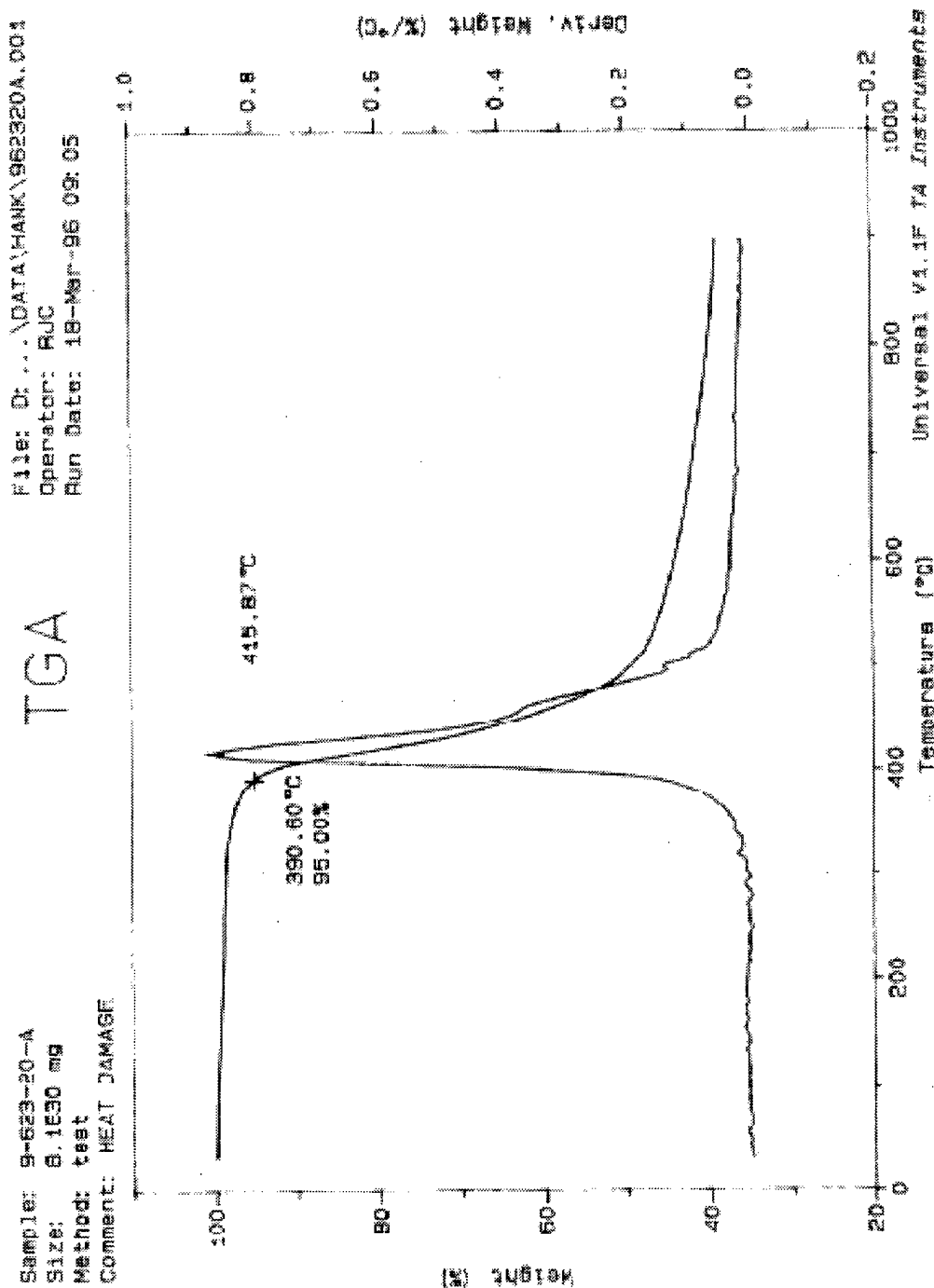
Figure C-25
TGA RESULTS SHOWING WEIGHT LOSS VERSUS TEMPERATURE OF THE 977-3 NEAT
RESIN AMBIENT SAMPLE THAT WAS HEAT DAMAGED AT 329°C FOR 20 MIN

APPENDIX C
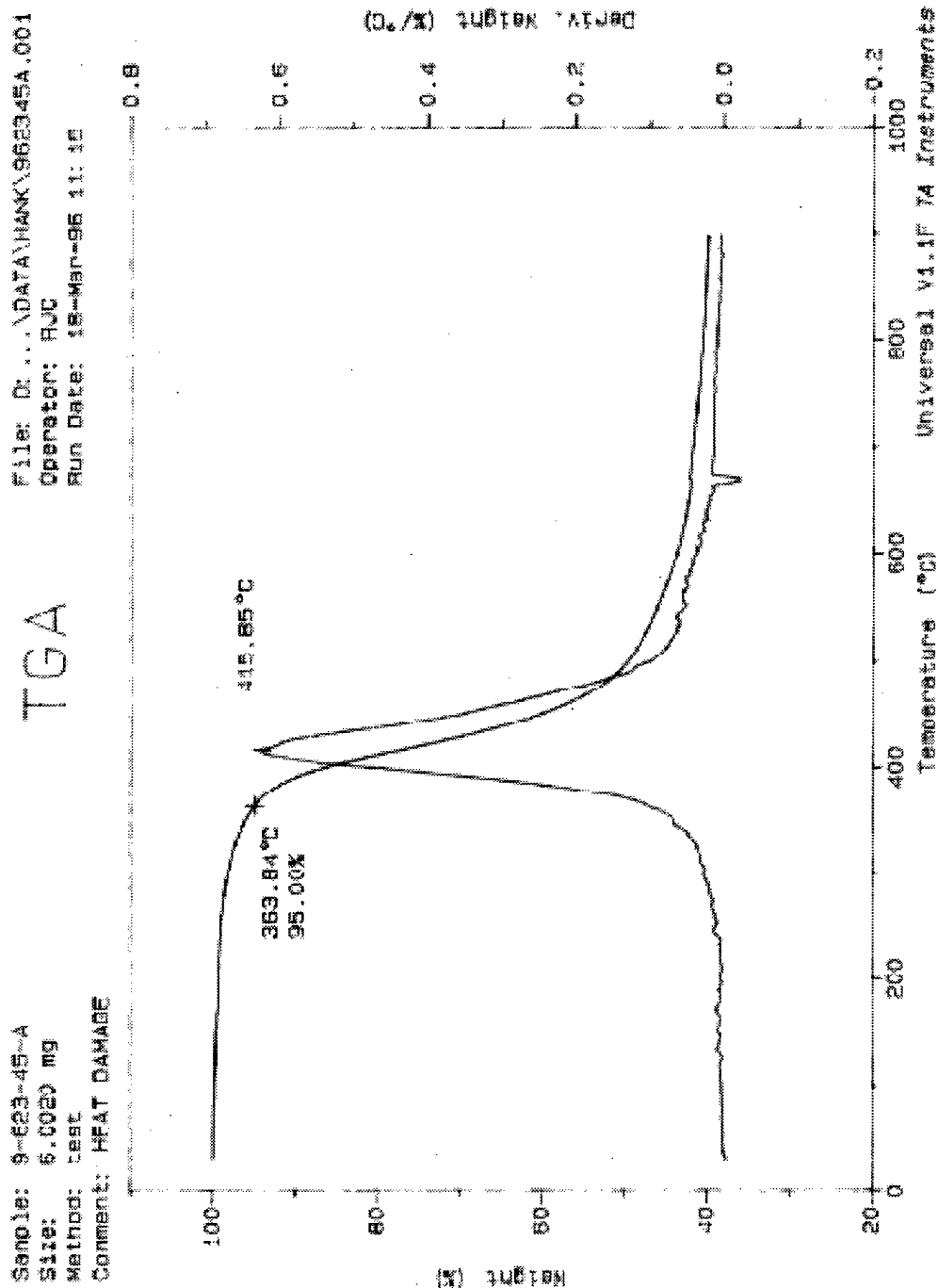
Figure C-26

TGA RESULTS SHOWING WEIGHT LOSS VERSUS TEMPERATURE OF THE 977-3 NEAT
RESIN AMBIENT SAMPLE THAT WAS HEAT DAMAGED AT 329°C FOR 45 MIN

APPENDIX C
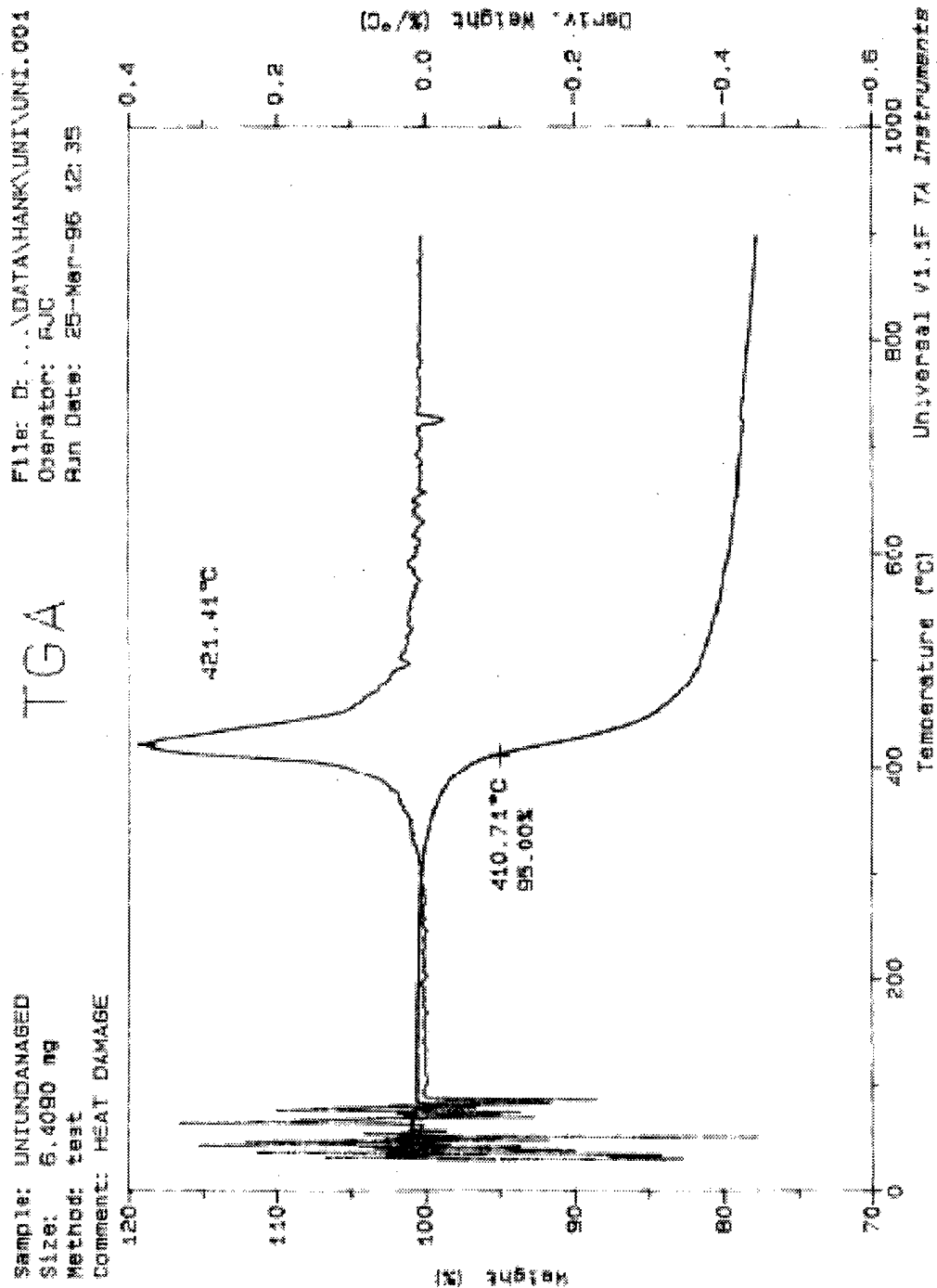
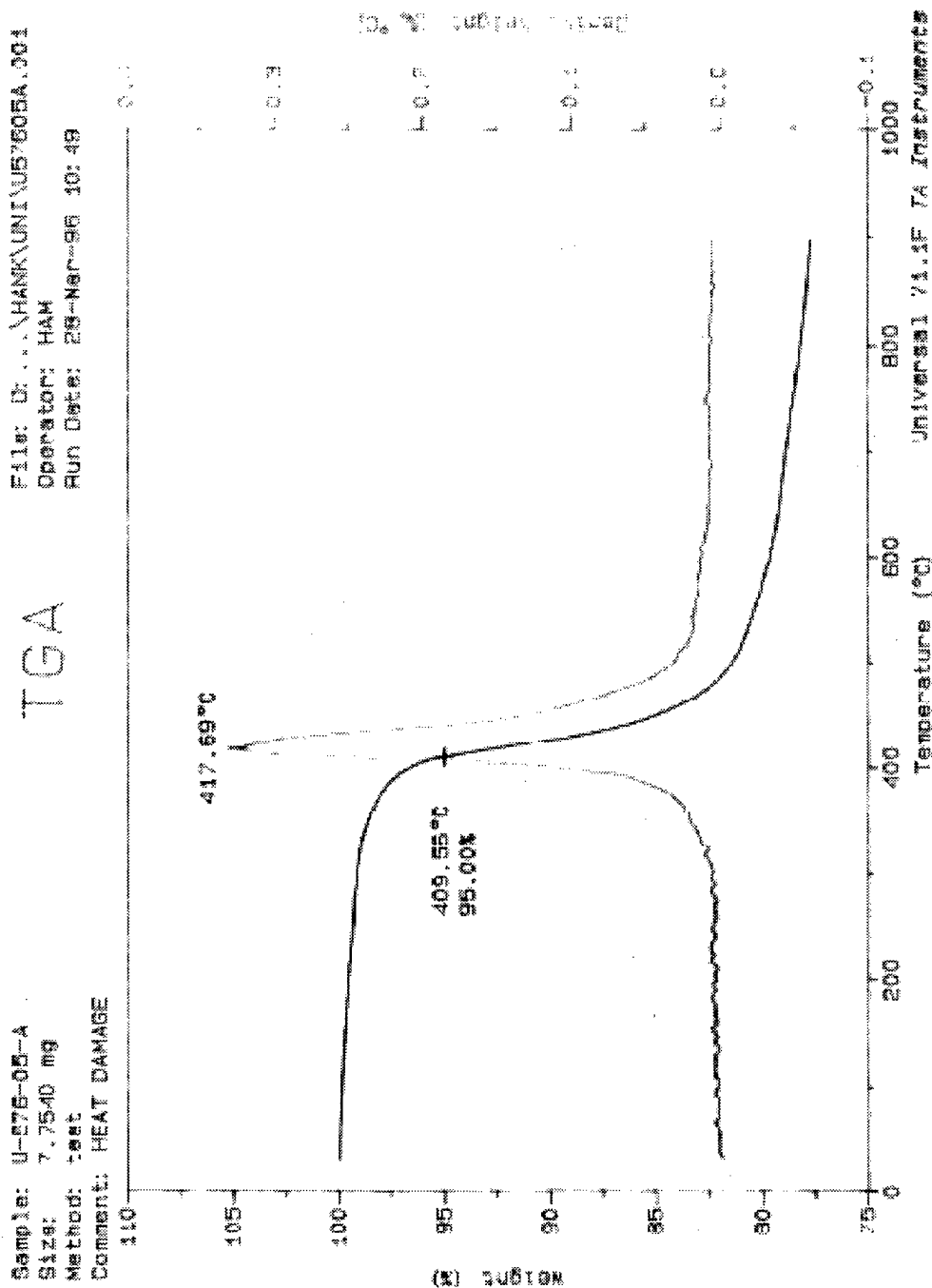Figure C-27
TGA RESULTS SHOWING WEIGHT LOSS VERSUS TEMPERATURE OF THE UNDAMAGED
IM6/977-3 UNIDIRECTIONAL LAMINATE SATURATED SAMPLE

APPENDIX C
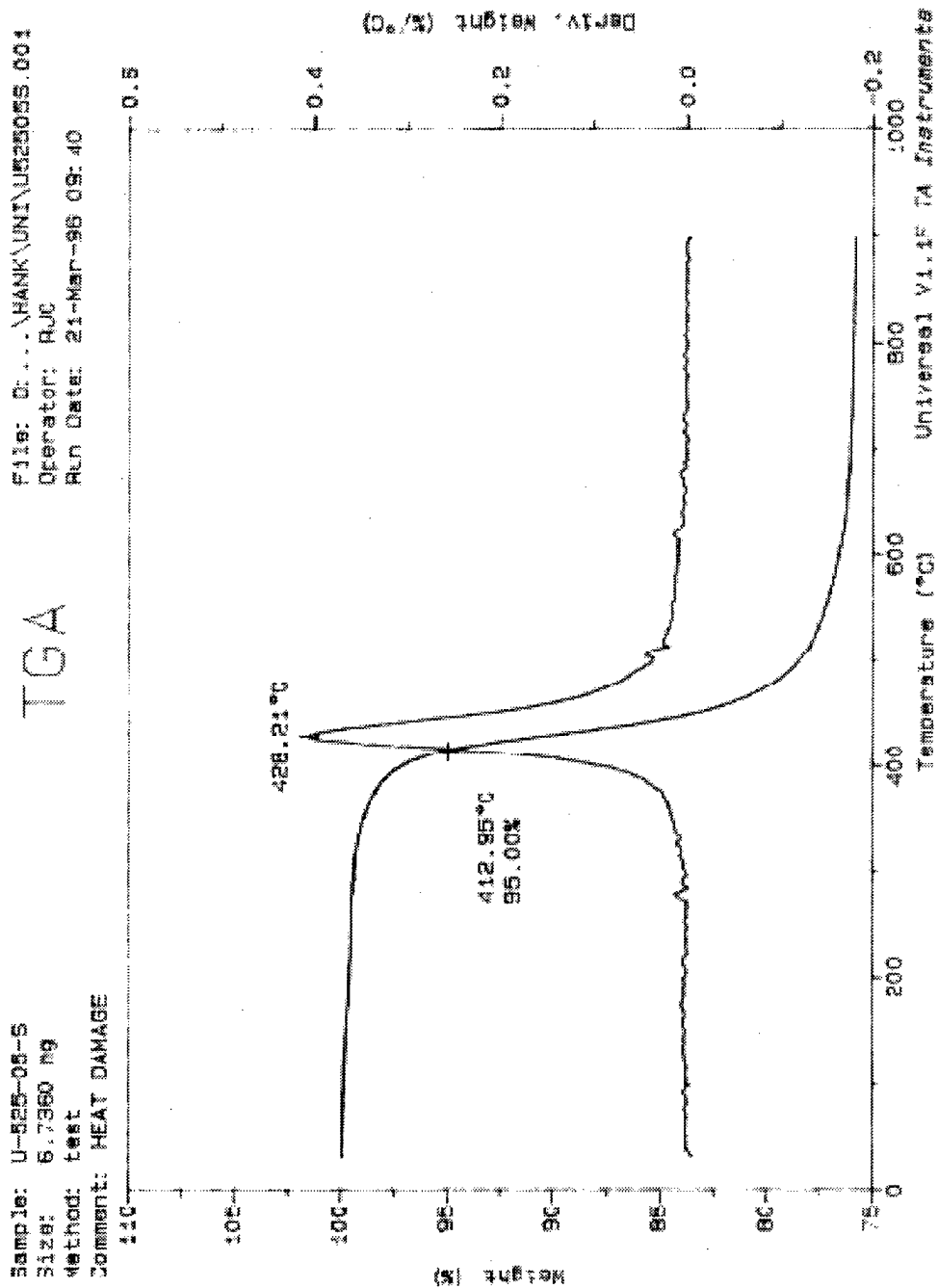
Figure C-28
TGA RESULTS SHOWING WEIGHT LOSS VERSUS TEMPERATURE OF THE IM6/977-3
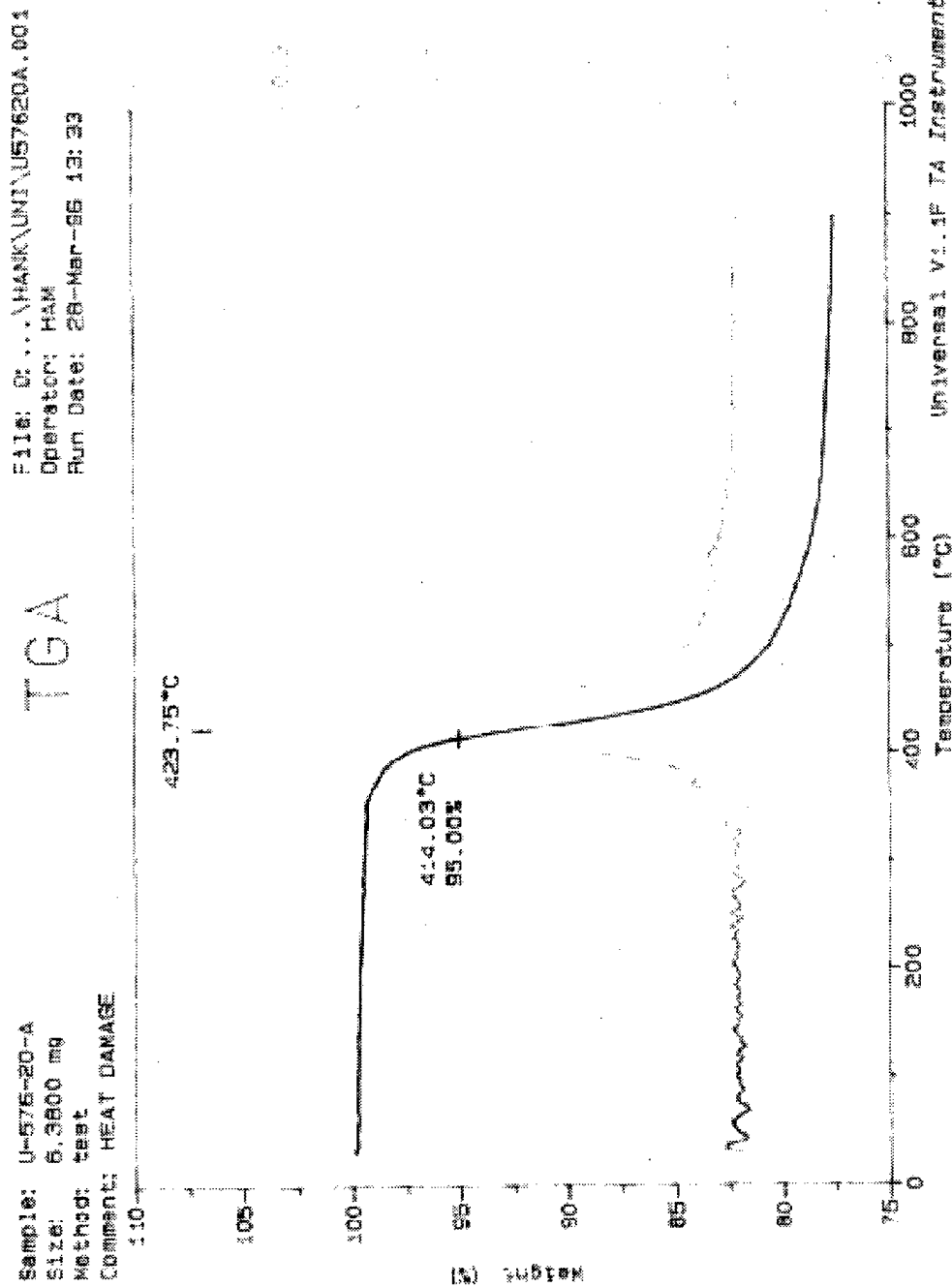UNIDIRECTIONAL LAMINATE SATURATED SAMPLE THAT WAS HEAT DAMAGED AT
274°C FOR 5 MIN
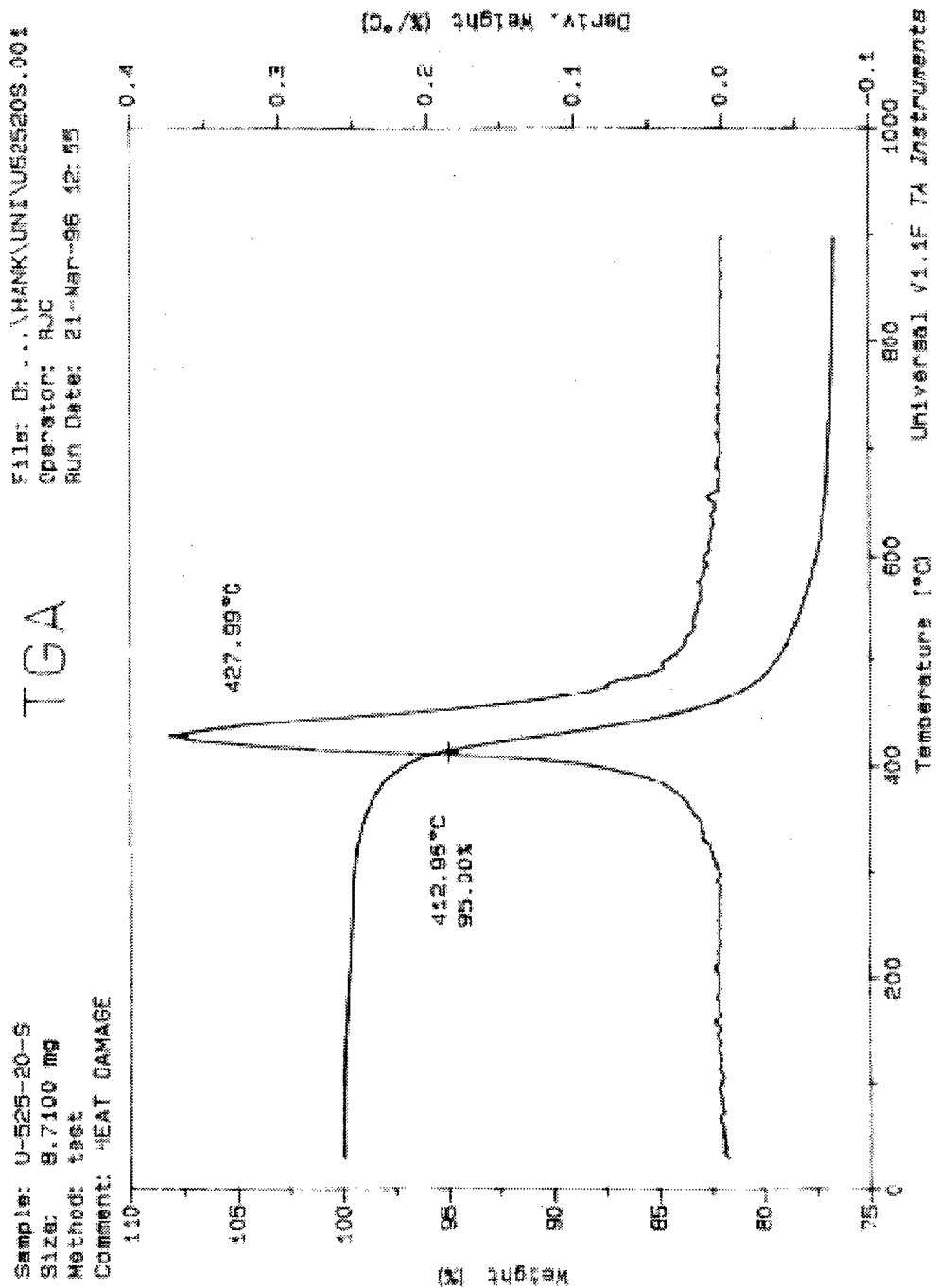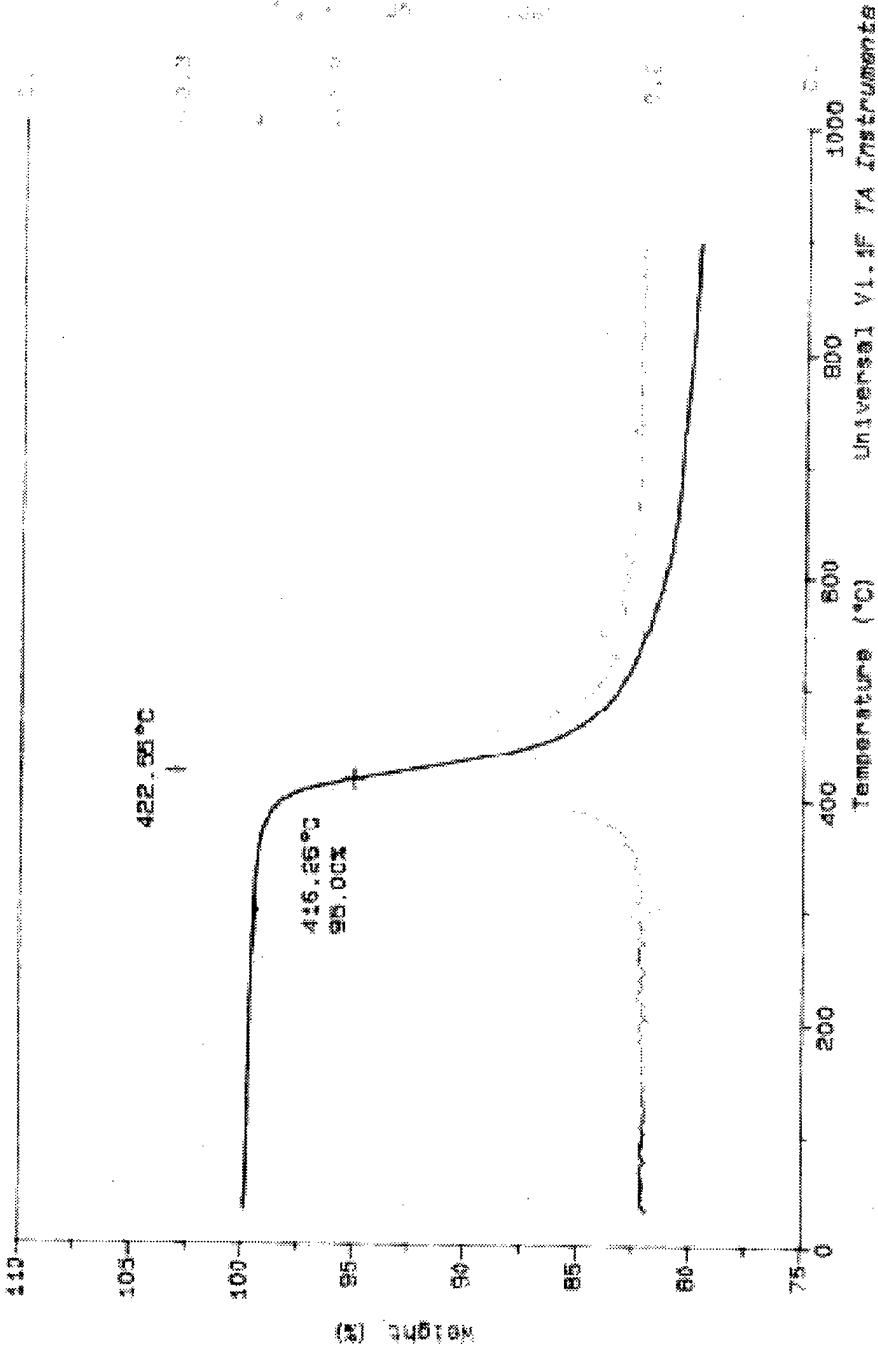
Figure C-29

TGA RESULTS SHOWING WEIGHT LOSS VERSUS TEMPERATURE OF THE IM6/977-3
UNIDIRECTIONAL LAMINATE SATURATED SAMPLE THAT WAS HEAT DAMAGED AT
274°C FOR 20 MIN

APPENDIX C
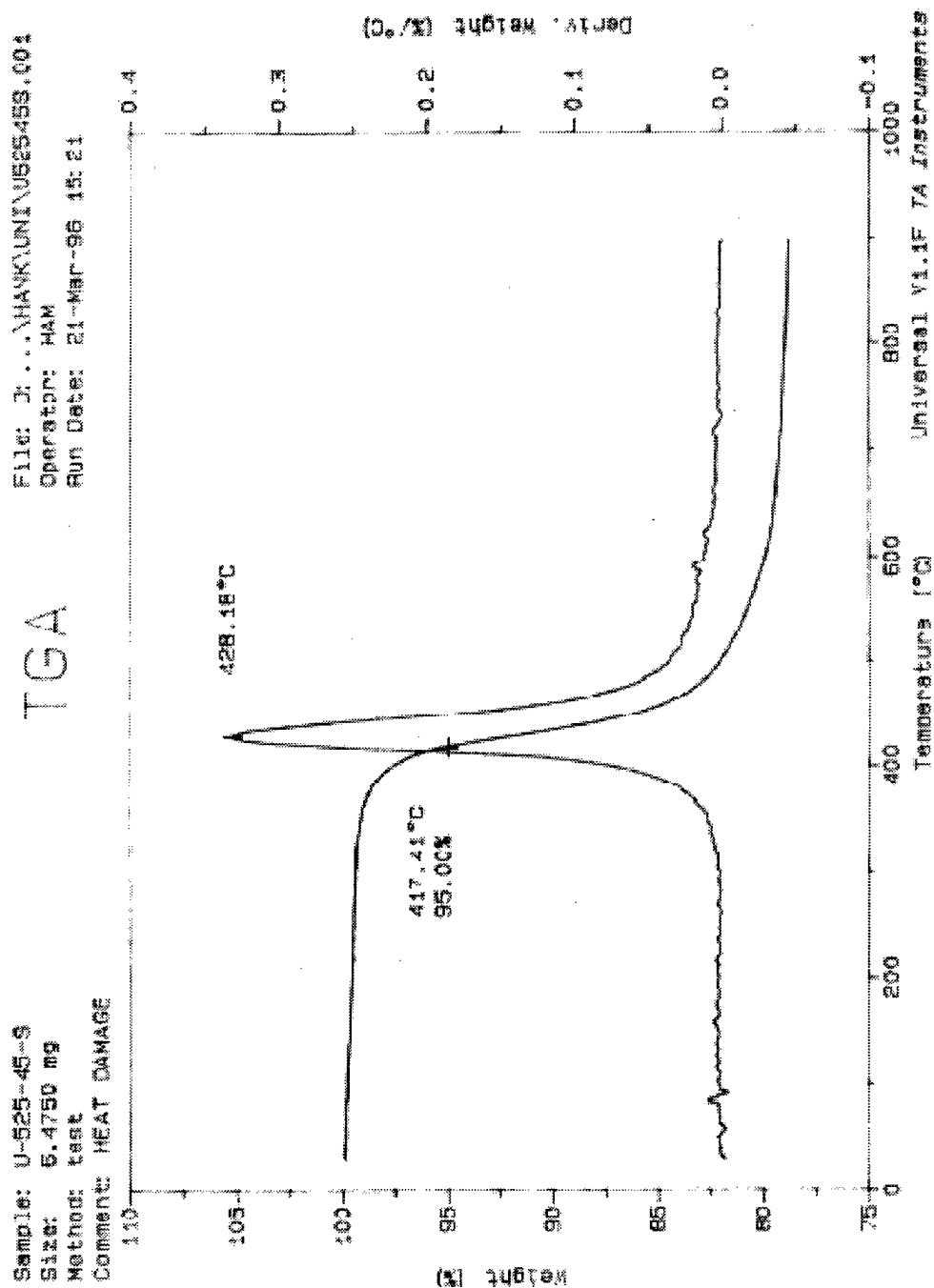
Figure C-30

TGA RESULTS SHOWING WEIGHT LOSS VERSUS TEMPERATURE OF THE IM6/977-3
UNIDIRECTIONAL LAMINATE SATURATED SAMPLE THAT WAS HEAT DAMAGED AT
274°C FOR 45 MIN
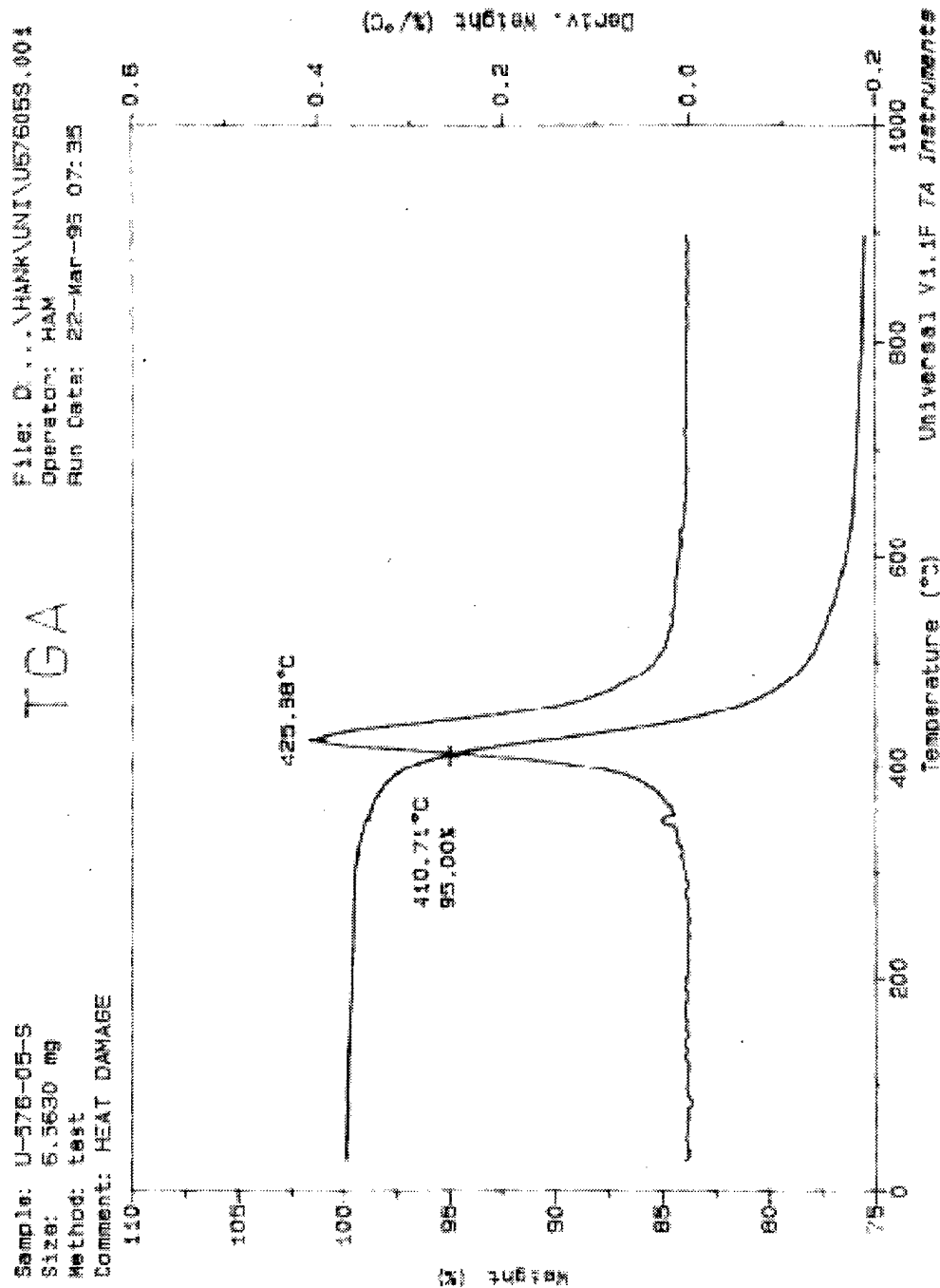
Figure C-31
TGA RESULTS SHOWING WEIGHT LOSS VERSUS TEMPERATURE OF THE IM6/977-3
UNIDIRECTIONAL LAMINATE SATURATED SAMPLE THAT WAS HEAT DAMAGED AT
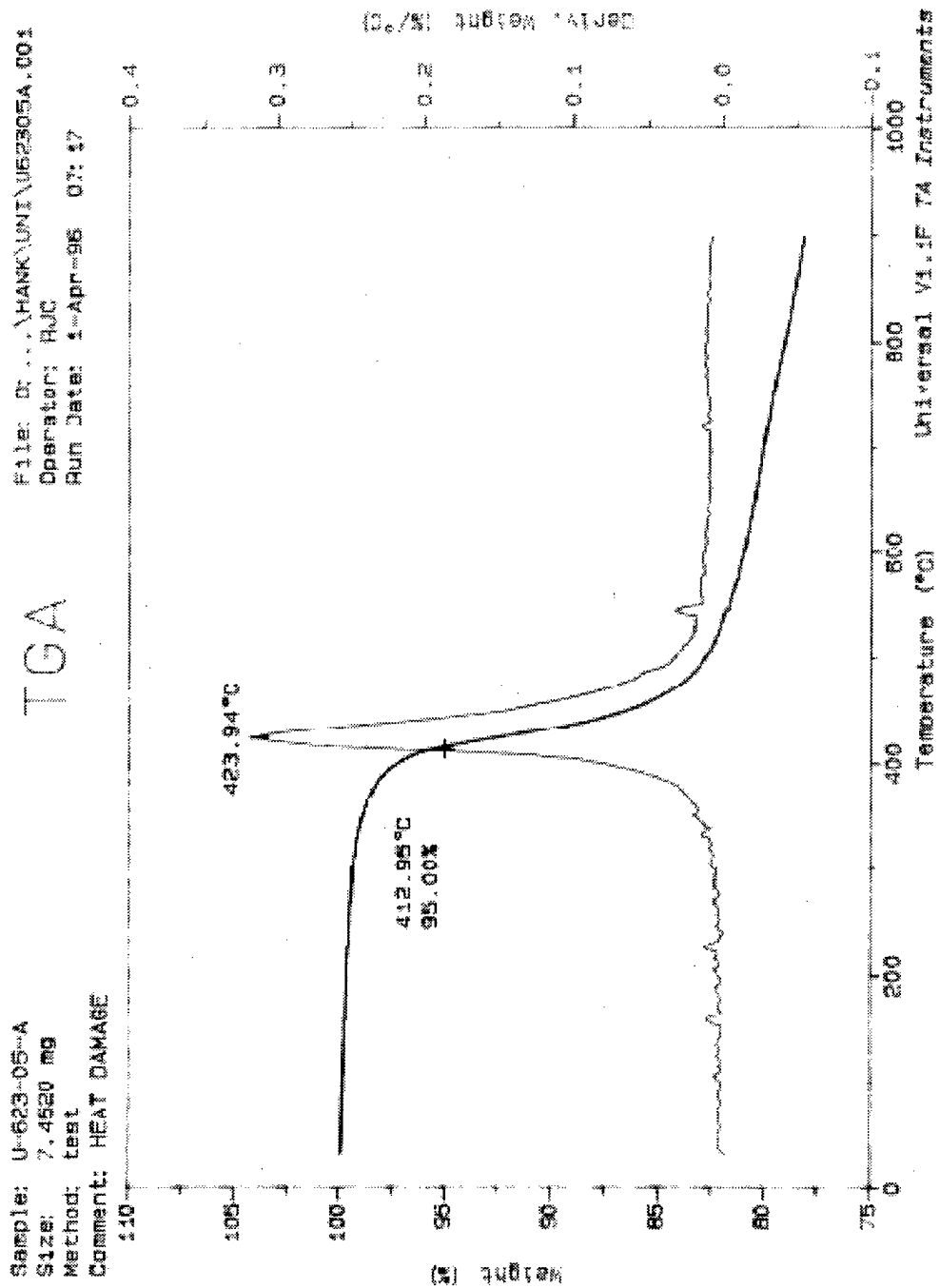302°C FOR 5 MIN
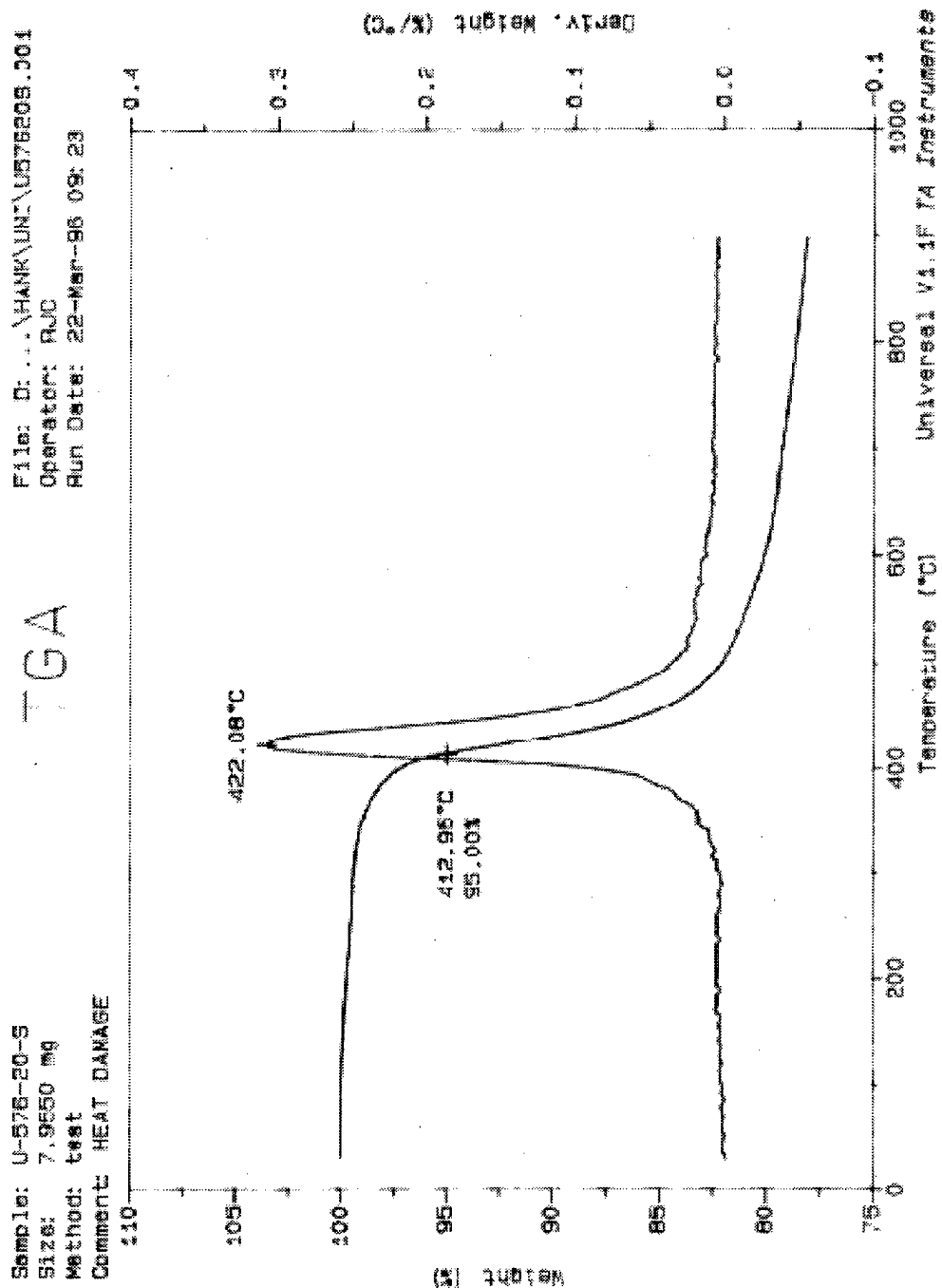
Figure C-32

TGA RESULTS SHOWING WEIGHT LOSS VERSUS TEMPERATURE OF THE IM6/977-3
UNIDIRECTIONAL LAMINATE SATURATED SAMPLE THAT WAS HEAT DAMAGED AT
302°C FOR 20 MIN
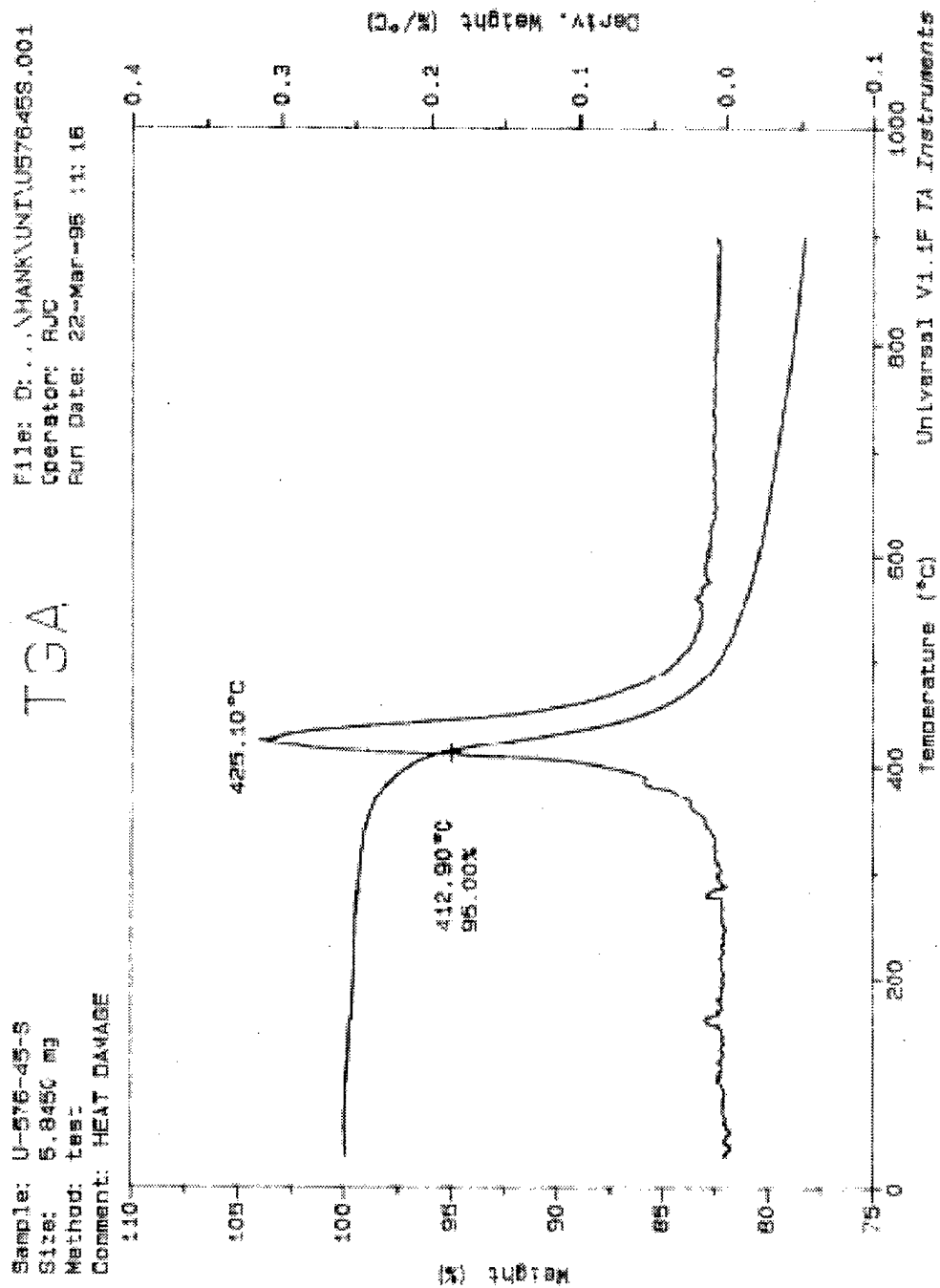
Figure C-33
TGA RESULTS SHOWING WEIGHT LOSS VERSUS TEMPERATURE OF THE IM6/977-3
UNIDIRECTIONAL LAMINATE SATURATED SAMPLE THAT WAS HEAT DAMAGED AT
302°C FOR 45 MIN

APPENDIX C
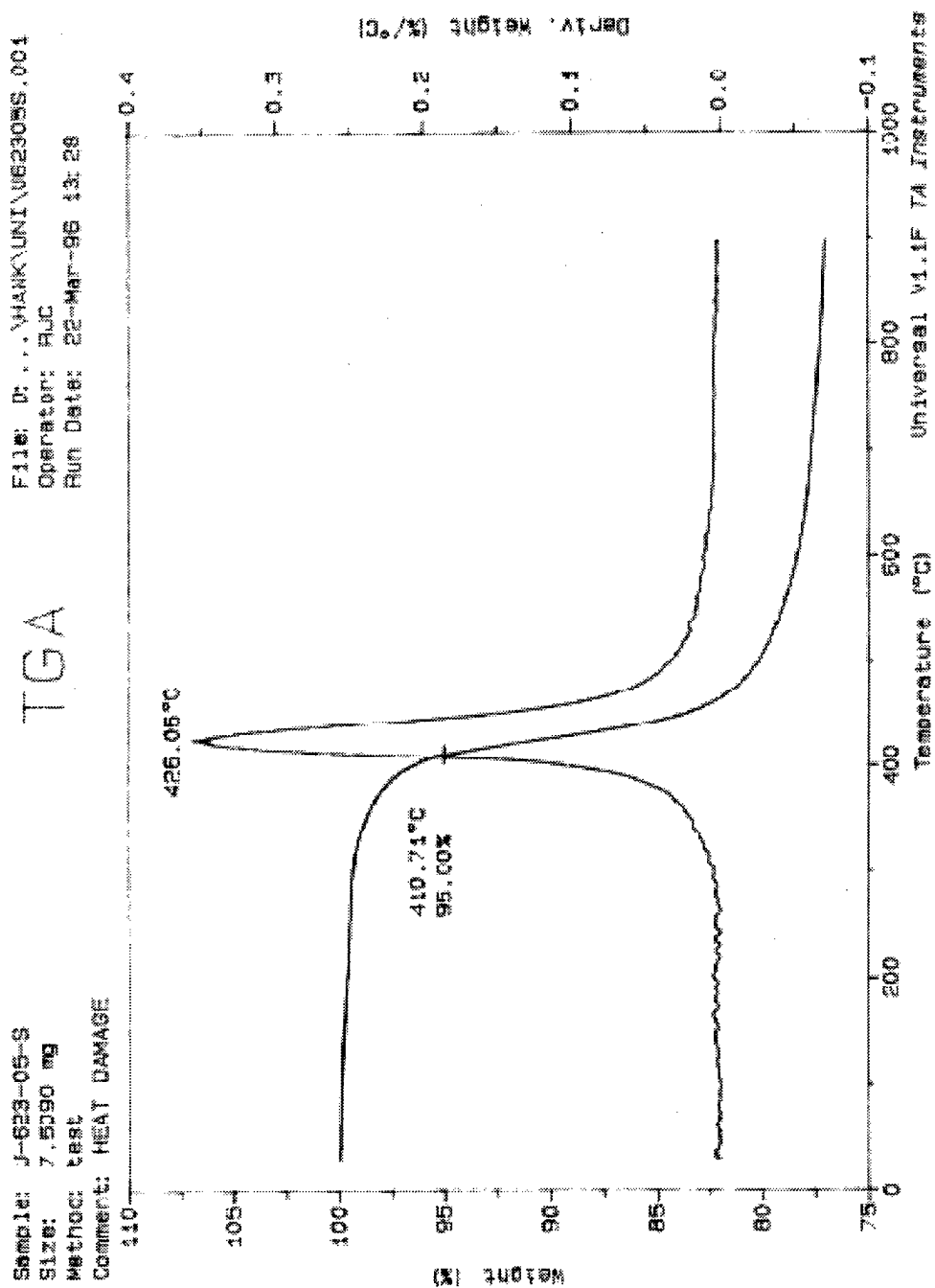
Figure C-34

TGA RESULTS SHOWING WEIGHT LOSS VERSUS TEMPERATURE OF THE IM6/977-3
UNIDIRECTIONAL LAMINATE SATURATED SAMPLE THAT WAS HEAT DAMAGED AT
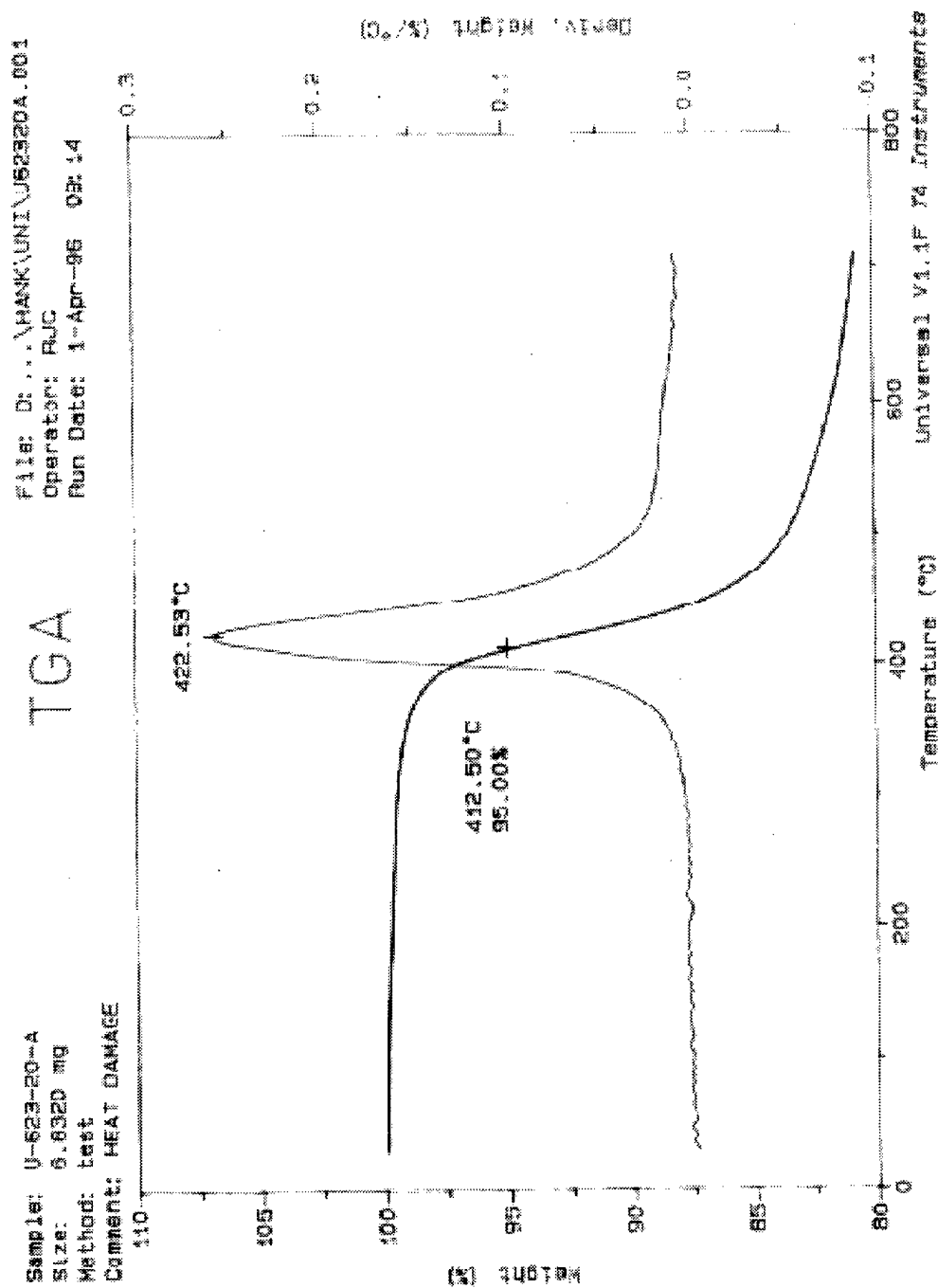329°C FOR 5 MIN

Figure C-35

TGA RESULTS SHOWING WEIGHT LOSS VERSUS TEMPERATURE OF THE IM6/977-3
UNIDIRECTIONAL LAMINATE SATURATED SAMPLE THAT WAS HEAT DAMAGED AT
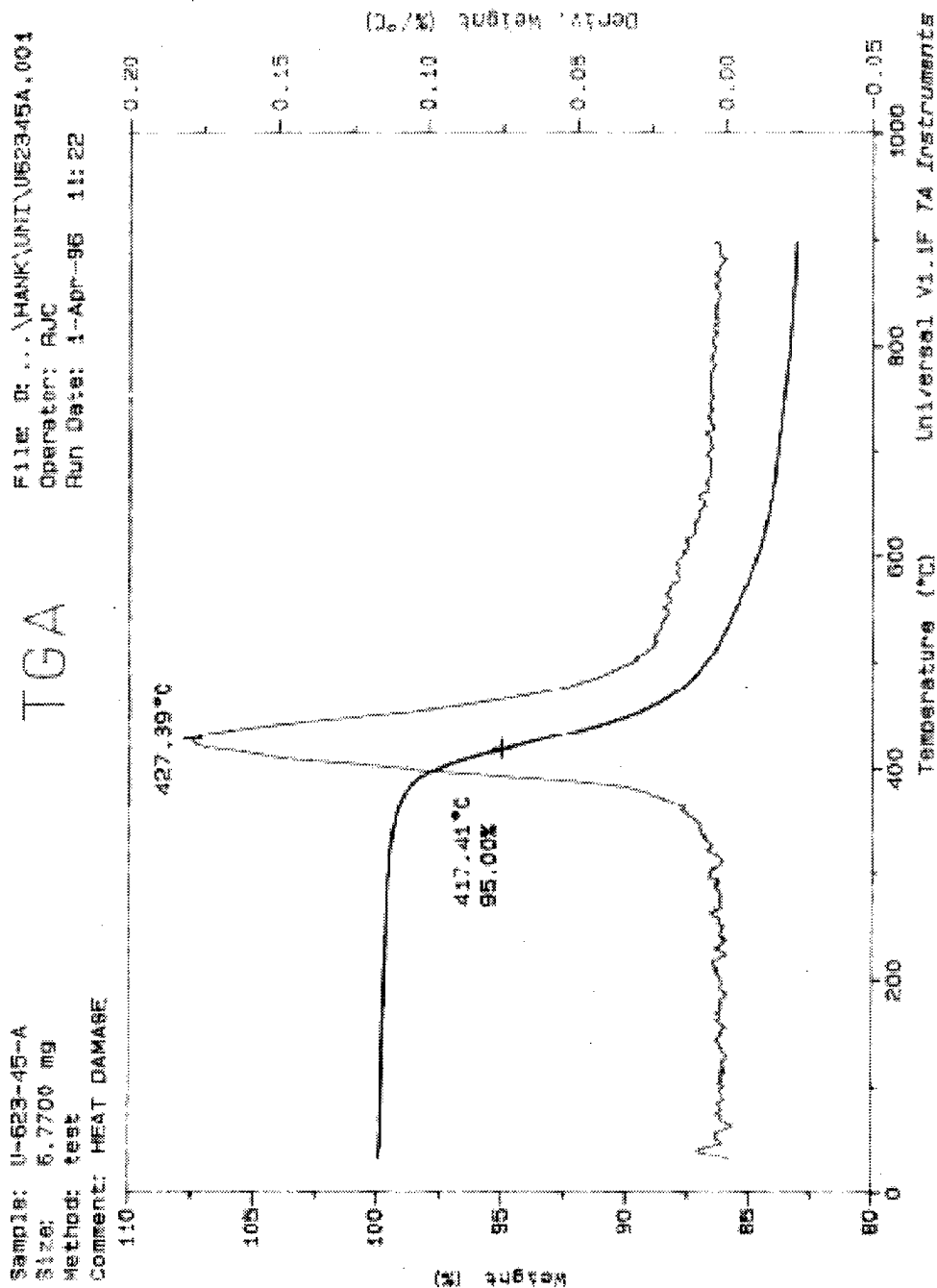329°C FOR 20 MIN

APPENDIX C

Figure C-36

TGA RESULTS SHOWING WEIGHT LOSS VERSUS TEMPERATURE OF THE IM6/977-3
UNIDIRECTIONAL LAMINATE SATURATED SAMPLE THAT WAS HEAT DAMAGED AT
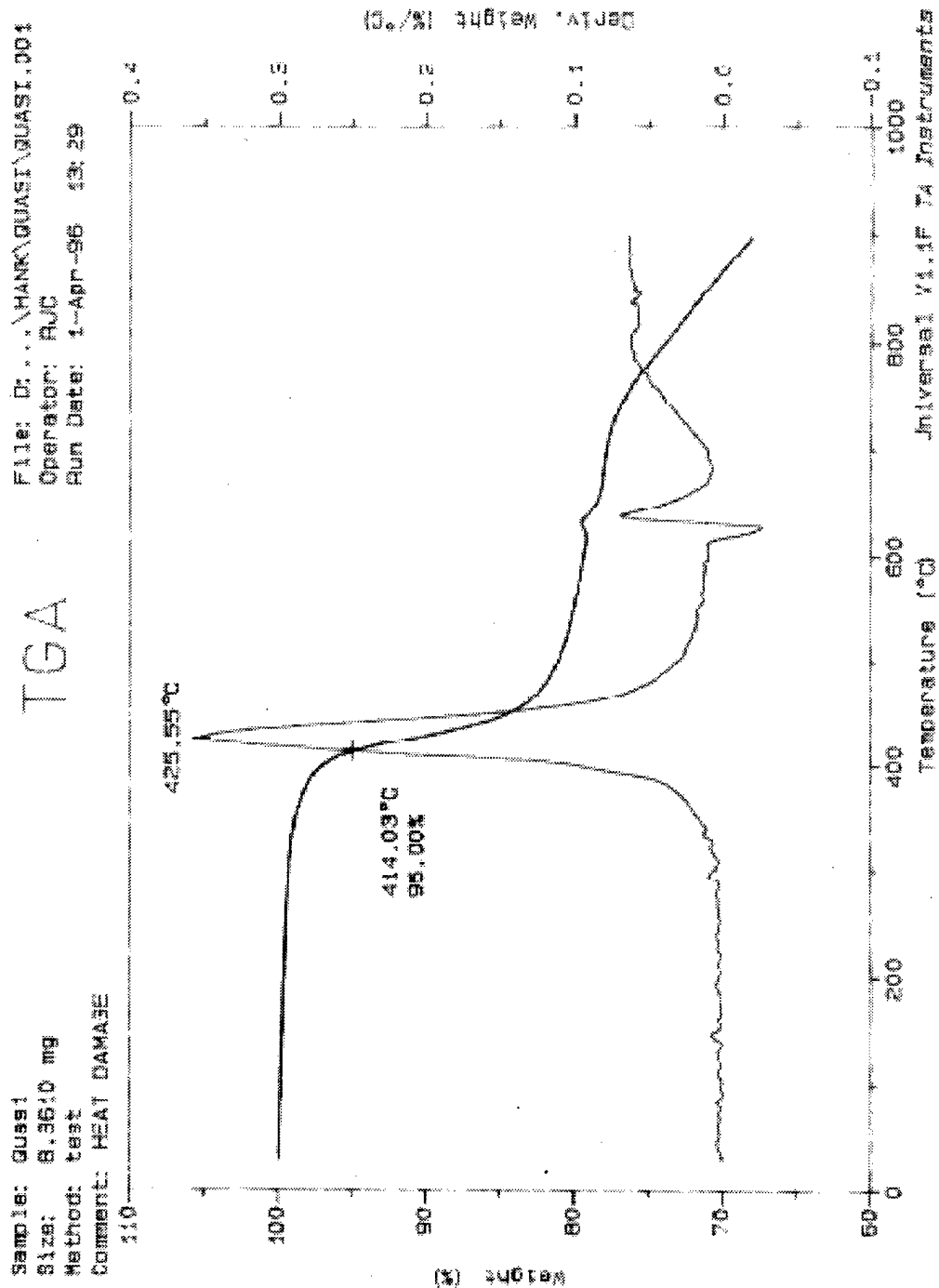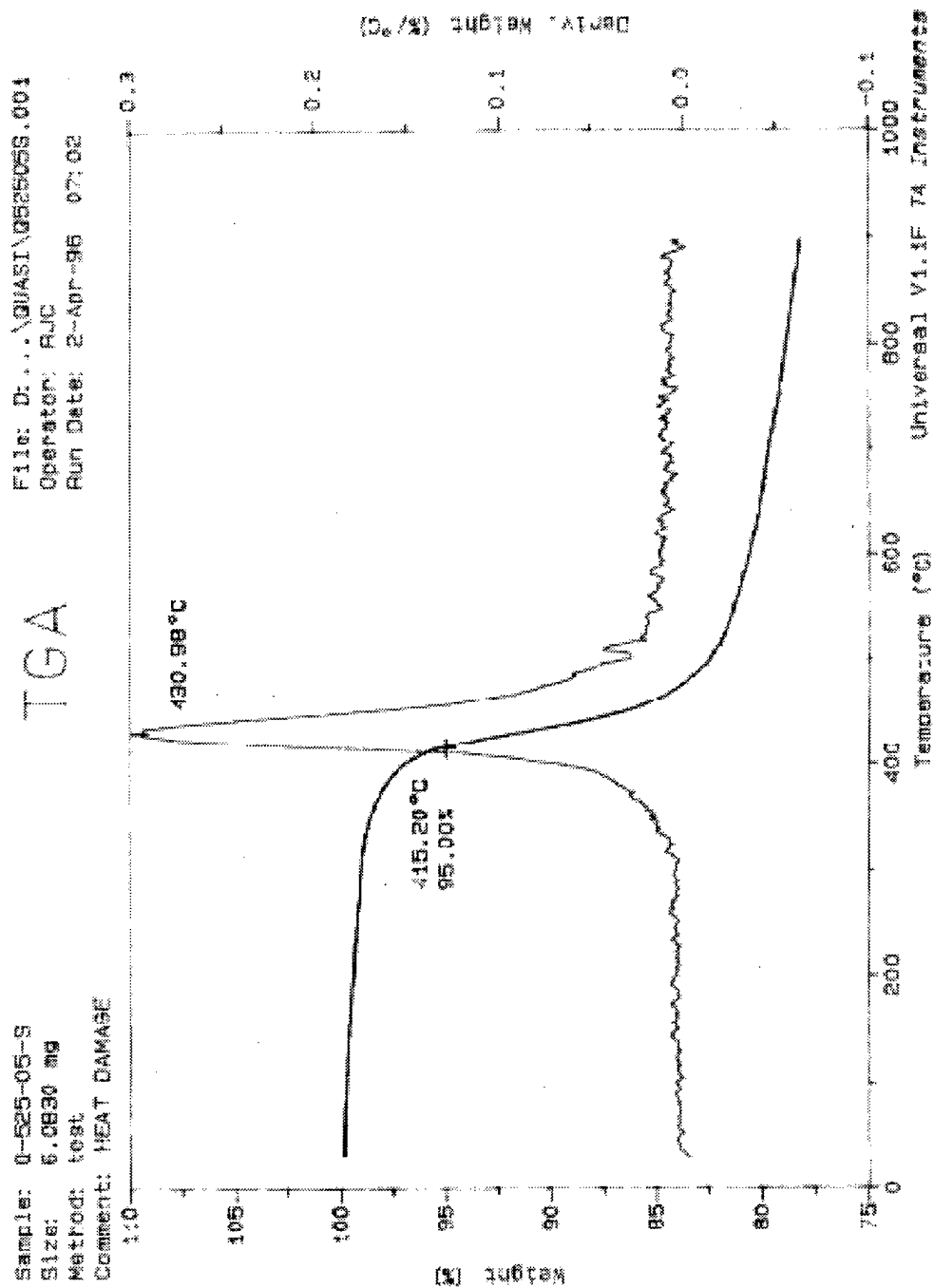329°C FOR 45 MIN

Figure C-37

TGA RESULTS SHOWING WEIGHT LOSS VERSUS TEMPERATURE OF THE IM6/977-3
UNIDIRECTIONAL LAMINATE DRY SAMPLE THAT WAS HEAT DAMAGED AT
274°C FOR 5MIN

Figure C-38
TGA RESULTS SHOWING WEIGHT LOSS VERSUS TEMPERATURE OF THE IM6/977-3
UNIDIRECTIONAL LAMINATE DRY SAMPLE THAT WAS HEAT DAMAGED AT
274°C FOR 20 MIN

Figure C-39

TGA RESULTS SHOWING WEIGHT LOSS VERSUS TEMPERATURE OF THE IM6/977-3
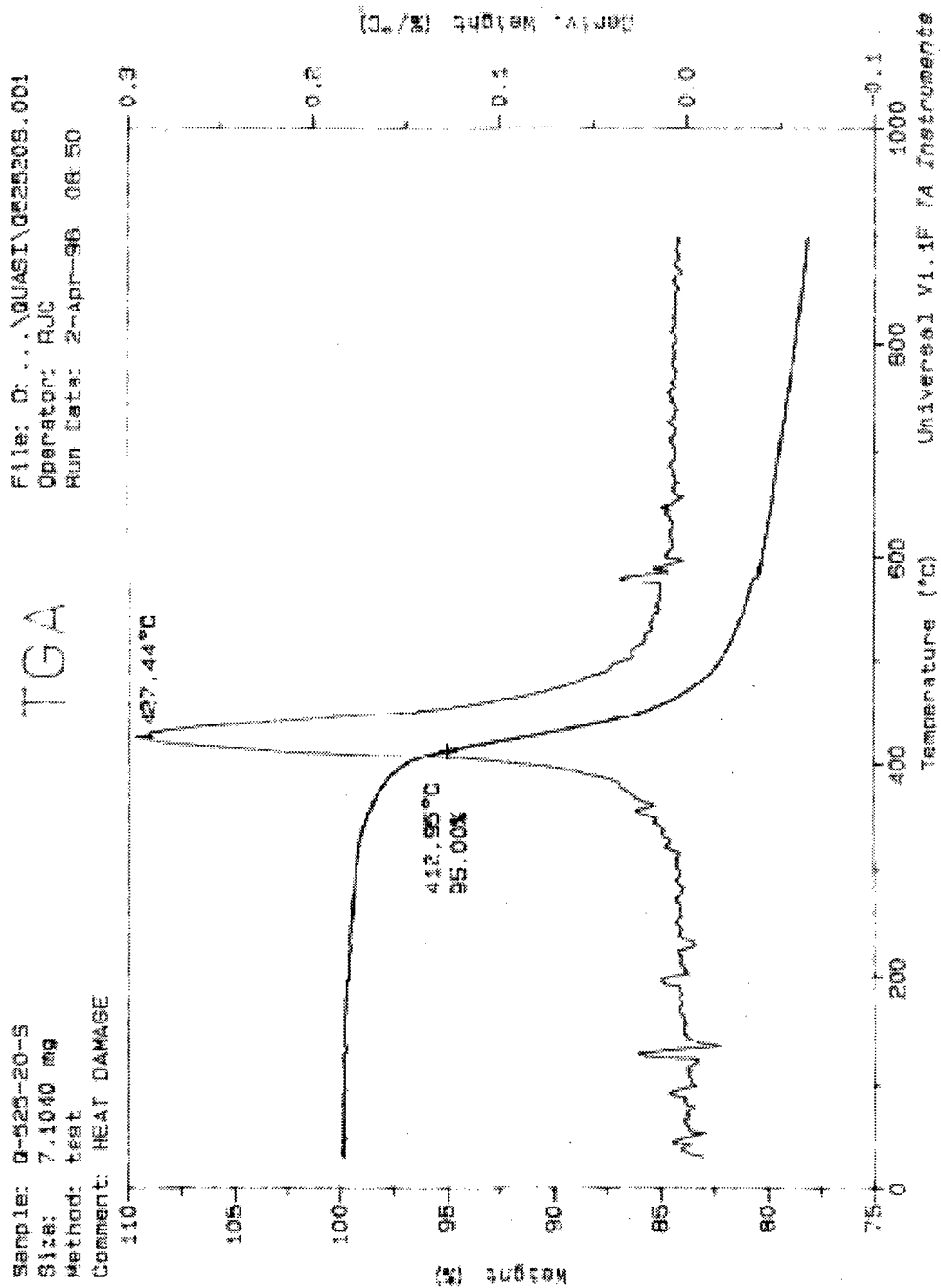UNIDIRECTIONAL LAMINATE DRY SAMPLE THAT WAS HEAT DAMAGED AT
274°C FOR 45 MIN

APPENDIX C

Figure C-40
TGA RESULTS SHOWING WEIGHT LOSS VERSUS TEMPERATURE OF THE IM6/977-3
UNIDIRECTIONAL LAMINATE DRY SAMPLE THAT WAS HEAT DAMAGED AT
302°C FOR 5 MIN

Figure C-41
TGA RESULTS SHOWING WEIGHT LOSS VERSUS TEMPERATURE OF THE IM6/977-3
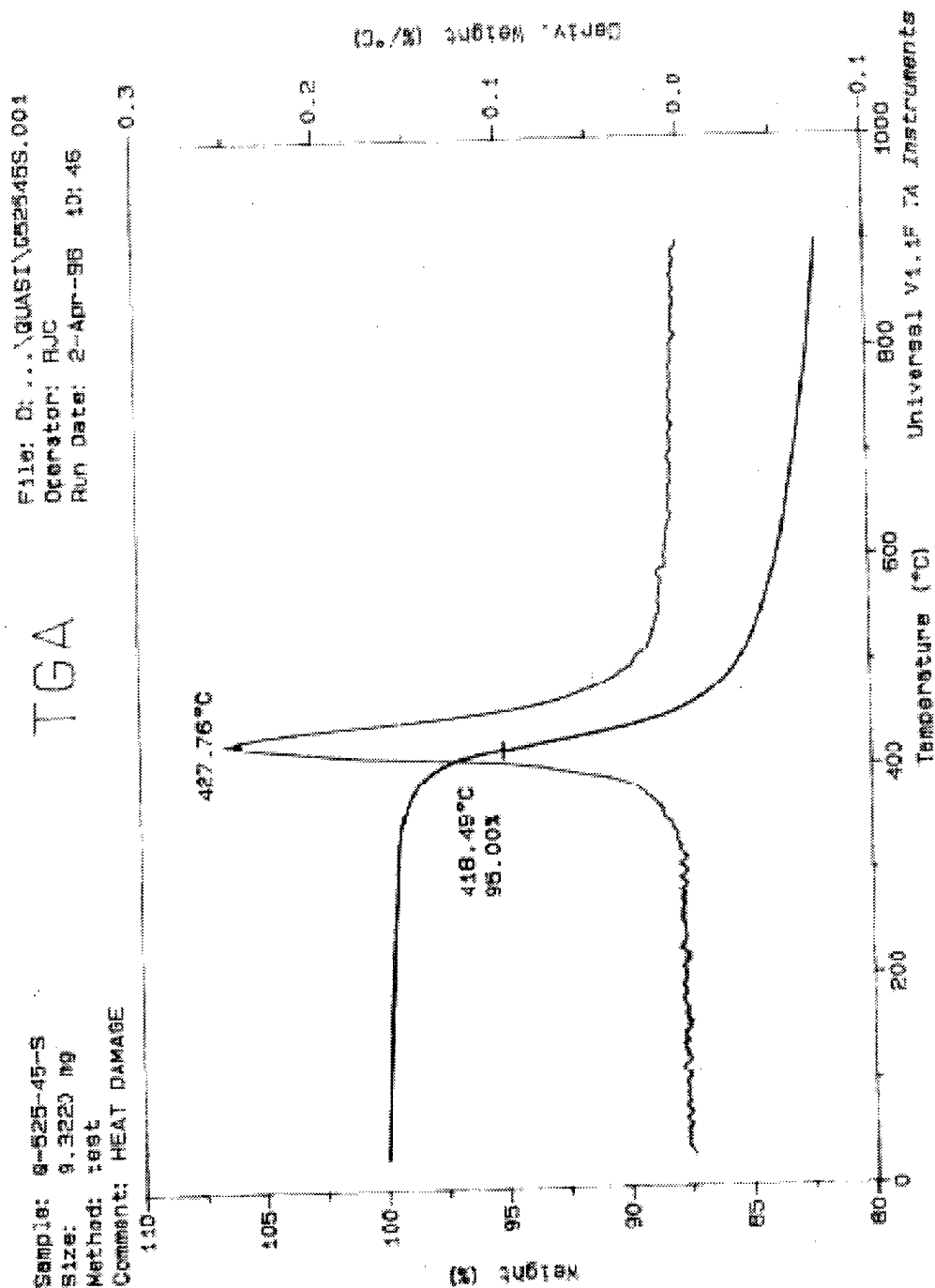UNIDIRECTIONAL LAMINATE DRY SAMPLE THAT WAS HEAT DAMAGED AT
302°C FOR 20 MIN

Figure C-42
TGA RESULTS SHOWING WEIGHT LOSS VERSUS TEMPERATURE OF THE IM6/977-3
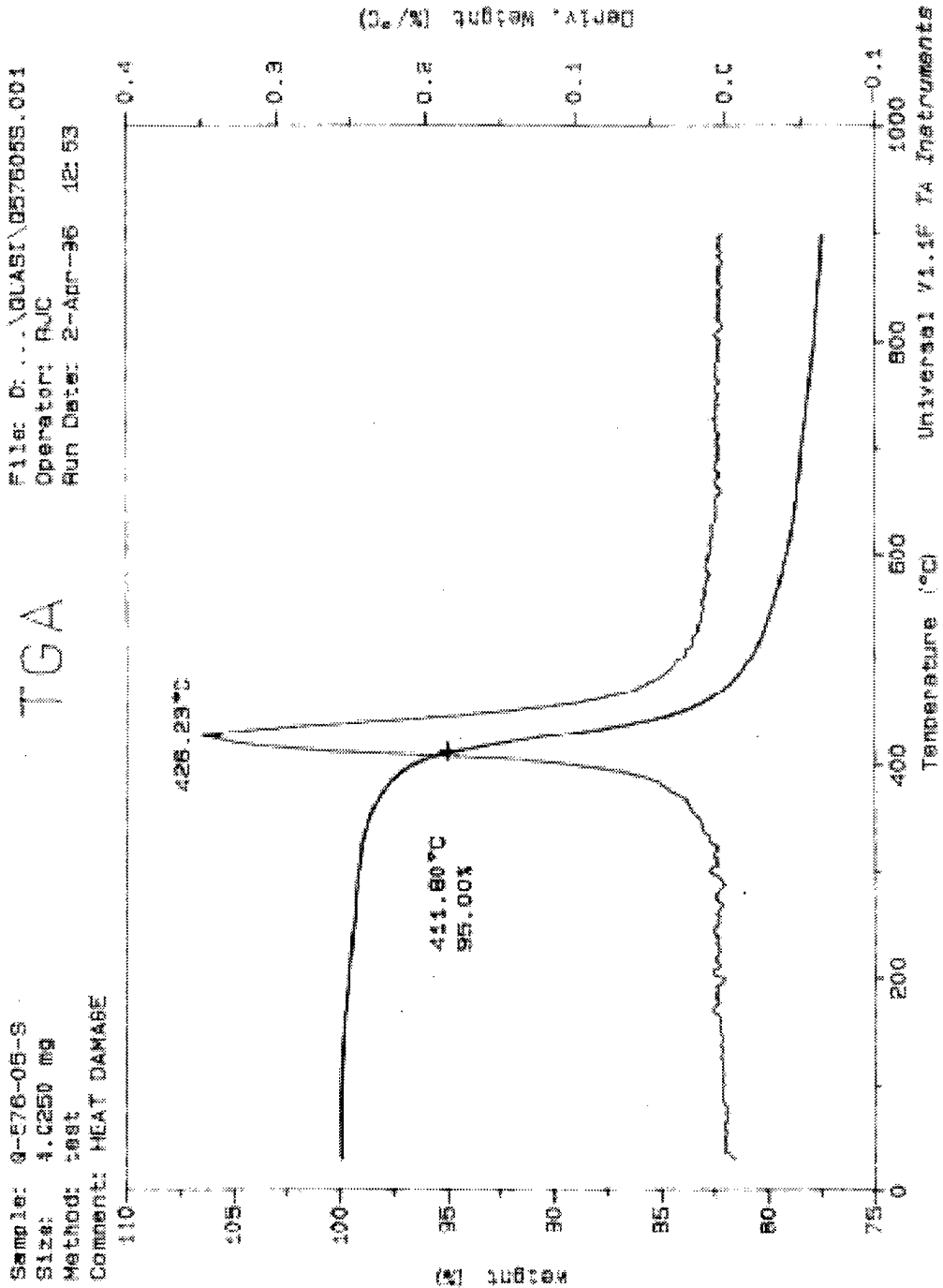UNIDIRECTIONAL LAMINATE DRY SAMPLE THAT WAS HEAT DAMAGED AT
302°C FOR 45 MIN

Figure C-43
TGA RESULTS SHOWING WEIGHT LOSS VERSUS TEMPERATURE OF THE IM6/977-3
UNIDIRECTIONAL LAMINATE DRY SAMPLE THAT WAS HEAT DAMAGED AT
329°C FOR 5 MIN

Figure C-44
TGA RESULTS SHOWING WEIGHT LOSS VERSUS TEMPERATURE OF THE IM6/977-3
UNIDIRECTIONAL LAMINATE DRY SAMPLE THAT WAS HEAT DAMAGED AT
329°C FOR 20 MIN

Figure C-45
TGA RESULTS SHOWING WEIGHT LOSS VERSUS TEMPERATURE OF THE IM6/977-3
UNIDIRECTIONAL LAMINATE DRY SAMPLE THAT WAS HEAT DAMAGED AT
329°C FOR 45 MIN

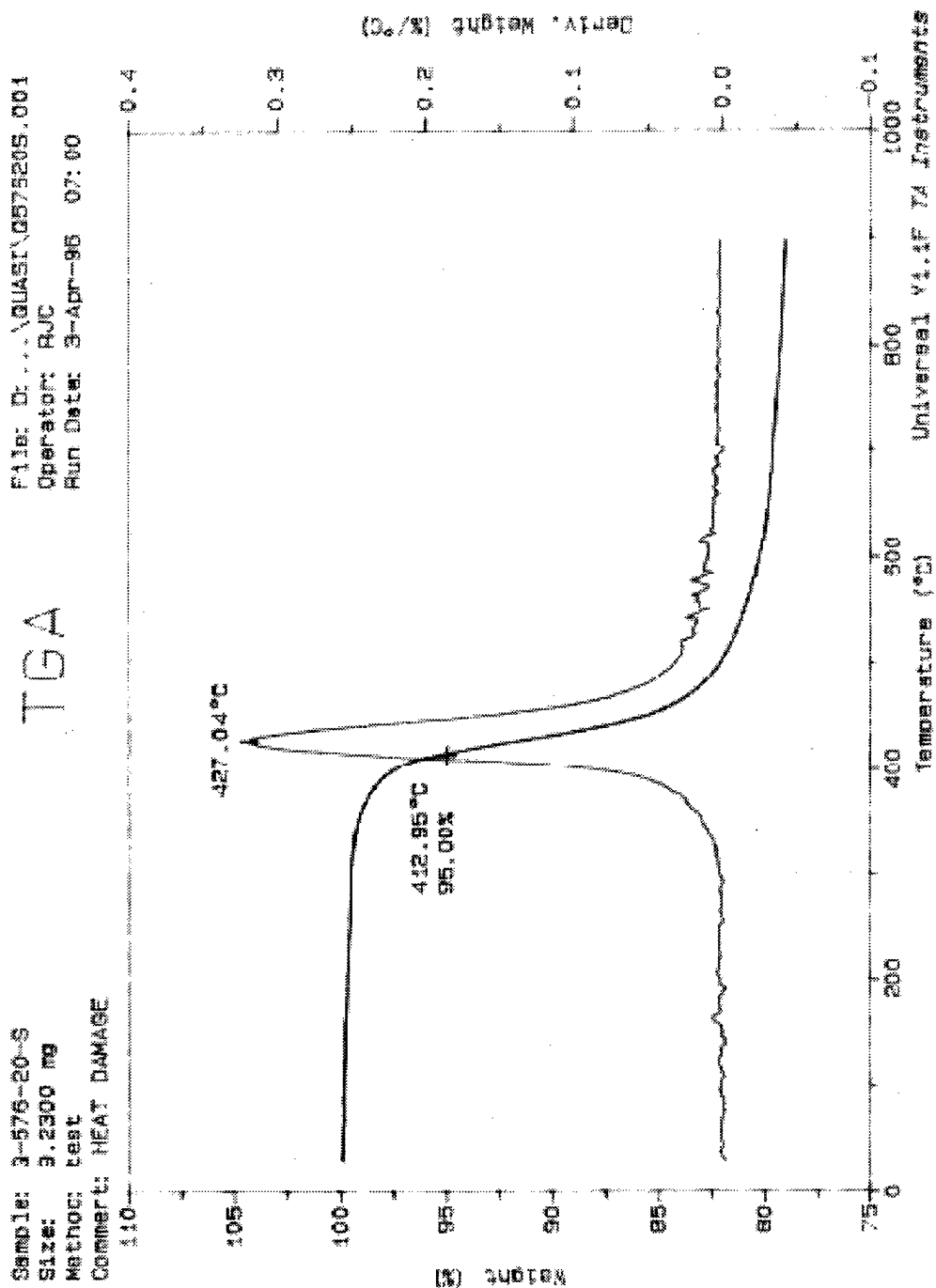APPENDIX C

Figure C-46

TGA RESULTS SHOWING WEIGHT LOSS VERSUS TEMPERATURE OF THE IM6/977-3
UNIDIRECTIONAL LAMINATE AMBIENT SAMPLE THAT WAS HEAT DAMAGED AT
274°C FOR 5 MIN

Figure C-47

TGA RESULTS SHOWING WEIGHT LOSS VERSUS TEMPERATURE OF THE IM6/977-3
UNIDIRECTIONAL LAMINATE AMBIENT SAMPLE THAT WAS HEAT DAMAGED AT
274°C FOR 20 MIN

Figure C-48

TGA RESULTS SHOWING WEIGHT LOSS VERSUS TEMPERATURE OF THE IM6/977-3
UNIDIRECTIONAL LAMINATE AMBIENT SAMPLE THAT WAS HEAT DAMAGED AT
274°C FOR 45 MIN

Figure C-49

TGA RESULTS SHOWING WEIGHT LOSS VERSUS TEMPERATURE OF THE IM6/977-3
UNIDIRECTIONAL LAMINATE AMBIENT SAMPLE THAT WAS HEAT DAMAGED AT
302°C FOR 5 MIN

APPENDIX C

Figure C-50

TGA RESULTS SHOWING WEIGHT LOSS VERSUS TEMPERATURE OF THE IM6/977-3 UNIDIRECTIONAL LAMINATE AMBIENT SAMPLE THAT WAS HEAT DAMAGED AT 302°C FOR 20 MIN
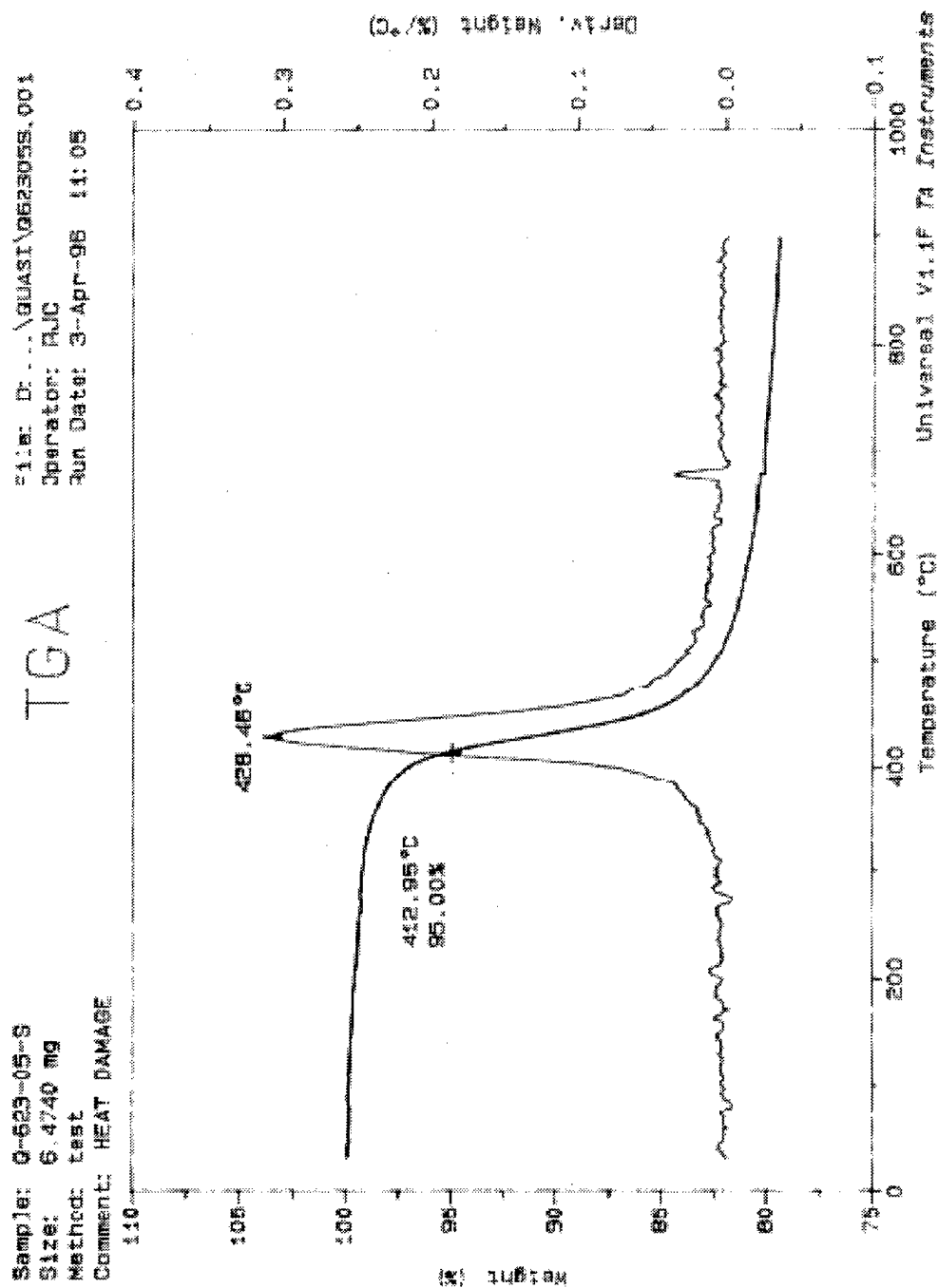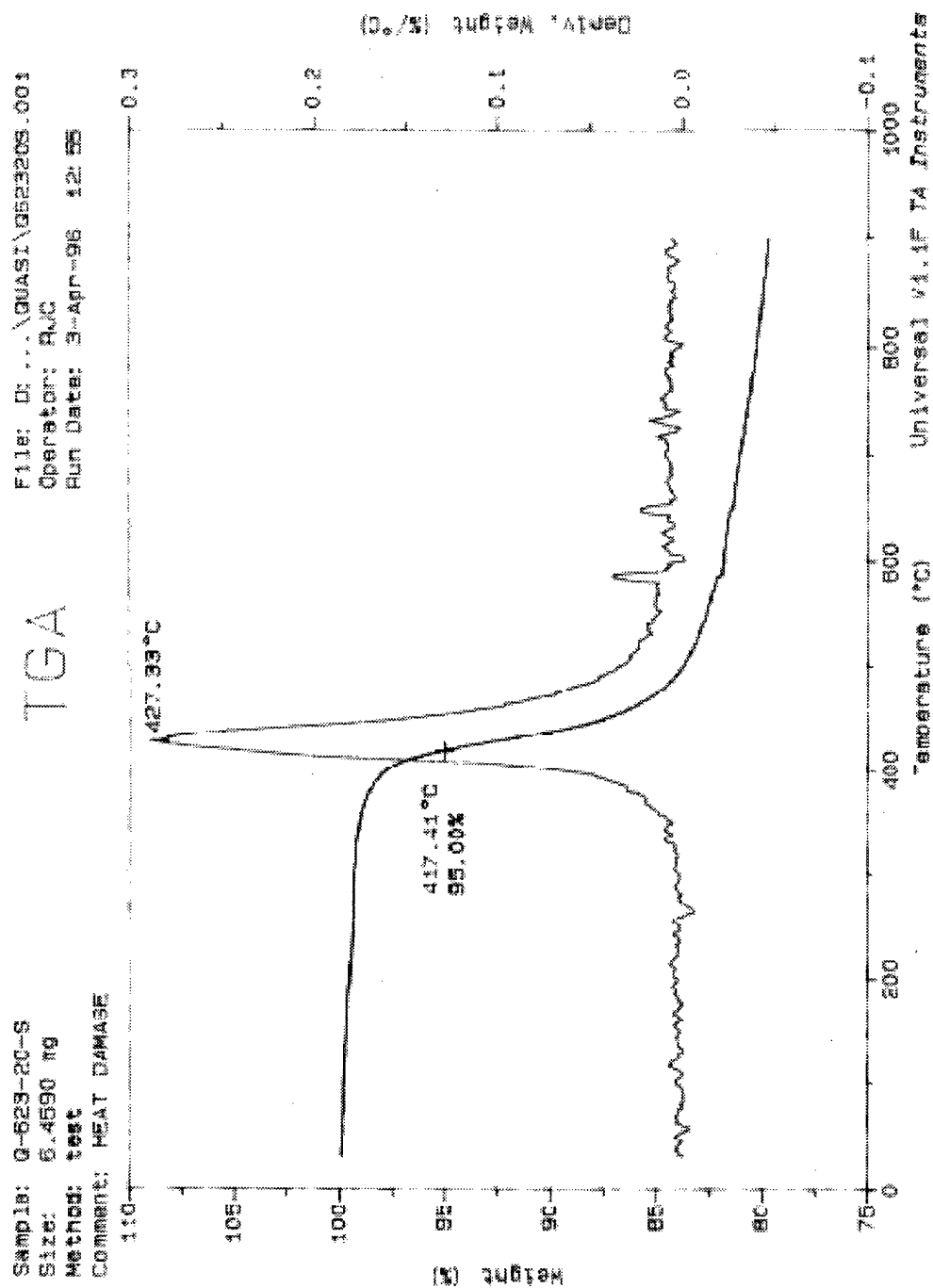
Figure C-51
TGA RESULTS SHOWING WEIGHT LOSS VERSUS TEMPERATURE OF THE IM6/977-3
UNIDIRECTIONAL LAMINATE AMBIENT SAMPLE THAT WAS HEAT DAMAGED AT
302°C FOR 45 MIN

Figure C-52

TGA RESULTS SHOWING WEIGHT LOSS VERSUS TEMPERATURE OF THE IM6/977-3 UNIDIRECTIONAL LAMINATE AMBIENT SAMPLE THAT WAS HEAT DAMAGED AT 329°C FOR 5 MIN

Figure C-53

TGA RESULTS SHOWING WEIGHT LOSS VERSUS TEMPERATURE OF THE IM6/977-3
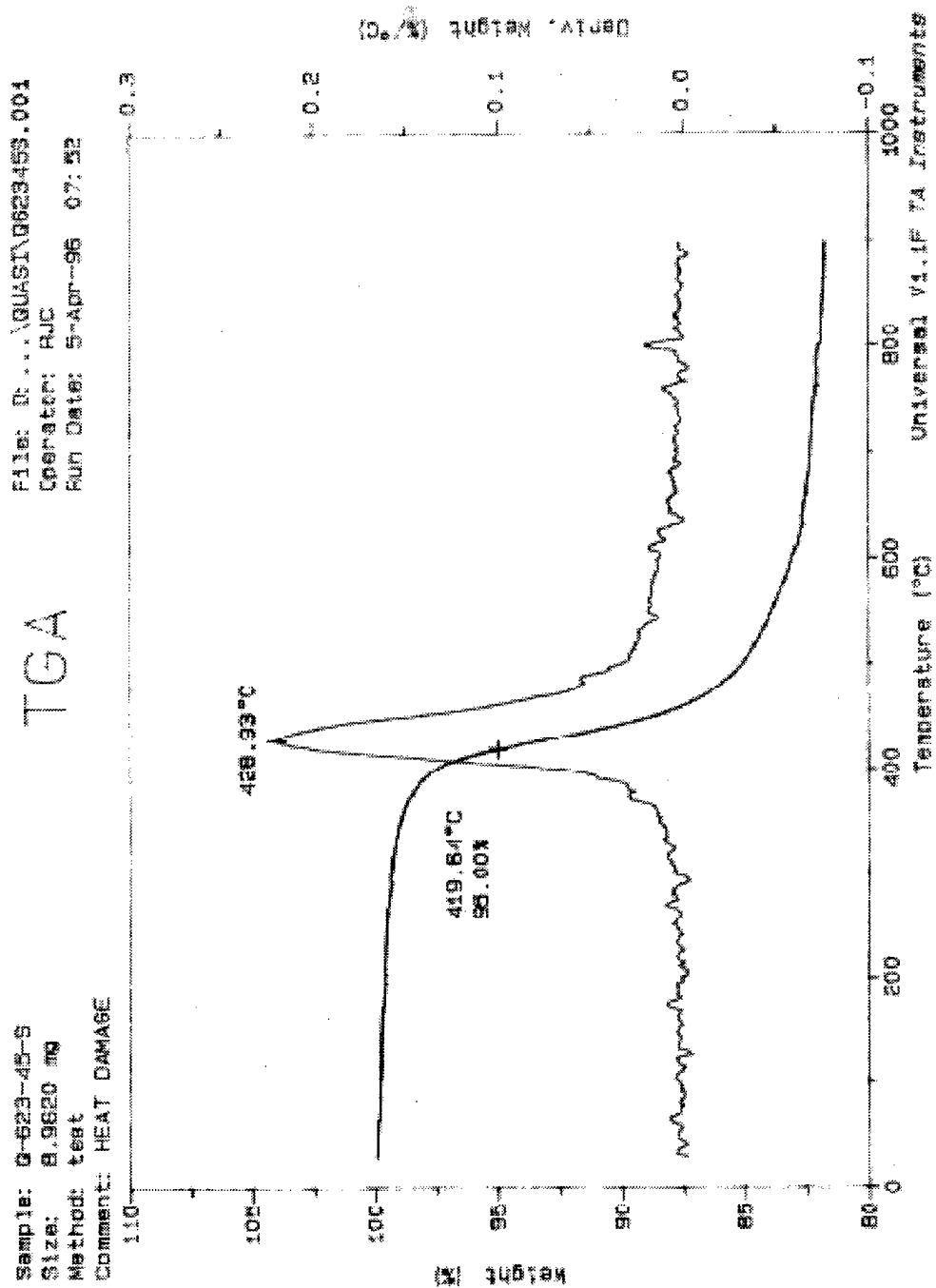UNIDIRECTIONAL LAMINATE AMBIENT SAMPLE THAT WAS HEAT DAMAGED AT
329°C FOR 20 MIN

Figure C-54
TGA RESULTS SHOWING WEIGHT LOSS VERSUS TEMPERATURE OF THE IM6/977-3
UNIDIRECTIONAL LAMINATE AMBIENT SAMPLE THAT WAS HEAT DAMAGED AT
329°C FOR 45 MIN

Figure C-55
TGA RESULTS SHOWING WEIGHT LOSS VERSUS TEMPERATURE OF THE UNDAMAGED
IM6/977-3 QUASI-ISOTROPIC LAMINATE SATURATED SAMPLE

Figure C-56
TGA RESULTS SHOWING WEIGHT LOSS VERSUS TEMPERATURE OF THE IM6/977-3
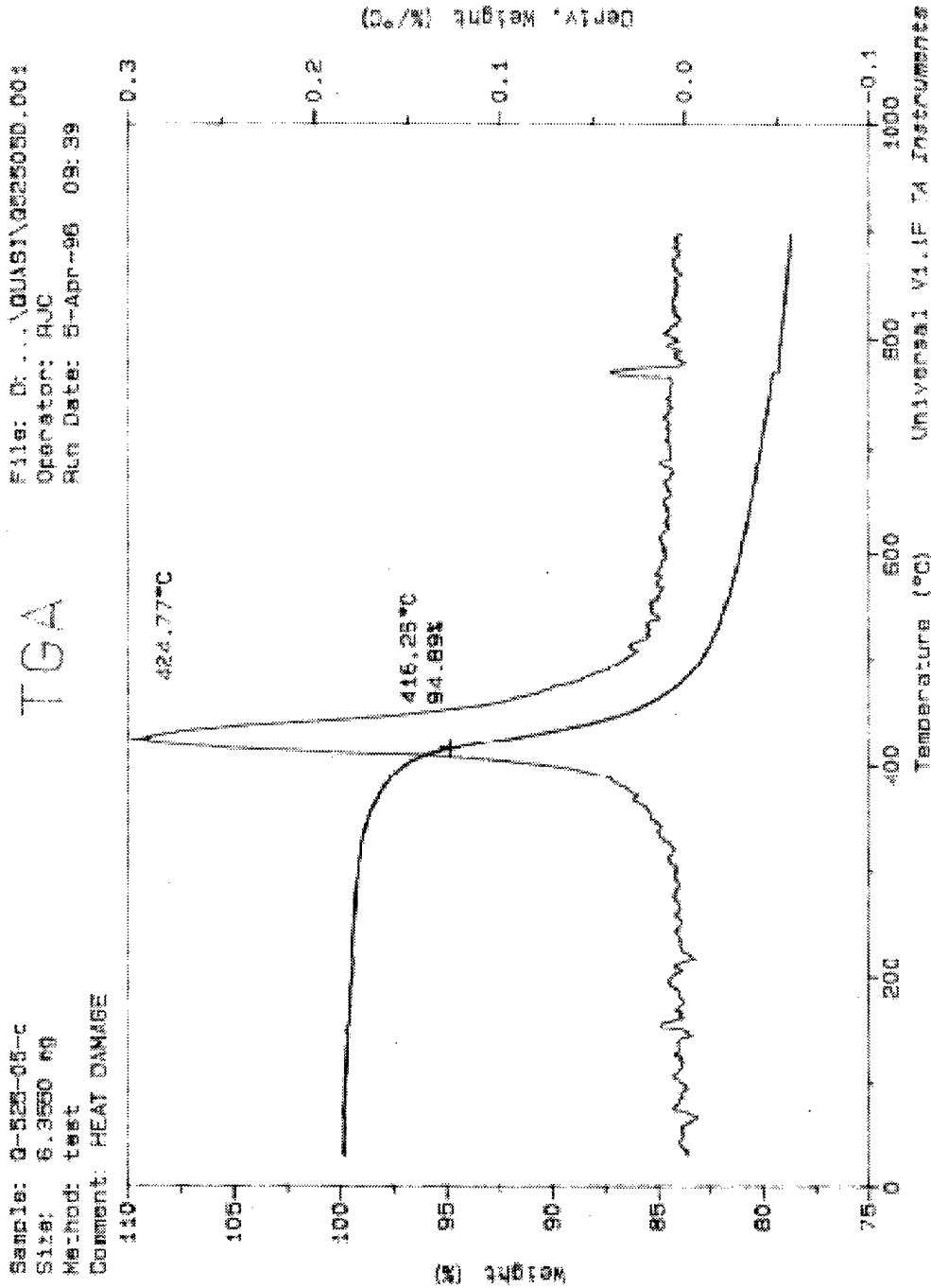QUASI-ISOTROPIC LAMINATE SATURATED SAMPLE THAT WAS HEAT DAMAGED AT
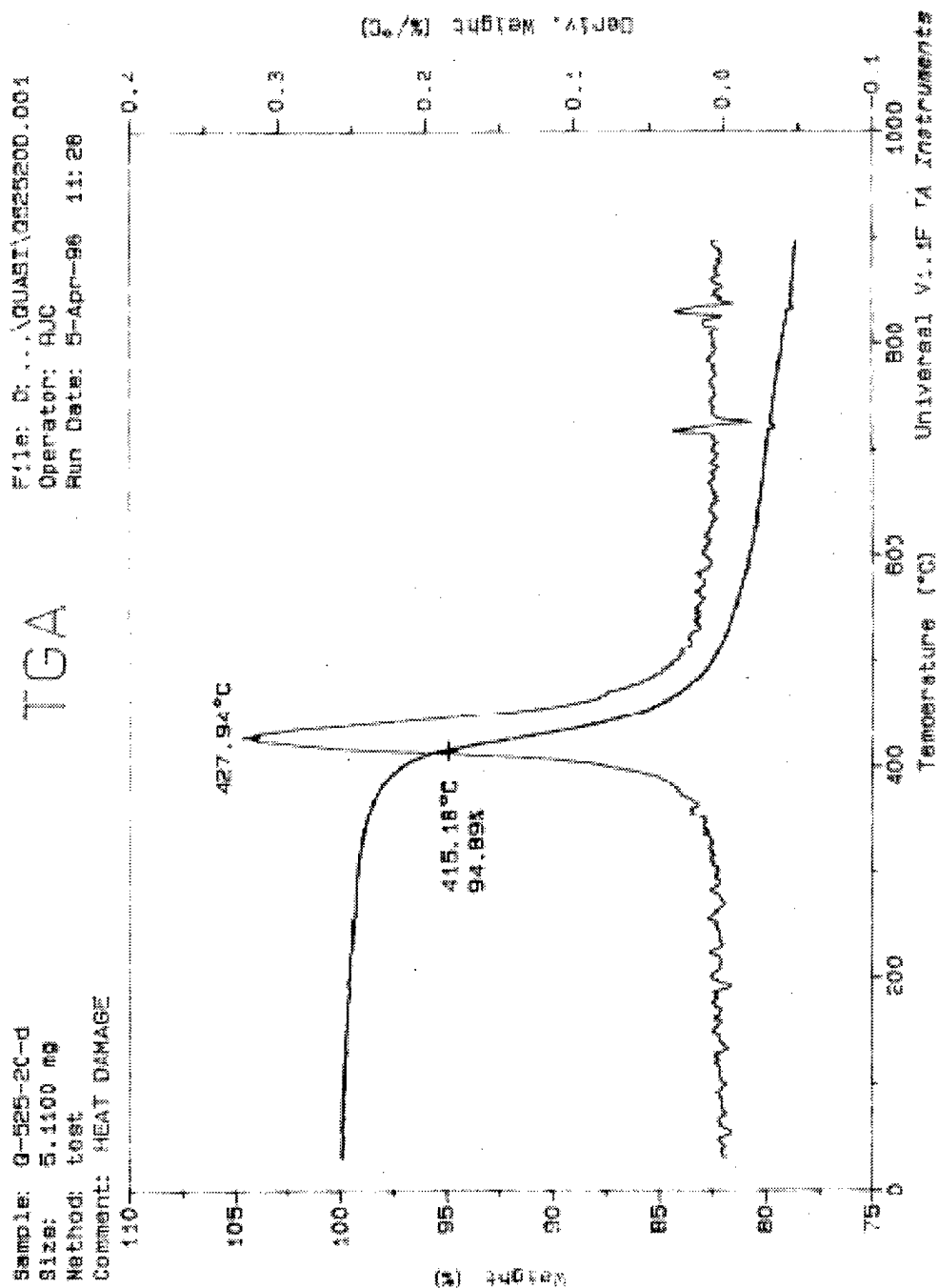274°C FOR 5 MIN

Figure C-57

TGA RESULTS SHOWING WEIGHT LOSS VERSUS TEMPERATURE OF THE IM6/977-3
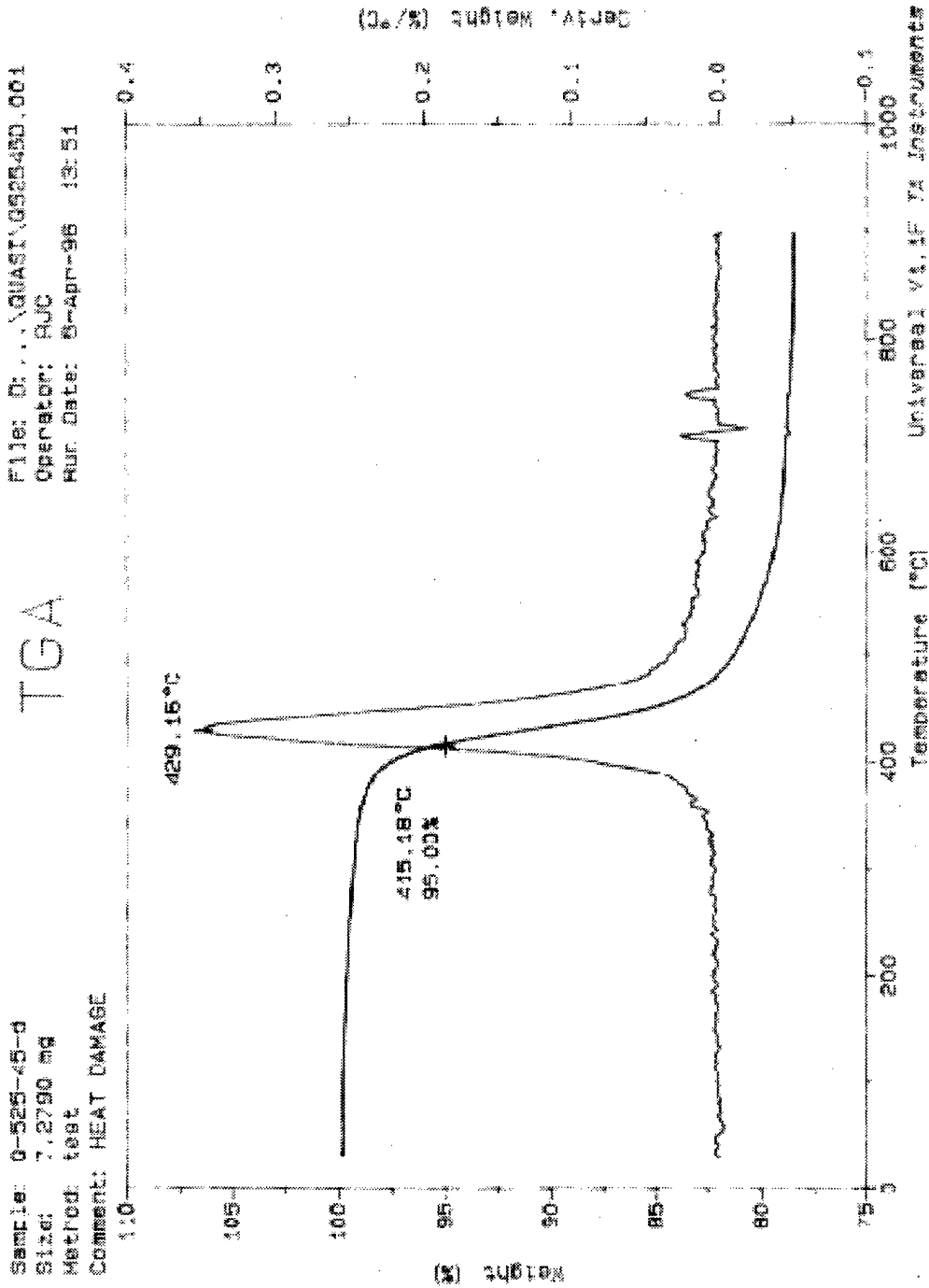QUASI-ISOTROPIC LAMINATE SATURATED SAMPLE THAT WAS HEAT DAMAGED AT
274°C FOR 20 MIN

APPENDIX C

Figure C-58

TGA RESULTS SHOWING WEIGHT LOSS VERSUS TEMPERATURE OF THE IM6/977-3
QUASI-ISOTROPIC LAMINATE SATURATED SAMPLE THAT WAS HEAT DAMAGED AT
274°C FOR 45 MIN

APPENDIX C

Figure C-59

TGA RESULTS SHOWING WEIGHT LOSS VERSUS TEMPERATURE OF THE IM6/977-3
QUASI-ISOTROPIC LAMINATE SATURATED SAMPLE THAT WAS HEAT DAMAGED AT
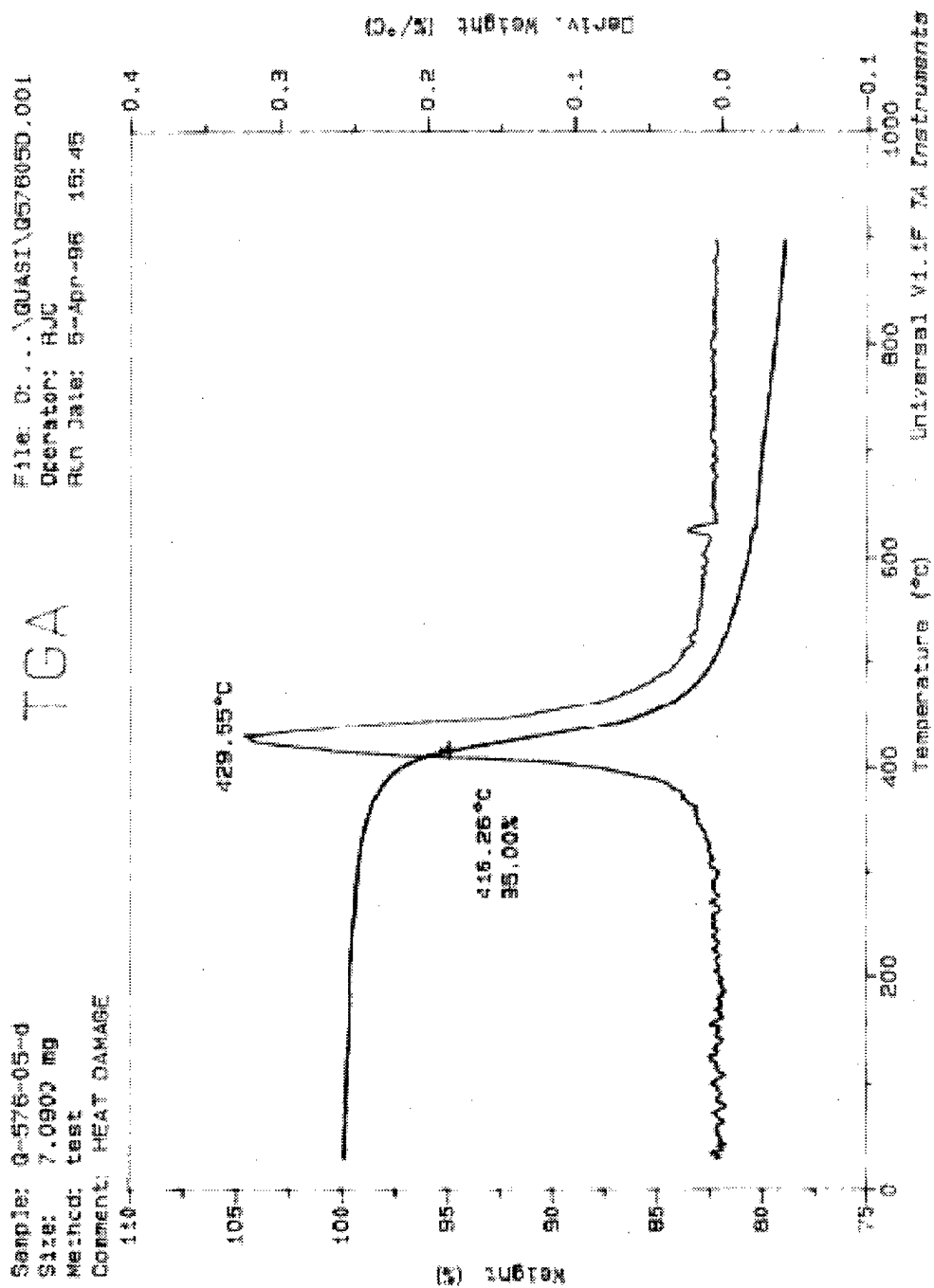302°C FOR 5 MIN

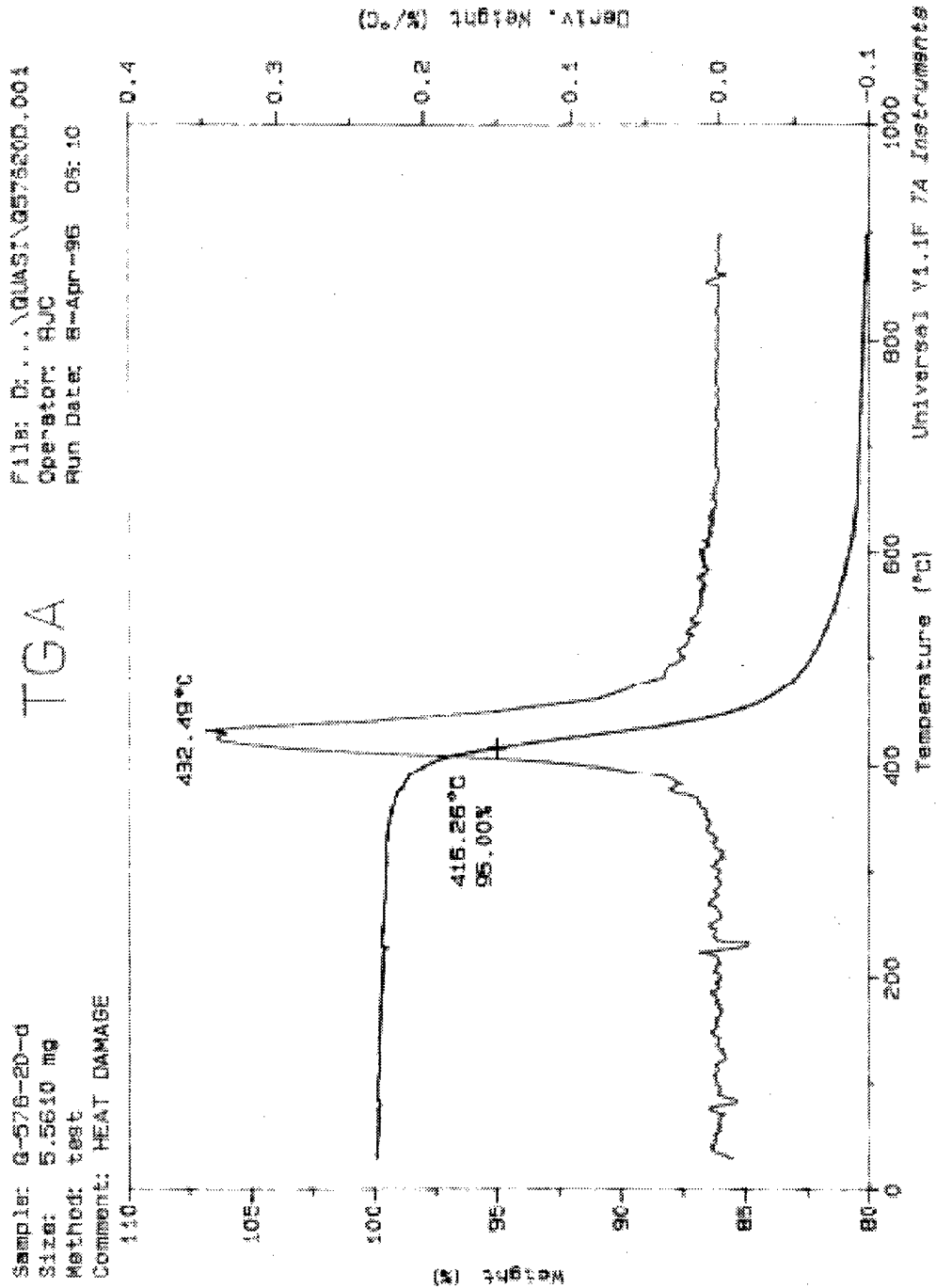APPENDIX C

Figure C-60

TGA RESULTS SHOWING WEIGHT LOSS VERSUS TEMPERATURE OF THE IM6/977-3 QUASI-ISOTROPIC LAMINATE SATURATED SAMPLE THAT WAS HEAT DAMAGED AT 302°C FOR 20 MIN

APPENDIX C
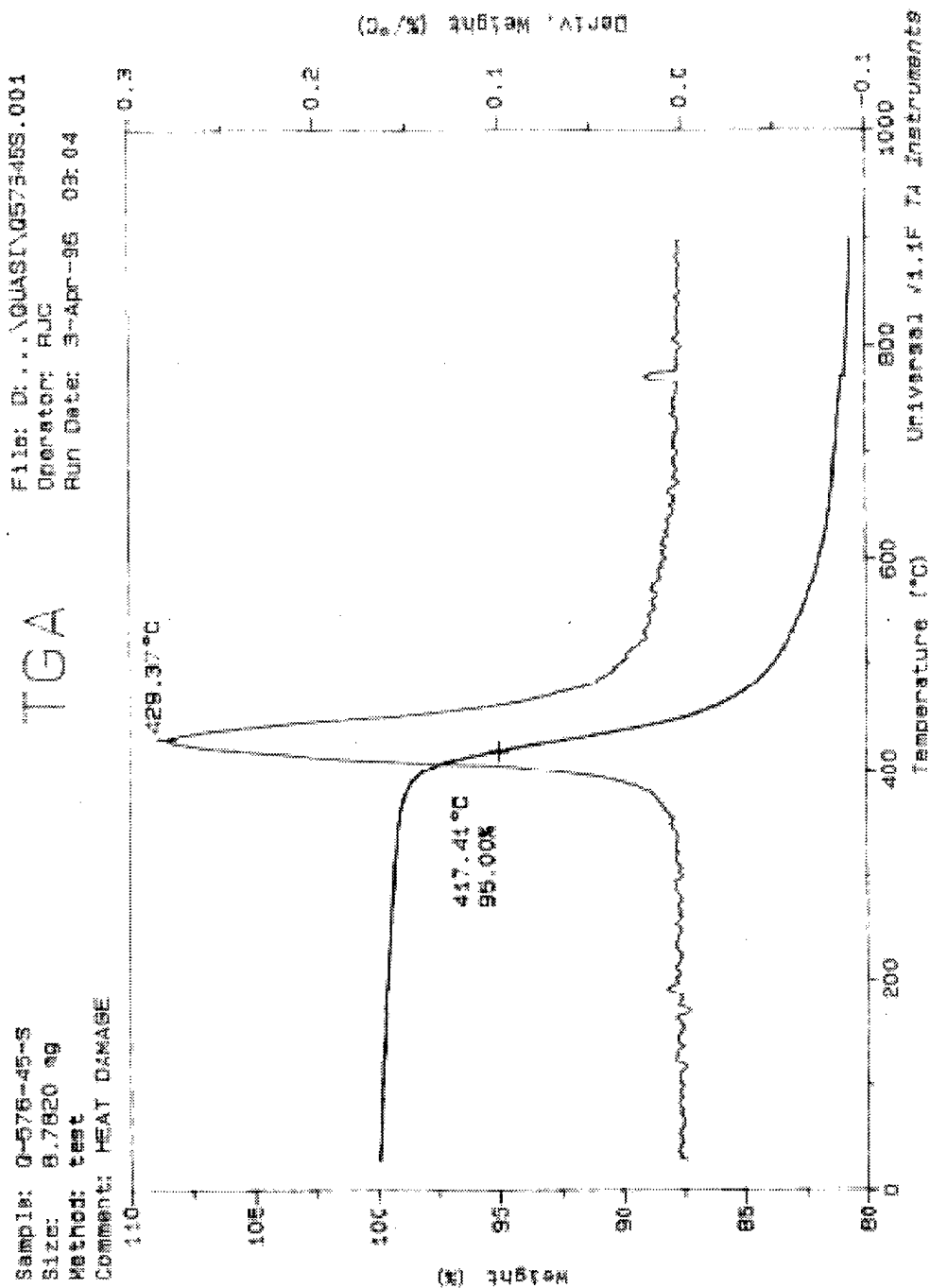
Figure C-61

TGA RESULTS SHOWING WEIGHT LOSS VERSUS TEMPERATURE OF THE IM6/977-3
QUASI-ISOTROPIC LAMINATE SATURATED SAMPLE THAT WAS HEAT DAMAGED AT
302°C FOR 45 MIN

Figure C-62

TGA RESULTS SHOWING WEIGHT LOSS VERSUS TEMPERATURE OF THE IM6/977-3 QUASI-ISOTROPIC LAMINATE SATURATED SAMPLE THAT WAS HEAT DAMAGED AT 329°C FOR 5 MIN

Figure C-63

TGA RESULTS SHOWING WEIGHT LOSS VERSUS TEMPERATURE OF THE IM6/977-3
QUASI-ISOTROPIC LAMINATE SATURATED SAMPLE THAT WAS HEAT DAMAGED AT
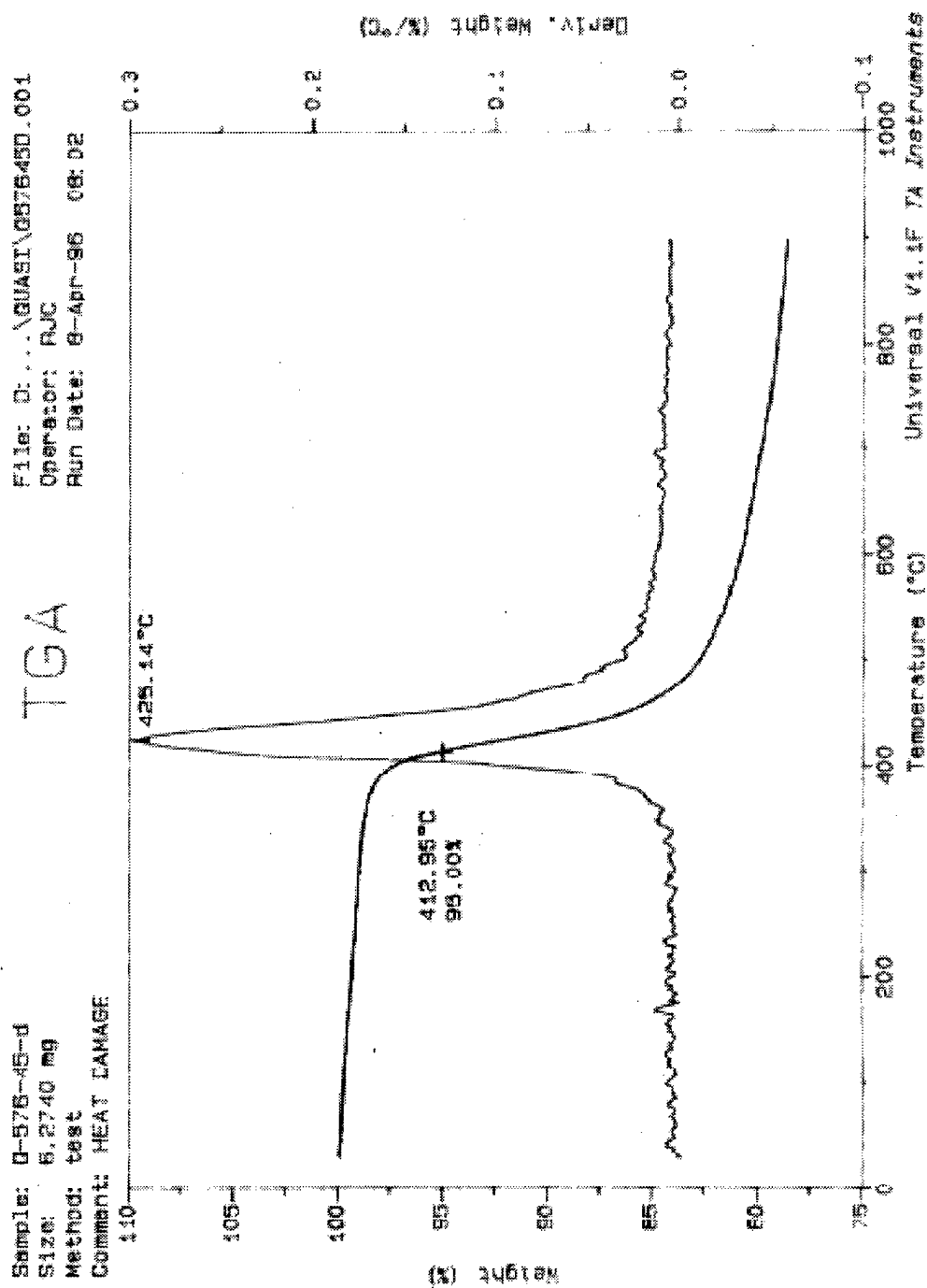329°C FOR 20 MIN

Figure C-64
TGA RESULTS SHOWING WEIGHT LOSS VERSUS TEMPERATURE OF THE IM6/977-3
QUASI-ISOTROPIC LAMINATE SATURATED SAMPLE THAT WAS HEAT DAMAGED AT
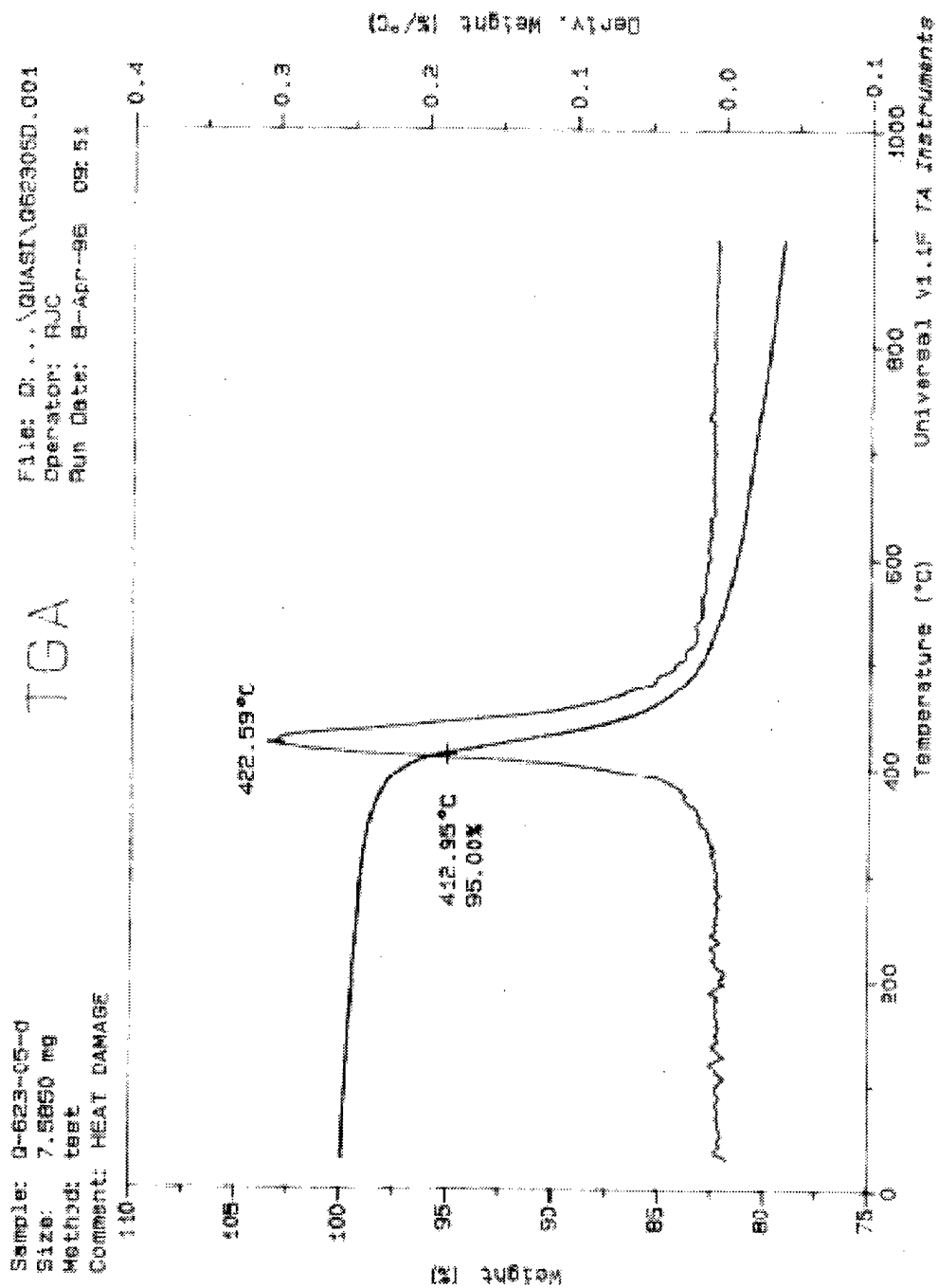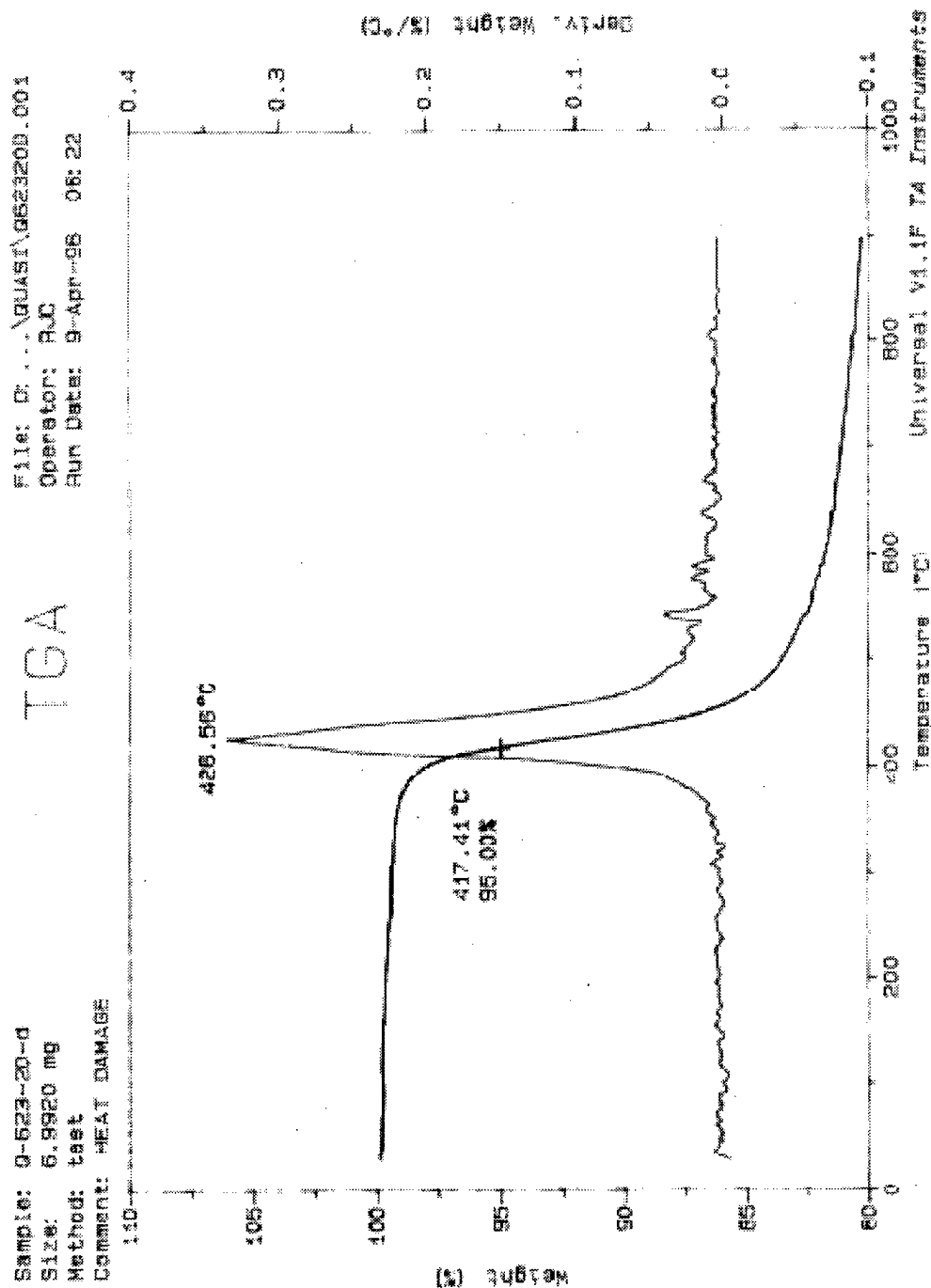329°C FOR 45 MIN

Figure C-65

TGA RESULTS SHOWING WEIGHT LOSS VERSUS TEMPERATURE OF THE IM6/977-3
QUASI-ISOTROPIC LAMINATE DRY SAMPLE THAT WAS HEAT DAMAGED AT
274°C FOR 5 MIN

APPENDIX C

Figure C-66

TGA RESULTS SHOWING WEIGHT LOSS VERSUS TEMPERATURE OF THE IM6/977-3
QUASI-ISOTROPIC LAMINATE DRY SAMPLE THAT WAS HEAT DAMAGED AT
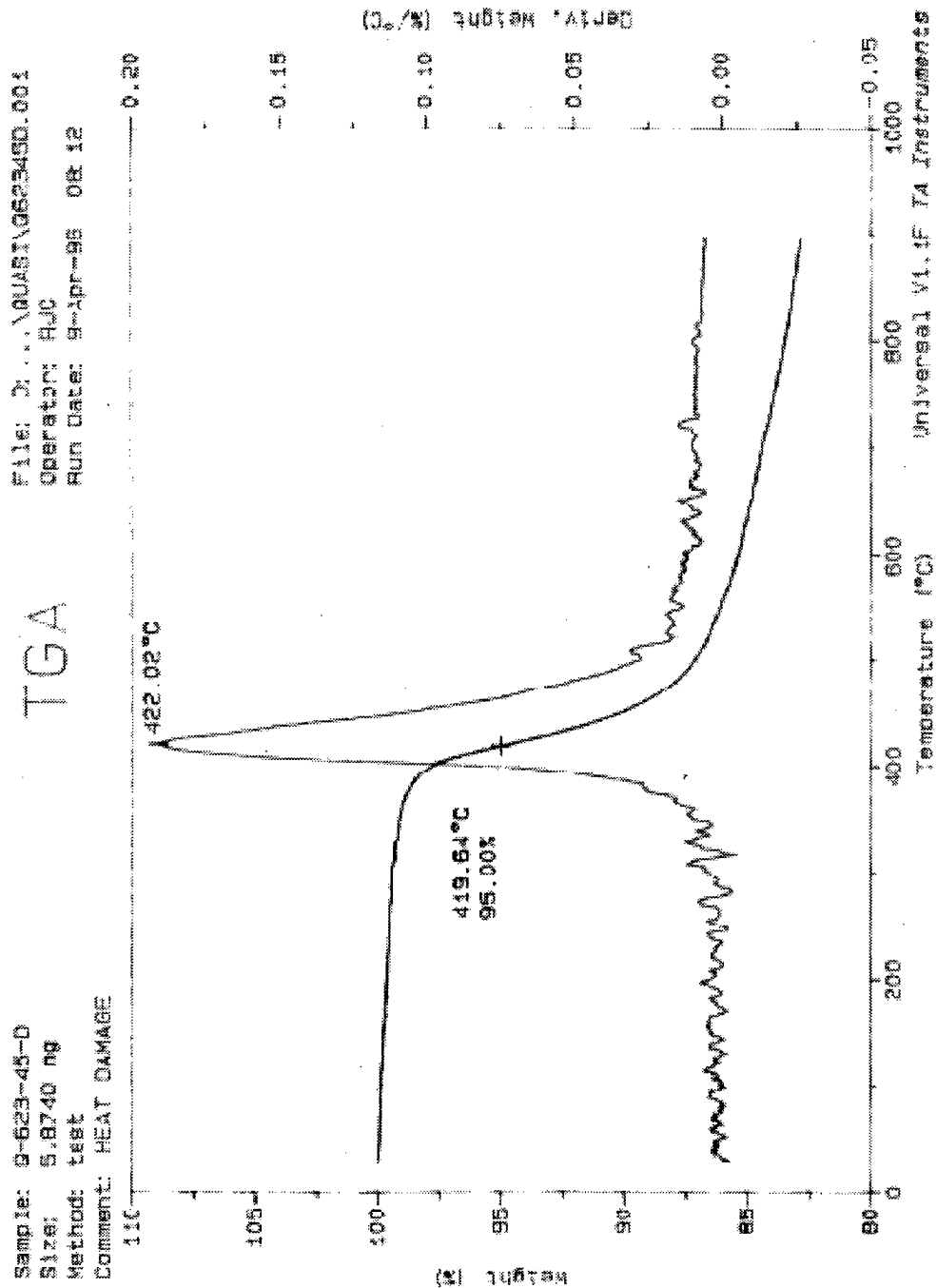274°C FOR 20 MIN

Figure C-67

TGA RESULTS SHOWING WEIGHT LOSS VERSUS TEMPERATURE OF THE IM6/977-3
QUASI-ISOTROPIC LAMINATE DRY SAMPLE THAT WAS HEAT DAMAGED AT
274°C FOR 45 MIN

APPENDIX C

Figure C-68

TGA RESULTS SHOWING WEIGHT LOSS VERSUS TEMPERATURE OF THE IM6/977-3
QUASI-ISOTROPIC LAMINATE DRY SAMPLE THAT WAS HEAT DAMAGED AT
302°C FOR 5 MIN

Figure C-69

TGA RESULTS SHOWING WEIGHT LOSS VERSUS TEMPERATURE OF THE IM6/977-3
QUASI-ISOTROPIC LAMINATE DRY SAMPLE THAT WAS HEAT DAMAGED AT
302°C FOR 20 MIN

Figure C-70
TGA RESULTS SHOWING WEIGHT LOSS VERSUS TEMPERATURE OF THE IM6/977-3
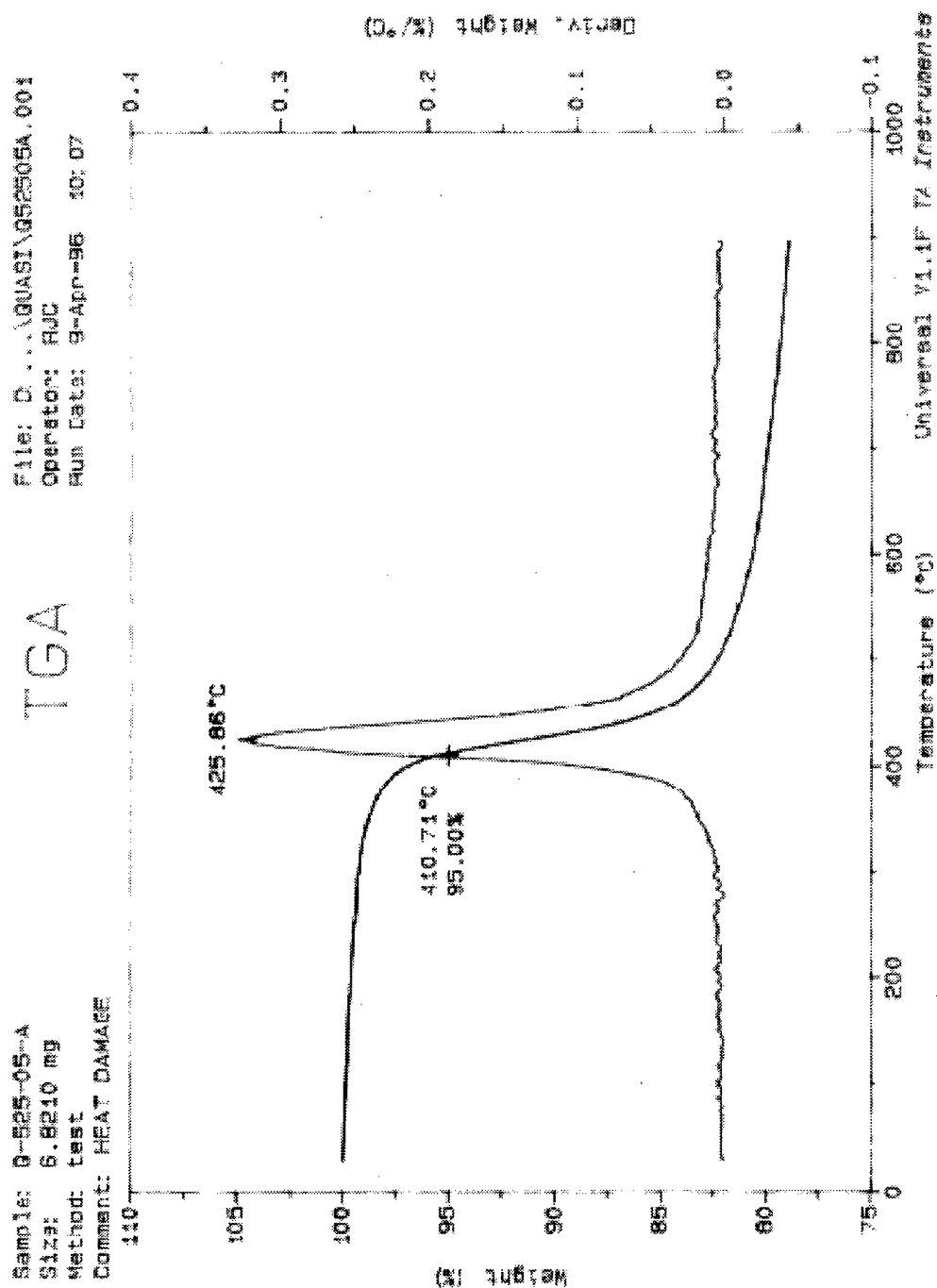QUASI-ISOTROPIC LAMINATE DRY SAMPLE THAT WAS HEAT DAMAGED AT
302°C FOR 45 MIN

APPENDIX C

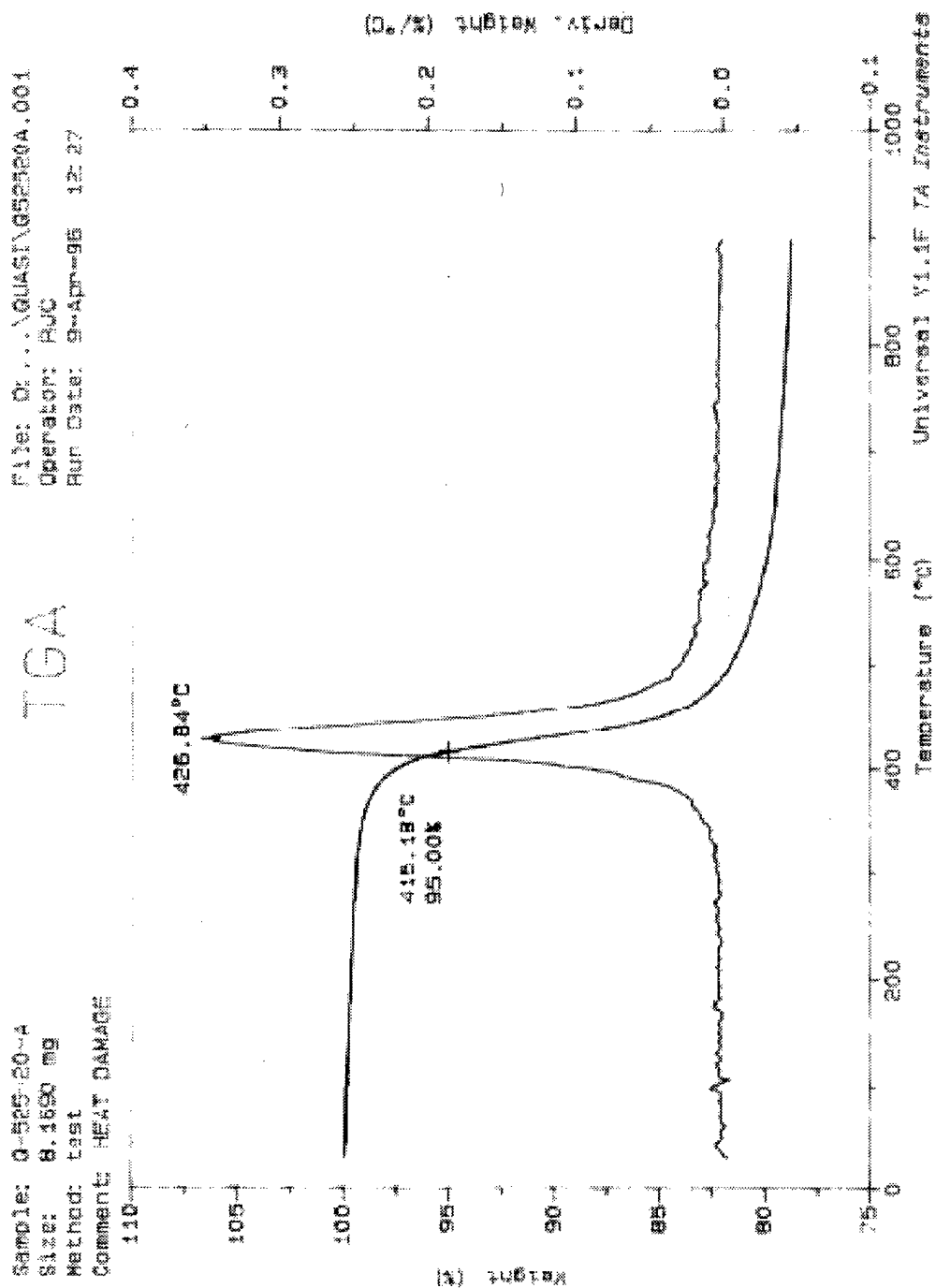Figure C-71

TGA RESULTS SHOWING WEIGHT LOSS VERSUS TEMPERATURE OF THE IM6/977-3
QUASI-ISOTROPIC LAMINATE DRY SAMPLE THAT WAS HEAT DAMAGED AT
329°C FOR 5 MIN

Figure C-72

TGA RESULTS SHOWING WEIGHT LOSS VERSUS TEMPERATURE OF THE IM6/977-3
QUASI-ISOTROPIC LAMINATE DRY SAMPLE THAT WAS HEAT DAMAGED AT
329°C FOR 20 MIN

Figure C-73

TGA RESULTS SHOWING WEIGHT LOSS VERSUS TEMPERATURE OF THE IM6/977-3
QUASI-ISOTROPIC LAMINATE DRY SAMPLE THAT WAS HEAT DAMAGED AT
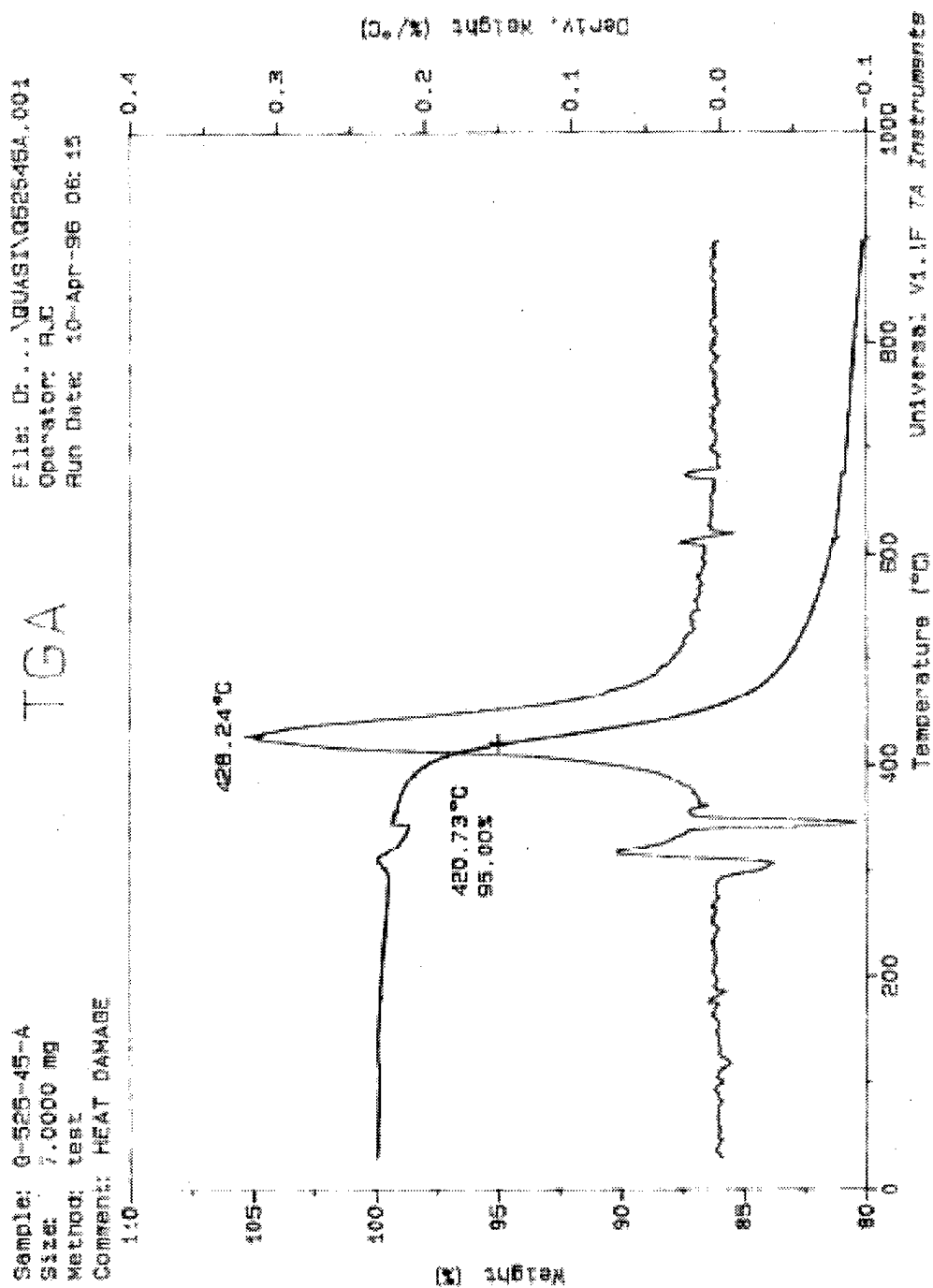329°C FOR 45 MIN

APPENDIX C

Figure C-74

TGA RESULTS SHOWING WEIGHT LOSS VERSUS TEMPERATURE OF THE IM6/977-3
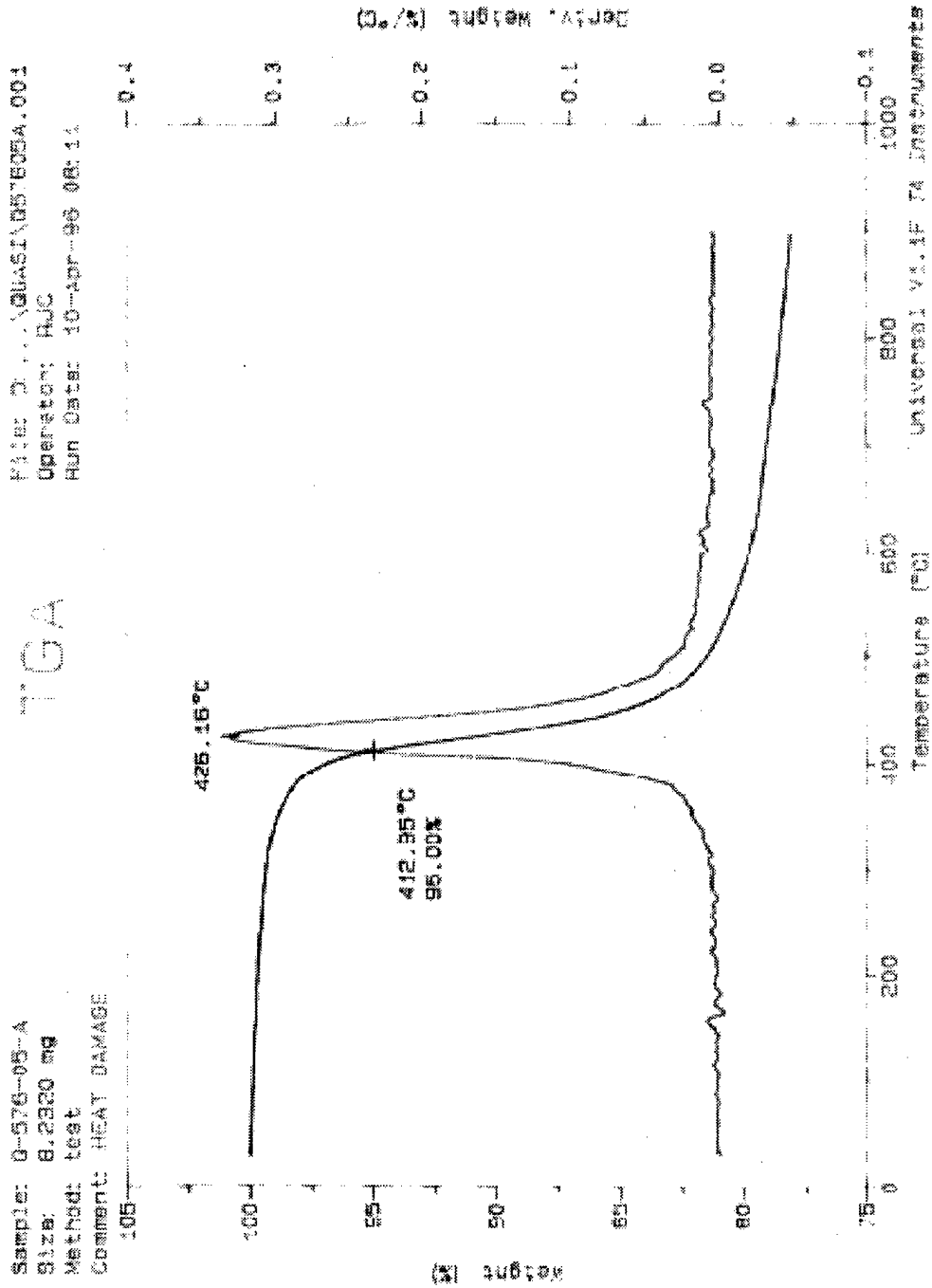QUASI-ISOTROPIC LAMINATE AMBIENT SAMPLE THAT WAS HEAT DAMAGED AT
274°C FOR 5 MIN

173   APPENDIX C

Figure C-75
TGA RESULTS SHOWING WEIGHT LOSS VERSUS TEMPERATURE OF THE IM6/977-3
QUASI-ISOTROPIC LAMINATE AMBIENT SAMPLE THAT WAS HEAT DAMAGED AT
274°C FOR 20 MIN

Figure C-76
TGA RESULTS SHOWING WEIGHT LOSS VERSUS TEMPERATURE OF THE IM6/977-3
QUASI-ISOTROPIC LAMINATE AMBIENT SAMPLE THAT WAS HEAT DAMAGED AT
274°C FOR 45 MIN

APPENDIX C

Figure C-77
TGA RESULTS SHOWING WEIGHT LOSS VERSUS TEMPERATURE OF THE IM6/977-3
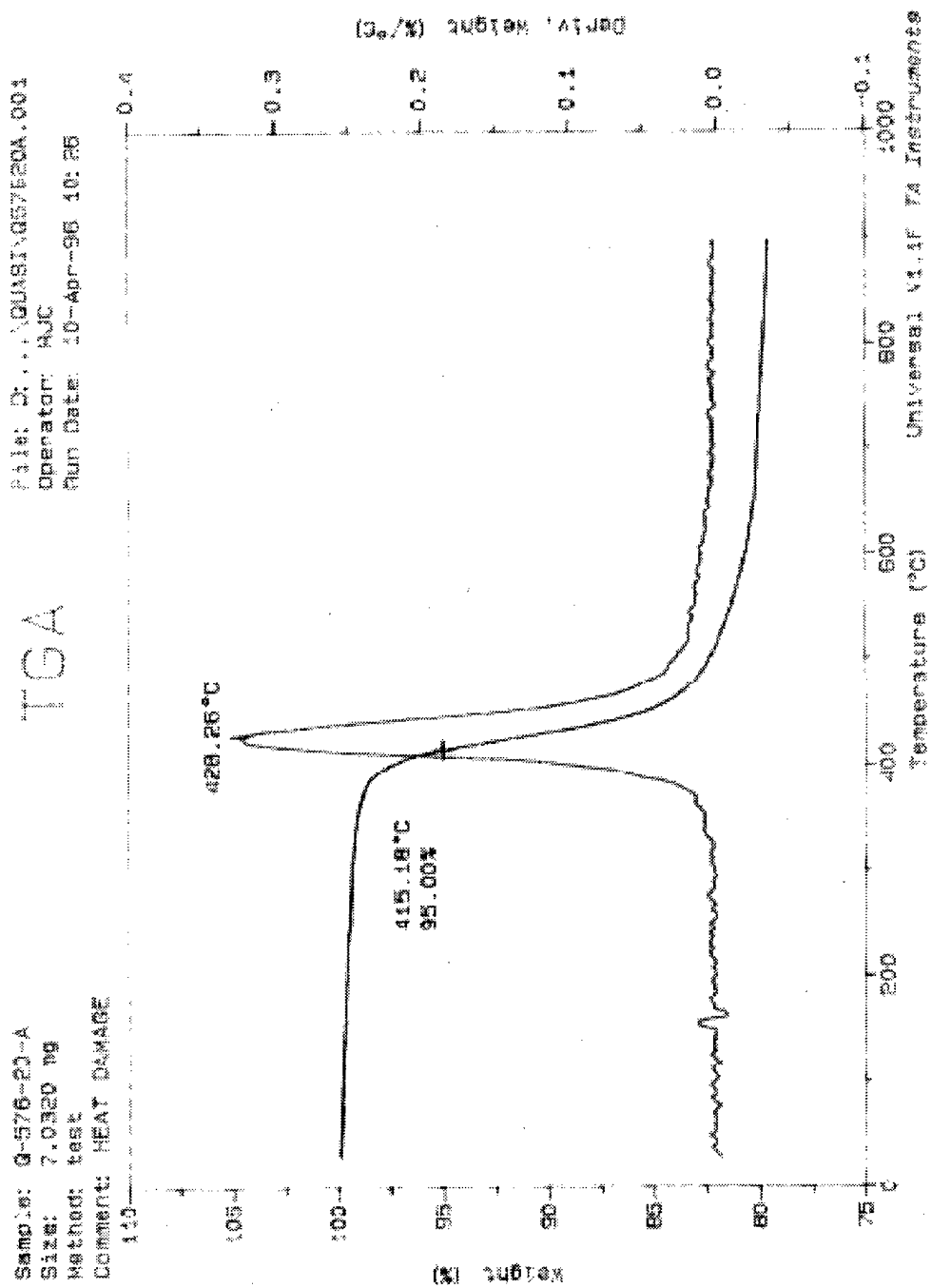QUASI-ISOTROPIC LAMINATE AMBIENT SAMPLE THAT WAS HEAT DAMAGED AT
302°C FOR 5 MIN

APPENDIX C

Figure C-78

TGA RESULTS SHOWING WEIGHT LOSS VERSUS TEMPERATURE OF THE IM6/977-3
QUASI-ISOTROPIC LAMINATE AMBIENT SAMPLE THAT WAS HEAT DAMAGED AT
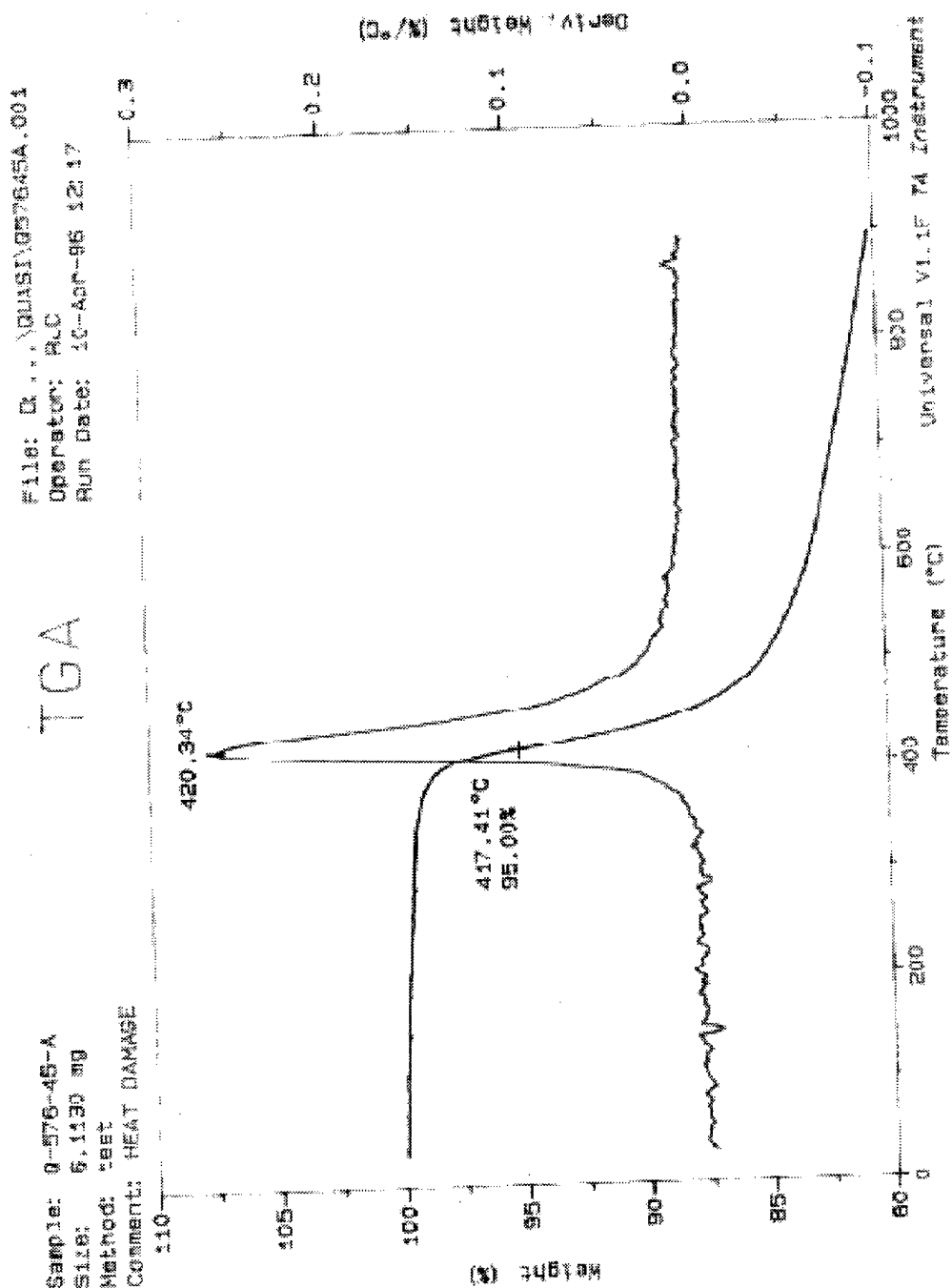302°C FOR 20 MIN

Figure C-79

TGA RESULTS SHOWING WEIGHT LOSS VERSUS TEMPERATURE OF THE IM6/977-3
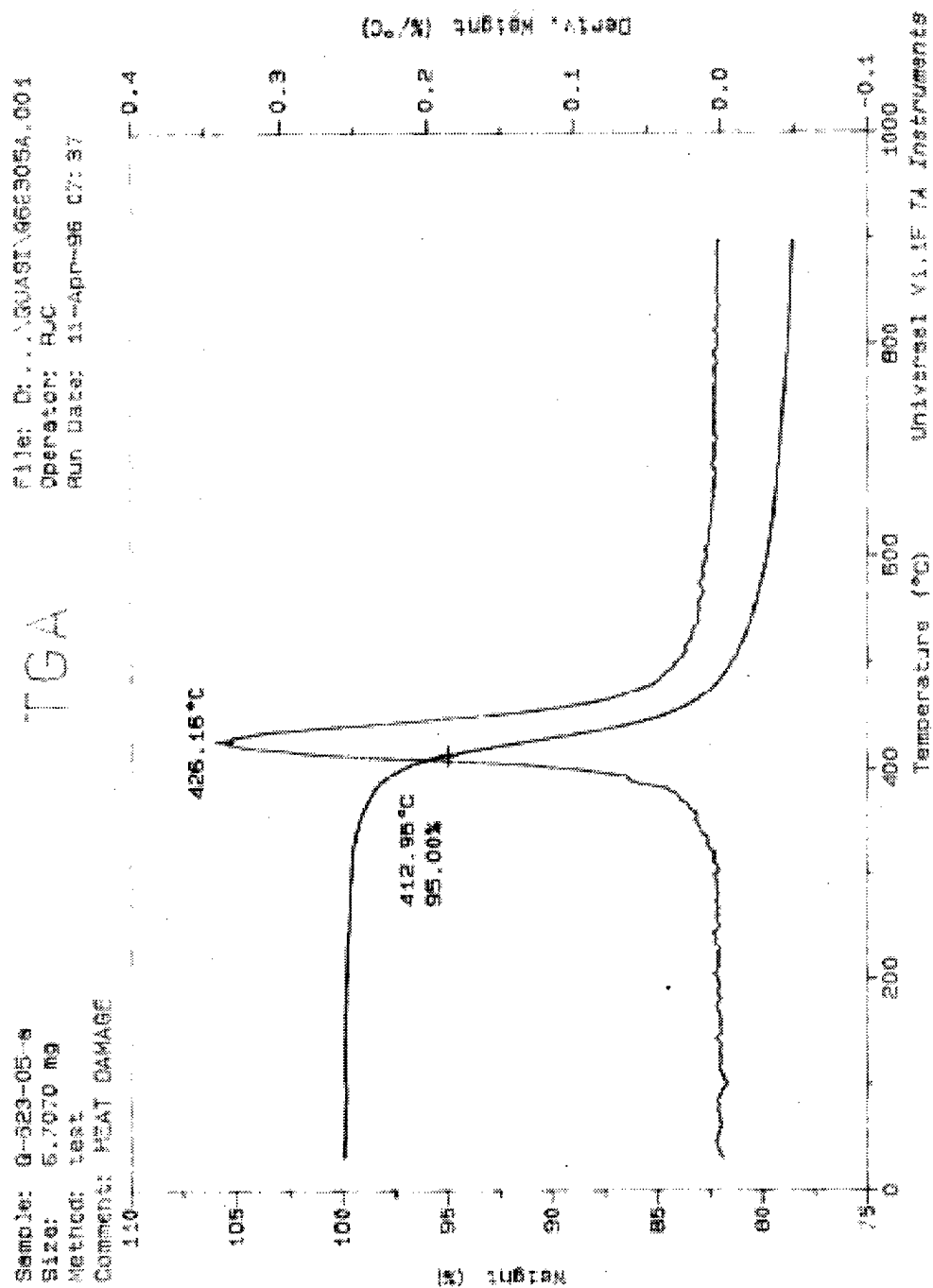QUASI-ISOTROPIC LAMINATE AMBIENT SAMPLE THAT WAS HEAT DAMAGED AT
302°C FOR 45 MIN

Figure C-80
TGA RESULTS SHOWING WEIGHT LOSS VERSUS TEMPERATURE OF THE IM6/977-3
QUASI-ISOTROPIC LAMINATE AMBIENT SAMPLE THAT WAS HEAT DAMAGED AT
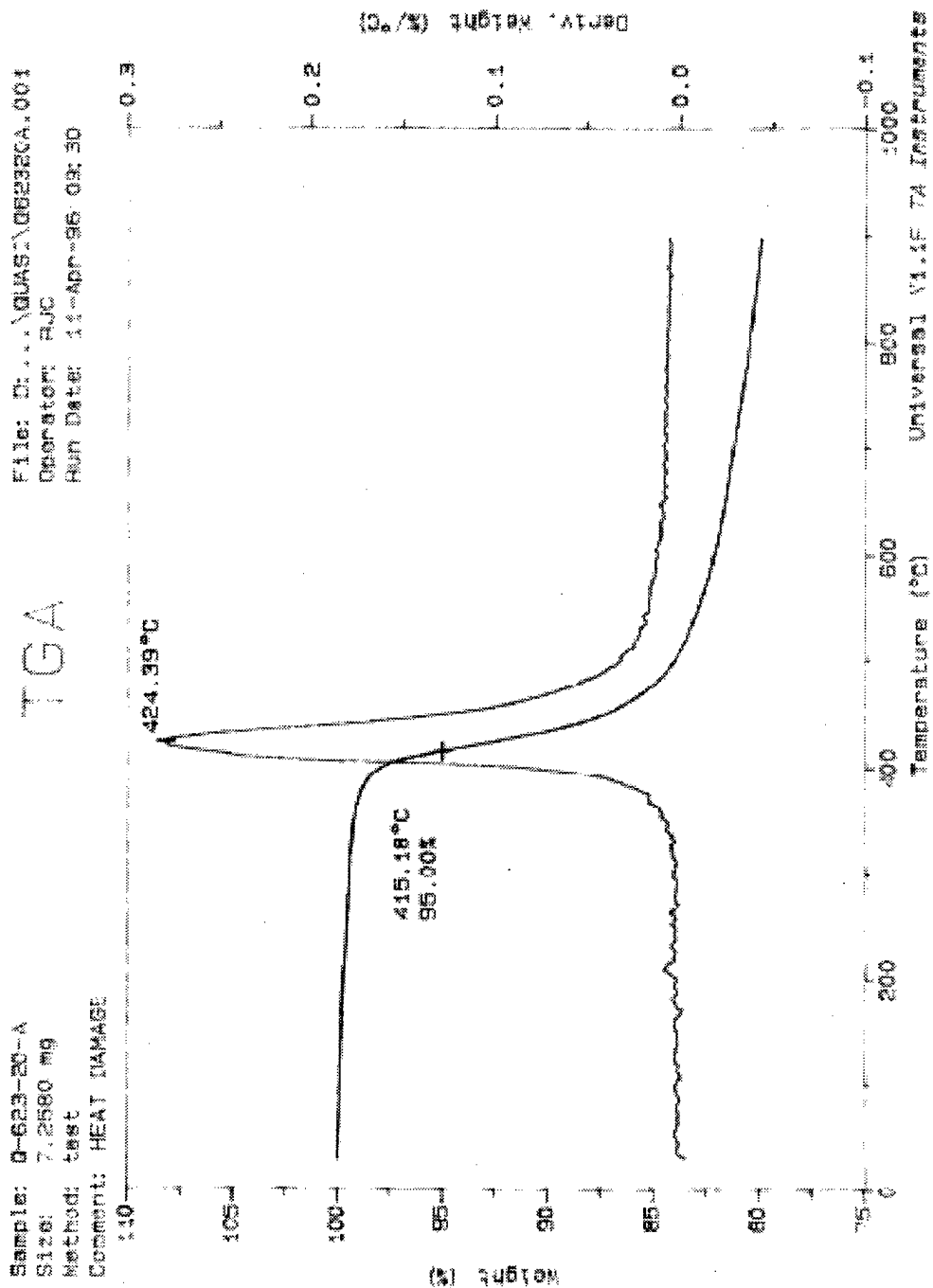329°C FOR 5 MIN

　　　　　　　　　　　　　　　　　　APPENDIX C

Figure C-81

TGA RESULTS SHOWING WEIGHT LOSS VERSUS TEMPERATURE OF THE IM6/977-3
QUASI-ISOTROPIC LAMINATE AMBIENT SAMPLE THAT WAS HEAT DAMAGED AT
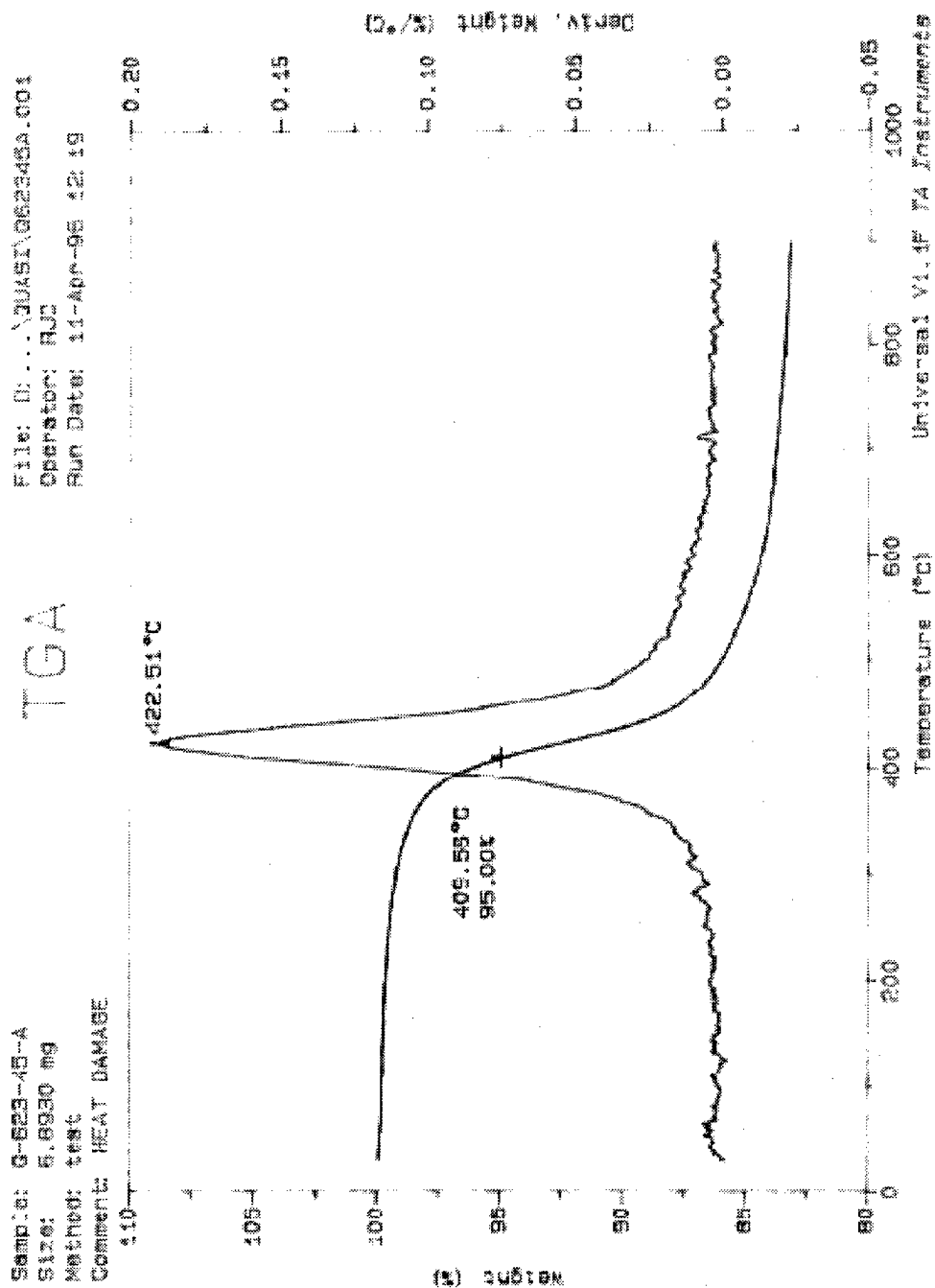329°C FOR 20 MIN

APPENDIX C

Figure C-82

TGA RESULTS SHOWING WEIGHT LOSS VERSUS TEMPERATURE OF THE IM6/977-3
QUASI-ISOTROPIC LAMINATE AMBIENT SAMPLE THAT WAS HEAT DAMAGED AT
329°C FOR 45 MIN

THIS PAGE INTENTIONALLY LEFT BLANK

DISTRIBUTION:

NADEP Cherry Point, NC	(1)
NADEP Jacksonville, F	(1)
NADEP North Island, CA	(1)
ONR Arlington, VA	(1)
NAVSURFWARCEN West Bethesda, MD	(1)
NAVSURFWARCEN Indian Head, MD	(1)
NAVAIRWARCENACDIV Patuxent River, MD (4.3.3.1)	(1)
NAVAIRWARCENACDIV Patuxent River, MD (4.3.4.3)	(5)
NAVAIRWARCENACDIV Patuxent River, MD (Technical Publishing Team)	(1)
Materials Directorate Wright Laborator Wright-Patterson AFB, OH	(2)
Villanova University Villanova, PA	(1)
Rust College Holly Springs, MS	(1)
DTIC	(1)